Johan Morren
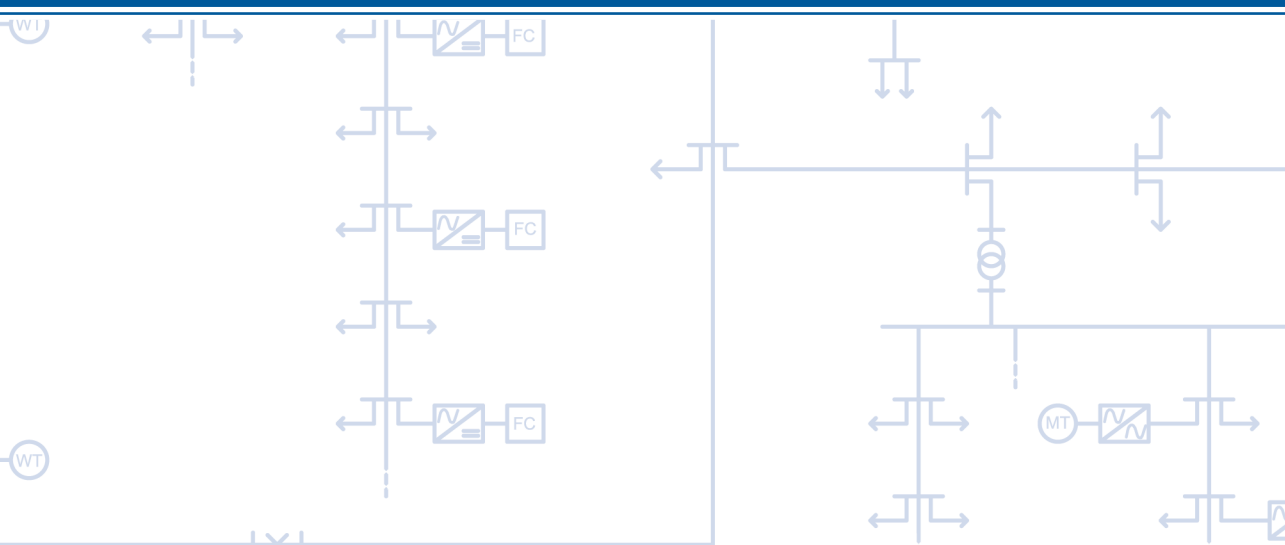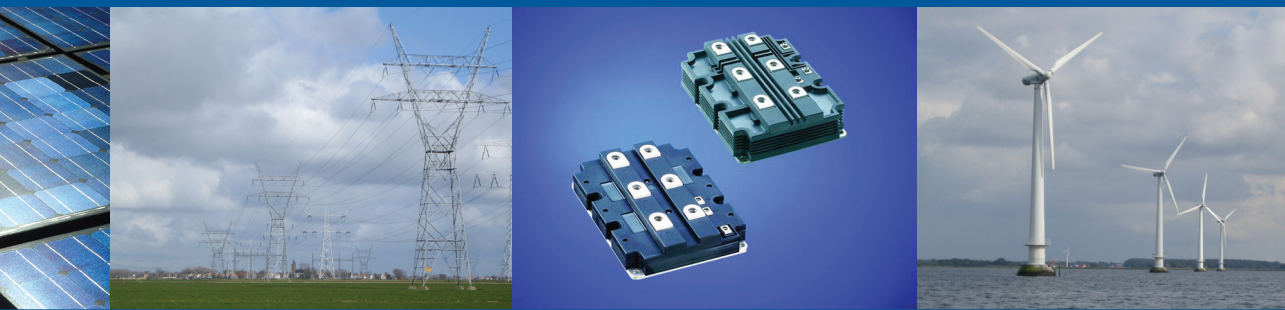
Grid support by power electronic converters of Distributed Generation units

Grid support by power electronic converters of Distributed Generation units

Grid support by power electronic converters of Distributed Generation units

PROEFSCHRIFT

ter verkrijging van de graad van doctor
aan de Technische Universiteit Delft,
op gezag van de Rector Magnificus prof. dr. ir. J.T. Fokkema,
voorzitter van het College voor Promoties,
in het openbaar te verdedigen op maandag 13 november 2006 om 12.30 uur
door

Johannes MORREN

elektrotechnisch ingenieur

geboren te Ede

Cover design by Hans Teerds
Cover pictures: ABB, Capstone, Hans Teerds

Summary

Grid support by power electronic converters of Distributed Generation units

Johan Morren

For several reasons an increasing number of small Distributed Generation (DG) units are connected to the grid. Most DG units are relatively small and connected to the distribution network. The introduction of DG causes several problems, which are mainly related to the differences between DG units and conventional generators: they are located at other places in the network, they are operated in another way, they use other technologies, and they can not always control their power. Four problems have been considered in this thesis: damping of harmonics, voltage control, the behaviour of DG units during grid faults, and frequency control.

A large part of the DG units are connected to the grid via power electronic converters. The main task of the converters is to convert the power that is available from the prime source to the correct voltage and frequency of the grid. The flexibility of the converters offers the possibility however to configure them in such a way that, in addition to their main task, they can avoid or solve some of the problems they cause.

The general objective of this thesis is to investigate how the power electronic converters can support the grid and solve some problems.

An increasing number of power electronic interfaced DG units will result in an increase of the capacitance in the grid, as most converters have a capacitor in their output filter. This capacitance can resonate with the network reactance. An active damping controller is defined in chapter 3, which can easily be implemented in the DG unit control. With this damping controller the DG unit converter can significantly increase the contribution to damping and reduce the harmonics in the network. Conditions are derived for which the converter works and it is analysed how large its contribution can be.

The connection of DG units to the network will result in a change in voltage. The maximum allowable voltage change is limited by regulations and standards. They limit the maximum percentage of DG that can be connected to a network. The DG units can consume reactive power to limit the voltage increase they cause by supplying active power to the grid. Especially in networks that have a high X/R ratio a significantly

higher penetration of DG can be allowed in this way. Most networks are rather resistive however. By applying converter overrating, generation curtailment, or the use of a variable inductance, also in these networks the maximum penetration level can be increased considerably. An approach has been presented to determine the maximum allowable DG unit penetration.

Most grid operators require the disconnection of DG units when faults like short-circuits and voltage dips occur in the network. An important reason for this requirement is that the grid operators fear that DG units disturb the classical protection schemes that are applied. Chapter 5 shows that power electronic interfaced DG units do not necessarily disturb the protection schemes however, as they do not supply large short-circuit currents. Thus, disconnection of these DG units is not necessary. The units can then be used to support the grid (voltage) during the fault.

Most types of DG unit can remain connected to the network in case of a grid fault. Appropriate control strategies have been presented. For one type of DG unit, namely a wind turbine with a doubly-fed induction generator, ride-through is more difficult. Some special measures have been proposed to protect this type of turbine. The key of the technique is to limit the high currents in the rotor circuit with a set of shunt resistors, without disconnecting the converter. In this way the turbine remains synchronised and it can supply (reactive) power to the grid during and immediately after a voltage dip.

Nowadays the grid frequency is stabilised by the conventional power plants. The goal of the frequency control is to maintain the power balance and the synchronism between the synchronous generators in the system. Most DG units do not participate in the frequency control. An increasing DG penetration level can therefore result in larger frequency fluctuations after disturbances. A method has been developed to let DG units participate in frequency control. For most individual DG units this is not possible, because they can not control their power source or because they are too slow. With a combination of different types of DG unit it is possible to support the frequency control however. Requirements are derived which can be used to determine the percentage of each of the DG unit types that is required to obtain a good overall response. Controllers have been presented that implement the frequency control on the DG units.

The different control strategies that have been defined in this thesis can all be implemented simultaneously in the control of a DG unit. A state diagram is derived that can be used to achieve the appropriate control in each situation. The control operates autonomously. Only the grid voltage at the DG unit terminal needs to be measured. In this way a multi-functional DG unit is obtained that can autonomously support the grid in several ways. Implementation of the grid support controller requires in most cases only adaptation of the control software. It can thus be implemented at low cost.

Samenvatting

Netondersteuning door vermogenselektronische omvormers van decentrale opwekeenheden

Johan Morren

Om diverse redenen neemt het aantal kleine decentrale opwek (Distributed Generation, DG) eenheden toe. De meeste DG eenheden zijn relatief klein en aan het distributienet gekoppeld. De introductie van DG leidt tot diverse problemen, welke hoofdzakelijk gerelateerd zijn aan de verschillen tussen DG eenheden en conventionele opwekkers: ze bevinden zich op andere plaatsen in het netwerk, worden op een andere manier bedreven, gebruiken andere technologieën en kunnen niet altijd hun vermogen regelen. Vier problemen zijn beschouwd in dit proefschrift: demping van harmonischen, spanningsregeling, het gedrag van DG eenheden bij netfouten en frequentieregeling.

Een groot gedeelte van de DG eenheden is via vermogenselektronische omvormers aan het net gekoppeld. De belangrijkste taak van deze omvormers is om het vermogen dat de primaire bron levert om te zetten naar de juiste spanning en frequentie van het net. De flexibiliteit van de omvormers biedt echter de mogelijkheid om ze zodanig te configureren dat ze, in aanvulling op hun eigenlijke taak, sommige problemen die ze zelf veroorzaken kunnen vermijden of oplossen.

Het doel van dit proefschrift is te onderzoeken hoe de vermogenselektronische omvormers het net kunnen ondersteunen en sommige problemen kunnen oplossen.

Een toenemend aantal vermogenselektronisch gekoppelde DG eenheden zal leiden tot een toename van de capaciteit in het net, aangezien de meeste omvormers een condensator in hun uitgangsfilter hebben. Deze capaciteit kan resoneren met de netwerkinductiviteit. In hoofdstuk 3 is een 'active damping controller' gedefinieerd die eenvoudig geïmplementeerd kan worden in de regeling van de DG eenheid. Met deze regeling kan de omvormer van de DG eenheid de bijdrage aan de demping aanzienlijk verhogen en de harmonischen in het net reduceren. Voorwaarden waarvoor waarvoor de omvormer werkt zijn afgeleid en de grootte van zijn bijdrage is geanalyseerd.

De koppeling van DG eenheden aan het net zal een verandering in spanning veroorzaken. De maximaal toegestane spanningsverandering wordt beperkt door regels en standaarden. Ze beperken het maximum DG percentage dat aan een net gekoppeld

kan worden. De DG eenheden kunnen reactief vermogen opnemen om de spanningstoename, die ze veroorzaken door actief vermogen aan het net te leveren, te beperken. Speciaal in netwerken die een hoge X/R verhouding hebben kan op deze manier een significant hogere DG penetratie toegestaan worden. De meeste netwerken hebben echter een veel lagere X/R verhouding. Door overbelasting van de converter of beperking van de opwek, of door een variabele inductiviteit te gebruiken, kan ook in deze netwerken een hogere DG penetratie toegestaan worden. Een aanpak om de maximaal toegestane DG eenheid penetratie te bepalen is gepresenteerd.

De meeste netbeheerders eisen de afkoppeling van DG eenheden wanneer fouten zoals kortsluitingen en spanningsdips plaatsvinden in het netwerk. Een belangrijke reden voor deze eis is dat ze vrezen dat DG eenheden de klassieke beveilingsconcepten verstoren. Hoofdstuk 5 laat zien dat vermogenselektronisch gekoppelde DG eenheden niet noodzakelijkerwijs de beveiliging verstoren, aangezien ze geen grote kortsluit-stroom leveren. Daarom is afkoppeling van deze DG eenheden niet nodig. De eenheden kunnen dan gebruikt worden om gedurende de fout het net te ondersteunen.

De meeste typen DG eenheid kunnen dus aan het net gekoppeld blijven in het geval van een fout. Regelstrategieën om dit mogelijk te maken zijn gepresenteerd. Voor één type DG eenheid, namelijk een wind turbine met dubbelgevoede inductiegenerator, is het moeilijker om tijdens een fout netgekoppeld te blijven. Speciale maatregelen zijn voorgesteld om dit type wind turbine te beveiligen. De kern van de techniek is om de hoge stromen in het rotorcircuit te beperken met een set parallelweerstanden, zonder de omvormer af te koppelen. Op deze manier kan de turbine gesynchroniseerd blijven en kan ze gedurende en direct na de spanningsdip (reactief) vermogen aan het net leveren

Vandaag de dag wordt de netfrequentie gestabiliseerd door de conventionele centrales. Het doel van de frequentieregeling is om de vermogensbalans en het synchronisme tussen de synchrone generators in het net te handhaven. De meeste DG eenheden participeren niet in de frequentieregeling. Een toenemende DG penetratie kan daarom resulteren in grotere frequentiefluctuaties na verstoringen. Een methode om DG eenheden te laten participeren in frequentieregeling is ontwikkeld. Voor de meeste individuele DG eenheden is dit niet mogelijk, omdat ze hun vermogensbron niet (snel genoeg) kunnen regelen. Met een combinatie van verschillende typen DG eenheid is het echter mogelijk frequentieregeling te ondersteunen. Er zijn vereisten afgeleid die gebruikt kunnen worden om het percentage te bepalen van elk type DG eenheid (of groep van typen) dat nodig is om een goede totaalreponsie te behalen. Regelaars zijn gepresenteerd die de frequentieregeling implementeren in de DG eenheden.

De verschillende regelstrategieën die gedefinieerd zijn in dit proefschrift kunnen allemaal gelijktijdig geïmplementeerd worden in de regeling van een DG eenheid. Er is

een toestandsdiagram ontworpen dat in elke situatie de geschikte regeling bepaald. Deze regeling werkt autonoom. Alleen de netspanning aan de klemmen van de DG eenheid behoeft gemeten te worden. Op deze manier is een multi-functionele DG eenheid verkregen die autonoom op verschillende manieren het net kan ondersteunen. De implementatie van de regelingen vereist in de meeste geval alleen maar een aanpassing van de regelsoftware. De regelingen kunnen dus meestal tegen weinig kosten geïmplementeerd worden.

Contents

Chapter 3. Harmonic damping contribution of DG unit Converters   25

Chapter 4. Voltage control contribution of DG units   47

Chapter 5. Ride-through and grid support during faults 67

Chapter 6. Frequency-control contribution of DG units 93

Chapter 7. Implementation of grid support control   123

Chapter 8. Conclusions and recommendations   133

References   139

Appendix A: Network model description   145

Appendix B: Converter model description   149

Appendix C: DG unit model description   155

Chapter 1

Introduction

1.1. Background

Over the last years an increasing number of Distributed Generation (DG) units are connected to the grid. This development is driven by governmental policy to reduce greenhouse gas emissions and conserve fossil fuels, as agreed in the Kyoto protocol, by economical developments such as the liberalisation and deregulation of the electricity markets, and by technical developments. Most DG units are relatively small and connected to the distribution network (DN). A large percentage of the sources are connected to the grid via power electronic converters.

The introduction of DG results in a different operation of the electrical power system. The conventional power system is characterised by a power flow from a relatively small number of large power plants to a large number of dispersed end-users. Electrical networks transport the electrical energy using a hierarchical structure of transmission and distribution networks. In a limited number of control centres the system is continuously monitored and controlled. [Bla 04], [Don 02]

The changes due to the introduction of DG are mainly caused by the differences in location and operation principle between the DG units and the conventional generators and loads. The most important differences are:

- The DG units are mostly connected to the DN; this introduces generators in the DN, which historically only contained loads [Bar 00], [Had 04].
- A large percentage of the DG units are connected to the grid via power electronic converters, which have a behaviour that is fundamentally different from the behaviour of the conventional synchronous machine based generators [Jóo 00], [Kna 04].
- Several types of DG unit are based on renewable energy sources like sun and wind, which are uncontrollable and have an intermittent character [Ack 02], [Püt 03].
- Most DG units behave as 'negative loads' and do not participate in the conventional control of the network [Jen 00].

1.2 Problem definition

The introduction of DG causes several problems. The four problems that will be investigated in this thesis are described in this section. They are all caused by the differences in location and operation principle between DG units and the conventional generators and loads, described in the previous section. First three problems with a local impact are considered. The fourth issue has a global impact, meaning that the system as a whole is affected [Slo 03b].

Damping of harmonics – An increasing number of power electronic interfaced DG units will result in an increase of the capacitance in the grid, as most converters have a capacitor in their output filter [Lis 06]. Manufacturers try to decrease filter inductors to make the inverter more cost-effective. At the same time the capacitance has to be increased to let the cut-off frequency of the filter remain the same [Ens 04]. The output capacitance can form a resonance circuit with the network reactance. In conventional grids the amount of capacitance is low, implying high resonance frequencies and a limited chance that the resonance circuits are excited. With an increasing amount of capacitance the resonance frequency will decrease and may be more easily excited by harmonics. As a result there is an increasing risk for resonances, oscillatory responses, and a high level of harmonic distortion [Ens 04]. How large the amplitude of the harmonic voltages and currents will be, depends on the damping in the network.

Voltage control - The objective of voltage control is to maintain the RMS value of the voltage within specified limits, independent of the generation and consumption [Mil 82], [Kun 94]. Conventional voltage control in the high-voltage transmission network is mainly performed by the large power plants. In DNs voltage control is done by tap changers on distribution transformers. This control is relatively slow and compensates for the current-depending voltage drop along the line, based on the assumption that only loads are connected to the network. Introduction of DG units in the DN will change the power flow in a part of the network. In addition some DG units have a primary energy source that fluctuates [Jen 00], especially those that are based on renewable energy sources such as wind and sun. As a result the DG unit power may fluctuate. The changes in magnitude and direction of the power will result in changing voltages, due to the current-depending voltage drop along the line, which has a relatively high impedance in the low-voltage and medium-voltage grid [Jen 00], [Str 02]. The voltage fluctuations can range from slow (hours) to fast (milliseconds). It may become difficult to keep the voltage within the specified limits and to meet requirements regarding flicker [Bar 00], [Tan 04].

Fault behaviour - In power systems many types of fault can occur, such as for example voltage dips and short-circuits [Bol 00]. Fault behaviour concerns the response of the DG units to these faults. The introduction of DG units in the DN can disturb the classical protection schemes that are applied [Kum 04]. This holds especially for DG units that are based on synchronous machines. The response of power electronic interfaced DG units to a fault will depend on the control implementation. Most grid operators require that DG units are disconnected from the grid during faults [Nav 05]. This minimises the risk that the grid protection schemes are disturbed. Disconnection may become undesirable however, when the percentage of DG in a network is increasing. It can result in a large power generation deficit and will require a larger power reserve of other generators.

Frequency control - Nowadays the grid frequency is stabilised by the conventional power plants. The goal of the frequency control is to maintain the power balance and the synchronism between the synchronous generators in the system [Kun 94]. The inertia of the synchronous machines plays an important role in maintaining the stability of the power system during a transient situation, e.g. during and after a disturbance. The more rotational mass the synchronous generator has, the less the generator rotor will respond to an accelerating or decelerating tendency due to a disturbance [Kun 94]. The large amount of rotating mass in the present interconnected power systems tends to keep the system stable following a disturbance. With an increasing penetration level of DG this stabilising task can become increasingly difficult because of the decreasing level of inertia in the grid [Kna 04]. Most DG units are connected to the grid by power electronic converters, and therefore the direct relation between power and frequency is lost [Jóo 00]. As a result, disturbances might result in larger frequency deviations.

1.3. Objective and research questions

Most of the problems discussed in the previous section occur in the medium and low voltage networks, where generally no control is available. Although several types of DG unit employ electric generators that are coupled directly to the grid, the trend is to use a power electronic interface [Jóo 00]. The main task of these power electronic converters is to transfer the active power to the grid. The flexibility of the converters offers the possibility to configure them such that, in addition to their main task, they support the grid and solve or mitigate some of the mentioned problems. The general objective of this thesis is based on these observations and is defined as:

> *Investigate if and how the power electronic converters of the DG units can be used to solve some of the problems caused by the introduction of DG, taking into account the requirements that are imposed by the network and the DG unit itself.*

Based on this objective and the problem definition given above, four main research questions have been defined:

a) *Damping of harmonics: How and to what extent can the power electronic converters contribute to the damping in the grid?*

b) *Voltage control: How and under which conditions can the power electronic converters of the DG units contribute to steady-state voltage control and how large can this contribution be?*

c) *Fault behaviour: How should the power electronic converters of the DG units react to short-circuits and voltage dips in order to avoid disturbance of the grid protection, to support the grid, and to protect the DG unit from malfunctioning?*

d) *Frequency control: How and to what extent can power electronic interfaced DG units contribute to primary frequency control and the inertia of the system?*

The main differences between the four research items are the grid parameters that are controlled (frequency, power, voltage) and the time scale of the phenomena. In power systems three time scales are generally distinguished, namely steady state, dynamic, and transient. Fig. 1.1 shows the time scales in which the phenomena fit.
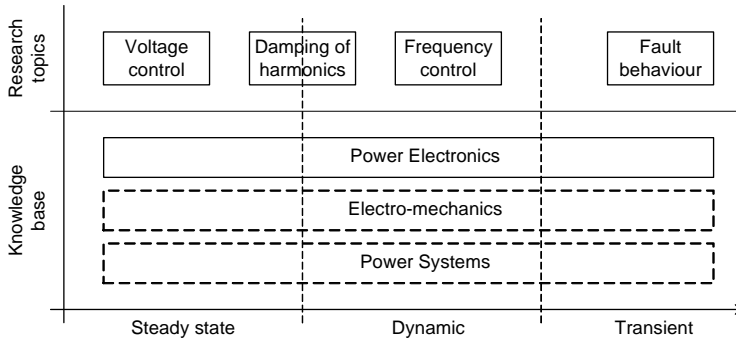
Fig. 1.1. Time scales in which the different problems occur and that are covered by the DG unit connection technologies

For these research items several knowledge bases play a role, namely power systems, electro-mechanics and power electronics. These three knowledge bases cover all time frames, as shown in Fig. 1.1. In this thesis the problems are considered from the point of view of the power electronics knowledge base, which all power electronic interfaced DG units have in common.

1.4. Approach

The goal of this thesis is to investigate how DG unit converters can support the grid and how they can solve the problems mentioned in the previous section. The approach for each of the topics is more or less the same.

Simplified models of the network and the DG units are derived. They are used to give a mathematical description of the problem. Based on this description mathematical analyses are done to quantify for which combination of parameters problems occur and how large the problems are. In the same way it is investigated how large the support can be. The results of the analyses are presented in a number of graphs. The values in these graphs are mostly in per unit to keep the results as general applicable as possible.

In the next step it is investigated how the grid support can be achieved by DG units. In this stage controller implementations and control strategies are derived. For some of the topics it is obvious how the control should be implemented. For the other topics appropriate control schemes, which can be implemented as additional control, will be described. The performance of the controllers is demonstrated with (time-domain) case study simulations.

Three types of DG unit will be considered in this thesis. They represent the three different groups of DG units that are important with respect to frequency control: fuel cells (static, controllable power source), micro-turbines (rotating, controllable power source), and wind turbines (rotating, uncontrollable power source). The models that are used are described in appendix C. The models of the converters that the DG units use are described in appendix B.

For each of the topics one or more realistic cases are studied to investigate the performance of the proposed controllers. They are performed on a number of case study networks, which are simplifications of some Dutch MV and LV networks. The three networks are described below. More information is given in appendix A.

Urban network - The 'Testnet' in Lelystad is a 10 kV cable distribution network in a residential area. It consists of a HV/MV distribution substation with a number of radial feeders. Three wind turbines with a total installed capacity of about 1.5 MW and a CHP

plant of about 2.5 MW are connected to this network. The network is rather lightly loaded and can be considered as a 'strong' network.

Rural network - The second network is an extensive rural 10 kV cable network in the north of the Netherlands. Some small wind turbines are connected to a feeder of the network. The feeder has a relative high impedance, which in some cases results in large voltage changes. The feeder can be considered as a 'weak' network.

Low-voltage network - The network in Vroonermeer-Zuid is a typical 400 V low-voltage network. It is of special interest because it contains a large penetration of solar cell inverters. One network, with a peak solar generation capacity of 235 kW and an average load of 26 kW, is considered. The network is of particular interest because severe problems with harmonic distortion and resonances have been noted.

All case study simulations are done in Matlab Simulink. Several models that are used are in the *dq0* reference frame. The advantage of using this reference frame is that all signals are constant in steady state, resulting in a large increase in simulation speed. The basic principles of deriving models in the *dq0* reference frame are presented in appendix E. For the models in this thesis only the *d-* and the *q*-axis are modelled, as only symmetrical situations are considered.

1.5 Outline

This section presents an outline of the thesis.

Chapter 2 – Chapter 2 gives a review of the relevant basics of power systems, Distributed Generation, and power electronics. This information can be helpful to understand the remaining part of the thesis.

Chapter 3 – In chapter 3 is investigated how power electronic converters can improve the relative damping in the grid. Relative damping is a function of frequency and therefore the analyses are done in the frequency domain. As a first step, transfer functions of power electronic converters are obtained. They are used to determine the damping contribution of the converter, by looking at the location (in the real-imaginary plane) of the resonant poles of the system. The influence of the converter is shown to be small, and therefore an active damping controller is proposed to increase the contribution to damping. Conditions are derived for which the active damping controller

works, and it is analysed how large its contribution can be. With some case studies the capabilities of the proposed damping controller are shown.

Chapter 4 - The voltage change caused by DG units depends on a number of parameters such as the short-circuit power of the network and the ratio between the inductance and the resistance (X/R ratio) of the grid. Chapter 4 starts with deriving relations between these parameters. The analyses show that voltage control possibilities with reactive power are limited, due to the low X/R ratio of (cable) distribution networks. The chapter describes a number of solutions to improve the possibilities for voltage control. It then continues with deriving equations that can be used to determine the maximum DG penetration that is possible when the voltage change caused by the DG units should stay below a certain limit. With some cases it is demonstrated how the relations derived in the chapter can be used to determine the maximum DG penetration level in practical situations.

Chapter 5 – Synchronous machines and power electronic converters have a completely different response to faults. Chapter 5 starts with comparing the responses. To a certain extent the converter response can be freely chosen, in contrast with a machine that has an inherent response. The flexibility of the converter control enables minimisation of the influence on the classical protection, as will be shown. When DG units do not disturb the protection they can stay connected during a fault and support the grid. The effectiveness of this support is investigated. To enable fault ride-through some measures have to be taken for some DG units. These measures will be presented. A special case during short-circuits is a wind turbine with a doubly-fed induction generator. It is analysed at the end of chapter 5.

Chapter 6 - Chapter 6 investigates how and to which extent power electronic interfaced DG units can contribute to frequency control. It starts with a description of the response of a conventional power system to load unbalances and frequency deviations. The response depends mainly on the inertia of the systems and the ability of the generators to increase their output power. For the most important DG unit types it will be investigated whether they can increase their output power and whether they have inertia or that a 'virtual inertia' can be emulated. With a good mix of types of DG units frequency control support is possible. A method to determine such a mix will be derived. The method is used to derive a number of figures that show the minimum and maximum allowable penetrations levels of different combinations of conventional generation and different types of DG. Time-domain simulation of a case study shows that frequency control is possible with the proposed mix.

Chapter 7 – The different grid support strategies and controllers are discussed in separate chapters. Chapter 7 investigates how the different support strategies can be implemented in one converter. The chapter develops a state diagram that can be implemented in the DG unit control.

Chapter 8 – General conclusions and recommendations for further research are given in chapter 8.

1.6 Intelligent power systems research project

The research presented in this thesis was performed within the framework of the 'Intelligent Power Systems' project. The project is part of the IOP-EMVT program (Innovation Oriented research Program – Electro-Magnetic Power Technology), which is financially supported by SenterNovem, an agency of the Dutch Ministry of Economical Affairs. The 'Intelligent Power Systems' project is initiated by the Electrical Power Systems and Electrical Power Processing groups of the Delft University of Technology and the Electrical Power Systems and Control Systems groups of the Eindhoven University of Technology. In total 10 PhD students, who work closely together, are involved in the project.

The research focuses on the effects of the structural changes in generation and consumption which are taking place, like for instance the large-scale introduction of distributed (renewable) generators [Rez 03].
   Such a large-scale implementation of distributed generators leads to a gradual transition from the current 'vertically-operated power system', which is supported mainly by several big centralised generators, into a future 'horizontally-operated power system', having also a large number of small to medium-sized distributed (renewable) generators. The project consists of four parts, as illustrated in Fig. 1.2.

The first part investigates the influence of decentralised generation without centralised control on the stability and dynamic behaviour of the transmission network. As a consequence of the transition in the generation, fewer centralised plants will be connected to the transmission network as more generation takes place in the distribution networks, close to the loads, or in neighbouring systems. Solutions that are investigated include the control of centralised and decentralised generation, the application of power electronic interfaces and monitoring of the stability of the system.

The second part focuses on the distribution network, which becomes 'active'. There is a need for technologies that can operate the distribution network in different modes and support the operation and robustness of the network. The project investigates how the power electronic converters of decentralised generators or power electronic interfaces between network parts can be used to support the grid. Also the stability of the distribution network and the effect of the stochastic behaviour of decentralised generators on the voltage level are investigated. The research presented in this thesis has been performed in this part of the project

In the third part autonomous networks are considered. When the amount of power generated in a part of the distribution network is sufficient to supply the local loads, the network can be operated autonomously but as a matter of fact remains connected to the rest of the grid for reliability reasons. The project investigates the control functions needed to operate the autonomous networks in an optimal and reliable way.

The interaction between the grid and the connected appliances has a large influence on the power quality. The last part of the project analyses all aspects of the power quality. The goal is to support the discussion between the polluter and the grid operator who is responsible for compliance with the standards. The realisation of a power quality test lab is an integral part of this part of the project.
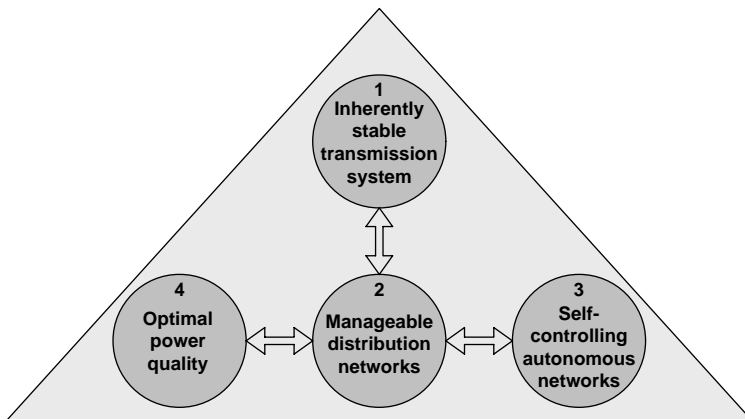
Fig. 1.2. The four parts of intelligent power systems research project

Chapter 2

Distributed Generation and Power Electronics

Over the last years an increasing number of small, Distributed Generation (DG) units are connected to the grid. Power electronics plays an important role in the connection of these DG units to the grid. This chapter discusses some important aspects related to DG, power electronics and the conventional power system, which might help to understand this thesis.

2.1 The conventional electricity network

Over the past century the electrical power systems have evolved to the concept that large power plants provide the optimal cost-effective generation of electricity. The electrical energy is transported from these sources to the end-user using a hierarchical structure of high-voltage transmission networks and medium-voltage and low-voltage distribution networks (DNs), as shown in Fig. 2.1. To ensure both a high security and availability, most of the networks have been meshed, to provide alternative routing in case of faults. They are protected from critical failures and natural phenomena, such as lightning strikes, with mechanical and electronic protection schemes. The networks are characterised by a power flow from a relatively small number of large power plants to a large number of dispersed end-users [Don 02].

The conventional arrangement of the power system offers a number of advantages. Large generating units can be made energy efficient and can be operated with a relatively small crew. The interconnected high-voltage transmission network allows generator reserve requirements to be minimised and the most efficient generating plant to be used at any time [Slo 03b].

Due to a number of developments an increasing number of DG units are connected to the power system. The introduction of DG results in differences in the operation of the power system. Most DG units are relatively small and connected to the distribution network. This results in an increase in the number of generators and it can result in a

change in the direction of the power flow. In addition, several DG unit types are based on renewable energy sources like sun and wind, which are uncontrollable, and have an intermittent character. This can result in unpredictable and fluctuating power flows in the network. Unlike the conventional generators, most DG units do not participate in the control of the network [Jen 00].
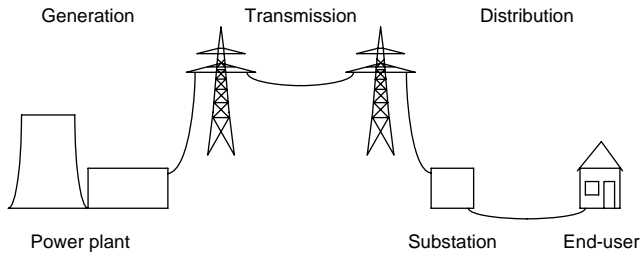
Fig. 2.1. Schematic representation of an electrical power system

2.2 Distributed Generation: drivers and definitions

The increasing interest in and application of DG is driven by political, environmental, economical and technical developments.

The current political intent to reduce greenhouse gas emissions and conserve fossil fuels, as agreed in the Kyoto protocol, has resulted in a drive to clean and renewable energy [Sco 02]. Governments started programmes to support the exploitation of renewable energy sources such as wind and solar power.

The world-wide move to liberalisation of the electricity markets is considered to have a positive influence on the increase of DG. A deregulated environment and open access to the DN is likely to provide better opportunities for DG units [Jen 00]. They require lower capital costs and shorter construction times. Besides this, it is becoming increasingly difficult to find sites and permissions for the construction of new large power plants and transmission facilities as high-voltage overhead lines [Püt 03]. As DG units are mostly connected to the DN, extension of the transmission network might not be necessary.

Besides this, DG is being increasingly applied just to help to provide for the ever-expanding demand for electric power. Benefits of generating power close to the loads include the use of waste heat for heating or cooling (combined heat and power (CHP), co-generation) and the availability of standby power for critical loads during periods when electricity from the utility is unavailable [Wal 01]. Another important reason is just

that a number of DG technologies have reached a development stage which allows for large-scale implementation within the existing electric utility systems [Püt 03].

No general accepted definition of Distributed Generation exists and there are even a number of other names for DG, such as 'embedded generation', 'dispersed generation', 'decentralised generation', and 'distributed energy resources' [Ack 01], [Don 02], [Pep 05]. Although all the definitions are more or less the same, there are some small differences. Distributed Generation is grid-connected, whereas dispersed generation can be stand-alone. The term decentralised generation stresses the geographical distribution, whereas the term embedded generation stresses the fact that the generated power is used locally [Ack 01]. Distributed resources also incorporate storage devices. In this thesis the term 'Distributed Generation' (abbreviated as 'DG') is used. For a single generator the term 'Distributed Generation unit' ('DG unit') is used.

Generally, Distributed Generation units can be defined as generation units that are connected to the distribution network and that have a relatively small capacity [Püt 03]. This definition implies a wide range of different possible generation schemes. At one side there are large industrial-site generating plants rated at tens of MW capacity, whereas at the other side there are small units of a few kW, typical of domestic DG installations. Distributed Generation should not be confused with renewable generation. DG technologies include renewable energy sources but are not limited to these sources. The renewable technologies include photovoltaic systems, wind turbines, small hydro generators and wave energy generators. Non-renewable technologies include combined heat and power (CHP, co-generation), internal combustion engines, fuel cells and micro-turbines [Jen 01], [Püt 03].

2.3 Distributed Generation technologies

This section describes the three types of DG unit that are considered throughout the thesis: fuel cells, micro turbines, and wind turbines. These three types are representative for the three main groups of DG units (see section 1.4). They will be described as far as is necessary to understand their use in this thesis. A description of the model implementation is given in appendix C.

2.3.1 Fuel cells
Fuel cells are electrochemical devices. A fuel cell system generally consist of three main parts, as shown in Fig. 2.2; a fuel processor (reformer) which converts fuels such as natural gas to hydrogen, the fuel cell itself, where the electrochemical processes take

place and the power is generated and the power conditioner, which converts the DC voltage to AC and enables grid-connection.
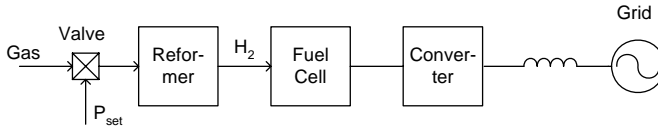
Fig. 2.2. Fuel cell system

Fuel cell basics - Fig. 2.3 shows the basic diagram of a fuel cell itself, consisting of a positive (anode) and a negative (cathode) electrode and an electrolyte. The fuel is electrochemically oxidised on the anode, while the oxidant is electrochemically reduced on the cathode. The ions created by the electrochemical reactions flow between the anode and the cathode through the electrolyte, while the electrons resulting from the oxidation at the anode flow through an external circuit to the cathode, completing the electric circuit [Bor 01].
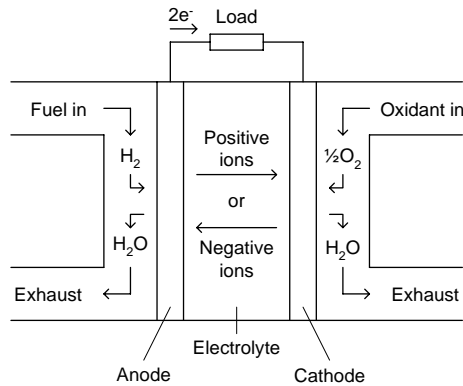
Fig. 2.3. Basic fuel cell diagram

Most fuel cells use gaseous fuels and oxidants. Mostly hydrogen and oxygen are used. The electrolyte of the fuel cell serves as ion conductor. Single fuel cells produce only about 1 V. Therefore a large number of fuel cells are used in series and parallel to form a stack with a considerable output power.

The fuel cells that exist nowadays can be classified by the electrolyte they use: alkaline fuel cell (AFC), molten carbonate fuel cell (MCFC), phosphoric acid fuel cell (PAFC), proton exchange membrane fuel cell (PEMFC) and solid oxide fuel cell (SOFC). The last two types are the most widely used. The PEMFC has an electrolyte that is a layer of solid polymer (usually a sulfonic acid polymer) that allows protons to be transmitted from one face to the other. Because of the limitations imposed by the thermal properties of the membrane, PEM fuel cells operate at a temperature that is

much lower than that of other fuel cells (~ 90 °C). SOFCs operate at temperatures of 650 to 1000 °C. This allows more flexibility in the choice of fuels. Solid oxide fuel cells have a non-porous metal oxide electrolyte material. Ionic conduction is accomplished by oxygen ions.

Characteristics and interface - Most fuel cells have a reformer which converts the fuel (mostly natural gas) to the hydrogen that is necessary for the electrochemical processes. The processes in the reformer change rather slow, because of the time that is needed to change the chemical reaction parameters after a change in the flow of reactants. This will limit the speed with which fuel cells can change their output power. Typically the response time is several tens of seconds.

   Voltage and current depend on parameters such as the number of stacked fuel cells and the kind of fuel used. For grid-connected fuel cells an inverter is needed to convert the DC voltage to AC voltage.

2.3.2 Micro turbines

Micro turbines are small gas turbines with power levels up to several hundreds of kilowatts. Essentially micro turbines can be considered as small versions of conventional gas-fuelled generators. The important differences are that they run at much higher speeds and are connected to the grid with a power electronic converter (PEC).

Micro turbine basics - There are basically two micro turbine types. The one that will be considered in this thesis is a high-speed single-shaft unit with the electrical generator on the same shaft as the compressor and turbine. The speed of the turbine is mainly in the range of 50,000 – 120,000 rpm [Zhu 02]. It needs a frequency converter for connection to the grid.

   A micro-turbine system consists of several parts, which are shown in Fig. 2.4. The first is a compressor in which air is compressed. The compressed air, together with the fuel, is fed to the combustor. The output of the combustor is used to drive the gas turbine. The gas turbine drives the electrical generator, which operates at high speed, ranging from 1500 to 4000 Hz. To match this with the grid frequency a back-to-back frequency converter is used. The electrical generator is mostly a permanent magnet synchronous machine.

Characteristics and interface – The gas turbine and permanent magnet generator are completely decoupled from the grid by the PEC. The characteristics of the micro turbine are therefore mainly determined by the converter. The response of the system to changes in the power setpoint depends on the gas turbine properties.
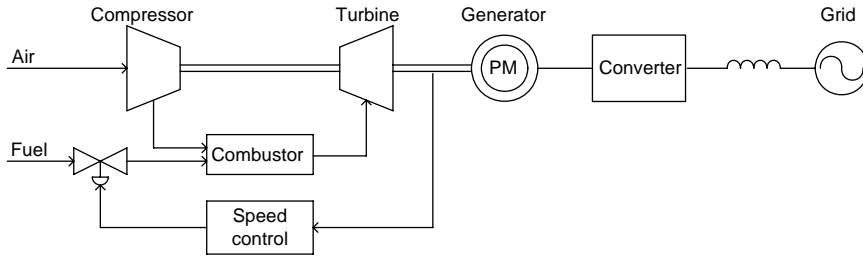
Fig. 2.4. Micro turbine system

2.3.3 Wind turbines

Wind turbines convert aerodynamic power into electrical energy. In a wind turbine two conversion processes take place. The first converts the aerodynamic power that is available in the wind into mechanical power. The next one converts the mechanical power into electrical power. Wind turbines can be either constant speed or variable speed. In this thesis only variable speed wind turbines will be considered.

Wind turbine basics - The mechanical power produced by a wind turbine is proportional to the cube of the wind speed. The rotational speed of the wind turbine for which maximum power is obtained is different for different wind speeds. Therefore variable speed operation is necessary to maximise the energy yield.

Variable speed turbines are connected to the grid via a PEC that decouples the rotational speed of the wind turbine from the grid frequency, enabling variable speed operation. Two basic concepts exist for variable speed turbines. The first concept has an electric generator with a converter connected between the stator windings and the grid, see Fig. 2.5a. The converter has to be designed for the rated power of the turbine. The generator is mostly a (permanent magnet) synchronous machine. Some types do not have a gearbox: the direct-drive concept. An alternative concept is a wind turbine with a doubly-fed induction generator (DFIG), which has a converter connected to the rotor windings of the wound-rotor induction machine, see Fig. 2.5b. This converter can be designed for a fraction (~ 30%) of the rated power.

Wind turbine control - Since electrical and mechanical dynamics in a wind turbine are of different time scales (i.e. the electrical dynamics are much faster than the mechanical dynamics), the whole system has two hierarchical control levels [Han 04]. The lower level controls the electrical generator (small time constants). It has the goal to control the active and reactive power of the wind turbine. The higher level controls the wind turbine (large time constants) and consists of the pitch and speed control.
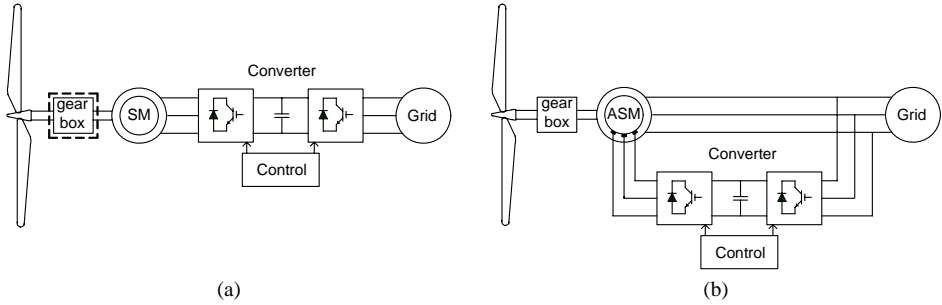
Fig. 2.5. Variable speed wind turbines: (a) with full-size converter; (b) with doubly-fed induction generator

The task of the speed controller is to maintain the optimal tip speed ratio λ over different wind speeds, by adapting the generator speed. The control is based on a pre-determined power-speed curve, as shown in

Fig. 2.6. Based on the measured rotational speed of the turbine, the optimal power and torque are determined. The error between the actual and the reference torque is sent to a PI controller. This gives a setpoint for the current controller of the turbine, which controls the torque to achieve the required speed.
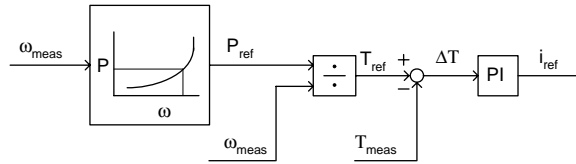
Fig. 2.6. Speed controller of variable speed wind turbine

Characteristics and interface –The output power of the wind turbine is not controllable. Due to the large inertia of the wind turbine blades, the output power of the turbine will vary slowly. In case of wind turbines with a full converter the response to grid events is mainly determined by the PEC. In case of a turbine with a DFIG the response is a mix of the induction machine response and the converter response.

2.4 Power Electronic Converters

Power electronic converters play an increasingly important role in modern electrical engineering. They are an essential part for the integration of DG units into the grid. The voltage generated by most DG units cannot be connected to the grid directly. The power electronic interfaces are necessary to match both the voltage level and frequency of the

DG unit and the grid [Bla 04]. This section first explains the basic operation principle of an IGBT-based voltage source converter (VSC), which is the PEC that is used by most DG units. Afterwards it discusses under which conditions the operation of another converter topology (a current source converter) is similar to that of a VSC.

2.4.1 Basic principle

In the early days of power electronics most systems were based on thyristor technology. The introduction of newer types of switches, such as IGBTs, largely increased the control possibilities and thus the number of applications for PECs. Thyristors only have turn-on capability. To turn them off, one has to wait until the next zero crossing of the current. This limits their application. IGBTs can be turned on and off at will and at much higher frequencies than a thyristor. In this way complete control over current and voltage can be obtained. Most modern converters that are used to connect DG units to the grid will be based on IGBT technology or similar technologies such as Mosfets.

As an example to explain the operation of PECs the single-phase half-bridge shown in Fig. 2.7 is considered. This one-leg converter is nowadays the basic block for other converters, such as single-phase full-bridge and three-phase full-bridge converters. The description is based on [Moh 95]. For ease of explanation it is assumed that the midpoint 'o' of the DC input voltage is available, although this is not always the case.
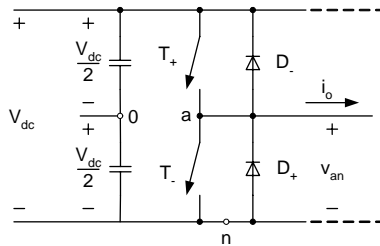
Fig. 2.7. Half-bridge converter

The converter switches T_+ and T_- are controlled by a Pulse Width Modulation (PWM) circuit. The objective of the modulation circuit is to have the inverter output sinusoidal with magnitude and frequency controllable. In order to produce a sinusoidal output waveform at a desired frequency, a sinusoidal control signal at the desired frequency is compared with a triangular waveform with amplitude v_{tri}, as shown by yhe signals in Fig. 2.8a. The frequency of the triangular waveform establishes the inverter switching frequency f_s. The reference signal v_{ref} is used to modulate the switch duty ratio and has a frequency f_1, which is the desired fundamental frequency of the inverter output voltage.

(a)

(b)
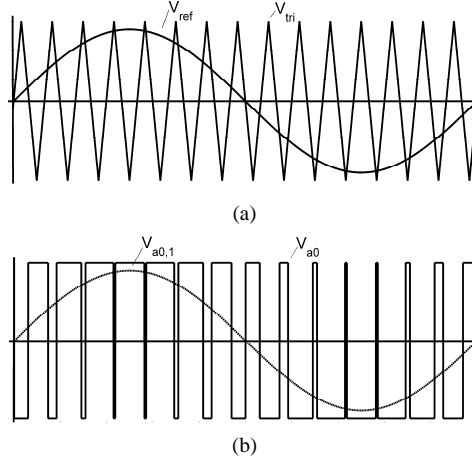
Fig. 2.8. Pulse Width Modulation signals; (a) comparison of V_{ref} and V_{tri}, (b) converter output voltage V_{a0} and its fundamental frequency component $V_{a0,1}$

The switches T_+ and T_- shown in Fig. 2.7 are controlled based on the comparison of v_{ref} and v_{tri}. When $v_{ref} > v_{tri}$ T_+ is turned on and $v_{a0} = $ ½V_{dc}. When $v_{ref} < v_{tri}$ T_- is turned on and $v_{a0} = $ -½V_{dc}. Since the two switches are never on or off simultaneously, the output voltage v_{a0} switches between ½V_{dc} and -½V_{dc}. The voltage v_{a0} and its fundamental frequency component are shown in Fig. 2.8b. It can be seen that the inverter output voltage is not a perfect sine wave and contains voltage components at harmonic frequencies of f_1. The harmonics appear at sidebands around the switching frequency and its multiples (see appendix F). A filter is generally connected between the inverter and the grid, to reduce the harmonics.

The amplitude of the fundamental frequency component is $\hat{v}_{a0,1} = m_a \cdot 1/2 V_d$ and can be controlled independently from the grid voltage, by controlling the amplitude modulation ratio m_a which is defined as $m_a = v_{con}/v_{tri}$.

For the simulations in this thesis mostly reduced models of PECs are used, in which the switching of the individual switches is not modelled. The switches are replaced by controlled voltage sources which are directly controlled by the reference waveforms. Generally, in the modulation circuit the reference waveforms are compared with the carrier waveform to control the semiconductor switches. Appendix F shows that in the lower frequency range, the frequency components in the reference waveform and the generated voltage waveform are equal, provided that the switching frequency is high enough. Therefore in the frequency range from zero up to half the switching frequency the reduced model can be used.

2.4.2 Control

Usually the VSC is connected to the grid through a filter. The filter forms a high impedance for the harmonic voltages that are present in v_{a0} and it enables current control. The filter can be implemented in different ways, but will always contain at least one inductor. The inverter bridge can then be considered as a controlled voltage source behind an inductor, as shown in Fig. 2.9, with the voltage v_{a0} a replica of v_{ref}. By changing v_{ref} it can control the current injected into the grid or absorbed from the grid. Most converters control the current in a feedback loop. For frequencies far enough below the bandwidth of the controller, the converter can then be considered as a controlled current source.
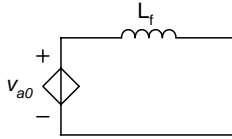
Fig. 2.9. Voltage source converter as controlled voltage source behind filter impedance

In the previous subsection the reference signal v_{ref} was assumed to be pure sinusoidal. This is not necessary true however. It is possible, for example, to introduce certain harmonic components in v_{ref}. These harmonics will also appear in v_{a0} then, if the switching frequency is high enough. In this way the converter can be used for harmonic compensation.

A schematic diagram of a current-controlled VSC is shown in Fig. 2.10. The inverter bridge with the power electronic switches is separated from the grid by a filter, which contains at least an inductor, but mostly also a capacitor. The current injected into the grid is controlled by the current controller. The reference value for the current controller is mostly obtained from a higher-level controller, which either controls the output power or the DC-link voltage. Besides this, the controller can perform other tasks, such as for example reactive power control and harmonic compensation.

2.4.3 Voltage and current source converters

The converter described in the previous subsections is a voltage source converter (VSC). This type of converter generates a voltage v that is a replica of v_{ref}. In open loop it behaves as a voltage source. Also a current source converter (CSC) can be used. These converters generate a current i, which is a replica of the reference current i_{ref}. In open loop they behave as a current source. By applying feedback control a VSC can be controlled as a current source and a CSC as a voltage source.

The operation and control of a CSC are dual to that of a VSC. The DC-link of the CSC behaves as a current source instead of voltage source and normally consists of an

inductance. The filter of a CSC contains at least a capacitor, which provides a small parallel impedance for the current harmonics in *i*.
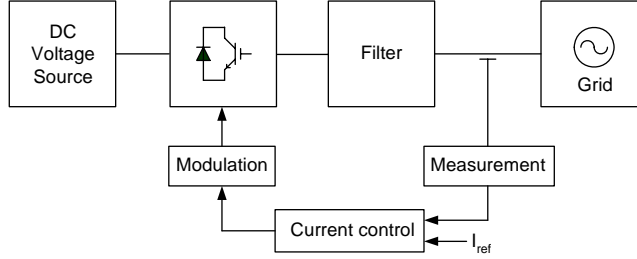
Fig. 2.10. Schematic diagram of current controlled voltage source inverter

The VSC is the preferred topology nowadays. This is because of switch technology, which favours switches with a reverse conduction diode and the cost, weight and size, which favour capacitors over inductors [Jóo 00]. In the thesis it is assumed that the DG units are connected to the grid with a VSC. The results are also valid for a CSC however. This subsection will show under which conditions the operation of a CSC can considered to be the same as that of a VSC.

When the filter consists of a capacitor and an inductor, the CSC can be controlled such that it behaves as a voltage source inverter. A schematic diagram of the CSC is shown in Fig. 2.11. A voltage control loop is implemented on the converter. It controls the voltage across the filter capacitance. When this voltage control loop is fast enough the converter can be considered as a controlled voltage source behind an inductance, as is shown in Fig. 2.9 for the VSC.
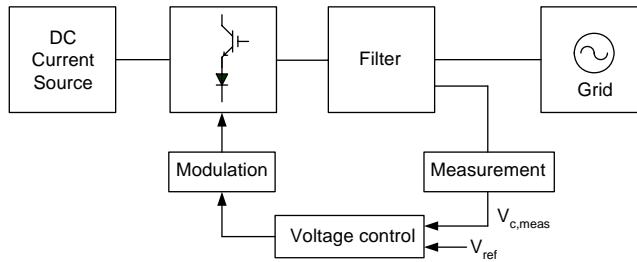
Fig. 2.11. Schematic diagram of voltage controlled current source converter

In a second control loop a current controller can be implemented that generates the input for the voltage control loop that controls the capacitor current. As long as the bandwidth of the voltage control loop is significantly larger than the bandwidth of the current control loop, the behaviour of the CSC is equal to that of the VSC.

2.5 Literature review

2.5.1 Introduction

This section discusses the most important literature on the introduction of DG in the power system, with emphasis on DG and power electronics. The last years showed a large increase in the literature on DG, but only some important publications that are related to the content of this thesis will be discussed. In this section a more general overview will be presented. Later, in each chapter, more specific literature related to the respective chapter will be discussed.

The paragraph consists of three subsections. In subsection 2.5.2 general publications on DG are discussed. Subsection 2.5.3 will discuss publications concerning grid support by DG units. Subsection 2.5.4 will discuss literature on 'microgrids'. The concept of 'microgrids' is introduced for island networks that are completely based on PECs.

2.5.2 Distributed Generation

This section gives a limited overview of the literature on DG. One of the first books on DG is [Jen 00]. It focuses mainly on the interaction between DG units and the grid and concludes that interconnection issues for a single generator are well understood but that the effect of many generators requires more research. A significant penetration of DG changes the nature of a distribution network but also affects the transmission network. At present most DG is considered as negative load over which the distribution utility has no control. This should change to achieve a more reliable system. Another book is [Bor 01] in which an extensive description is given of several DG unit types. With respect to the interconnection issues it is concluded that it is especially important to bring all concerned parties to a common understanding.

A large number of papers and reports on DG have been written. For this thesis only the publications that treat the electrical aspects of DG units and their interaction with the grid are important. An extensive overview is presented in [Don 02]. It investigates the interaction of DG with a typical urban network. Some of the most important conclusions are:

- The voltage rise caused by a single unit is a function of DG power and short circuit power of the grid at the point of connection.
- The short-circuit power in the grid rises because of the DG short-circuit current contribution. This can result in unacceptable short circuit levels in some cases and settings in distance relays, over-current relays, short-circuit current indicators, etc. may have to be changed.
- DG units with a PEC can have a positive impact on the voltage profile.

- Network reliability can be improved. DG will support the grid and may prevent blackouts in times of supply shortages.

Another discussion of the impact of DG on DN operation is given in [Ack 02]. The paper compares different DG technologies and investigates a number of operation issues such as the impact on losses, voltage, power quality, short-circuit power and reliability. It is concluded that the impact of DG on the operational aspects of the distribution network depends on the DG penetration level as well as on the DG technology. Critical issues, such as for example the impact of DG on the protection system, can be solved by using the right technology and detailed studies on beforehand.

In [Tra 03] the impact of DG on LV networks is investigated. It is concluded that the main constraints are related to the steady-state operation: the voltage profile and the currents in the branches. No significant fault current contribution of the DG units is expected, and therefore no major changes in the grid protection is required.

2.5.3 Grid support by DG units

This thesis investigates how DG unit converters can support the grid. This subsection summarises other publications that propose grid support by DG unit converters.

One of the first papers that discussed the issue appeared in 2000 [Jóo 00]. It proposed the provision of 'ancillary services' by the DG unit converters. Ancillary services are defined as services provided in addition to real power generation [Jóo 00]. They include, amongst others, reactive power control, provision of spinning reserve, frequency control, and power quality improvement. The paper proposes to configure the DG unit converters such that they can behave as a STATCOM, a Dynamic Voltage Restorer, and an Active Filter. The first two devices are mainly used for voltage control, while the third is used for harmonic compensation. The paper only presents some ideas. It does not go into detail on implementation and effectiveness.

Another concept is that of Flexible Distributed Generation, which is proposed in [Mar 02], [Mar 04]. It is similar to the concept of ancillary services and proposes the use of DG unit converters to mitigate unbalance, flicker and harmonics. The focus of the papers is on the use of fuzzy logic controllers and adaptive linear neuron structures for parameter tracking and estimation.

Using DG units for voltage control has been proposed in a number of other papers. In [Bar 02] it is concluded that the voltage control should be implemented as a droop controller. This enables operation without any communication. In [Mog 04] a voltage control algorithm is proposed that is based on active power curtailment and reactive power control. A control algorithm is proposed to switch between the two control modes. Voltage control in weak, rural lines is investigated in [Kas 05]. It is concluded that a significant distance should be maintained between DG units to avoid dynamic

interaction. Proper coordination between multiple DG units can be obtained by a proper definition of upper and lower thresholds and time delays with which the controllers start operating. In [Bol 05] analytical expressions are derived for the voltage along a line with uniformly distributed DG applying voltage control.

2.5.4 Microgrids

The concept of 'microgrids' has received considerable interest last years [Hat 06]. Microgrids are small low-voltage networks that can be connected to the main power network or can be operated autonomously. When they are not connected to the main power system they are operated in a similar way as the power system of physical islands. In essence a microgrid consists of a combination of generation sources, loads and energy storage, which are generally connected to the network with PECs. Microgrids have been studied in several research projects. A key issue is the control of the power flow and the network voltage by the PECs. Most controllers that have been proposed are based on droop lines [Aru 04], [Eng 05].

A key challenge for microgrids is to ensure stable operation during faults and various network disturbances. Transitions from a situation in which a microgrid is connected to the main network to a situation in which it is islanded are likely to cause large mismatches between generation and loads, posing a severe frequency and voltage control problem [Hat 06]. Several protection techniques and control strategies have been proposed to ensure a stable operation and to protect the generators [Kat 05], [Peç 05].

There are a number of important differences between the control applied in microgrids and the grid support by DG units considered in this thesis. The main difference is that the DG units in this thesis are assumed to be connected to a conventional power system. They only have to support the control that is performed by the conventional generators, tap changers and so on. They do not have to control the whole network. A main issue of this thesis is to investigate how large the support of the DG units can be. This question is generally not considered in the microgrid publications. Another difference is that most microgrids use some kind of a centralised controller to control the interaction between a microgrid and the main network, while the DG units in this thesis operate autonomously.

Chapter 3

Harmonic damping contribution of DG unit converters

3.1. Introduction

Power electronic converters (PECs) have an output filter to reduce the harmonic distortion and EMI. The connection of power electronic interfaced DG units to the distribution grid will result in an increase of the capacitance in the grid, as most output filters contain a capacitor. Manufacturers try to decrease filter inductors to make the inverter cost-effective. This requires an increase in capacitance to keep the cut-off frequency of the filter the same. The capacitance can resonate with the network reactance [Ens 04]. In conventional grids the total capacitance was low, and the resonance frequency was high. In most cases it was much higher than the dominant harmonics in the grid and thus the chance that these resonance circuits were excited was small. An increasing amount of capacitance results in a decreasing resonance frequency however. It may get values in a range that is more easily excited by harmonics.

To avoid resonances, oscillatory responses, and a high level of harmonic distortion, there should be enough damping in the grid. In passive grids the damping is obtained from the resistance of the loads and lines. The main goal of this chapter is to investigate how PECs (can) contribute to the damping. The output impedance of converters can be represented as a complex number. The real part of this frequency-dependent complex output impedance represents the resistance and thus the damping contribution of the converter. For some converter types it can have a negative value, meaning that harmonics and resonances are amplified instead of attenuated. In the ultimate case the negative damping can become larger than the positive damping in the network, which results in instability.

From constant power loads it is known that they can cause stability problems [Ema 04]. A short review of this instability will be given in section 3.2, as it lays down some basic principles that will be valuable in understanding this chapter. The need for damping is not limited to the quasi-stationary case however, it is important at all frequencies.

Therefore the analyses will be done in the frequency domain. As a first step, frequency domain models of PECs are obtained in section 3.3. Only a limited number of converter types can be discussed in this chapter. A more in debt investigation of the operation of PECs shows that they consist of a limited number of functional blocks. Most blocks can be characterised by their transfer function. It will become clear then, that there are only a few types of converter. In section 3.4 the transfer functions are used to determine the frequency-dependent output impedance of the most-used converter types and to see how these converters influence the damping in the grid. Section 3.5 proposes an active damping controller that can be implemented as an additional controller on DG unit converters. The section first describes the control and its implementation, followed by an investigation of possible limitations on the contribution. In section 3.6 the results of some case studies are presented to demonstrate the functionalities of the active damping controller. Only single-phase converters will be considered in this chapter.

3.2. Incremental impedance

Power electronic loads that are tightly regulated can sink a constant power from the grid. This implies that they have a negative incremental impedance characteristic, which can cause instability, as is known [Ema 04], [Mid 76], [Sud 00], [Wil 95]. As an introduction to this chapter this type of instability is shortly revised. Understanding the quasi-stationary case may be helpful in understanding the remaining part of the chapter which concerns the, more general, frequency-dependent case.

Consider a load (or source) as shown in Fig. 3.1a. It is assumed to work at power factor one. The incremental impedance is defined as the small-signal deviation of the voltage over that of the current:

$$R^{'} = \frac{\Delta v}{\Delta i} \tag{3.1}$$

Three types of devices are distinguished here: a resistive load (constant impedance load), a constant power load and a constant power source, as shown in Fig. 3.1b – d. Fig. 3.1c shows that a constant power load has negative incremental impedance. This may result in stability problems. The constant impedance load and the constant power load both have positive incremental impedance and no stability problems are expected.

Historically most loads in the electricity network are constant impedance loads, which means that their impedance is independent of the voltage. These loads have positive incremental impedance. PECs can be programmed as constant power loads in quasi-stationary situations, which implies negative incremental impedance.
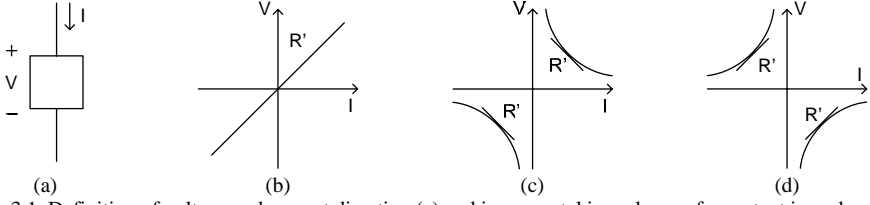
Fig. 3.1. Definition of voltage and current direction (a) and incremental impedance of: constant impedance load (b), constant power load (c), and constant power source (d)

The problems caused by constant power loads can be explained with the network model shown in Fig. 3.2. It shows a grid with a constant power load R_{CPL}' and a constant impedance load R_l. The grid is modelled by a voltage source V_g, a resistance R_g, an inductance L_g, and a capacitance C_g.
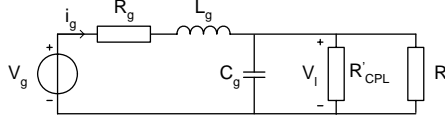
Fig. 3.2. Model of network with constant power load R_{CPL}' and constant impedance load R_l

As the constant power load is a nonlinear device, small-signal variations around an operation point have to be considered. The average power consumed by the load is:

$$P_{CPL} = V_{l,0}I_{l,0} \tag{3.2}$$

When a small-signal perturbation is applied to the voltage, the power becomes:

$$P_{CPL} = \left(V_{l,0} + \Delta V_l\right)\left(I_{l,0} + \Delta I_l\right) \tag{3.3}$$

By neglecting the second-order term it can be obtained that [Ema 04]:

$$\frac{\Delta V_l}{\Delta I_l} = -\frac{V_{l,0}}{I_{l,0}} = R_{CPL}^{'} \tag{3.4}$$

where $V_{l,0}$ and $I_{l,0}$ give the load voltage and current in the operation point. They are assumed to be in phase with each other, meaning that the load only draws active power from the grid. From (3.4) it can be noted that, with the sign convention of Fig. 3.1a, a small decrease in voltage results in a small increase in current. As a result of this increasing current the voltage drops further: an unstable situation. When the overall equivalent resistance of the grid becomes negative the system becomes unstable.

That constant power loads can cause stability problems is well-known. It is however less known that also power electronic sources can have negative incremental impedance. Most single-phase inverters need a sinusoidal reference waveform for their

current control. This waveform can be internally generated, but it is also possible to use a copy of the grid voltage. The converter current is then:

$$i(t) = -k \cdot v(t) \tag{3.5}$$

where the value for the constant k is determined by the average power that should be supplied to the grid. This constant is adapted relatively slow. The incremental impedance for this constant power source is thus:

$$R'_{CPS} = -\frac{1}{k} = -\frac{V_0}{I_0} \tag{3.6}$$

This type of converter also has a negative incremental impedance. It depends on the total resistance of the grid whether the network will become unstable.

3.3. Frequency domain analysis of power electronic converters

The goal of this chapter is to investigate whether PECs can contribute to the damping in the grid. As both the converter behaviour and the damping are frequency-dependent, frequency domain analyses will be done. This section describes how linear frequency domain models for the converters can be obtained by determining their transfer functions. The frequency-dependent converter output impedance can be obtained by determining the transfer function from the output current to the output voltage of the converter. Using transfer functions will make analysis easier. As will be shown in this section, it is possible to reduce a large number of converter types to a small number of transfer functions.

3.3.1 Converter description

PECs exist in a wide variety of topologies, with different components, and with all types of control. Only grid-connected voltage source converters will be investigated in this thesis as they are used by a large majority of the DG units. A general description of such a converter is given in section 2.4. The converter is assumed to be single-phase.

The converter generally has two control levels. The output impedance of the converter is mainly determined by the low-level current control, as its bandwidth is much higher than that of the high-level control. The phenomena considered in this chapter are normally at higher frequencies and therefore it will be enough to consider only the low-level current control.

Converters can be considered to be built up from a number of basic blocks. These blocks are shown in Fig. 3.3:

- The core of the converter is formed by the power electronic switches.
- The switches are connected to the grid through a filter, which consists of capacitor(s) and/or inductor(s) and/or resistor(s). It has the task to suppress the higher harmonics that are produced by the power electronic switches.
- The firing of the switches is controlled by the modulator, which transforms the signals from the controller, to the control signals for the semiconductor switches.
- In order to be able to operate, the converter requires knowledge about the actual current and voltage. So, measurements are necessary. Often only the RMS value is known. Therefore a sine-wave has to be created in some way.
- The sine wave reference can be generated internally and then synchronised with the grid or it can be a copy of the grid voltage.
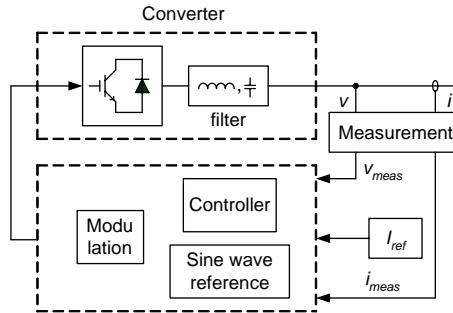
Fig. 3.3. Block diagram of voltage source converter with current controller

3.3.2 Basic building blocks

Fig. 3.3 shows the most important blocks that are needed in a converter. This subsection gives possible implementations of these blocks, together with their transfer functions.

Modulator – The modulator is a device that converts continuous signals to on/off signals for the switches. The first type that is often used derives its on/off signals from v_{ref}, for instance by comparison of a triangular carrier with v_{ref}. The second type derives its on/off signals from i_{ref}, for instance by hysteresis control. The block diagrams for these two modulation types are shown in Fig. 3.4a and b respectively. As long as the frequency of the input waveform is much smaller than the frequency of the modulator (and the switching frequency), the transfer of the modulator is approximately ideal. Phenomena with a frequency much higher than the modulating frequency are not transferred through the modulator. Frequencies between these two borders are transmitted partly. The approximate transfer functions of the modulators are shown in Fig. 3.4c and d respectively.

(a)

(b)

(c)

(d)
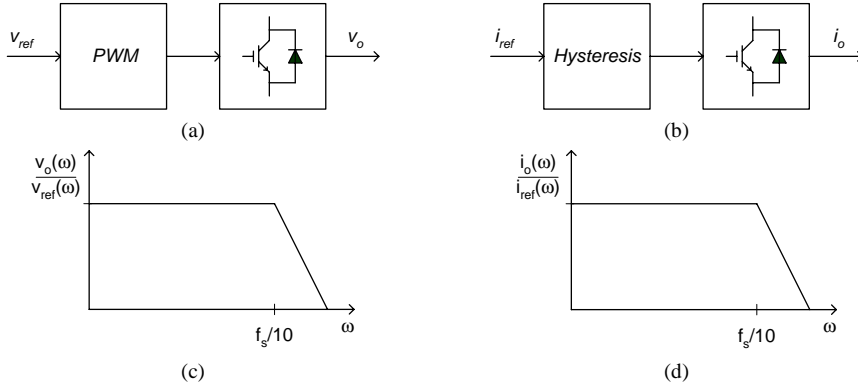
Fig. 3.4. Modulator block diagrams and transfer functions; (a) and (c): Pulse Width Modulation; (b) and (d) Hysteresis modulation

Controller - Two basic principles are used as controller in a single-phase converter, the Proportional-Integral (PI) controller and the Proportional-Resonant controller (PR). PI-controllers are the most classical controllers. When the reference signal is constant, zero steady-state error is achieved by the integral term of the controller. When the reference current is a sinusoidal signal however, straightforward use of the PI controller would lead to steady-state error due to the finite gain at the operating frequency. For these situations PR-controllers are proposed, which have infinite gain at a specified frequency. With this type of control it is possible to realise a zero steady-state error at the operating frequency (50Hz). The transfer function for a PI controller is:

$$G_{PI}(s) = \frac{sK_p + K_i}{s} \qquad (3.7)$$

whereas the transfer function for a PR controller is:

$$G_{PR}(s) = K_p + \frac{K_r s}{s^2 + \omega_0^2} \qquad (3.8)$$

Fig. 3.5 shows the transfer functions of the two controllers.

(a)

(b)
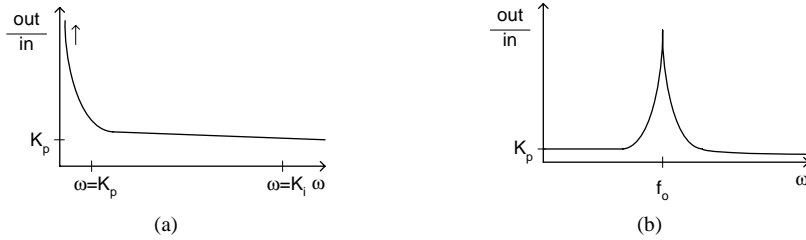
Fig. 3.5. Controller transfer functions; (a) Proportional-Integral (PI) controller; (b) Proportional-Resonant (PR) controller

Sine wave reference - Both for the modulation and the controller a reference sine wave can be needed. There are basically two categories of reference generators. The reference can be a copy of the grid voltage or the converter controller can have an internal, predefined sine wave that is synchronised to the grid with a phase-locked loop (PLL). Some inverters combine the reference source and the synchronisation with the grid voltage by using the waveform of the grid voltage as the basis for the reference waveform that is used by the modulator. The advantage of this technique is its simplicity. The disadvantage is that if the grid voltage is distorted, also the current is distorted. The schematic diagram of this type of sine reference is shown in Fig. 3.6a, and its transfer function in Fig. 3.6c. The schematic diagram for a sine wave reference based on a PLL is shown in Fig. 3.6b, whereas Fig. 3.6d shows its transfer function.
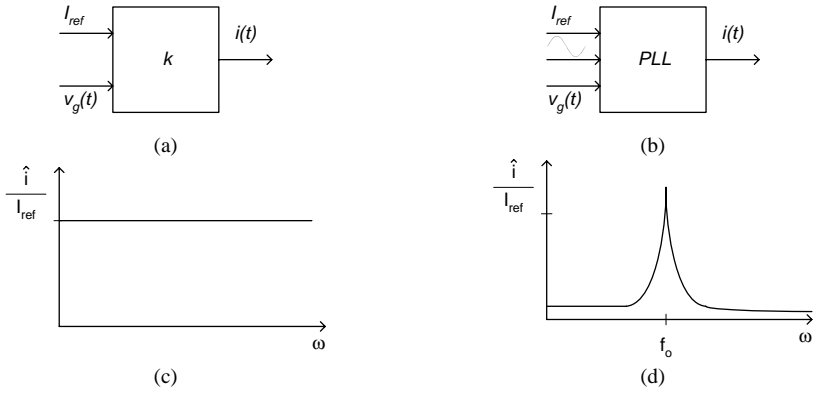
Fig. 3.6. Sine wave reference block diagrams and transfer functions; (a) and (c): reference based on grid voltage; (b) and (d) internally generated reference synchronised with PLL

Measurement - In order to enable feedback control, but also to obtain a reference for the sine wave, measurement of the grid voltage and grid current is necessary. In order to avoid high-frequency noise, the measured signals are filtered first. After this filtering the signal is sampled with a certain sampling rate. In general the bandwidth of the measurement system is determined by the bandwidth of its filter.

Converter and filter - The transfer function of the converter is mainly determined by its filter. This filter is designed to avoid that higher harmonics created by the power electronic switches are injected in the grid. Therefore the filter cut-off frequency has to be lower than the switching frequency of the converter and the cut-off frequency of the overall transfer is determined by the filter. The transfer function is similar to those given in Fig. 3.4, with a cut-off frequency determined by the filter.

3.3.3 Model comparison

In this chapter transfer functions in the Laplace domain are proposed as a method to investigate the behaviour of PECs. It should be investigated whether the models based on transfer functions correctly represent the behaviour of a real converter. Especially the fact that modulation and switching are neglected requires attention.

As a base case for comparison the single-phase full-bridge converter described in appendix B.1 is used. In this model the pulse-width modulation and the switching of the IGBTs is taken into account. The output conductance up to the 31st harmonic is determined for the full converter and for the converter model based on transfer functions. The fundamental grid voltage is perturbed with a small harmonic voltage with a fixed frequency and amplitude. The response of the output current of the converter model to this perturbing voltage is determined and from this the output conductance is determined. The results are shown in Fig. 3.7a.

For the full model the results are disturbed by the fact that the converter itself also produces harmonic currents, independent from the harmonic voltages with which it is perturbed. Subtracting these harmonics from the results of Fig. 3.7a gives Fig. 3.7b. The maximum deviation between the results of the full model and the transfer function model is less than 5%. This shows that the model based on transfer function gives a good representation of the full model.

(a) (b)
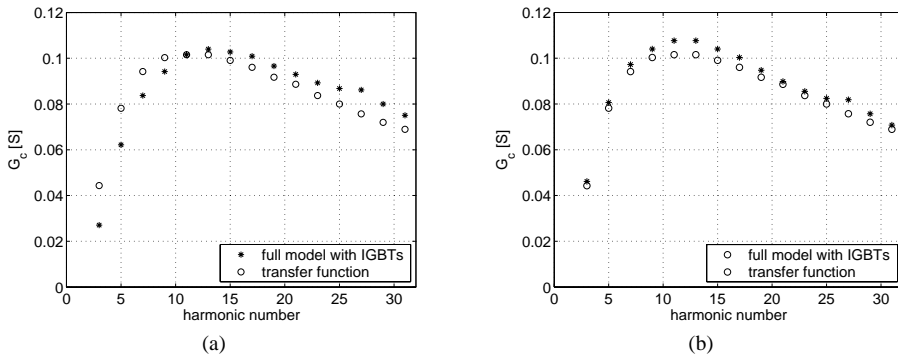
Fig. 3.7. Output conductance of full model (*) and model based on transfer functions (o); (a) uncompensated model; (b) model compensated for harmonic distortion of converter itself

3.4 Damping capability of converter

3.4.1 Converter output impedance

This subsection analyses the output impedance of PECs, to see the damping capability of the converter. The output admittance of a converter can be obtained by determining

the transfer function from grid voltage to converter output current. The real part of this frequency-dependent complex value gives the output conductance of the converter as a function of frequency. The value of the conductance determines the damping contribution of the converter and will plays a role in the damping of harmonics and resonances in the grid. For ease of explanation a converter operating at power factor one is analysed. The results are also valid for other power factors however.

By combining blocks from the groups defined in the previous section, basic converter models can be constructed. Two important converter models are considered. The first one, shown in Fig. 3.8a, uses PWM modulation and has a PR controller and a sine wave reference based on the grid voltage. The second one, shown in Fig. 3.8b, is the same except the sine wave reference, which is obtained from a PLL. Both converters have an LCL-filter. A description of the converter and its parameters are given in appendix B.1.
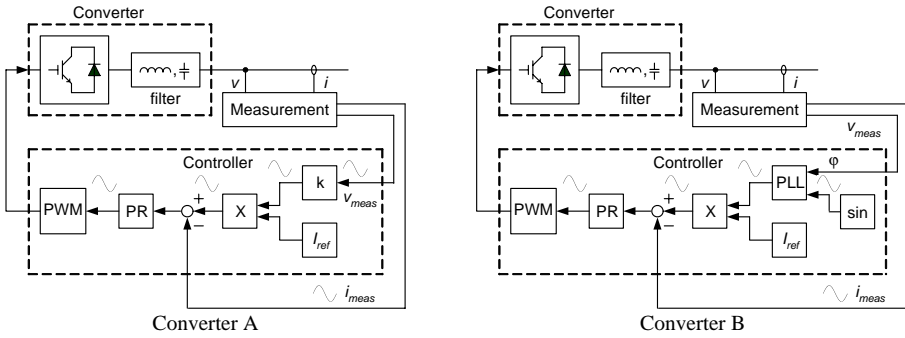
Fig. 3.8. Converter model with reference current as a function of the grid voltage (a) and with reference current based on PLL (b)

The bode diagrams for the transfer function from output voltage to output current, $i_o(s)/v_o(s)$, of both converters are determined for three different values of K_p (the proportional constant of the PR controller). This parameter showed to have the largest effect on the magnitude and angle of the output conductance. Fig. 3.9 shows the bode diagrams for the two converters. They give the frequency-dependent output conductance of the converter. For a phase value in the range -90º – 90º (± 360º) the incremental conductance has a negative value. Fig. 3.9a shows that the incremental output conductance of converter 'A' is thus negative for a large frequency range (approximately 5 – 400 Hz). For a large value of K_p it is even negative up to ~ 10 kHz. For converter type 'B' the phase angle is always outside the range -90º – 90º. So this converter will always have a positive influence on damping.
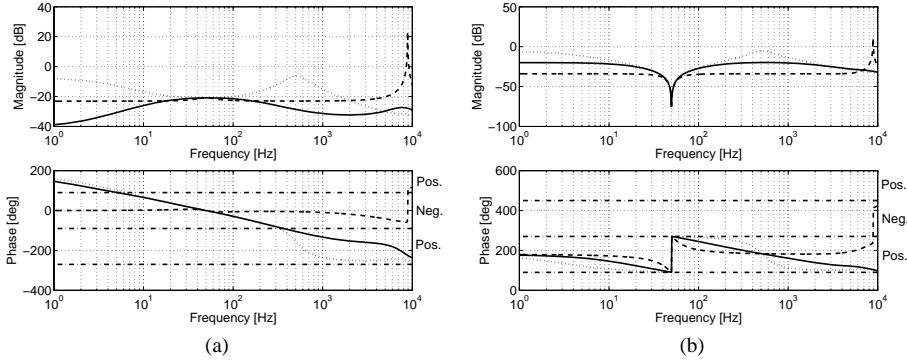
Fig. 3.9. Bode diagram for output conductance of converter A (a) and converter B (b) for $K_p = 2$ (dotted), $K_p = 10$ (solid) and $K_p = 50$ (dashed) ($K_r = 10000$, $L_{fc} = 0.2$ mH, $L_{fg} = 0.8$ mH, $C_f = 2$ μF)

3.4.2 Damping contribution in the grid

The real part of the frequency-dependent complex-valued output admittance of a converter can be considered as its conductance. The previous subsection investigated how the value of this conductance depends on the converter type and control. This section considers the contribution of the converter output conductance to the damping in the network.

The network of Fig. 3.10 is used for the analysis. It gives the lumped representation of a real existing 230 V network [Ens 02]. In this network problems were noticed with a high harmonic distortion, which could be explained from the negative incremental impedance of solar cell converters. The line impedance of the network is modelled by R_g and L_g. The resistance R_l represents the load and C_l consists of the capacitance of the load and other converters. The resonance frequency of the network is a function of L_g and C_l. It gives a complex-conjugate pole-pair in the real-imaginary plane. The influence of the converter on the relative damping of these poles will be investigated. The model of the network is described in appendix A.3 and the converter model in appendix B.1.
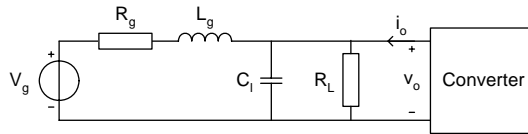
Fig. 3.10. Network model with converter

The influence of several converter (controller) parameters on the damping of the resonant poles was investigated. In each analysis the root-locus of the resonant poles was determined as a function of the parameter under investigation. Parameters that were varied are the control parameters K_p and K_r, the rated power of the converter and filter

parameters. As an example Fig. 3.11 shows the root-locus for varying K_p for both converters. This parameter showed to have the largest influence on the relative damping. Note that even for this parameter the influence is limited.

The only parameter with a larger influence on the location of the poles is the rated power of converter A. The system becomes even unstable for large values of the rated power. This is because the negative damping of the converter becomes larger than the positive damping in the grid. The network of appendix A.3 for example becomes unstable when a ~100 kW converter with negative incremental impedance is connected to it. The short-circuit power of the network is ~500 kW.

(a)   (b)
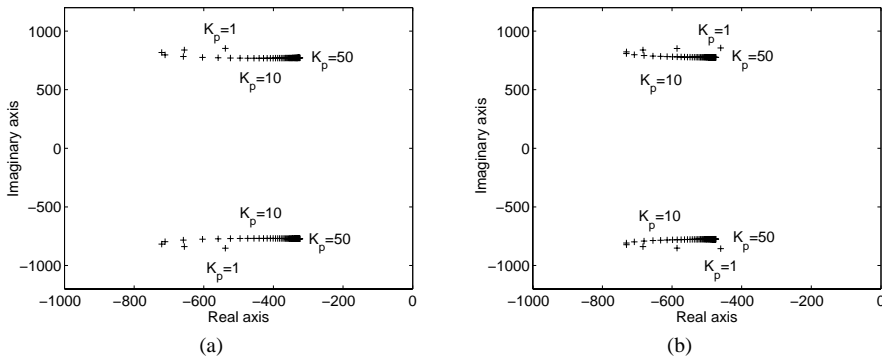
Fig. 3.11. Stability network with converter A (a) and converter B (b) for changing K_p

3.5 Active damping

3.5.1 Introduction

The previous sections showed that in the most favourable case PECs have a slightly positive influence on the damping in the grid. In order to have a robust grid which is not sensitive to disturbances, a much higher damping is required. This section proposes an additional control loop on PECs, which gives the output impedance of the converter a resistive behaviour. The 'emulated resistance' will increase the damping of the grid, making it less sensitive to harmonics and oscillations.

The type of control presented in this section is different from the active filters that have been investigated extensively. These active filters, which can be implemented as specific devices (for example [Aka 97]), or as a secondary function on power electronic generators or loads (for example [Mac 04]), are used to compensate for specific harmonics. The parameters of the power system and the sources of pollution are often unknown however and can be time-varying, making this type of control difficult. Contrary, the controller presented in this section presents a damping resistor for a large

harmonic spectrum and can be implemented easily. Complete compensation of harmonics will not be possible with the proposed controller, but generally this will not be needed.

The control strategy proposed in this chapter is comparable to those presented in [Tak 03], [Ryc 06a], and [Ryc 06b]. In [Tak 03] the control is implemented on a three-phase converter however. Their control is difficult to implement on single-phase converters, as it is based on the *dq*-transformation. The control strategy proposed in this chapter is more similar to the one in [Ryc 06a] and [Ryc 06b]. In these publications also a single-phase converter is considered. The publications present experimental verifications of the operation of the active damping controller. The mentioned publications focus mainly on the implementation however, while this section extensively investigates how large the contribution of the damping controller can be in a practical network.

3.5.2 Damping controller operation principles

This subsection gives a description of the controller that emulates a resistive output impedance for the converter. The controller is additional to the controllers that perform the primary task of the converter: transferring the DG unit power to the grid. The transfer of power is done at the fundamental frequency. The additional damping controller should thus not affect the fundamental frequency.

For the analysis a DG unit converter is assumed to be connected to the grid at a point of common coupling with voltage v_n, as shown in Fig. 3.12. The DG unit converter is represented as a voltage source, with voltage v_{dg}, behind the filter impedance. The voltage v_n is assumed to be distorted by harmonics. It can be split up in its fundamental frequency part $v_{n,f}$ and a part containing the other harmonics, $v_{n,h}(s)$:

$$v_n(s) = v_{n,f} + v_{n,h}(s) \tag{3.9}$$
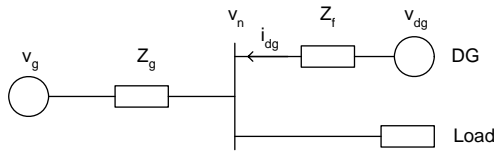
Fig. 3.12. DG unit converter connected to point of common coupling with voltage v_n

In order to obtain a resistive behaviour for the harmonic frequencies, the converter should inject a harmonic current into the grid which is 180° out of phase with the grid voltage. This gives for the total converter current:

$$i_{dg}(s) = i_{dg,f} + i_{dg,h}(s)$$
$$= G_f v_{n,f} - G_d v_{n,h}(s)$$

(3.10)

The variable G_f determines the active power that is supplied to the grid and G_d is the damping conductance for the non-fundamental components. It is assumed that the converter works at power factor one, but this is not necessary.

The active damping controller injects a harmonic current $i_{dg,h}(s)$ to obtain a conductance G_d at the converter terminal. It superimposes a harmonic voltage on the converter voltage v_{dg}, such that the required harmonic current is obtained. The current has to flow through the filter of the converter and depends on the voltage difference between the voltage created by the PEC $v_{dg,h}(s)$ and the node voltage $v_{n,h}(s)$:

$$i_{dg,h}(s) = \frac{v_{dg,h}(s) - v_{n,h}(s)}{Z_f(s)}$$

(3.11)

with $Z_f(s)$ the filter impedance. From this equation the voltage $v_{dg,h}(s)$ that is needed to obtain a certain output conductance can be determined:

$$v_{dg,h}(s) = (1 - G_d Z_f(s)) v_{n,h}(s)$$

(3.12)

Fig. 3.13 shows a schematic diagram of the complete converter control. The middle part shows the conventional current control which uses a PR controller. It controls the fundamental component of the voltage and current.
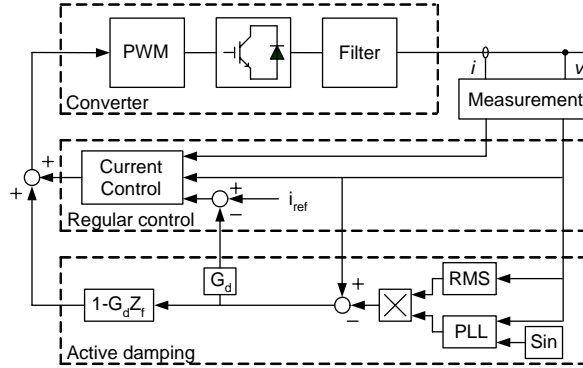
Fig. 3.13. Block diagram of converter, current control and active damping controller

The active damping controller is shown at the bottom. It consists of two loops. The first one, which is similar to the control presented in [Ryc 06], subtracts a term $G_d \cdot v_{n,h}$ from the reference current. This implies that in case of an ideal controller the output current is given by:

$$i_{dg}(s) = i_{ref} - G_d v_{n,h}(s) \tag{3.13}$$

i.e., a resistive behaviour for the non-fundamental components. The PR-controller that is used has infinite gain for 50Hz, but the gain drops quickly for higher frequencies. That implies that the controller is less effective for these frequencies. Therefore a second (feed-forward) control loop is implemented that also works for higher frequencies. As the damping controller should not influence the fundamental component of the converter current and voltage, this component is first subtracted from the measured voltage. The fundamental component is obtained from a predefined sine-wave which is synchronised with the grid via a PLL.

The poles that are related to the resonance circuit of L_g and C_l in the network of Fig. 3.10 are shown in Fig. 3.14 for different values of G_d. Fig. 3.14a shows the root-locus of the poles when the damping controller is implemented on a converter of type 'A' and Fig. 3.14b when it is implemented on converter of type 'B'. In both cases the damping constant has a significant influence on the location of the poles. For increasing value of G_d the poles move to the left, further from the imaginary axis and closer to the real axis, implying increasing relative damping.

(a) (b)
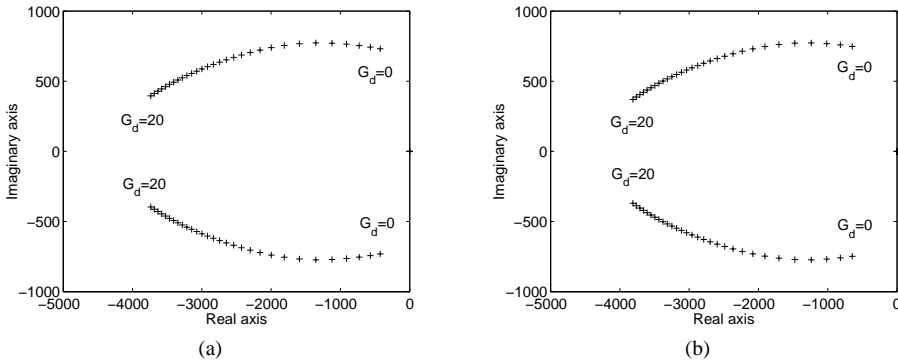
Fig. 3.14. Resonant poles in the grid for different values of damping conductance G_d: converter type 'A' (a) and converter type 'B' (b)

3.5.3 Influence of type and location of the harmonic source

From the point of view of a DG unit harmonics can have two different origins. In the first one, shown in Fig. 3.15a, the harmonic voltages are caused by closely located harmonic sources such as a load that draws harmonic current from the grid. In the second one, shown in Fig. 3.15b, the harmonic voltages are caused by background harmonic distortion, originating from remote harmonic source. They can be modelled as a harmonic voltage source in series with the substation voltage. The resonance circuit that is 'seen' by the harmonics is different for the two cases. The first case can be

modelled by a harmonic current source and a parallel resonance circuit formed by the capacitance C_l (formed by other loads and DG units) and the grid inductance L_g (formed by cable and transformer inductance). Fig. 3.16a shows the resonance circuit and the corresponding impedance (as a function of frequency). The circuit has a high impedance at its resonance frequency. Background harmonic distortion, the second case, can be modelled as a harmonic voltage source and a series resonant network formed by L_g and C_l, see Fig. 3.16b. In this case, the circuit has a low impedance at the resonance frequency.

The damping controller on the DG unit can also be considered as a (compensating) harmonic current source. For this case always the parallel resonance circuit of Fig. 3.16a is valid. This implies that the converter can compensate harmonics most easily when they are close to the resonance frequency.
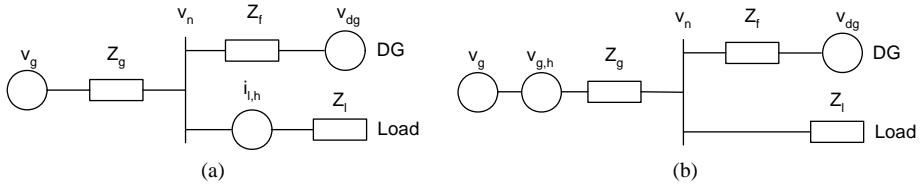
Fig. 3.15. Harmonic source locations
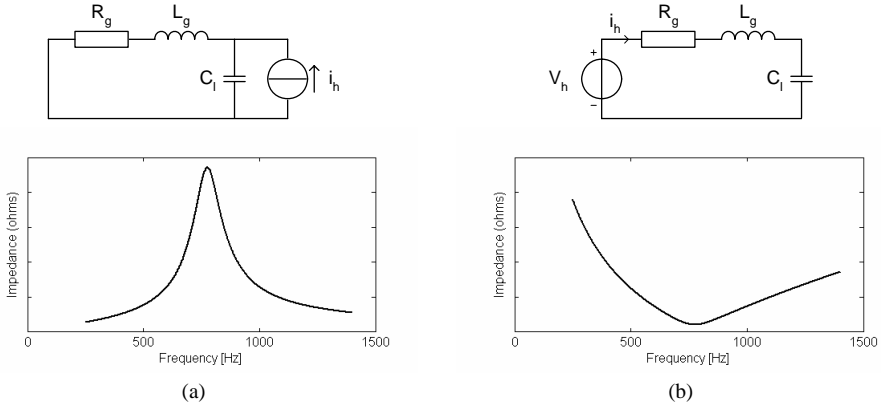
Fig. 3.16. Parallel (a) and series (b) resonance circuits and resonance impedances as a function of frequency

3.5.4 Value of emulated damping conductance
The emulated damping conductance of the converter will determine how large the damping of resonances and harmonics is. This subsection will lay down a relation between G_d and the damping that is obtained in a certain network.

The voltage v_n depends on the value of the damping conductance G_d. The ratio between the grid current in case of damping, $i_{g,d}$ and without damping, $i_{g,0}$ and between the voltage with damping, $v_{n,d}$ and without damping, $v_{n,0}$ is given by:

$$\frac{i_{g,d}(s)}{i_{g,0}(s)} = \frac{v_{n,d}(s)}{v_{n,0}(s)} = \frac{s^2 C_l L_g + s R_g C_l + 1}{s^2 C_l L_g + s\left(R_g C_l + G_d L_g\right) + 1 + G_d R_g} \tag{3.14}$$

At the resonance frequency f_r, the term $s^2 C_l L_g + 1$ is zero. The equation reduces then to:

$$\frac{i_{g,d}}{i_{g,0}} = \frac{v_{n,d}}{v_{n,0}} = \frac{1}{1 + G_d L_g / \left(R_g C_l\right)} \tag{3.15}$$

These equations indicate how large the value of G_d should be to obtain a certain reduction of harmonics in the grid voltage. Fig. 3.17 shows some relations for a typical example. For different frequencies it is shown how the harmonic currents (a) and voltages (b) can be attenuated as a function of the emulated damping conductance G_d. The figure shows that for harmonics at the resonance frequency of the grid a much smaller G_d is required to obtain a certain reduction. For harmonics below and above the resonance frequency a much larger value of G_d is required. For lower frequencies a slightly larger G_d is required than for higher frequencies. The parameters that have been used to obtain Fig. 3.17 are given in table 3.1 and appendix A.3

(a)   (b)
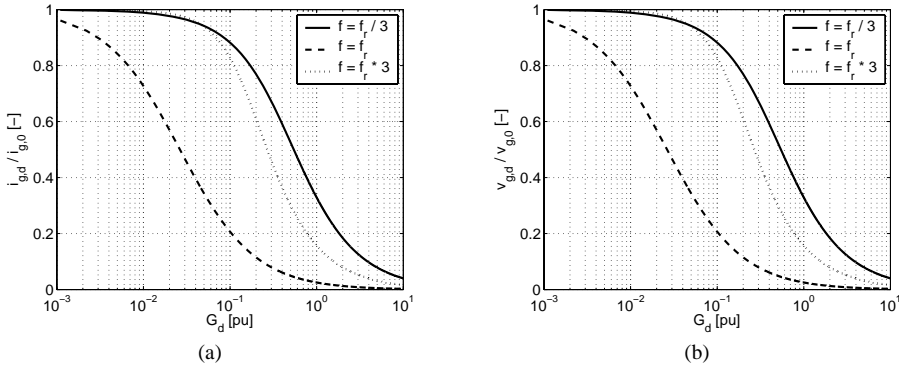
Fig. 3.17. Reduction in harmonic voltages as a function of emulated damping conductance G_d: damping of harmonic currents (a) and damping of harmonic voltages (b)

Table 3.1 Parameters of network and DG unit converter

Parameter	Value [p.u.]	Parameter	Value [p.u.]	Parameter	Value [p.u.]
L_g	0.44	f_r	777	$v_{g,h}$	0.07
R_g	0.91	L_f	2.9	$i_{l,h}$	0.008
C_l	105	$P_{dg,nom}$	0.01		
R_l	200	G_f	0.01		

3.5.5 Limitations and operation range

In order to determine the feasibility of the proposed solution it is important to determine the limiting factors. Possible limitations are:

- Converter current
- (dc-link) voltage of converter
- switching frequency of converter

Current - To compensate the harmonic voltages, the converter has to draw a certain harmonic current from the grid, which is given as:

$$i_{dg,h}(s) = -G_d v_{n,h}(s) \tag{3.16}$$

From this equation and (3.14) the current $i_{dg,h}$ can be calculated as a function of the attenuation of the voltage and current harmonics. The results are shown in Fig. 3.18. The nominal converter current is used as base value. The harmonic current has to be added to the fundamental frequency current. The graphs can be used in combination with the graphs of Fig. 3.17. Fig. 3.17 gives the reduction for a certain emulated damping conductance, while Fig. 3.18 gives $i_{dg,h}$ for this reduction. The figure shows that high currents may be required to obtain a significant damping.
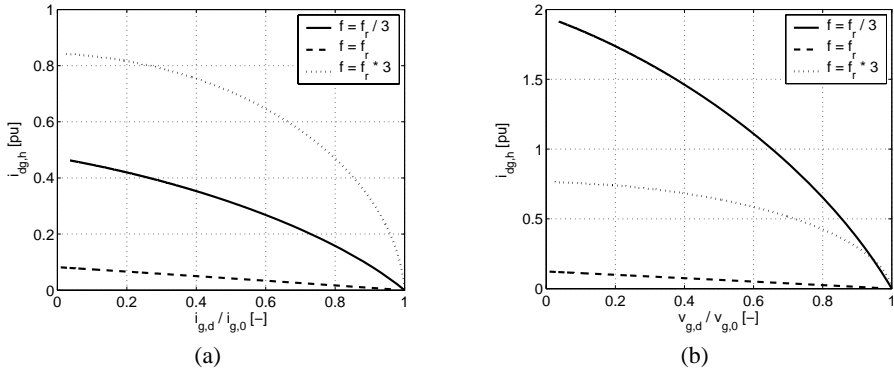
Fig. 3.18. Harmonic current that should be created by converter as function of reduction in harmonic current (a) and voltage (b) that should be achieved (in per unit with nominal converter current and voltage as base values)

Voltage - The damping controller superimposes a harmonic voltage on the voltage that has to be supplied by the converter. Equation (3.12) shows that the required harmonic voltage depends on the frequency. For frequencies far below the resonance frequency of the filter, the filter can be considered as the sum of its inductances. The filter impedance and thus the voltage drop across the filter increase linearly with the frequency. The voltage that can be supplied is limited by the dc-link voltage of the converter. This will

limit the maximum damping that can be achieved. The voltage $v_{dg,h}$ as a function of the attenuation of the voltage and current harmonics can be calculated by combining (3.12) and (3.14). The results are shown in Fig. 3.19.
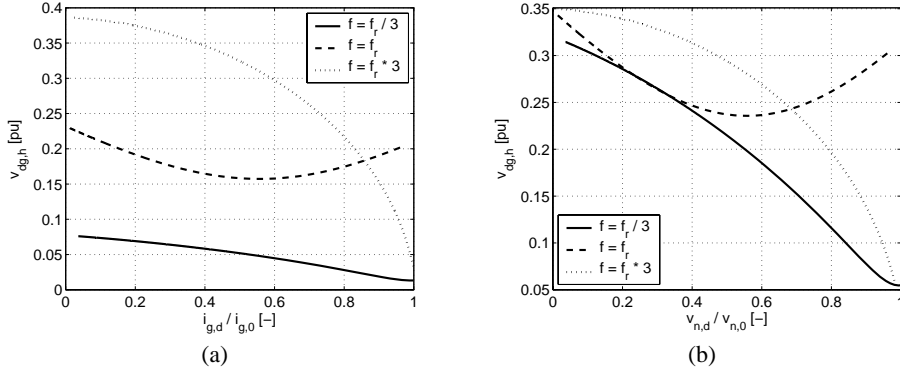
Fig. 3.19. Harmonic voltage that should be created by converter as function of reduction in harmonic current (a) and voltage (b) that should be achieved (in per unit with nominal converter current and voltage as base values)

The graphs can be used in combination with the graphs of Fig. 3.17. Those graphs give the reduction that can be obtained for a certain emulated damping conductance, while Fig. 3.19 gives $v_{dg,h}$ for this reduction. In case of distortion at the resonance frequency of the network, the voltage $v_{dg,h}$ has a minimum for a reduction of ~ 50%. For other frequencies the voltage increases for increasing reduction.

Frequency – The frequency range in which the damping control can operate is limited by the maximum switching frequency of the converter. The switching frequency should be at least twice as high as the harmonic component to be damped, to be able to modulate the required harmonic voltages. In case of low-power converters this will generally pose no problems as they have a high switching frequency.

3.6 Case studies

The damping controller proposed in the previous section reduces the harmonic distortion in the network. It does not only damp specific harmonics, such as active filters do, but it influences the whole harmonic spectrum of the network. This implies that it also reduces possible oscillations that can occur during transient phenomena such as voltage dips. This section presents the results of some case studies. They show the positive influence of converters with emulated damping resistance on the quality of the

grid voltage and current. The model of Fig. 3.20 is used for the case studies. It consists of a Thévenin equivalent of the network, a load that is modelled by a capacitor and a constant power source and a converter. For the converter the reduced model is used, which is described in appendix B. The parameters are given in table 3.1 and B.1. The constant power load consumes 8 kW. The emulated output conductance of the converter is 0.5 S.
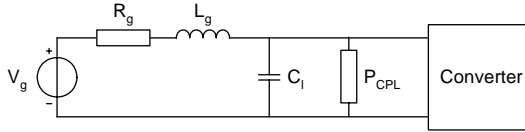
Fig. 3.20. Case study network with constant power load P_{CPL} and converter

The first case shows that the converter can damp harmonic voltages and currents in the grid. The voltage in case of background harmonic distortion in the network is shown in Fig. 3.21a. In first instance the damping controller does not work, but at time $t = 1$ s it is put into operation, resulting in a large reduction in harmonic distortion. In the second case the load draws harmonic current from the network. The voltage for this case is shown in Fig. 3.21b. Again a large reduction in harmonic distortion is obtained.

| (a) | (b) |
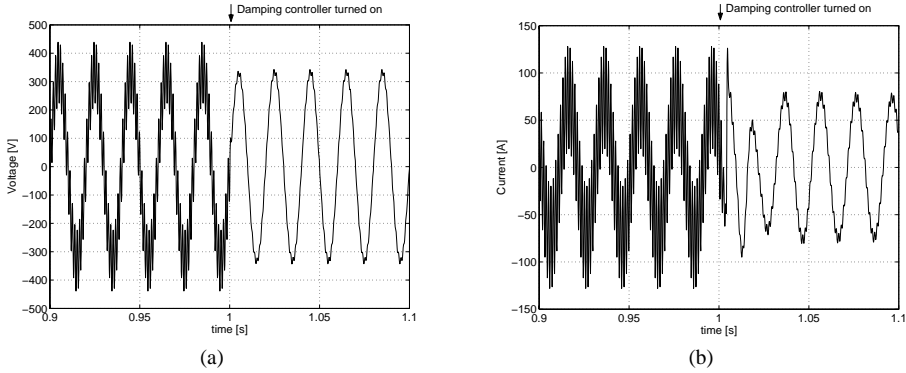
Fig. 3.21. Damping of harmonic voltage (a) and current (b) (at $t = 1$ s the active damping controller is activated)

The second case shows that the damping controller also can be used to avoid negative impedance instability. At time $t = 1$ s the power consumed by the constant power load increases to 24 kW. As a result the grid impedance plus the converter output impedance is smaller than the negative incremental impedance of the constant power load. This results in the oscillations in the converter terminal voltage shown in Fig. 3.22. At time $t = 1.05$ s the active damping controller is turned on and the system stabilises again.

44
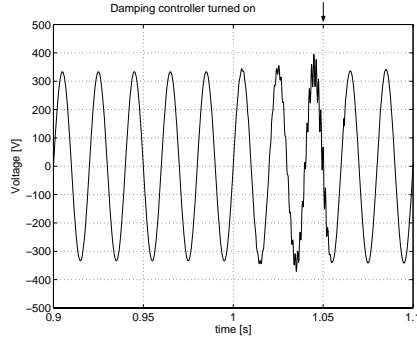
Fig. 3.22. Avoidance of instability: converter terminal voltage (at $t = 1$ s the load is reduced, resulting in a negative damping and oscillating voltage, at $t = 1.05$ s the active damping controller is activated)

The third case analyses the response to a voltage dip. The dip is modelled as a 50% drop in the voltage v_g that lasts from $t = 0.95$ s to $t = 1.05$ s. The resulting converter terminal voltage is shown in Fig. 3.23b. Due to the dip oscillations will occur in the resonance circuit formed by L_g and C_l. At the time that the voltage drops the damping controller is not inserted, and some oscillation in the voltage can be noted. During the dip, at time $t = 1$ s the controller is put into operation. As a result, there are no oscillations in the voltage at the moment that the dip is cleared.
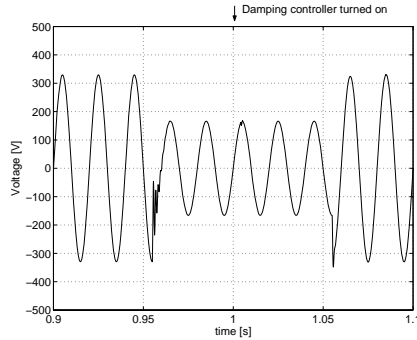
Fig. 3.23. Converter terminal voltage during voltage dip (A voltage dip occurs at $t = 0.95$ s, resulting in some oscillations in the voltage. The dip clears at $t = 1.05$ s without oscillations, as the damping controller is turned on at $t = 1$ s.)

3.7 Concluding remarks

The increasing number of DG units results in an increasing number of PECs in the grid. Due to the output capacitance of these and other converters there is a chance on the occurrence of harmonics, badly damped transients and oscillations. This chapter

investigated whether the DG unit converters can contribute to the damping in the grid. The contribution of converters with conventional control showed to be limited. Converters that use a sine wave reference that is a copy of the grid voltage can even have a negative influence.

An additional control loop can be implemented on the DG unit converter to give the output impedance of the converter a resistive behaviour for a large frequency range. In this way the damping in the network is increased. With this controller, harmonics can be mitigated, negative impedance instability can be avoided, and oscillatory responses due to for example voltage dips can be avoided. Due to the active damping controller the voltage and current of the converter will increase. This will limit the maximum damping contribution of the converter. Harmonics at the resonance frequency of the grid can be compensated easily. A 90% reduction requires only a ~10% increase in current and voltage (for a converter with a rated power of 1% of the short-circuit power of the grid). Harmonics at three times the resonance frequency require a ~80% increase in current and a ~180% increase in voltage however, to obtain a reduction of 90%.

Chapter 4

Voltage control contribution of DG units

4.1. Introduction

In conventional power systems the generators are generally connected to the high-voltage transmission network, whereas the loads are connected to the medium- and low-voltage distribution networks (DNs). This results in a power flow from a higher to a lower voltage level. Due to the line impedance the voltage decreases from the substation to the end of the feeder [Mas 02]. To compensate for this voltage drop, the voltage is stepped up at the HV/MV and MV/LV substation, as is shown in Fig. 4.1. The voltage in the DN can be controlled continuously by the automatic tap changers on the HV/MV distribution transformer, whereas the MV/LV transformers normally have manual off-load tap changers with a fixed value.
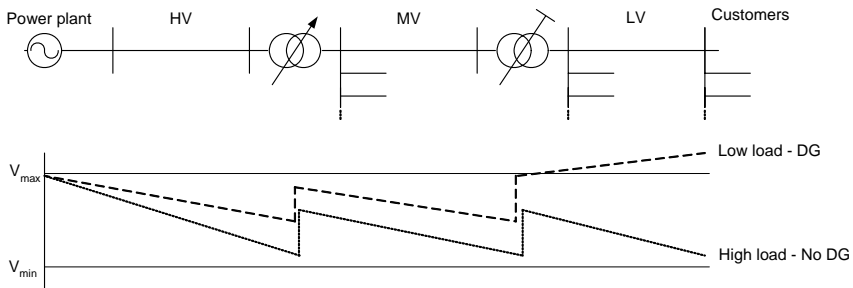
Fig. 4.1. Voltage profile from power plant to customer with all voltages expressed relative to their nominal value

When DG units are connected to the MV or LV network, the voltage profile in the line will change [Bon 01], [Con 01], [Dug 02], [Lie 02], [Mas 02], [Soe 05], [Vu 06]. The voltage might even increase in low load situations [Bon 01], as is shown by the dashed line in Fig. 4.1. In principle the automatic tap changer at the HV/MV transformer can lower the voltage. However, also feeders without DG can be connected to the same substation and

it may become difficult to keep the voltage in all feeders within the allowable range. In general, too large voltage fluctuations at the MV network make it difficult to keep the voltage in the LV network within specified limits [Pro 05], as the tap changers on the MV/LV transformer generally have fixed settings. Therefore, although the official voltage limits for a 10kV DN are mostly +/- 10%, in practice they are mostly more stringent. The total voltage fluctuation at the MV/LV transformer is usually required to be smaller than 5%. In several countries the maximal allowed voltage rise caused by a single DG unit is maximum 2% or 3% [Nav 05].

The impact of DG units on the voltage profile has widely been considered as a serious drawback and limitation for the maximum amount of DG that can be connected to the grid. In most publications on this topic it is concluded that above a certain DG penetration level the voltage changes become too large [Koj 02], [Dai 03], [Ing 03], [Bol 05], [Vu 05]. Several publications conclude that voltage control by reactive compensation is difficult, as the X/R ratio in DNs is low [Sco 02], [Str 02], [Pro 05].

Several solutions have been proposed to limit the voltage change caused by DG. Some of the solutions are based on coordinated control between the DG units and the tap changers and line drop compensators at the substation [Str 02], [Cal 05]. Other papers focus on the use of DG units for voltage control [Woy 03], [Sun 04b], [Tan 04]. These papers mainly concentrate on the implementation of appropriate controllers and the interaction and communication between several DG units that contribute to voltage control [Mar 04], [Mog 04]. Also power electronics based solutions such as a Distribution STATic COMpensator (D-STATCOM) or a Dynamic Voltage Restorer (DVR) have been proposed [Saa 98], [Gru 00], [Sun 04a].

Summarizing, most publications conclude that a problem can occur, they determine how large the voltage change will be and they propose solutions to limit the voltage change. It is not determined however, what the maximum allowable penetration level of DG units is, with respect to the voltage change they cause.

The goal of this chapter is to determine the maximum (with respect to the voltage change they cause) allowable penetration level of DG units, assuming that the DG units compensate (a part of) the voltage change they cause. Several techniques to increase the amount of reactive power that the DG unit can compensate are considered and it is investigated how they can be used to increase the maximum penetration level of DG.

The chapter starts in section 4.2 with discussing some basic theory and proposing several voltage control techniques. For each of the techniques it is investigated how effective it is in compensating the voltage deviations caused by the DG units, depending on the X/R ratio of the line impedance. Section 4.3 presents a device that can be used to increase the inductance of the grid. Section 4.4 presents a procedure to determine the

maximum penetration level of DG (with respect to the voltage change they cause). In this section the theory and techniques of section 4.2 are used. In section 4.5 the theory is applied to some practical cases.

4.2 Reactive power control

Power electronic converters can supply or absorb reactive power to control the grid voltage. In this section first the basic theory on reactive compensation is summarised, followed by an analysis of the effectiveness of reactive power for voltage control. Reactive power compensation will not always be enough to keep the voltage within the allowed borders. Solutions are proposed to improve the possibilities for voltage control.

4.2.1 Basic theory

This subsection investigates the influence of active and reactive power on the grid voltage. Fig. 4.2 shows a simplified network. The grid is modelled by a voltage source $\underline{V}_s$ and a short-circuit impedance $\underline{Z}_{sc}$. A constant current load and a DG unit are connected to the network. The voltage at their terminals is $\underline{V}_{dg}$. The voltage $\underline{V}_{dg}$ without DG unit connected is chosen as the reference voltage. All equations and results in this chapter are in per unit with the short-circuit power $S_{sc} = 100$ MVA and the supply voltage $V_s = 10$ kV as the base values (unless otherwise stated).
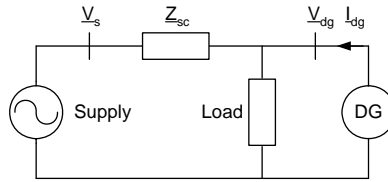
Fig. 4.2. Network diagram with Thévenin equivalent of grid, load, and DG unit

When the DG unit supplies current to the network the voltage $\underline{V}_{dg}$ will change to $\underline{V}_{dg,new}$. The difference between the two voltages is:

$$\Delta \underline{V}_{dg} = \underline{Z}_{sc} \underline{I}_{dg} \qquad (4.1)$$

This voltage change has a component $\Delta V_{dg,r}$ in phase with V_{dg} and a component $\Delta V_{dg,x}$ perpendicular to V_{dg}. According to [Mil 82], and neglecting the load, the two components can be approximated by:

$$\frac{\Delta V_{dg,r}}{V_{dg}} \approx \frac{1}{S_{sc}} \left[P_{dg} \cos \varphi_{sc} + Q_{dg} \sin \varphi_{sc} \right] \qquad (4.2)$$

$$\frac{\Delta V_{dg,x}}{V_{dg}} \approx \frac{1}{S_{sc}} \left[P_{dg} \sin \varphi_{sc} - Q_{dg} \cos \varphi_{sc} \right] \tag{4.3}$$

with P_{dg} and Q_{dg} the active and reactive power supplied by the DG unit, and with:

$$\tan \varphi_{sc} = \frac{X_{sc}}{R_{sc}} \tag{4.4}$$

The voltage $\underline{V}_{dg,new}$ is obtained by adding (4.2) and (4.3) to V_{dg}:

$$\underline{V}_{dg,new} = \left(V_{dg} + \Delta V_{dg,r} \right) + j \cdot \Delta V_{dg,x} \tag{4.5}$$

The phasor diagram is shown in Fig. 4.3, for a specific situation in which the voltage without DG unit is below the lower voltage limit. When the DG unit is connected the voltage increases to a value between the two limits.
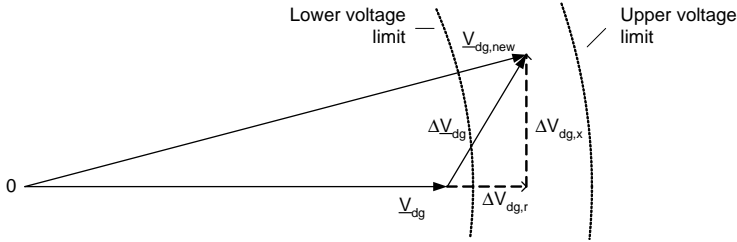
Fig. 4.3. Phasor diagram of voltage change due to DG unit power

Under the assumption that $V_{dg} \cong \underline{V}_s$, the following approximation holds [Mil 82]:

$$\frac{\Delta V_{dg}}{V_{dg}} \cong \frac{S_{dg}}{S_{sc}} \tag{4.6}$$

The equations (4.2) - (4.6) are very useful, as they are expressed in terms of quantities that describe the characteristics of the network; short-circuit power S_{sc} and X/R ratio (i.e. $\tan \varphi_{sc}$) of the network, and the active and reactive power P_{dg} and Q_{dg} of the DG unit.

4.2.2 Effect of X/R ratio on voltage deviation and voltage control possibilities

The equations in the previous subsection show that the voltage change due to the active and reactive power of the DG unit depends on:

- the X/R ratio of the short-circuit impedance (given by $\tan \varphi_{sc} = X_{sc}/R_{sc}$)
- the ratio between the rated DG unit power S_{dg} and the short-circuit power at the point of connection S_{sc},

Voltage control with reactive power is traditionally applied in the high-voltage transmission grid. The impedance is dominated by the reactance of the overhead lines

and the transformers, offering good possibilities for reactive compensation. At lower voltage levels voltage control with reactive power is more difficult because the line impedance is mainly resistive. In addition the voltage increase due to the active power of a DG unit is relatively large because of the relatively high resistance. Fig. 4.4a shows the voltage change due to the DG unit in the network of Fig. 4.2 for 3 different X/R ratios. The impedance is 1 p.u. in all three cases. The DG unit has a rated power of 0.2 p.u. and operates at 90%. The margin in power (and current) is used to consume reactive power to reduce the voltage. The figure shows that for X/R = 1/3 and 1 the voltage is higher than the upper voltage limit. Only for X/R = 3 the voltage stays below the limit. The whole range of voltages that can be achieved is shown by the circle and ellipses in Fig. 4.4b. The figure shows that in case of a large X/R ratio the voltage never exceeds the voltage limits, whereas for a low X/R ratio the voltage is too large in most cases.
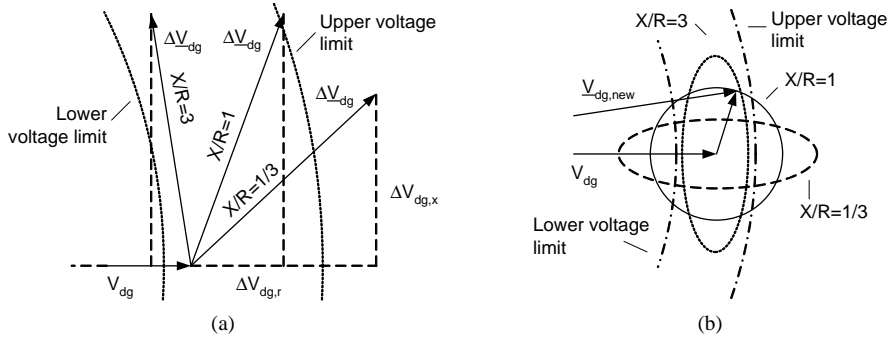
Fig. 4.4. Phasor diagrams: (a) Voltage change caused by DG unit for different X/R ratios (V_{dg} = 1 p.u., Z_{sc} = 1 p.u., S_{dg} = 0.2 p.u., P_{dg} = 0.18 p.u., Q_{dg} = 0.087 p.u.); (b) Range of $\Delta\underline{V}_{dg}$ for different X/R ratios (V_{dg} = 1 p.u., Z_{sc} = 1 p.u., S_{dg} = 0.2 p.u.)

Especially cable networks have a low X/R ratio. The voltage range that can be realised has been analysed for two distribution cable networks in the Netherlands: one rural network and one urban network. The parameter values are summarized in table 4.1. More information on the networks can be found in Appendix A. For three different nodes in the network the short-circuit power, the X/R ratio and the distance between the node and the substation are given. Node 1 is at the substation, node 3 is at the end of a feeder, and node 2 halfway the feeder. Both the short-circuit power and the X/R ratio of the grid decrease for increasing distance to the substation.

When a DG unit is connected to node 1, its active power causes only a small voltage increase, because of the high short-circuit power and the high X/R ratio, which are mainly determined by the transformer impedance. Due to the high X/R ratio the DG unit can easily control the voltage by absorbing a small amount of reactive power, as is

shown by the solid line in Fig. 4.5a and b for the urban and the rural DN respectively. Node 2 is located further from the substation. Due to the cable between node and substation both the short-circuit power and the X/R ratio are lower. The reactive power required for compensation (dashed line) is approximately equal to the active power. For node 3, which has a low short-circuit power and a low X/R ratio the required reactive power is larger than the active power (dotted line).

Table 4.1. Parameters of a two typical Dutch cable networks

Urban network				Rural network			
Node	S_{sc} [MVA]	X_{sc}/R_{sc}	Distance [km]	Node	S_{sc} [MVA]	X_{sc}/R_{sc}	Distance [km]
1	233	16	0	1	153	41	0
2	105	1.25	5	2	103	2.2	7
3	60	0.75	10	3	21	0.35	14
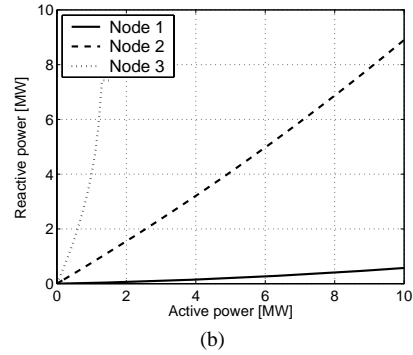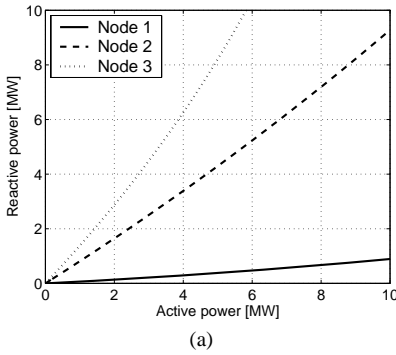
Fig. 4.5. Reactive power that is required to compensate the voltage change that is caused by active power at a certain node: (a) urban network; (b) rural network

From the analysis, which is representative for most cable DNs, some conclusions can be drawn: DG unit connected at locations close to the substation (node 1) can easily perform voltage control (high X/R ratio) but it is hardly necessary as the voltage deviations are small due to the high short-circuit power. Further from the substation the short-circuit power is lower and voltage control may be necessary, but is more difficult because of the low X/R ratio. The larger the distance from the substation, the more voltage control is needed and the more difficult it is, because of the low X/R ratio.

4.2.3 Overrating and generation curtailment

The DG unit will not always be able to supply the reactive power that is necessary for compensation, because its converter current is limited. Problems are most likely to

occur in low-load / high-generation situations. When the DG unit supplies a large power, there is a chance that the upper voltage limit is exceeded. As the DG unit supplies a large active power, the margin for reactive power consumption is limited or even zero. The maximum amount of reactive power that can be consumed is:

$$Q_{dg,\max} = \sqrt{\left(V_{dg}\, I_{dg,\max}\right)^2 - P_{dg}^2} \qquad (4.7)$$

with the maximal converter current defined as:

$$I_{dg,\max} = \frac{S_{dg,nom}}{V_{dg,nom}} \qquad (4.8)$$

A possibility to improve the voltage control capability is to increase the maximum current ($I_{dg,max}$) that is allowed for the DG unit converter. The basic principle is shown in Fig. 4.6a. The phasor diagram shows a voltage increase V_p due to the active power and a compensating voltage V_Q (solid line) due to the reactive power. The compensating term is limited to the maximum current times the grid impedance (represented by the circle) and therefore it can not bring the voltage below the upper limit of $\underline{V}_{dg}$. When the maximum current is increased also V_Q (dotted line) can be increased, such that $\underline{V}_{dg,new}$ is below the limit. Fig. 4.7a shows for three ratios of X/R how large the overrating of the converter should be to obtain a certain voltage compensation. Fig. 4.7c shows the overrating for a converter with higher rated power.
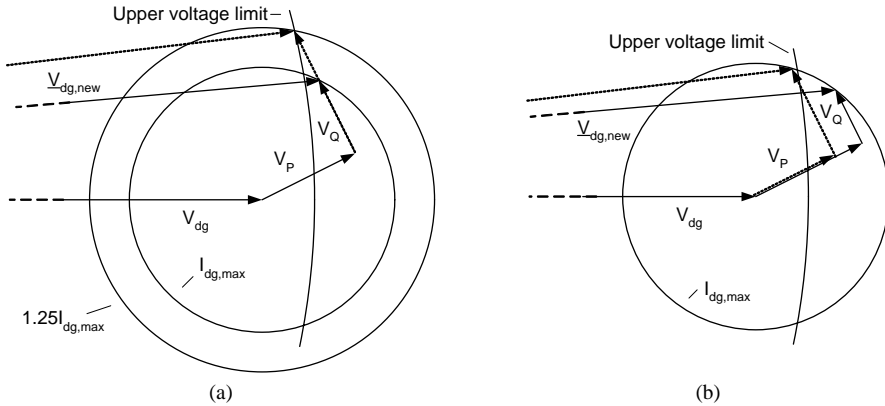
Fig. 4.6. Phasor diagrams showing strategies to improve the voltage control capabilities of converters; (a) converter overrating; (b) active power reduction

Another possibility is to lower the amount of active power that is supplied by the DG unit when the upper voltage limit is exceeded (generation curtailment). As the active current decreases the reactive power that can be consumed increases, as can be

seen from (4.7). The phasor diagram in Fig. 4.6b shows the principle of generation curtailment. Due to the reduction in active power V_P will decrease and the margin for reactive power will be larger, resulting in a larger V_Q. Fig. 4.7b and d show how far the active power should be reduced to obtain a certain reduction in voltage (due to decrease of V_P and the increase of V_Q). The likelihood of the coincidence of low load and high generation determines the total energy that is lost when curtailment is applied. As the price of electricity is primarily driven by load demand, and curtailment occurs typically during periods of low load, the value of the curtailed energy is likely to be low [Str 02].
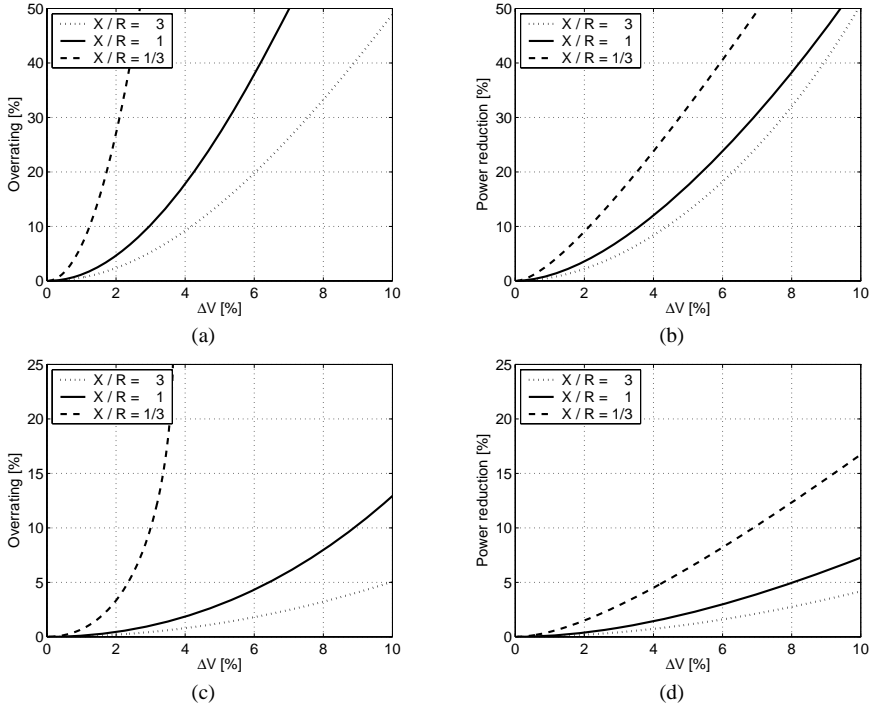
Fig. 4.7. Measures to improve the voltage control capabilities of converters as a function of the required voltage change: (a) converter overrating ($S_{dg,nom} = 0.1$ p.u.); (b) active power reduction ($S_{dg,nom} = 0.1$ p.u.); (c) converter overrating ($S_{dg,nom} = 0.4$ p.u.); (d) active power reduction ($S_{dg,nom} = 0.4$ p.u.);

The graphs in Fig. 4.7 show that the overrating that is needed to obtain a certain voltage change strongly depends on the X/R ratio and the rated power of the converter. The required curtailment is less dependent on the X/R ratio, but it depends strongly on the rated power of the converter. The figure shows further that, especially for converters with a high rated power, only a small percentage of overrating or curtailment is needed to achieve a significant voltage change.

4.3 Variable inductance

The limited effect of reactive power compensation in cable networks is mainly due to the low inductance of the cables. Increasing the inductance will increase the effectiveness of reactive compensation. A higher inductance can be undesirable in normal situations however, because of the large voltage drop across it. A solution can be to use a variable inductance. This subsection investigates the usefulness of such a device and presents a possible implementation.

4.3.1 Variable inductance value

A typical example of a network in which a variable inductance can be useful is shown in Fig. 4.8. The loads and DG units are aggregated and connected to the end of the line. Branch A has both a load and a DG connected whereas branch B only has a load. Due to the DG the voltage in branch A can become too high in cases of high generation and low load. The tap-changer at the distribution transformer can decrease the voltage at the substation, but this can result in a too low voltage at the end of feeder B. A variable inductance, in combination with reactive power control by the DG unit, can avoid violation of the voltage limits [Ton 05].
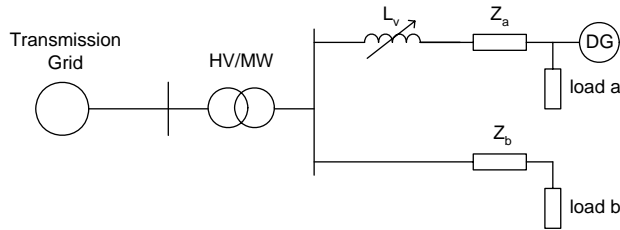
Fig. 4.8. Model of network with variable inductance, DG unit and loads

The inductance value that is needed to obtain a certain voltage change depends on the line impedance, the load and the active and reactive power supplied or consumed by the DG unit converter. The voltage drop across the inductance depends on the active and reactive power of DG unit and load. The active power supplied by the DG unit will result in a voltage increase, whereas the reactive power that is consumed results in a voltage drop. The voltage drop that can be achieved as a function of the value of the variable inductance is shown in Fig. 4.9. A variable inductance of 10mH equals ~3 p.u.. The curves are shown for 4 values of the difference between the reactive power of the DG unit and the load. The results of Fig. 4.9a have been obtained for $P_{dg} - P_l = 0.025$ p.u. and the results of Fig. 4.9b for $P_{dg} - P_l = 0.05$ p.u..
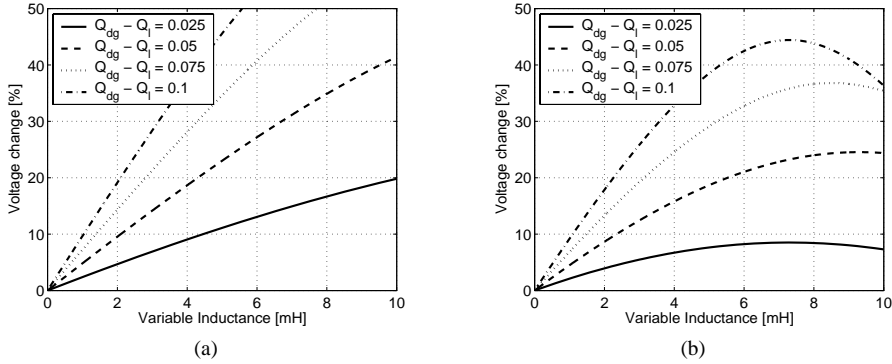
Fig. 4.9. Voltage drop that can be achieved with reactive power as a function of a variable inductance for different values of the reactive power; (a) $P_{dg} - P_l = 0.025$ p.u.; (b) $P_{dg} - P_l = 0.05$ p.u.

The voltage change that is achieved increases with increasing inductance. Above a certain inductance it decreases again however. At that point the voltage change due to the active power starts dominating the voltage change due to the reactive power. This implies that there is a maximum in the voltage change that can be achieved with a variable inductance. For a larger value of $P_{dg} - P_l$ the maximum is reached at a lower inductance and a lower voltage change. The figure shows further that with a small inductance already a high voltage change can be achieved. It is assumed that the DG unit has the capability to consume enough reactive power. In reality measures like overrating or generation curtailment might be necessary to achieve the required amount of reactive power.

4.3.2 Implementation

A device with a variable inductance can be implemented in different ways. In this section an implementation is used that is similar to the thyristor controlled reactor circuit [Boh 89] and the advanced series compensation concept proposed by [Par 97]. The device will be called a 'Variable Inductor' ('VI'). It consists of an inductor in parallel with two anti-parallel thyristors, as shown in Fig. 4.10a. The current through and the voltage across the inductor are shown in Fig. 4.10b. The thyristors are fired with phase shift α, with respect to the zero crossing of the current. When thyristor 'T1' is fired (with angle α) the current through the inductance remains constant. The turn-on of 'T1' shunts L_v, effectively removing it from the circuit. This condition lasts until the thyristor current becomes zero. Then 'T1' turns off and the current through L_v starts decreasing. The process is repeated in the negative half cycle using 'T2'. By changing the firing angle of the thyristors the time can be determined that the inductor will be inserted during each period. This results in an average (equivalent) inductance. Snubber

components are necessary to avoid over-voltages by switching transients. During normal operation the device can be by-passed.

(a)   (b)
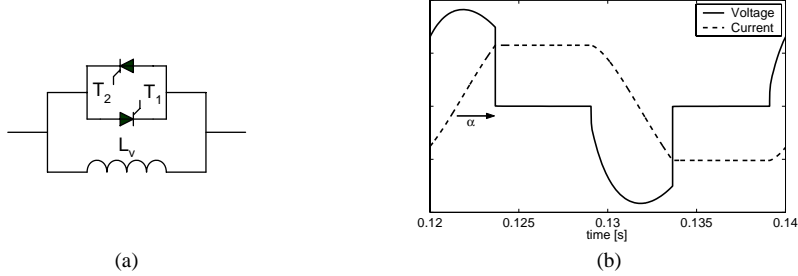
Fig. 4.10. Variable Inductor: (a) circuit; (b), thyristor voltage and current for 45 degrees firing angle

Introducing the VI in the line will increase the voltage control capabilities of the DG unit converter. Fig. 4.11a shows the voltage at the DG unit terminal of Fig. 4.8, for a sequence of conditions. At $t = 0.4$ s reactive power control is applied (without VI). This has a limited effect because of the small network inductance. When the VI is inserted ($t = 0.7$ s), a significant reduction in voltage can be obtained. In both last cases the DG unit is absorbing maximum reactive power ($I_{dg,max} = 165$ A). The inductance L_v has a value of 20 mH (~6 p.u.), $Z_a = 4.5$ p.u. with an X/R ratio of 1/3, and the load consumes no power. The voltage across and the current through the VI are shown in Fig. 4.11b. The figure shows the period in which the VI is turned on. The firing angle is ~45° (this means an effective inductance of 10 mH). Oscillations occur in the voltage across the VI. This is caused by resonance between the VI and the cable capacitance. It results in a THD of about 4%.

(a)   (b)
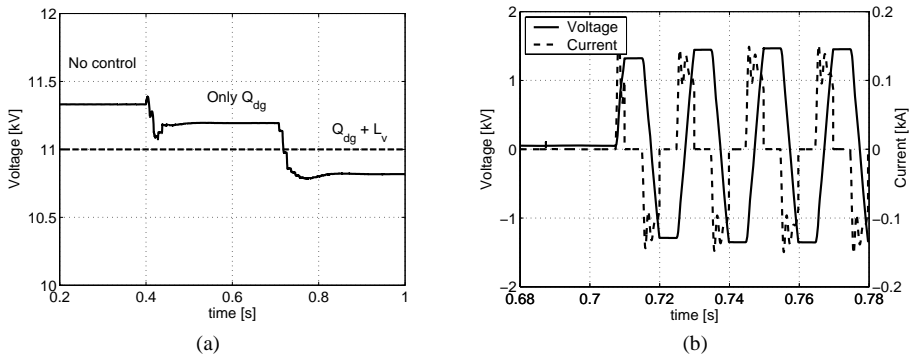
Fig. 4.11. Effect of Variable Inductor (VI): (a) voltage at the DG unit terminal; (b) voltage over and current through VI; (0 - 0.4 s: no control and no VI; 0.4 - 0.7 s: control only with DG unit, without VI; 0.7 - 1 s: control with both VI and DG unit

4.4 Maximum DG penetration

4.4.1 Introduction

This section will determine how many DG units can be connected to a network when the voltage change caused by the DG units should stay below a certain limit. The DG units are assumed to absorb as much reactive power as possible to limit the voltage increase they cause. The strategies and devices proposed in the previous sections are used to achieve a further increase in maximum allowable DG unit penetration. The maximum penetration level will be determined in three steps:

- Firstly the penetration level is determined when the DG units use the maximum possible reactive power to compensate the voltage change they cause.
- Secondly it is investigated how (much) the penetration level can be increased by using overrating and generation curtailment.
- The third step investigates how the VI can be used to achieve a further increase in the penetration level.

In section 4.5 the results of this section are applied to two practical cases.

4.4.2 DG only

Violation of the voltage limit is most likely to occur in high-generation situations. In that case the DG unit operates at, or close to, its nominal power and the reactive power capability is limited. The active power that is supplied to the grid will result in an increase of V_{dg} due to the voltage drop across the line impedance. As P_{dg} is independent of V_{dg} this results in a decrease of the active current ($P_{dg}=V_{dg}I_{dg}\cos\varphi$) and thus in an increase of the reactive power margin. In this way the converter can undo a part of the voltage increase caused by its active power. First only the margin obtained in this way will be used and the maximum penetration level for this case will be determined. The voltage change caused by the DG unit active and reactive power can be calculated from:

$$\underline{V}_{dg} = \underline{V}_s + \underline{Z}_{sc}\,\frac{\underline{S}_{dg}^*}{\underline{V}_{dg}^*} \tag{4.9}$$

The maximum amount of installed DG unit power ($P_{dg,nom}$) that is possible for a particular limit can be calculated by solving (4.7) – (4.9) iteratively. The maximum allowable installed DG unit power is shown in Fig. 4.12 as a function of the maximum voltage change, and for different X/R ratios. The results are obtained for a DG unit that absorbs the maximum available reactive power.

The X/R ratio of the network strongly influences the maximum installed DG unit power. Fig. 4.12 shows that for an X/R ratio of 3 the voltage change becomes never

larger than ~1.5%. This implies that in this network a large amount of DG can be installed. Also for lower X/R ratios the maximum penetration level can be increased, by absorbing reactive power. According to (4.6) the DG unit power without compensation is 0.04 p.u. for a 4% voltage change. For example in a network with X/R = 1 the maximum installed DG unit power can be ~ 0.09 p.u. when a 4% voltage change is allowed and the maximum amount of reactive power is absorbed.

Fig. 4.12. Maximum allowable installed DG unit power (per unit of short-circuit power) as a function of maximum allowable voltage change for different X/R ratios (V_{dg}=1)

4.4.3 Overrating and curtailment

It has been shown in the previous section that the voltage control capability of a DG unit can be improved by converter overrating and generation curtailment. Fig. 4.13 shows for three different values of the allowed voltage change the maximum installed DG as a function of the converter overrating. The curves are shown for X/R = 1 (Fig. 4.13a) and for X/R = 1/3 (Fig. 4.13b). (For X/R = 3 no curves are shown as for this X/R ratio the voltage change is low already, as can be seen from Fig. 4.12.)
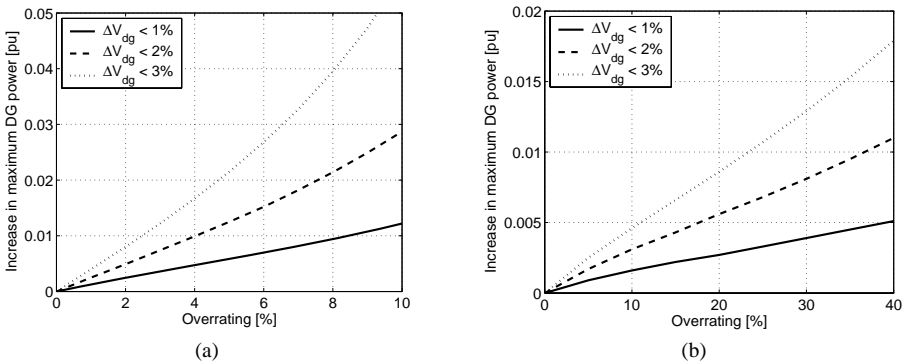
Fig. 4.13. Increase in maximum allowable installed DG unit power (per unit of short-circuit power) as a function of converter overrating; (a) X/R = 1; (b) X/R = 1/3; (V_{dg} = 1 p.u.)

The results are obtained by solving (4.7) – (4.9) for an increasing overrating of the converter. Comparing the results shows that overrating is much more effective for the higher X/R ratio. For X/R = 1/3 the effect is rather limited.

The increase in installed power that can be achieved with generation curtailment is shown in Fig. 4.14a and b for an X/R ratio of 1 and 1/3 respectively. Comparing the graphs with Fig. 4.13 shows that, especially for lower X/R ratios, curtailment is more effective than converter overrating. Due to the high resistance the reduction in active power is very effective.
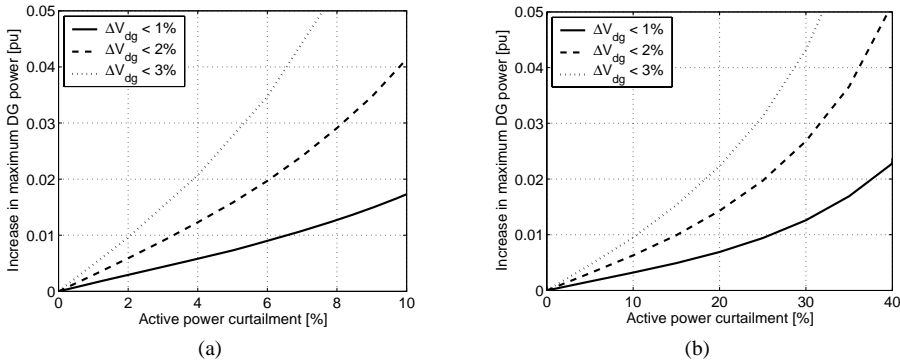
Fig. 4.14. Increase in maximum allowable installed DG unit power (per unit of short-circuit power) as a function of active power curtailment; (a) X/R = 1; (b) X/R = 1/3; (V_{dg} = 1 p.u.)

The values that are obtained from the curves of Fig. 4.13 and Fig. 4.14 can be added to the values obtained from Fig. 4.12. This gives the allowable penetration level when for example a combination of reactive compensation and generation curtailment is applied.

4.4.4 Variable Inductance

This section investigates how a VI can increase the maximum DG unit penetration. The increase in DG penetration that can be achieved is shown in Fig. 4.15, as a function of the inductance value. The curves are shown for three different voltage changes and for X/R = 1 (Fig. 4.15a) and X/R = 1/3 (Fig. 4.15b). The results are obtained for a case without load. The VI increases the network inductance. When the DG unit absorbs too much reactive power voltage instability will occur. This implies that the range in which the VI works correctly is limited.

The VI shows to be more effective in the network with the highest X/R ratio. In both cases a significant increase in allowable penetration level can be achieved however. An inductance of 0.5 p.u., for example, results already in an increase of 0.03 p.u. and 0.01 p.u. respectively.
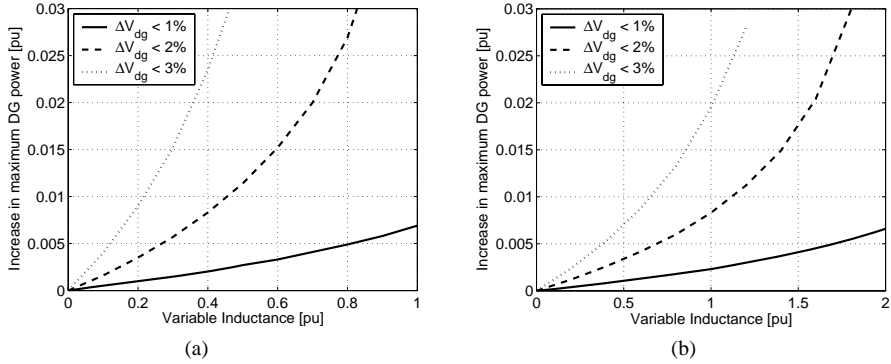
Fig. 4.15. Increase in maximum allowable installed DG unit power (per unit of short-circuit power) as a function of variable inductance; (a) X/R = 1; (b) X/R = 1/3; (S_l = 0, V_{dg} = 1 p.u.)

4.4.5. Discussion

The results in this section show that the maximum allowable DG unit power becomes significantly higher when the DG units absorb reactive power to compensate a part of the voltage change they cause. The allowable penetration level can be increased further by overrating, generation curtailment and the application of a variable inductance.

The results are obtained under the assumption that V_{dg} = 10 kV. When it is higher also $Q_{dg,max}$ will be higher. Therefore the voltage change caused by the DG unit can be kept smaller. Fig. 4.16 shows how the results of Fig. 4.12 change for increasing V_{dg}. For the lowest X/R ratio (Fig. 4.16a) the influence is rather limited, but for X/R=1 (Fig. 4.16b) the maximum allowable power increases significantly.
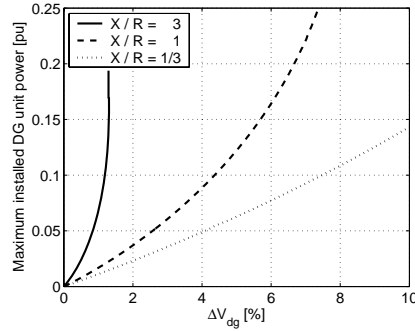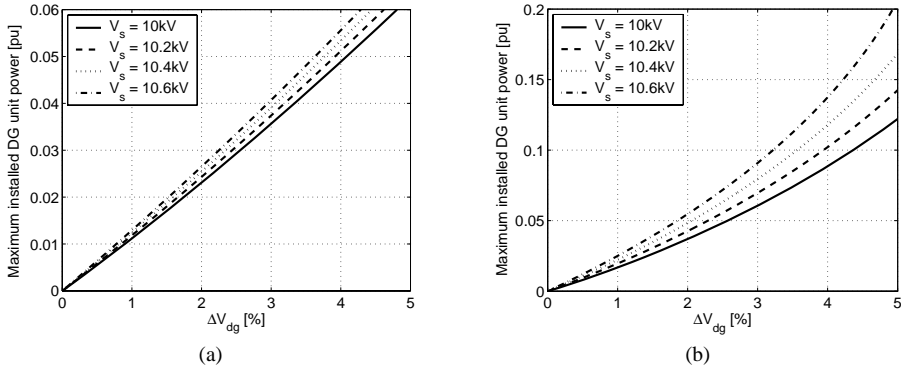

Fig. 4.16. Maximum allowable installed DG unit power (per unit of short-circuit power) as a function of maximum allowable voltage change for different values of V_{dg}; (a) X/R = 1/3; (b) X/R = 1;

A higher V_{dg} will also affect converter overrating and active power curtailment. Fig. 4.17a shows, for different values of V_{dg}, the increase in power that can be achieved by

converter overrating. Fig. 4.17b shows the same for active power curtailment. Both graphs show that a higher V_{dg} has a considerable influence on the active power that can be installed. For voltages above the nominal grid voltage, a higher penetration level of DG can thus be allowed.

(a) (b)
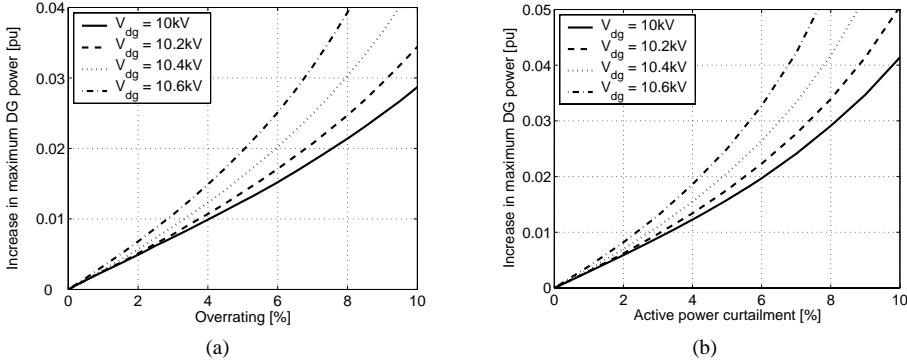
Fig. 4.17. Increase in maximum allowable installed DG unit power (per unit of short-circuit power) as a function of converter overrating (a) and active power curtailment (b) for different values of V_{dg}; X/R = 1;

In this chapter it was assumed that, besides the limitations imposed by the maximum converter current, there are no limitations on the reactive power supplied by the DG units. In reality there might be other limitations, such as for example the maximum current that is allowed in the network, or the minimum power factor that is allowed by grid operators. Other issues that have not been considered, but that can be important are the influence on the losses in the network and the optimal location of the DG units.

4.5 Cases

Several voltage control techniques are considered in this chapter. The analyses can be used to determine the voltage change that is be caused by DG units and to determine maximum allowable penetration levels. This will be demonstrated with two cases.

4.5.1 Case 1
The influence of a 1.5 MW wind turbine connected to node 3 of the rural network described in appendix A.2 is considered. Currently three constant speed wind turbines are connected with a total rated power of about 1.5 MW. The network has a rather low short-circuit power and the wind turbines cause large voltage fluctuations. This can be seen from Fig. 4.18, which shows for a period of one week the power supplied by the

turbine and the voltage at its terminals. (The active power was measured for each wind turbine separately. The power shown in the figure is the total active power for the three turbines.) For the analysis the wind turbines are replaced by a single variable speed wind turbine with a synchronous generator and a PEC, with a rated power of 1.5 MW.
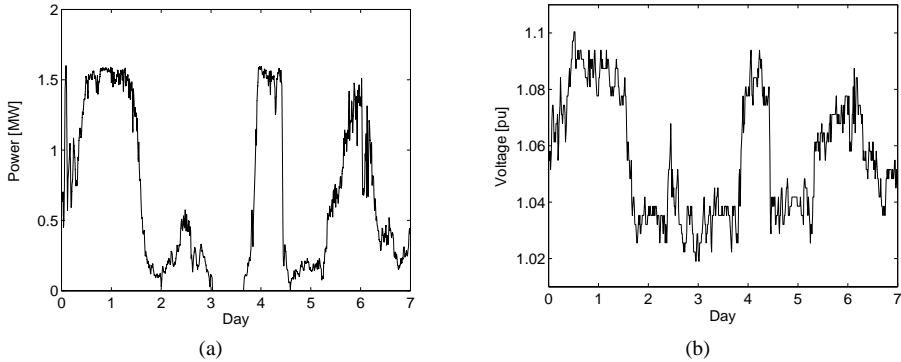
(a)   (b)
Fig. 4.18. Wind turbine output power (a) and voltage and wind turbine terminals (b)

The effect of the wind turbine on the voltage is determined in a number of steps:

1. The voltage change due to the introduction of one or more DG units can be determined approximately by (4.6). The short-circuit power at the node to which the wind turbine is connected is 21 MVA, with an X/R ratio of 0.35. According to (4.6) the maximum rated power of the DG unit is 0.6 MW when the maximum allowable voltage change is 3%. The wind turbine has a rated power of 1.5 MW, implying a maximum voltage change of ~ 7%. This is in compliance with Fig. 4.18.
2. The change in voltage caused by the wind turbine is thus too large. In the previous paragraphs several solutions are proposed to overcome this problem. Their usefulness will be considered.
   a. The wind turbine has a PEC and thus it can absorb reactive power. When a maximum voltage change of 3% is allowed, the maximum installed DG unit power will be 0.7 MW, as can be determined from Fig. 4.12. This is only slightly higher than in a case without voltage control. This is, of course, due to the low X/R ratio of the network.
   b. Overrating of the converter will increase its voltage control capability and therefore the maximum amount of power that can be installed. Fig. 4.13b shows that a 40% overrating of the converter results in a 0.4 MW increase in power that can be installed. The total installed power is then 1.1 MW, which is still too low.

c. Another solution is generation curtailment. Fig. 4.14b shows that 30% curtailment results in 0.8 MW increase in active power that can be installed. Adding this to the 0.7 MW for a case without control, the total installed DG power is 1.5 MW.

d. The third option that has been discussed is the usage of a variable inductance. Fig. 4.15 shows that the maximum variable inductance value is about 1.2 p.u.. The increase in installed power that can be obtained with this inductance is 0.5 p.u., which is too low.

3. Generation curtailment shows to be the only option that makes it possible to install the 1.5 MW wind turbine without violating the 3% voltage change limit. The highest 30% of the wind turbine power has to be curtailed. For a 1.5 MW wind turbine the maximal power that may be supplied is thus 1.05 MW. This means a significant reduction in the total energy that is produced. Fig. 4.18a shows the power output for one week. The total energy produced in this week is ~1100 MWh. When the power is limited to 1.05 MW the energy production is ~940 MWh, a reduction of ~15%.

4.5.2 Case 2

In the second case the maximum rated DG unit power that can be connected to node 4 of the Testnet will be determined. (Details of the network are given in appendix A.1.) This is done in a number of steps:

1. The short-circuit power at node 4 is 50 MVA, with an X/R ratio of 0.75. According to (4.6) the rated power of the DG should not be higher than 1.5 MW (for a voltage change of 3%).

2. To increase the maximum allowable DG unit penetration level the DG unit can absorb reactive power, possibly in combination with one of the proposed techniques. The following options to reach a penetration level of 5 MW are compared:

a. By absorbing maximum reactive power an installed power of 0.05 p.u. is allowable for a 3% voltage change, as can be seen from Fig. 4.12. This implies a maximum DG unit power of 2.5 MW.

b. Fig. 4.13a shows that a 10% overrating of the converter results in an additional increase in power of about 0.05 p.u.. The total power that can be installed in that case is thus about 5MW.

c. Fig. 4.14a shows that for example 8% curtailment results in a 2.5 MW increase in installed power, resulting in a total power of 5 MW.

d. To increase the allowable penetration level to 5 MW by using a VI is not possible without causing voltage instability, as can be seen from Fig. 4.15a.

3. A comparison can be made between the different solutions. The best solution can be defined in different ways. For example the highest annual energy yield or the lowest kWh-price.

    a. When the highest annual energy yield has to be obtained, overrating of the converter or the use of a VI will be the best solution, as generation curtailment will reduce the annual energy yield.

    b. Another possibility is to determine for which option the lowest price per kWh is obtained. For this case the DG units are assumed to be two wind turbines of 2.5 MW each. The cumulative wind power distribution function of one turbine is shown in Fig. 4.19. It shows how large the chance is that the active power of the wind turbine is below the value shown on the horizontal axis. In point 2.c it was concluded that an 8% curtailment was enough to allow the installation of 5 MW. For one wind turbine this implies a maximum power of 2.3 MW. The chance that the output power is below 2.3 MW is about 0.9, as can be obtained from Fig. 4.19. Curtailment implies thus that in 10% of the time 0.2 MW less is produced. This implies an annual energy loss of 175 MWh. When the price per kWh is known, the annual loss in revenues can be calculated. This can be compared with the investment costs of overrating or a VI to determine the most cost effective solution.
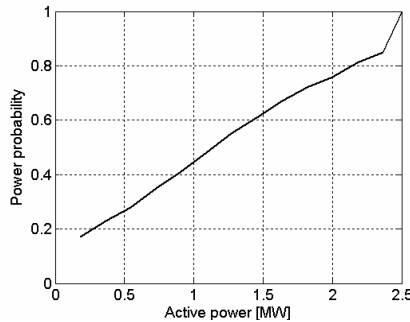
Fig. 4.19. Cumulative wind turbine output power distribution

4.5.3 Discussion and conclusion

From the two cases a number of conclusions can be drawn. They show in the first place that the allowable penetration level increases when the DG unit is able to absorb reactive power. The increase is higher for a higher X/R ratio. (15% increase in case 1, with an X/R ratio of 0.35 and a 40% increase in example 2, with an X/R ratio of 0.75.)

The effect of overrating is limited in networks with a low X/R ratio. Case 1 showed that a 40% overrating results in an increase in installed power of no more than 55%. In networks with a higher X/R ratio overrating will become more effective. Case 2 showed

that 10% overrating was enough to double the amount of DG power that can be installed.

Both examples show that generation curtailment is a good option. In the second case, for example, a curtailment of 8% was enough to allow an increase in rated power of 100%. In the first case a higher curtailment was required, about 30%; leading to a decrease in annual energy yield of only 15%

The VI will increase the total grid inductance. When the total inductance is high and the amount of reactive power that is consumed is large, voltage stability problems can occur. This stability problem poses a limit on the use of the VI.

4.6 Summary and conclusion

In this chapter the voltage control contribution of DG unit converters is investigated. Reactive compensation showed to be of limited effect because of the low inductance in DNs. Converter overrating and generation curtailment have been proposed as solutions to partially overcome these limitations. Section 4.3 proposed to use a variable inductance. An implementation with two anti-parallel thyristors was proposed for the variable inductance. It should be realised that this device will have a significant influence on the short-circuit power and the power quality of the DN.

Section 4.4 presented an approach to determine the maximum allowable DG penetration level, with respect to the voltage change that is caused by the DG units. The increase in voltage they cause, offers the possibility to increase the reactive power consumption to limit the voltage increase. Using this reactive power significantly increases the maximum allowable penetration level. Especially in networks with a high X/R ratio a significantly higher penetration level of DG can be allowed. For networks with a low X/R ratio generation curtailment and the use of a VI offer good possibilities to increase the DG unit penetration level, although its effect is limited: for too high values voltage instability occurs. The effect of overrating is limited in a network with a low X/R ratio.

Finally in section 4.5 the maximum DG penetration levels in some typical networks were determined. They showed that reactive power control by the DG unit increased the allowable DG power with 15 – 40% already, depending on the X/R ratio. A 10% overrating can increase the allowable penetration level by 50% in networks with an X/R ratio of ~1. 8% curtailment was in this network enough to achieve a 100% increase in allowable penetration level.

Chapter 5

Ride-through and grid support during faults

5.1 Introduction

Short-circuits regularly occur in power systems. They can be caused by lightning strikes, degradation of isolation material, and so on. They lead to the flow of large short-circuit currents. Protection systems protect the network by isolating the faulted area from the main grid. The removal of generators and loads from the main grid may result in power imbalance and frequency deviations, as will be discussed in chapter 6. The short-circuit currents that flow in the grid and the switching events that are taken by the protection system also result in voltage dips. The interaction between DG units and the grid during voltage dips is investigated in this chapter.

Most DG units will intentionally disconnect from the grid during a dip. There are several reasons for this disconnection. The first is that up to now most standards for DG require disconnection in case of a fault (for example IEEE-Std. 1547-2003), because DG units can disturb the protection schemes of the network. Another reason is that the power electronic converters (PECs) that connect the DG units to the grid may be sensitive to over-currents and over-voltages. The easiest way to avoid detrimental effects is to disconnect the DG unit. In networks with a large DG penetration level the disconnection will cause serious problems. Disconnection of all DG units may result in a large power generation deficit and in stability problems [Slo 02]. In addition they can not support the grid voltage and frequency during and immediately after the grid failure.

The goal of this chapter is to investigate how PEC-based DG units can support the grid (voltage) during faults and how damage to the DG unit can be avoided.

Section 5.2 analyses the response of DG units to voltage dips. In section 5.3 it is investigated how the disturbance of the classical grid protection by DG units can be minimised. Section 5.4 will investigate how DG units can support the grid voltage during dips and will determine how large this contribution is. During a fault the power that the DG unit can deliver to the grid is often limited because of the reduced grid

voltage. Section 5.5 discusses the consequences for the DG units and describes protection techniques that can be applied to avoid malfunctioning of the DG unit. A special case, when it comes to short-circuits and protection, is a wind turbine with a doubly-fed induction generator. It is analysed separately in section 5.6.

5.2 Fault response of DG units

During a fault a voltage dip is experienced by DG units connected to the grid. Their response depends on the type of DG unit, especially whether it is connected to the grid with a machine or a PEC. The response of an electrical machine is completely different from that of a converter. This paragraph compares their responses. The network shown in Fig. 5.1a is used to compare the voltage dip response of PECs and synchronous machines (SMs). It contains a DG unit and a load. The rated power of the DG unit is ~5% of the short-circuit power of the grid.

In the first case the DG unit is the SM shown in Fig. 5.1b. The stator current and voltage during the dip are shown in Fig. 5.2a and c. The response of the SM is determined by the fundamental electro-mechanical laws and physical construction of the machine, and by its excitation control. The initial short-circuit current reaches a high value, but decays after some time. The peak current mainly depends on the sub-transient reactance of the generator which is inherent to its physical construction and on the excitation of the machien. The machines are developed to be able to withstand these currents and dynamic forces for a certain time. Therefore no special protection is required for the SM.
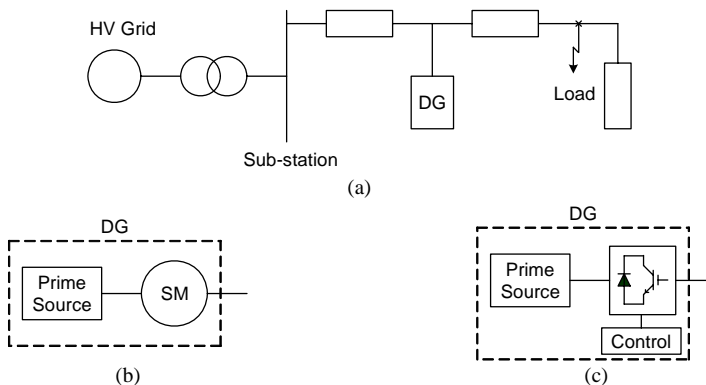
Fig. 5.1. Network with DG unit and fault: (a) network; (b) DG unit with synchronous machine; (c) DG unit with power electronic converter
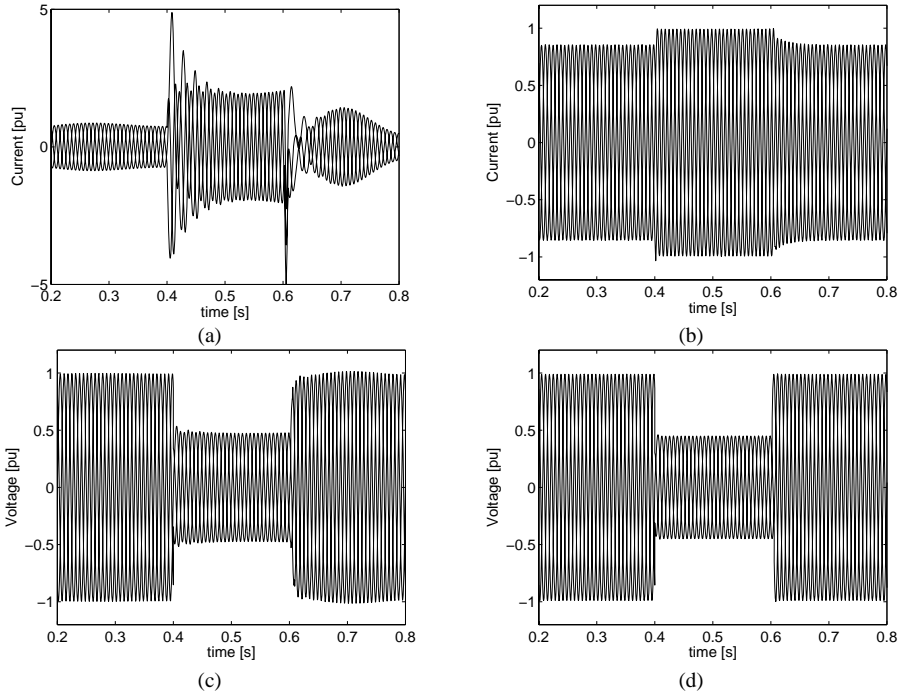
Fig. 5.2. Response to voltage dip: (a) synchronous machine current; (b) converter output current; (c) synchronous machine stator voltage; (d) converter output voltage;

In the second case the DG unit is the PEC shown in Fig. 5.1c. Fig. 5.2b and d show the output current and the terminal voltage. In contrast to the SM, the current is not determined by the converter construction but by its control. During normal operation PECs have a low-impedance output. This implies that when they are not controlled, they will supply a large current when the voltage drops. The current control of the converter limits the current however, to avoid breakdown of the semiconductor devices which are sensitive to high currents. When the controllers are fast enough the current can be limited as shown in Fig. 5.2b. Breakdown of the semiconductor switches is thus avoided and the converter can stay connected during the dip. When the current control loop is not fast enough there will be a short peak in the converter current.

In this example the converter current is limited to its nominal value. Other control strategies are possible however. In principle converter designers can implement a number of different control schemes in the same converter. In the installation phase and during operation the grid operators can choose the appropriate control.

5.3 Disturbance of protection during faults

5.3.1 Introduction

In distribution networks (DNs) protection schemes are applied to minimise the detrimental effect of faults in the DN. The connection of DG units will influence the operation of the protective devices. This has been discussed extensively in literature [Dug 02], [Kau 04], [Mäk 04], [Kum 05]. Most publications consider machine-based DG units and generally it is concluded that the DG units can prevent the proper operation of the feeder protection [McD 03], [Kum 04], [Ver 04]. This is not necessarily true however. Especially PEC-based DG units can limit their current during a fault and minimise he influence of the DG unit on the network protection.

This section will discuss shortly how the DG units can be controlled to minimise the influence on the protection. The most important problems mentioned in literature are [Kau 04], [Jer 04]:

1. Blinding of protection
2. False tripping (unnecessary disconnection of a healthy feeder)
3. Failure of reclosing
4. Islanding

The issue requires more research however, before general conclusions can be drawn.

5.3.2 Blinding of protection

DG units can prevent the proper operation of feeder protection [Dug 02], [Kau 04], [Mäk 04]. This happens when the fault current measured by the protective device decreases due to the short-circuit current supplied by the DG unit, as illustrated by Fig. 5.3a and b. In a situation without DG all fault current is flowing through the protective device at the beginning of the feeder (Fig. 5.3a). In a case with DG, the DG unit also supplies a part of the short-circuit current, resulting in a lower current through the protective device (Fig. 5.3b). The current can drop below the breaking current and as a result the breaker will not disconnect the feeder and the fault current continues to flow. This can cause damage to grid components.

An example will be given for the chance on blinding in a realistic case. When, without DG unit, a fault occurs at node 3 of the Testnet (see appendix A.1) a 3.5 kA current flows through the protective device. When a 5 MW DG unit is connected to node 2, this current reduces to 3.2 kA, in the case that the DG unit current is limited to its nominal value. This example shows that the reduction in current through the protective device is limited. In normal operation the nominal current through the protective device is only ~120 A. Discrimination between a normal situation and a fault will not be difficult.
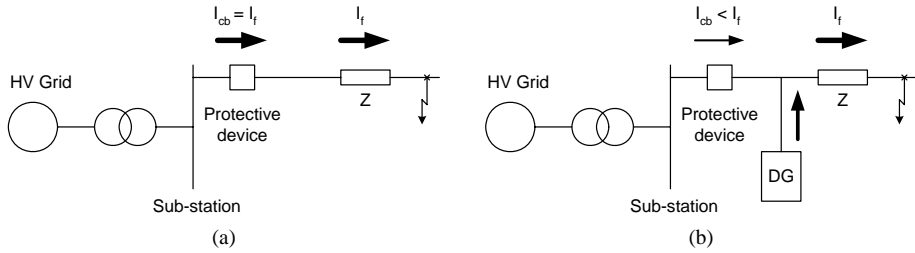
Fig. 5.3. Blinding of protection due to fault downstream of DG: (a) fault current I_f completely observed by protective device; (b) protective device is blinded because DG delivers a large part of fault current I_f

5.3.3 False tripping

It is concluded in a number of publications that DG units can cause false tripping and unnecessary disconnection of a healthy feeder [Kau 04], [Mäk 04]. This is explained with reference to Fig. 5.4, where a fault occurs in feeder 2. The DG unit connected to feeder 1 feeds this fault through the substation bus. The current of the DG unit can be large enough to trip protective device 1 in feeder 1, before protective device 2 is tripped. This type of malfunctioning can be avoided when a converter based DG unit is used however. Depending on the settings of the two protective devices the DG unit can limit its current during the fault to avoid tripping.
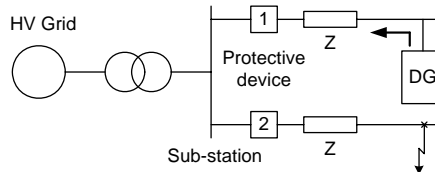
Fig. 5.4. False tripping of protective device 1 due to fault in another feeder

Again an example will be given. The fault is assumed to occur at node 3 (feeder B) of the Testnet, while a 5 MW DG unit is connected to feeder A. The fault current through the protective device of feeder B is 3.5 kA and through that of feeder A it is ~300 A, when the DG unit current is limited to its nominal value. The chance on false tripping is thus small.

5.3.4 Failure of auto-reclosing

Auto-reclosing is a fault clearing technique that is normally applied in networks with overhead lines. Most line faults are due to arcs caused by lightning over-voltages and they are self-clearing when the line is disconnected. When a fault is detected the circuit breaker is opened, which interrupts the current that is fed into the short-circuit and

therefore the arc will disappear. After a short period (~0.3s) the breaker is closed again automatically.

Many papers mention that DG units can prevent the successful operation of auto-reclosers [Dug 02], [Kau 04], [Mäk 04], [Kum 04]. When a DG unit is connected to the feeder, it can continue to supply current to the fault and as a result the arc may not disappear. To avoid problems PEC-based DG units can reduce their output current to almost zero during the period that the recloser is open. This increases the chance that an arc is cleared, as the DG unit feds almost no current into it.

5.3.5 Islanding

The fourth issue is islanding [Ye 04], [Kat 05], [Peç 05]. It occurs when a DG unit continues to energise a section of the utility system that has been separated from the main utility system. Islanding can pose a serious safety threat for maintenance personnel, if they expect a system to be de-energised. The islanded network will probably not comply with power quality and protection requirements. Therefore most grid operators do not permit islanded operation.

The big issue for DG units is to detect when the network becomes islanded. The detection method should be reliable. On one hand it has to be sure that the DG unit will disconnect in case of an island, while on the other hand unnecessary tripping should be avoided. A whole range of islanding detection techniques has been developed [Jer 04], [Ye 04], [Yin 04]. With these techniques unnoticed islanding can be avoided in most cases.

5.4 Grid support during dips

5.4.1 Introduction

So far faults have been investigated which occur close to the DG unit, i.e. in the same DN. They mostly result in a large short-circuit current. When the fault occurs further away (outside the DN), the DN protection will not react and disturbance of protection will not occur.

Faults further away result in a voltage dip. They are experienced as a reduction in rms voltage at the terminals of DG units and loads. The dip can be problematic for the loads connected to the network. Several types of loads, such as adjustable-speed drives, process-control equipment, and computers are very sensitive to voltage dips. Some of them disconnect when the rms voltage drops below 90% for longer than one or two cycles [Bol 00]. Also most DG units disconnect in case of a fault. This is mainly because of the current grid codes, as was explained already in the introduction of this chapter. When DG units stay connected to the grid however, they can supply active and reactive

power during the dip. In this way they can limit the depth of the voltage dip and thus reduce the chance that loads are disconnected.

On some places it is required already for larger DG units that they have ride-trough capability (stay connected) and support the grid voltage during dips. Fig. 5.5 shows an example (from E.On Netz, a grid operator in Northern Germany [E.On 03]). This requirement is for wind farms directly connected to the transmission grid. For voltages above the curve (in duration and voltage level), the turbine should stay connected. For voltages in the gray area, the turbine should supply reactive power.

This section will investigate how DG units can support the grid during voltage dips and how large their contribution can be. As a first step the effectiveness of reactive power is investigated. In most cases this is limited. Therefore techniques will be proposed to improve the voltage control capabilities, such as overloading of the converter and the use of a variable inductance.
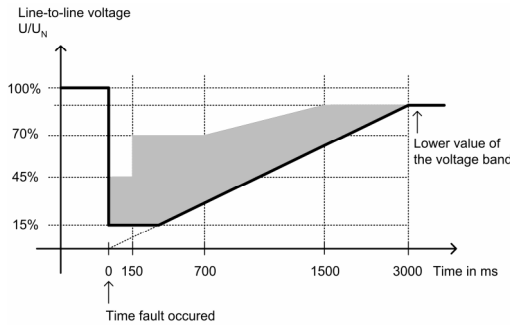
Fig. 5.5. E.On Netz requirements for wind park behaviour during faults ([E.On 03])

5.4.2 Voltage control with (re-)active power

In chapter 4 it has been concluded that voltage control with reactive power is mostly limited because of the low inductance in the grid and the limited current rating of the PECs. An additional problem in case of voltage dips is that due to the low voltage, the power that can be supplied to the grid without exceeding the rated converter current is lower than at nominal voltage. An important difference with chapter 4 is, however, that most voltage dips have a limited duration (generally < 1 s) and short-term overloading of the converter might be possible. For most converters in the MW-range a 100% overloading for a short time (~ 1s) could be acceptable (or the converter can be designed for it). This subsection will investigate how much DG units can increase the grid voltage in case of a dip. The basic theory on voltage control that is presented in chapter 4 is used to derive the results in this section. All results are in per unit with the

short-circuit power S_{sc} = 100 MW and the supply voltage V_s = 10 kV as the base values. The rated power of the DG unit is 0.1 p.u .in all cases.

Fig. 5.6a shows the voltage change that can be achieved with reactive power, as a function of the overloading of the converter. Curves are shown for three different X/R ratios. The active current of the converter is kept constant. (This means that the active power is directly proportional to the voltage.) Fig. 5.6b shows for three different X/R ratios how the results depend on the rated power of a 100% overrated DG unit. The figures show that a considerable overrating and installed power are required to obtain a significant voltage increase in voltage.
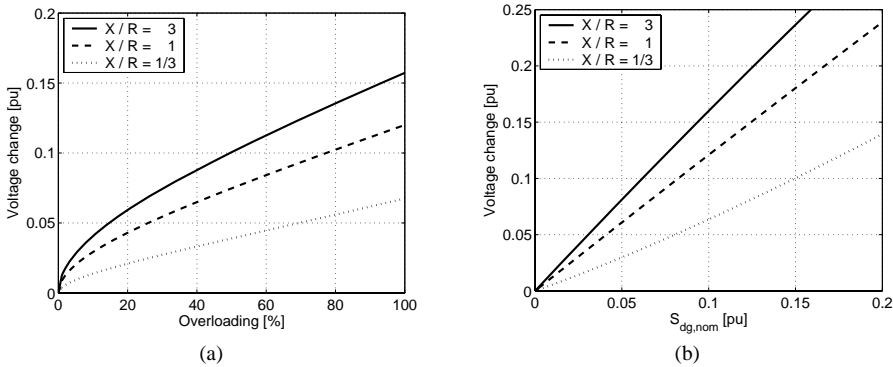
Fig. 5.6. Voltage increase that can be achieved during voltage dip by supplying reactive power; (a) as a function of converter overloading ($S_{dg,nom} / S_{sc}$= 0.1); (b) as a function of rated DG unit power (overrating of 100%)

In networks with a low X/R ratio it might be better to increase the active power to increase the voltage. The DG unit should be able to supply this power (fast enough). This will not always be possible. DG units with rotating parts can use their kinetic energy, such as will be proposed in chapter 6 for frequency control support. Fig. 5.7 shows the voltage change that be achieved by controlling active power. The reactive power is zero. Fig. 5.7a shows the voltage change that can be achieved by overloading the converter. Fig. 5.7b shows, for an overrating of 100%, how the voltage change that can be achieved depends on the rated power of the DG unit.

Comparing the figures shows that in case of a low X/R ratio active power is slightly more effective than reactive power. For the other two cases reactive power is more effective. This is partly due to the fact that for a given active power and current, the amount of reactive power that can be achieved by overloading the converter is higher than the active power. In general the increase in voltage that can be achieved is limited however.
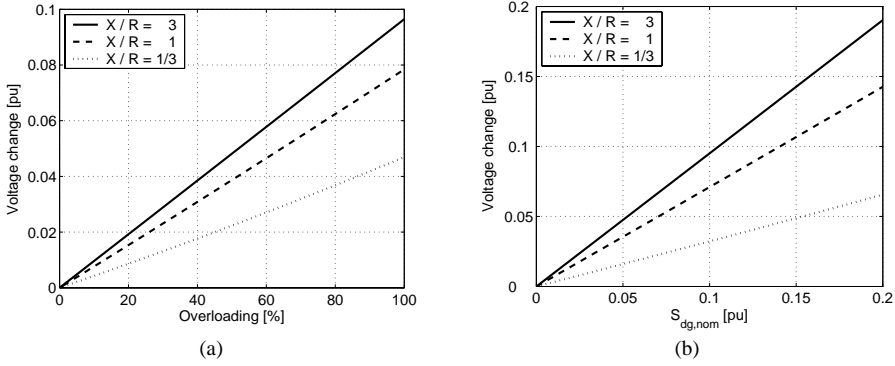
Fig. 5.7. Voltage change that can be achieved during voltage dip by supplying active power; (a) as a function of converter overloading ($S_{dg,nom}/S_{sc}$= 0.1, Q_{dg} = 0); (b) as a function of rated DG unit power (overrating of 100%, Q_{dg} = 0)

5.4.3 Variable inductance

The variable inductance proposed in chapter 4 can be very useful to compensate voltage dips, as it can increase the inductance between the fault and the DG unit. Fig. 5.8a shows the voltage change that can be achieved as a function of the inductance, for different values of the reactive power that is supplied by the DG unit. The maximum value of the variable inductance (20 mH) is ~6 p.u..
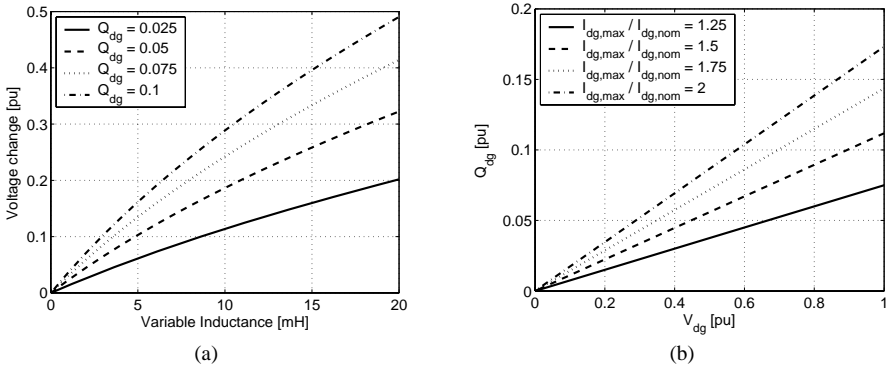
Fig. 5.8. Voltage change that can be achieved with variable inductance; (a) Voltage change as function of variable inductance and reactive power ($S_{dg,nom}/S_{sc}$= 0.1); (b) reactive power that is available as function of voltage and overloading ($S_{dg,nom}/S_{sc}$= 0.1)

The reactive power that can be supplied by the DG unit will depend on the grid voltage, the active power that is supplied by the converter and the maximum converter current, as has been defined in (4.7). Fig. 5.8b shows how much reactive power Q_{dg} can be supplied as a function of the grid voltage, for different values of the converter

overloading and a constant active current. Comparing the graphs of Fig. 5.8 to those of Fig. 5.6 and Fig. 5.7 shows that when a variable inductance is used, a much larger voltage change can be achieved.

5.4.4 Example

The results in this section showed that the voltage increase that can be achieved by the DG units is limited. Generally the DG units will not be capable to compensate a dip completely. A certain reduction of the dip depth (for example a 10 or 20% higher voltage) might be possible however. This subsection will give an example too show that such a small reduction can be very useful already.

The circles in Fig. 5.9 show the voltage dips that in a certain period have been measured at a 150 kV / 10 kV substation in the Netherlands. The solid line is a part of the so-called ITI-curve, which is defined by the American Information Technology Industry Council. When the voltage is above the line (in voltage level and duration), computer and telecommunication appliances should stay connected to the grid. In this case 40% of the dips are above the line. When a DG unit is connected that can achieve a 10% voltage increase, the ITI-curve can be lowered with 10% (the DG unit will increase the voltage during the dips by 10%). This is shown by the dashed line in Fig. 5.9. In this case the appliances should stay connected for 65% of all dips. When a DG unit is connected that can achieve a 20% voltage increase even 85% of all dips is above the line. This means that less appliances will disconnect.
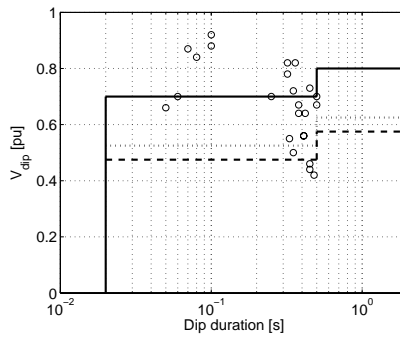
Fig. 5.9. Measured voltage dips and ITI voltage tolerance curves

The dips are assumed to be measured at the substation of the Testnet and the DG unit is assumed to be connected to node 3 of this network. From the figures presented in the previous subsections it can be seen how the DG unit can achieve a 10 or 20% increase in voltage. Fig. 5.6a for example shows that in case of compensation with reactive power an overrating of ~100% is needed (for $S_{dg,nom} / S_{sc} = 0.1$). When a variable

inductor is used, a lower overrating is required. From Fig. 5.8, in combination with Fig. 5.6, it can be concluded that with a 25% overrating and a variable inductance of ~8 mH, a 20% increase in voltage can be achieved (5% due to the grid impedance and 15% due to the variable inductance).

5.5 DG unit ride-through during voltage dips

5.5.1 Introduction

The previous paragraph investigated how DG units can support the grid voltage during dips. A prerequisite for grid support is that the DG units ride through the dip (stay connected). In paragraph 6.2 the response of PECs to voltage dips was investigated. When the current controllers of the converter are fast enough fault ride-through is no problem. Only the response of a converter has been investigated however, and not the response of the whole DG unit. This is done in this section.

A voltage dip manifests itself as a decrease in voltage amplitude at the converter terminal. To keep the power supplied to the grid constant, the current should increase. It will be limited by the current controller however, to avoid overloading of the converter. This will thus limit the power that the DG unit can supply to the grid during a dip. For some DG unit types the power limitation can be a problem. This section will present protection measures and control strategies that can be used to avoid problems. Three types of DG unit will be considered: wind turbines with a full-size converter, micro turbines and fuel cells. One specific DG unit, a wind turbine with a doubly-fed induction generator, will be discussed in section 6.6.

5.5.2 Variable speed wind turbine with full-size converter

Fault ride-through of variable speed wind turbines with a full-size converter has not gained much attention till now. In [Sac 02] a thorough investigation of the operation and control of the converter is given, but it does not investigate the impact on the wind turbine itself. The same holds for [Mul 05b] which presents a non-linear dc-link controller that enables fault ride-through. The issue is discussed in more papers, but all focus on the converter control and do not investigate how the wind turbine operation is affected.

Control principle - First the basic principles of a control strategy to enable fault ride-through are described. Variable speed wind turbines with a full-size converter generally use (permanent magnet) synchronous generators. The generator is connected to the grid by a back-to-back converter. A dc-link separates the two converters and therefore they can be controlled independently. During normal operation the generator-side converter

controls the rotational speed of the wind turbine to capture as much power as possible from the wind. A power setpoint P_{ref} is generated based on the measured wind speed. The power from the rectifier is fed to the dc-link. The grid-side converter supplies the dc-link power to the grid. The generator-side converter determines the overall power of the system and the inverter has to supply this power to the grid. Fig. 5.10a shows the control structure.

A fault in the network will result in a drop of the rms value of the voltage at the converter terminals and, due to the current limitation, in a reduction of the power that the inverter can supply to the grid. As a result the dc-link voltage will increase, as long as the power from the turbine is not decreased. To avoid a too high dc-link voltage, the grid-side converter should become the master, and determines the overall power. Its reference power is determined by the maximum power that can be supplied to the grid. The rectifier limits its power to avoid a too high dc-link voltage. This control structure is shown in Fig. 5.10b. As the power that the rectifier supplies to the dc-link will reduce, the speed of the generator will increase. Decreasing the mechanical power input by pitching the blades might be necessary to avoid overspeeding of the turbine. Pitching is a rather slow process however and thus the rotational speed will thus continue to increase for some time.
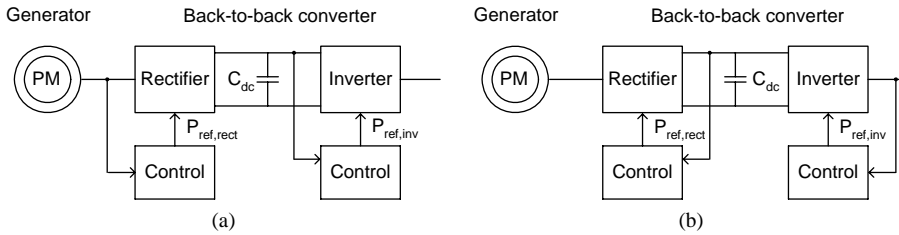
Fig. 5.10. Control of permanent magnet synchronous machine; (a) normal situation; (b) current limitation during voltage dip

Implementation - The control principles described above can be implemented in different ways. An important issue is to decide when the operation of the two converters has to be changed. One possibility is to monitor the grid voltage. When it drops below a predefined threshold, the control of the converters is changed: the rectifier starts controlling the dc-link while the inverter determines the maximum power that is supplied to the grid. Another possibility is to use the dc-link voltage as an indicator. When the currents in the grid converter are limited, it will not be able to supply all dc-link power to the grid during a dip, resulting in an increase in dc-link voltage. When the voltage exceeds a predefined level the rectifier has to reduce its power and can start controlling the dc-link voltage.

Analysis - The amount of energy stored in the dc-link is small. This requires fast control, as the voltage of the dc-link will change very fast when there is a mismatch between rectifier and inverter power. The dc-link voltage is given by

$$C_{dc} v_{dc} \frac{dv_{dc}}{dt} = P_{rect} - P_{inv}$$
(5.1)

with P_{rect} and P_{inv} the rectifier power supplied to the dc-link and the inverter power absorbed from the dc-link respectively. When a voltage dip occurs, P_{inv} will decrease, as the inverter current will be limited by the current controller. How far the voltage dc-link voltage increases depends on how fast P_{rect} is decreased. When the converter operates at nominal power, the per unit drop in power can be assumed to be equal to the per unit drop in voltage. Defining $\Delta v_{dc,max}$ as the maximum change in dc-link voltage that is allowed, the response time in which the rectifier power P_{rect} should be reduced is:

$$\Delta t_{rt} = \frac{C_{dc} v_{dc} \Delta v_{dc,\text{max}}}{r_{dip} P_{nom}}$$
(5.2)

with r_{dip} the dip ratio ($r_{dip} = 1 - V_g/V_{g,nom}$) and Δt_{rt} the delay caused by the complete ride-through control. The minimum value of C_{dc} is a function of the rated power of the converter P_{nom}, the switching frequency f_s, and the maximum allowable voltage ripple due to the switching $\Delta v_{dc,r}$. It can be approximated by:

$$C_{dc,\text{min}} = \frac{P_{nom}}{2 f_s \Delta v_{dc,r} v_{dc}}$$
(5.3)

By combining the two equations the maximum allowable delay can be determined:

$$\Delta t_{rt,\text{max}} = \frac{\Delta v_{dc,\text{max}}}{2 f_s r_{dip} \Delta v_{dc,r}}$$
(5.4)

Under some assumptions an approximate value for $\Delta t_{rt,max}$ can be obtained. Assuming $\Delta v_{dc,max}$ to be 4 times larger than $\Delta v_{dc,r}$, and for $r_{dip}= 1$, $\Delta t_{rt,max}$ should be smaller than 2 switching periods. As the switching frequency of MW-class converters is not very high (a few kHz at maximum) this maximum delay should be realisable.

The ride-through control will result in an increase of rotational speed, as the electrical torque will decrease, because of the reduction in electrical power. How far the rotational speed will increase depends on the inertia of the turbine and the pitch speed. The relation between power, inertia and rotational speed ω_{wt}, is given by:

$$J \omega_{wt} \frac{d\omega_{wt}}{dt} = P_a - P_e$$
(5.5)

with P_a and P_e the aerodynamic and electrical power respectively. Combining this equation with that for the inertia constant H, given in (5.2), and assuming $\Delta P_a = 0$ and the nominal active power of the turbine equal to the nominal apparent power, gives

$$\frac{1}{\omega_{wt}} \frac{d\omega_{wt}}{dt} = \frac{r_{dip}}{2H} - \frac{\Delta P_a(\theta)}{2HS_{nom}} \qquad (5.6)$$

where ΔP_a is the reduction in aerodynamic power due to the pitching of the blades, θ the pitch angle, and S_{nom} the nominal power of the wind turbine. The inertia constant of wind turbines is in the range $2 - 5$ [Knu 05]. This implies that in case of a 85% dip, and assuming ΔP_a to be zero, the change in rotational speed is between 9% and 21% per second. The pitch speed of wind turbines is normally less than 5° per second, but can increase to 10° during emergencies [Knu 05]. The reduction in power that is achieved for a certain pitch angle differs per turbine, but can rise to a 50% reduction for a 10° pitch angle. The increase in speed for the 85% dip mentioned before becomes than 4% to 9% for a one second dip.

Case study - A case study is done to demonstrate the proposed solution. The wind turbine is connected to node 4 of the Testnet (see appendix A.1). Data of a 1.5 MW direct-drive wind turbine with a permanent magnet generator is used to model the turbine. A description of the wind turbine model can be found in appendix C and [Pie 04]. The dc-link voltage of the converter is continuously measured. When it becomes larger than 1.05 p.u., the rectifier limits its power and starts controlling the dc-link voltage, while the inverter determines the maximum power flow to the grid. The controller used by the inverter is similar to the dc-link voltage controller used by the inverter during normal operation. It is described in appendix B. When the rotational speed of the wind turbines exceeds 1 p.u. the pitch angle is reduced to avoid overspeeding of the turbine.

The wind turbine operates at almost nominal power. A 50% - 0.5 s voltage dip is applied to the voltage source of the Thévenin equivalent of the grid. This results in a voltage dip at the wind turbine terminals, as shown in Fig. 5.11a. To avoid overloading of the converter, the converter currents are limited, as shown in Fig. 5.11b. As a result the power that the converter supplies to the grid decreases (Fig. 5.11c), resulting in an increase in the dc-link voltage (Fig. 5.11d). The grid converter now controls the power (with its setpoint determined by the maximum current), while the generator converter controls the dc-link voltage. It reduces the stator power to avoid a too high dc-link voltage. The controller causes some oscillations before a constant value is reached, as can be seen from the dc-link voltage (Fig. 5.11d) and stator power (Fig. 5.11e). The reduction in stator power results in an increase in rotational speed (Fig. 5.11f). The increase in speed is very small, due to the large inertia and the short dip duration.

Increasing the pitch angle to avoid overspeeding is not necessary. When the dip ends the generator converter becomes again the master and normal operation is resumed.
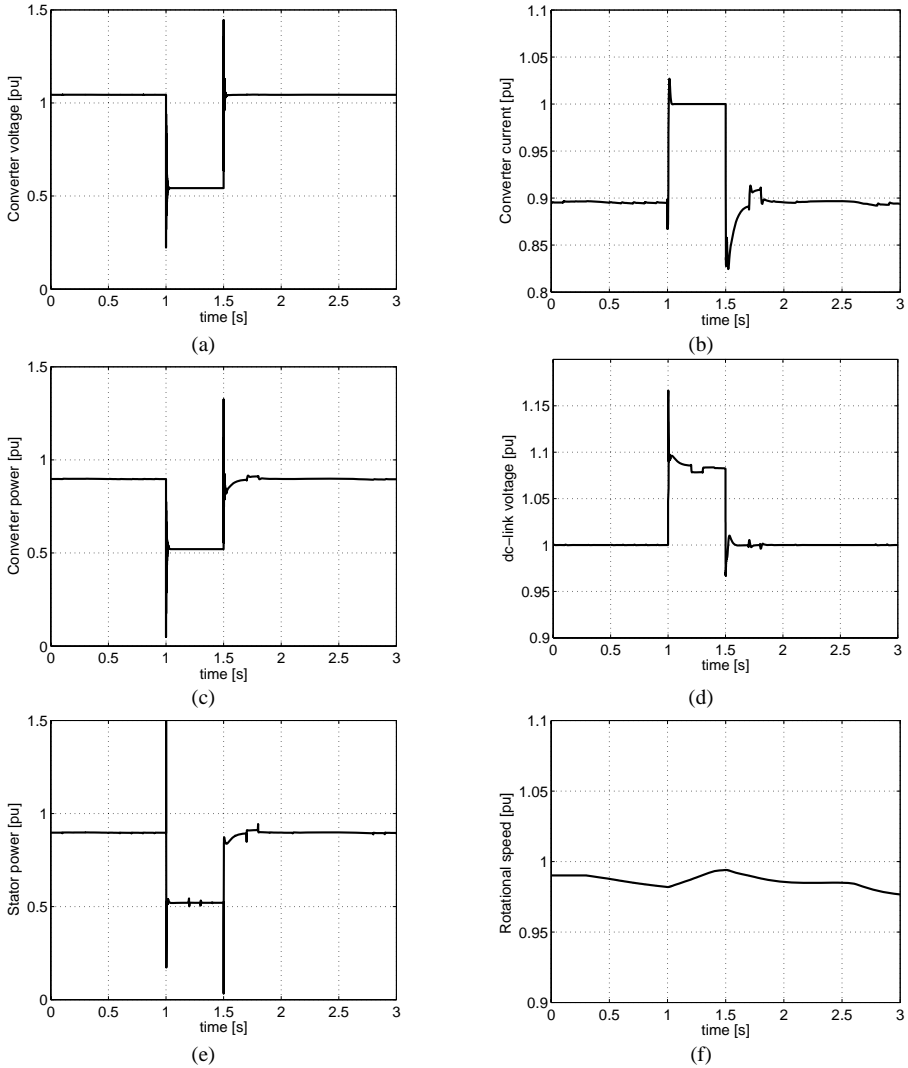
Fig. 5.11. Response of wind turbine with permanent magnet generator to 50% - 0.5 s voltage dip at $t = 1$ s: (a) grid voltage; (b) grid converter current; (c) grid converter power; (d) dc-link voltage; (e) stator power; (f) rotational speed of turbine

5.5.3 Micro turbine and fuel cell
The electrical part of a micro turbine is similar to that of the variable speed wind turbine described in the previous subsection: a (permanent magnet) synchronous generator and

a back-to-back converter. Fault ride-through can therefore be achieved in the same way. There are some differences however. The first is that the switching frequency of a micro turbine converter can be higher as the rated power of micro turbines is normally much smaller than that of wind turbines. This can imply a smaller response time Δt_{rt} as can be seen from (5.4). The second difference is that the gas turbines that are used in the micro turbine generally are fast controllable. This implies that no large increase in rotational speed will occur.

A fuel cell system is different from wind turbines and micro turbines. As a fuel cell is a dc-source it does not need a rectifier. Instead of that the system has mostly a dc-dc converter that connects the fuel cell to the dc-link. The main problem during a voltage dip is the same however. Due to the current limitation the inverter will supply less power to the grid, and the dc-link voltage will increase. The dc-dc converter can limit the current from the fuel cell to avoid a too high dc-link voltage. At the same time the fuel flow to the fuel cell has to be reduced.

5.6 Doubly-Fed Induction Generator

5.6.1 Introduction

The previous paragraph analysed the fault ride-through capability of DG units that are connected to the grid with a converter. This section will investigate the behaviour of a wind turbine with a doubly-fed induction generator (DFIG). Most modern variable speed wind turbines are based on this type of generator. Instead of a converter between the stator and the grid, it has a converter between the rotor windings and the grid, as shown in Fig. 2.5b. This has a major impact on the operation during grid faults. The voltage drop at the terminals will result in large, oscillatory currents in the stator windings of the DFIG. Because of the magnetic coupling between stator and rotor these currents will also flow in the rotor circuit and through the PEC. The high currents can cause thermal breakdown of the converter.

A possible solution to avoid destruction of the converter is to short-circuit the rotor windings of the generator with so-called crowbars during a fault, and disconnect the converter. Resuming normal operation without transients when the fault is cleared is not properly feasible however. First the converter has to be re-synchronised with the grid and the rotor. Most turbines using doubly-fed induction generators therefore are automatically disconnected from the grid nowadays, when a fault occurs [Slo 03a].

Worldwide there is an ambition to install more wind power. The interaction with the grid becomes increasingly important then [Slo 02]. It is worldwide recognized that to enable large-scale application of wind energy without compromising system stability,

the turbines should stay connected to the grid in case of a failure. They should – similar to conventional power plants – supply active and reactive power for frequency and voltage support immediately after the fault has been cleared, which is normally within a fraction of a second. For wind turbines connected to higher voltage levels most grid operators require fault ride-through capability already. An example of such a requirement was shown in Fig. 5.5.

A number of papers have been published that discuss the protection of DFIGs during grid disturbances. Some papers assume operation of a crowbar followed by disconnection of the wind turbine [Per 04]. Other papers propose the use of a crowbar and disabling of the converter, but without disconnecting the wind turbine from the grid [Sun 04b]. The generator operates then as an induction machine with a high rotor resistance. The transition back to normal operation will take time in this case and grid support during the fault is not possible. Other papers assume overrating of the converter [Pet 04], [Ana 05], to cope with the transient currents and voltages.

Some papers propose fault ride-through by using a kind of an 'active crowbar'. With this protection the generator can stay connected to the grid and it is not necessary to disconnect the converter. The most extensive and detailed publication on this type of protection is [Mor 05]. With the control proposed in this paper it is possible to keep the wind turbine connected to the network and to resume normal operation immediately after clearance of the fault. When the dip lasts longer than a few hundred milliseconds, the wind turbine can even support the grid during the dip. Most other papers give little or no information on the way in which the protection and the control is implemented [Hud 03], [Nii 04], [Dit 05], [Nii 05]. They also give only limited information on the behaviour of the rotor voltage and current during disturbances [Eka 03], [Dit 05], while these signals are very important. Rotor currents or voltages that are too high might destruct the converter in the rotor circuit.

This section proposes a method that makes it possible for wind turbines using DFIGs to stay connected to the grid during grid faults and support the grid. First the response of a DFIG to a voltage dip will be analysed. Then the protection technique is described. The section ends with a case study that shows the operation of the protection.

5.6.2 Fault response and protection of doubly-fed induction generator

This subsection will analyse the response of a DFIG to a dip in the voltage at its terminals. Appendix D gives a mathematical analysis and explanation of the fault response of an induction machine. The analysis and explanation of the voltage dip behaviour of the DFIG will be given with reference to this appendix. The response of a DFIG is to a large extent the same as that of an induction machine. The differences will be high-lighted in this and the following subsection.

The stator voltage equation of the induction machine is given in (D.1). In a stationary reference frame it is expressed as:

$$\vec{v}_s = R_s \vec{i}_s + \frac{d\vec{\psi}_s}{dt} \tag{5.7}$$

In normal operation the space-vectors rotate at a synchronous speed with respect to the reference frame. Ignoring the stator resistance, the derivative of the stator flux is directly proportional to the grid voltage. When the voltage drops to zero (in case of a fault at the generator terminals) the stator flux space-vector will stop rotating. This will produce a dc-component in the stator flux. The dc-component in the rotor flux of the machine is fixed to the rotor and will continue rotating, adding an alternating component to the dc-component of the stator flux. The maximum value that the currents reach depends mainly on the dip depth and the stator and rotor leakage inductance. How fast the dc-component will decay is mainly determined by the transient time constants of the stator and rotor, given by (D.14) and (D.15).

The voltage dip will cause large (oscillating) currents in the rotor circuit of the DFIG to which the PEC is connected. A high rotor voltage will be needed to control the rotor current. When this required voltage exceeds the maximum voltage of the converter, it is not possible any longer to control the current as desired. This implies that a voltage dip can cause high induced voltages or currents in the rotor circuit that can destroy the PEC.

In order to avoid breakdown of the converter switches there should be a by-pass for the rotor currents in case of a voltage dip. This can be achieved by connecting a set of resistors to the rotor winding via bi-directional thyristors, as shown in Fig. 5.12. When the rotor currents become too high the thyristors are fired and the high currents do not flow through the converter but into the by-pass resistors. Meanwhile it is not necessary to disconnect the converter from the rotor or the grid. Because generator and converter stay connected, the synchronism of operation remains established during the fault.

When the fault in the grid is cleared, or the dc offset in voltage and current has decayed far enough, the resistors can be disconnected by inhibiting the gating signals of the thyristors and the generator can resume normal operation. A control strategy has been developed that takes care of the transition back to normal operation. Without special control action large transients would occur. During the period that the resistors are connected to the rotor circuit the controller signal should be limited in a small band around the values they had at the moment that the fault occurred. The controllers will try to control the currents, the power, the rotational speed and so on to the reference values. This is not possible however as long as the by-pass resistors are connected to the rotor circuit. When the signals are not limited large overshoot in the signals will occur.
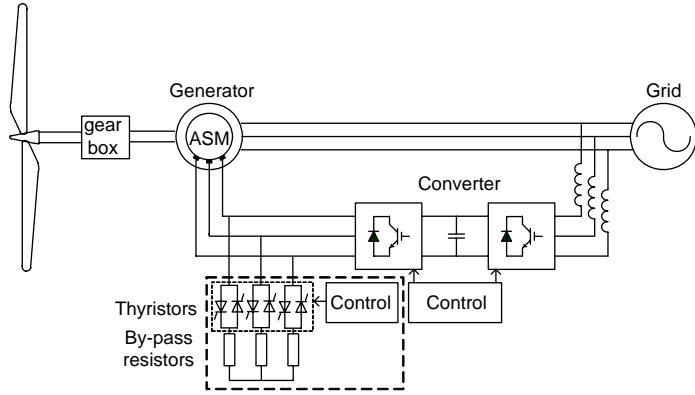
Fig. 5.12. DFIG by-pass resistors in the rotor circuit

5.6.3 Short-circuit current and by-pass resistor value

This subsection will derive an (approximate) equation for the stator and rotor currents of the DFIG during a fault. The fault current supplied to the grid is important to know for grid operators. When the value is known it is also possible to determine a good value for the by-pass resistors. To derive an (approximate) equation for the short-circuit current supplied by the DFIG the equations derived for the induction machine will be used (see appendix D). Two important assumptions that are made during the analysis of the induction machine are not valid for a DFIG. The first is that when the by-pass resistors are connected to the rotor in case of a fault, the resistance no longer can be neglected. The second is that the slip of a DFIG is not always close to zero, as is the case for an induction machine. The consequences of these differences for the short-circuit behaviour of the DFIG will be described in this section. A worst-case analysis will be done, which assumes that a short-circuit occurs at the stator of the machine and that the turbine operates at full power.

The maximum stator current of an induction machine in case of a short-circuit at the stator terminals is given by (D.25):

$$i_{s,\max} = \frac{\sqrt{2}V_s}{X_s^{'}}\left[e^{-\frac{T}{2T_s^{'}}} + \left(1-\sigma\right)e^{-\frac{T}{2T_r^{'}}}\right]\tag{5.8}$$

with X_s' the transient stator reactance, σ the leakage factor, T the period of the grid frequency, and T_s' and T_r' the transient time constants of the stator and rotor respectively. All parameters are defined in appendix D. The equation was obtained in two steps. First the term outside the rectangular brackets was determined. It represents the initial value of the current prior to the fault. In the next step the two terms inside the

brackets were determined. They represent the damping of the dc-components in the stator and rotor flux respectively.

The initial value of the current is determined under the assumption that the stator and rotor resistance can be neglected. When the by-pass resistors are connected in cause of a fault this assumption is no longer valid. This implies that (D.16) becomes:

$$I_s e^{j\omega_s t} = \frac{V_s e^{j\omega_s t}}{jX_s + R_{bp}}$$
(5.9)

and that the transient time constant of the rotor becomes:

$$T_r^{'} = \frac{L_r^{'}}{R_r^{'} + R_{bp}^{'}}$$
(5.10)

with $R_{bp}^{'}$ the resistance of the by-pass resistors, reduced on the stator side.

The two exponential functions inside the brackets in (5.8) are based on the assumption that the rotor and stator flux are 180° out of phase after half a period, implying that the current reaches its maximum value at at $t = T/2$. This assumption is approximately valid for an induction machine where the slip is small and where the stator and rotor flux are approximately in phase with each other, at the moment that the fault occurs. A doubly-fed induction generator can operate at a much larger slip however. This implies that at the moment of the fault the two flux vectors are not in phase with each other. When the DFIG is in over-synchronous mode the rotor flux will lead the stator flux and it will take less than half a period before the two fluxes are 180° out of phase (which gives the maximum current, see appendix D). When the DFIG is in under-synchronous mode, the opposite holds and it will take more than half a period.

When the voltage at the stator terminals drops to zero, the stator and rotor flux vector stop rotating, as explained in appendix D. In reality they will rotate slowly, depending on the stator and rotor resistance. The larger the resistance the faster they rotate. For an induction machine this rotation can be neglected because of the small resistance. For a DFIG with by-pass resistors the rotation is no longer negligible. This is another reason why it can take less than half a period before the first peak in the current is reached.

Taking into account these differences between an induction machine and a doubly-fed induction generator, (5.8) becomes:

$$i_{s,\max} = \frac{\sqrt{2}V_s}{\sqrt{X_s^{'2} + R_{bp}^{'2}}} \left[e^{-\frac{\Delta t}{T_s^{''}}} + (1-\sigma)e^{-\frac{\Delta t}{T_r^{'}}} \right]$$
(5.11)

where Δt gives the time after which the current reaches its first peak. It is dependent on the slip of the machine and the value of the by-pass resistors. For small by-pass resistor values, ($R'_{bp} \leq X'_s$), this equation showed to give a good approximation of the maximum current. For large resistance values it gives a too low value.

A larger by-pass resistance will result in a smaller T_r'. At the same moment Δt decreases. As a result the term inside the brackets in (5.11) stays approximately constant. As a rough approximation the maximum stator current is then given as:

$$i_{s,max} \approx \frac{2.4V_s}{\sqrt{X_s'^2 + R_{bp}'^2}} \tag{5.12}$$

The last part of this subsection describes how a good value for the by-pass resistance can be determined. On one hand the resistance should be high, to limit the short-circuit current. On the other hand it should be low to avoid a too high voltage in the rotor circuit. A too high voltage can result in breakdown of the isolation material of the rotor and the converter. It is further possible that when the voltage becomes higher than the dc-link voltage, large currents will flow through the anti-parallel diodes of the converter, charging the dc-link to an unacceptable high voltage. The thermal time constant of the rotor will be high enough to handle the short-circuit currents for a short period and the by-pass resistors should be designed for it.

An approximation of the maximum stator current is given by (5.12). As all parameters are transferred to the stator side, the maximum rotor current (reduced on the stator side) will have approximately the same value. The voltage across the by-pass resistors, and thus across the rotor and converter is:

$$\sqrt{2}V_r \approx R'_{bp}i'_{r,max} \tag{5.13}$$

Combining this with (5.12) the maximum value of the by-pass resistors can be determined:

$$R'_{bp} < \frac{\sqrt{2}V_{r,max}X'_s}{\sqrt{5.8V_s^2 - 2V_{r,max}^2}} \tag{5.14}$$

with $V_{r,max}$ the maximum allowable rotor voltage. Note that it only is an approximation, as it is based on a number of assumptions and approximations.

The minimum value is determined by the maximum current that is allowed in the rotor circuit of the induction generator or by the maximum value of stator short-circuit current that is allowed.

5.6.4 Simulation results

In order to show the effectiveness of the protection scheme, some simulation results will be presented. A model has been used in which the DFIG is connected to node 4 of the Testnet. Data of a 2.75 MW wind turbine with doubly-fed induction generator has been used for the simulations. The wind turbine model and the parameters are given in appendix B. The by-pass thyristors are activated when the rotor current exceeds 1.1 p.u. All values are referred to the stator with the nominal generator power and voltage as the base values. The maximum allowable rotor voltage is 0.35 p.u. The transient stator inductance is 0.2 p.u. The maximum value of the by-pass resistors is obtained from (5.14) as 0.06 p.u. A value of 0.05 p.u. is used.

In the first place the behaviour of the DFIG during a voltage dip of 85% (15% remaining voltage) and 200 ms is simulated. The stator voltage and current are shown in Fig. 5.13a and b and the rotor voltage and current are shown in Fig. 5.13c and d, respectively. A large peak in the stator and rotor current can be noted. The rotor current is not flowing through the converter however, but in the by-pass resistors. The power that is consumed by the resistors is shown in Fig. 5.13e. The rotor voltage oscillates to ~0.3 p.u. This is slightly below the maximum rotor voltage of 0.35 p.u. Due to the drop in stator power, the wind turbine will accelerate. Because of the large inertia of the wind turbine rotor the increase in rotational speed is limited however, as can be seen from Fig. 5.13f. When the dip lasts longer eventually the pitch controller can be used to reduce the aerodynamic power and to limit the increase in rotational speed.

After ~50 ms the by-pass resistors are disconnected and the DFIG can resume normal operation (at a lower voltage). The clearance of the voltage dip results again in high oscillating currents and the by-pass resistors will be turned on again to protect the converter. After the current has decayed far enough the resistors are disconnected again and the turbine can resume normal operation.

By appropriate control the wind turbine can supply reactive power during the dip, as is demanded by some grid connection requirements for wind turbines (see Fig. 5.5). When the by-pass resistors are de-activated the turbine can resume normal operation and supply reactive power. This will be shown in an example. The same network and wind turbine as in the previous example are used. Now a 50% - 1 s dip is applied. The stator voltage is shown in Fig. 5.14a and the active and reactive power supplied by the DFIG are shown in Fig. 5.14b and c respectively. It can be seen that ~0.25 p.u. reactive power is supplied, while the generator is still supplying ~0.5 p.u. active power. When more reactive power has to be supplied, the active power should be reduced, or a higher current should be allowed. Fig. 5.14d shows the rotor current. During the dip it is 1 p.u. The rotor voltage is shown in Fig. 5.14e and the rotational speed is shown in Fig. 5.14f.

Large reactive power peaks can be noted at the occurrence and clearance of the fault. They are cause by the (de-)magnetizing of the machine. The large amount of reactive power that is absorbed immediately after fault clearance may cause voltage stability problems and in a further study it should be investigated how it can be limited.
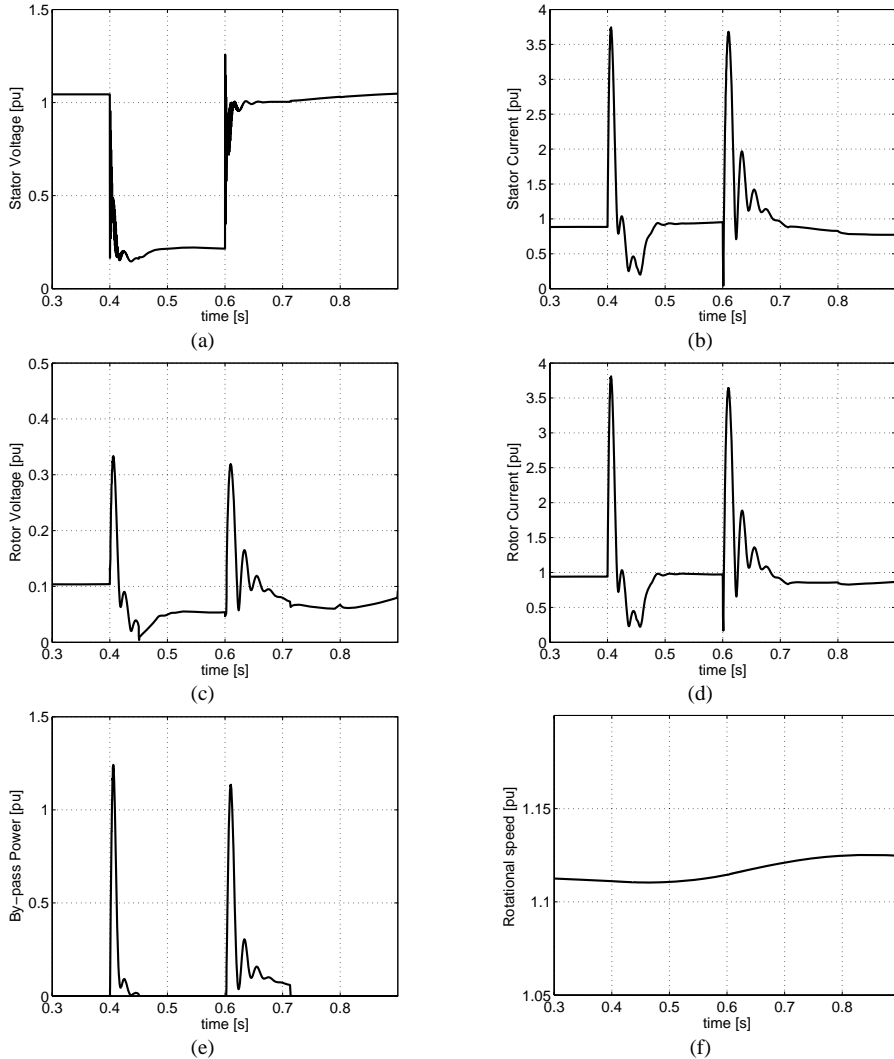
Fig. 5.13. Voltage dip of 85%, 0.2 s applied to DFIG with protection: (a) stator voltage; (b) stator current; (c) rotor voltage; (d) rotor current; (e) power consumed in by-pass resistors; (f) rotational speed of generator
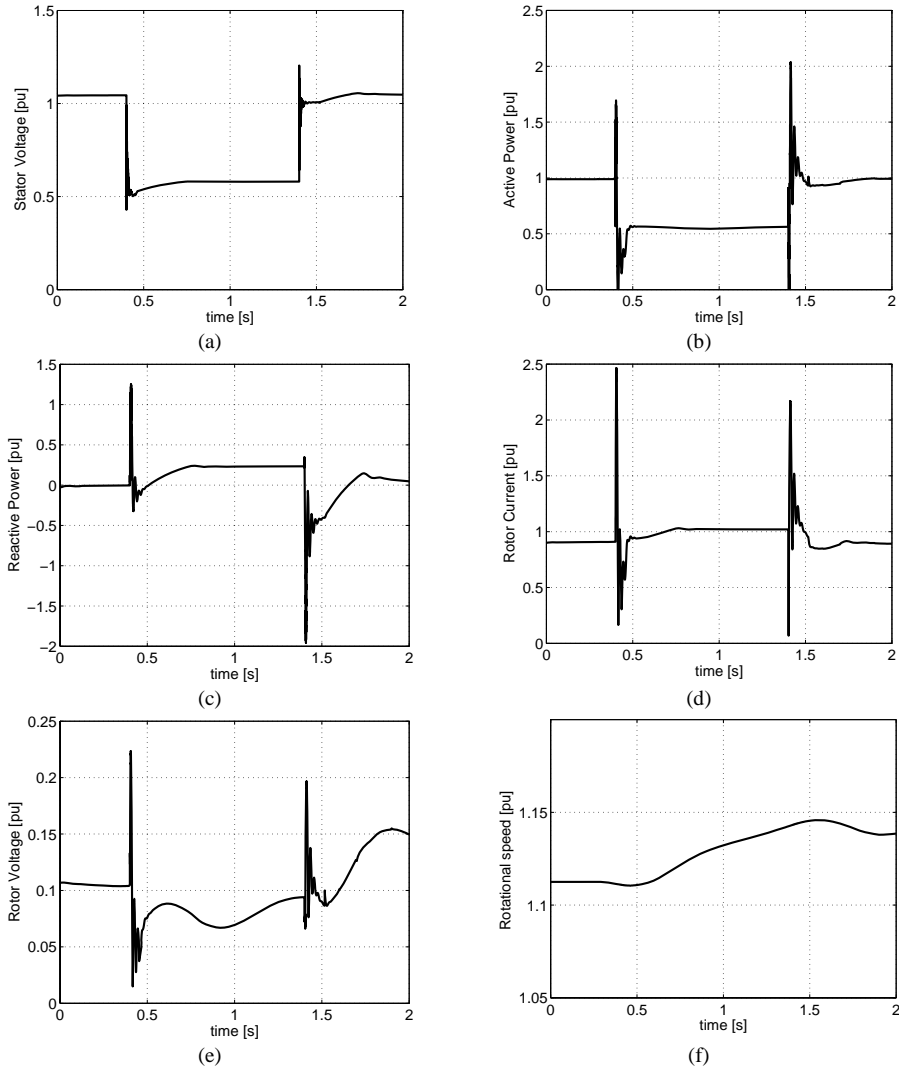
Fig. 5.14. Voltage dip of 50%, 1 s applied to DFIG with protection: (a) stator voltage; (b) DFIG active power; (c) DFIG reactive power; (d) rotor current; (e) rotor voltage; (f) rotational speed

5.7 Conclusion

Most distribution network operators require the disconnection of DG units when faults occur in the network. One reason for this requirement is that they fear that DG units disturb the classical protection schemes that are applied. It has been shown in this

chapter that disturbance of protection not necessarily occurs when power electronic interfaced DG units are controlled properly.

When DG units stay connected during faults, they can support the grid during a voltage dip. For some larger DG units directly connected to the transmission network this is often required already [E.On 03]. Voltage dips occur for a short period only. Overloading of a converter will mostly be possible for this short period. In combination with a variable inductance a significant reduction in dip depth can be achieved. It should be noted however, that in some cases the variable inductance can reduce the short-circuit current that flows in the network, causing blinding of protection. Before implementation of a variable inductance this issue should be considered.

In the last two sections of this chapter it has been shown that there are generally no problems to keep DG units connected to the grid during voltage dips. In case of a wind turbine with a doubly-fed induction generator some special measures have to be taken. The key of the technique is to provide a by-pass for the high currents in the rotor circuit with a set of resistors, without disconnecting the converter from the rotor or the grid. The wind turbine can resume normal operation when the voltage and current oscillations have decayed enough (generally within a few hundred milliseconds). In this way the turbine can supply reactive power to the grid during a voltage dip.

The short-circuits and the proposed protection techniques can result in large torque fluctuations in the gearbox of variable speed wind turbines. This important issue falls outside the scope of this thesis, but requires further attention.

92

Chapter 6

Frequency-control contribution of DG units

6.1 Introduction

In electrical power systems there must always be an equilibrium between the power that is generated and the power that is consumed, as there is hardly energy storage. An imbalance manifests itself by changes in the frequency, which arise from a change in kinetic energy of the rotating masses. For satisfactory operation of electrical power systems the frequency should remain as constant as possible. There are continuously small variations in the power balance due to variations in generation and load. Due to the large inertia of the synchronous generators in the grid, the frequency fluctuations are small. Larger variations are mostly due to disturbances such as short-circuits, which can result in opening of circuit breakers and loss of generation or load. Frequency changes are observed by all power stations and they respond by changing the power of their prime mover.

At this moment DG units do not contribute to frequency control and most DG units do not have inertia. An increasing penetration level of DG can therefore result in larger frequency deviations. This issue did not receive much attention so far. Some publications mention that most DG units are connected to the grid by power electronic converters (PECs), which have no inertia [Kna 04], [Rez 05]. Some other papers determined the inertia contribution of wind turbines [Eka 04], [Lal 04], [Lal 05], [Mul 05a].

The goal of this chapter is to investigate how and to what extent (combinations of different) DG units can contribute to frequency control. The chapter begins with a review of the response of a conventional power system to load imbalances and frequency deviations and then continues with a description of the conventional frequency control. Section 6.3 briefly describes the effect that different types of DG unit have on frequency control. In section 6.4 a method is derived to determine upper and lower boundaries for the penetration level of different types of DG unit. When DG units have to contribute to frequency control, they should be able to increase their output power. For generators based on renewable energy sources this is generally not possible,

as they operate at the maximum available power. Section 6.5 investigates if and how (fast) DG units can increase their output power. The proposed solutions are demonstrated with a case study simulation in section 6.6.

6.2 Classical power-frequency control

6.2.1 Introduction
The response of the power system and the synchronous generators to a change in power balance, together with the resulting frequency deviations can be divided into three phases.

In the first phase, when controllers have not yet been activated, the rotor of the synchronous generators releases or absorbs kinetic energy; as a result, the frequency changes. The response is mainly determined by the equation-of-movement of the system and is called inertial response here, as the inertia dampens the frequency deviations.

When the frequency deviation exceeds a certain limit, controllers are activated to change the power input to the prime movers. This is the second phase, the primary frequency control.

After restoration of the power balance there is still a steady-state frequency deviation. In the third phase, secondary frequency control, the frequency is brought back to its nominal value.

6.2.2 Inertial response
The power generated in a power system preferably matches the load power at all times. Initially, in order to avoid excessive control action, there is no control response to small imbalances. Therefore imbalance between generation and load will result in a change in frequency. The initial rate of change is determined by the system dynamics [Sac 03]:

$$\frac{d\left(\frac{1}{2}J\omega_e^2\right)}{dt} = P_g - P_l \tag{6.1}$$

with P_g being the power that is generated, P_l the power that is demanded by the loads, J the total inertia of the system and ω_e the grid frequency. The left-hand side of (6.1) is the derivative of the kinetic energy stored in the rotational mass of the generator. As a measure for this kinetic energy, in relation to the power rating, the so-called inertia constant H is often used, which is defined as:

$$H = \frac{J\omega_e^2}{2S} \tag{6.2}$$

with S being the nominal apparent power of the system. The inertia constant has the dimension time and gives an indication of the time that the system can provide nominal power by using only the energy stored in its rotating masses. Typical inertia constants for the generators of large power plants fall in the range of $2 - 9$ s, depending on both the type of power plant in which they are used and their nominal rotational speed [Gra 94]. A minimal value of H is necessary to avoid too large fluctuations in frequency.

6.2.3 Primary control

An imbalance between generated and consumed power will result in a change in the frequency. When this frequency deviation becomes too large, controllers are activated. These controllers adapt the amount of prime power in order to restore the power balance. Actually they control the speed of the turbine. The primary-control contribution of the generators is based on their so-called droop constant, which gives the additional power that is be supplied as a function of the frequency deviation:

$$\Delta P_G = -K_{pfc}\Delta f \tag{6.3}$$

The percentage of change in power as a function of the percentage of change in frequency for a generator, or a whole network, is often given by the so-called droop:

$$D_{pfc} = \frac{-\Delta f / f_{nom}}{\Delta P_G / P_{G,nom}} \cdot 100\% \tag{6.4}$$

with f_{nom} the nominal frequency, ΔP_G the change in the output power of the generator and $P_{G,nom}$ the nominal power of the generator. From this equation the droop constant K_{pfc} can be defined as:

$$K_{pfc} = \frac{100 \cdot P_{G,nom}}{D_{pfc} \cdot f_{nom}} \tag{6.5}$$

Fig. 6.1 shows an example of a droop characteristic.
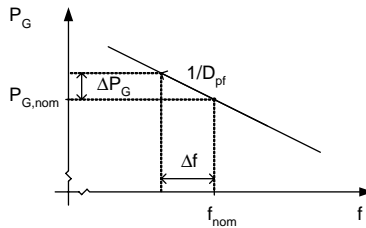
Fig. 6.1. Droop characteristic: Input power from prime mover, P_G, as a function of frequency

Two important parameters are the primary control reserve and the deployment time of the generator. The primary control reserve is, for a certain operational point, the maximum additional power that can be supplied by the generator. It is the difference

between the rated power and the power that is supplied at a given moment. The deployment time is the time that it takes to increase or decrease the output power to the new value. The values for different generators should be in the same range to minimise dynamic interaction [UCT 04]. A typical frequency response, such as might occur when a large generator is disconnected or when a large load is connected to the grid, is shown in Fig. 6.2.
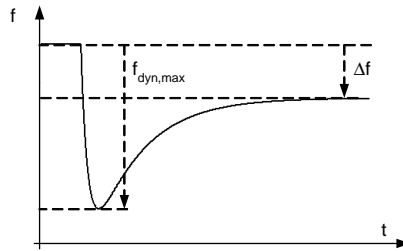
Fig. 6.2. Typical frequency response in a network in which a large generator is disconnected or a large load is connected

The maximum dynamic frequency deviation $f_{dyn,max}$ mainly depends on [UCT 04]:

- the amplitude and development over time of the power disturbance affecting the balance between power output and consumption;
- the kinetic energy of the rotating machines in the system;
- the number of generators subject to primary control, the primary control reserve and its distribution between these generators;
- the dynamic characteristics of the machines (including controllers);
- the dynamic characteristics and particularly the self-regulating effect of loads.

The quasi-steady-state frequency deviation Δf depends on the amplitude of the disturbance and the network power frequency characteristic, which is mainly influenced by [UCT 04]:

- the droop of all generators with primary control in a system;
- the sensitivity of consumption to variations in system frequency.

6.2.4 Secondary control

After the primary control has re-established the frequency, it will generally be different from the reference value. The goal of the secondary control is to bring the frequency back to the reference value (normally 50 Hz). This is done by increasing or decreasing the droop characteristic as shown in Fig. 6.3. As a result of the imbalance the frequency decreases from point 1 to point 2 on the curve and the output power increases correspondingly. In point 2 the system is stable again, but at another frequency. By increasing the entire droop characteristic the frequency can be brought back to its

nominal value, as is shown by the movement from point 2 to point 3. Secondary frequency control is not considered further.
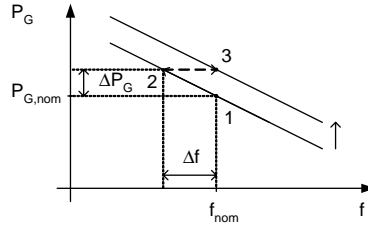
Fig. 6.3. Droop characteristic

6.3 Effect of DG units on frequency response

The response to frequency fluctuations of most DG units is fundamentally different from that of conventional generators. There are two main reasons for this difference. In the first place most types of DG unit have a PEC and therefore do not have an inherent inertial response. Secondly several types of DG unit are driven by an uncontrollable source and therefore they can only partly participate in primary frequency control (they can not increase but only decrease their power on demand).

Considering inertial response and primary frequency control separately, several groups of DG units can be distinguished. With respect to inertial response the ability to increase the power fast is the most important. In response to a decreasing frequency there are DG units that:

  I.   can increase their output power inherently by releasing kinetic energy (e.g. constant speed wind turbines).
 II.   can increase their output power fast (e.g. micro turbines and variable speed wind turbines (by using their kinetic energy)).
III.   can increase their output power slowly (e.g. fuel cells) or not (e.g. solar cells).

With respect to primary frequency control there are DG units that:

 IV.   are driven by a controllable power source (e.g. fuel cells and micro turbines).
  V.   are driven by an uncontrollable power source (e.g. solar cells and wind turbines).

In reality the distinction between the different groups will not be as strict as presented here. Often the changes are gradual. Photovoltaic systems for example often have a small amount of energy stored in their dc-link capacitor, which they can use to increase their output power for a short period. There are also DG units that belong in different groups, such as a micro turbine, which has a rotating machine (group II) and is driven by a controllable source (group IV).

DG units of group I have an inherent inertial response. The extent of their contribution to the inertia constant depends on the type and size of the machine. The DG units of group II have no inherent inertial response, but they have kinetic energy in their rotating mass, which they can use to increase their output power quickly. By implementing an additional control loop, it is possible to make this 'hidden inertia' available to the grid, as will be explained later. No contribution to inertial response is possible with the DG units in group III unless they are driven by controllable sources whose power can be changed rapidly.

Participation in primary frequency control is possible for the DG units in group IV as long as they have a primary control reserve margin (i.e., when they are not working at full power yet). At first sight DG units of group V are not able to participate in primary frequency control as they cannot control their prime energy source; however, it will be shown later that in some cases some of them can have a small contribution.

The introduction of DG units results in a mix of different generator types (conventional and DG). The response of this mix to load changes is different from the conventional system. For example, it can be expected that the primary control reserve of the system will decrease, resulting in larger frequency deviations during disturbances. The reduction of the inertia will result in larger and faster frequency fluctuations.

In this chapter a method to analyse the influence of DG units on the inertial response and the primary frequency control of the grid is developed. This method can also be used to synthesise a group with different combinations of DG units such that the mentioned control still works.

The method to determine and synthesise the response on system level is based on a summation of the individual responses. At system level the inertial response to a change in load change is determined primarily by the total (emulated) inertia of the system including DG units. The primary frequency control response to a load change is at system level primarily determined by the total primary control reserve that is available from both the conventional generators and the DG units.

In order to be able to determine the above-mentioned responses it is necessary to know for each type of DG unit:

- the behaviour that is inherent to its physical (construction) properties.
- its ability to increase its stationary power and the associated dynamics.
- the size of its (emulated) inertia.

Some DG units that do not have inertia or whose inertia is decoupled from the grid can be given an artificial inertia. Within certain limits this inertia can be chosen freely. The inertia obtained in this way is called 'emulated inertia'.

A description of the DG units and their responses is given in section 6.5. First section 6.4 describes a method to obtain a good mix of types of DG unit.

6.4 Method

In this section a method will be developed that can be used to analyse if and to what extent the inertial response and primary frequency control still work properly, with an increasing percentage of DG in the grid. Besides that a method will be developed that can be used to synthesise a group with different combinations of DG units (eventually with additional control) such that the mentioned control still works.

6.4.1 Primary control

The power P_i, that is generated by a certain generator i is written as the product of its nominal power $P_{nom,i}$ and its thus defined utilisation factor k_i:

$$P_i = k_i P_{nom,i} \tag{6.6}$$

For stable operation of power systems there should always be a balance between the power that is generated and the power that is supplied, thus

$$\sum_{i=1}^{N} k_i P_{nom,i} = \sum_{i=1}^{M} P_{load,i} \tag{6.7}$$

with $P_{load,i}$ the power consumed by load i.

In order to be able to contribute to primary frequency control DG units should have an utilisation margin Δk_i in which the utilisation factor can be increased in case of disturbances. The power margin $\Delta k_i P_{nom,i}$ can be considered as an equivalent of the primary control reserve of conventional power plants. It is different for different types of DG unit. For photovoltaic systems operating at their maximum power point for example, Δk_i is zero. For DG units which can control their prime energy source, such as for example fuel cells, it is $1-k_i$.

The total available power margin should at least be equal to the maximal change in power due to a disturbance, $P_{dist,max}$, that can be expected

$$\sum_{i=1}^{N} \Delta k_i P_{nom,i} \geq P_{dist,\max} \tag{6.8}$$

The maximum change in power that can occur is mostly the sudden disconnection of the largest generator (or interconnection) in a network, or the connection of the largest load. For instance in a grid with a large percentage of renewable generators it might be

impossible to fulfil the requirement of (6.8). Other DG units, such a for example micro turbines, might bridge the gap however.

The equations are used to determine how the actual power in a network can be spread over DG units and conventional power plants, such that the maintained primary control reserve (power margin) is large enough to re-establish the power balance after the largest possible disturbance. Some examples for networks with fuel cells (or more general: DG units of group IV) and wind turbines (or more general: DG units of group V) will be given.

In the first example requirements are given for the minimal required fuel cell utilization margin Δk_{fc}. The utilization margin of the conventional generator is set to 0.1 and the utilization margin of the wind turbine to zero. The maximum disturbance that can occur is a 10% increase in load power. The result is shown in Fig. 6.4a. For a given load power it is analysed how the generation can be spread over fuel cells (P_{fc}), wind turbines (P_{wt}) and conventional generators (P_c). For each combination of P_{fc}, P_{wt}, and P_c it is calculated what should be the minimal value of Δk_{fc}, such that the system is able to re-establish the power balance after the maximum disturbance. The regions in the figure correspond to the minimal required fuel cell utilization margins that are needed to be able to re-establish the power balance. For example for all combinations in the dark gray area the fuel cell utilization margin should be between 0.1 and 0.2. Each point in the triangle represents a certain combination of percentages of the three types. The combination always adds up to 100%. The more close a point is to a certain corner of the triangle, the higher the fraction of the respective generator type is. On the ribs one of the fractions is zero.
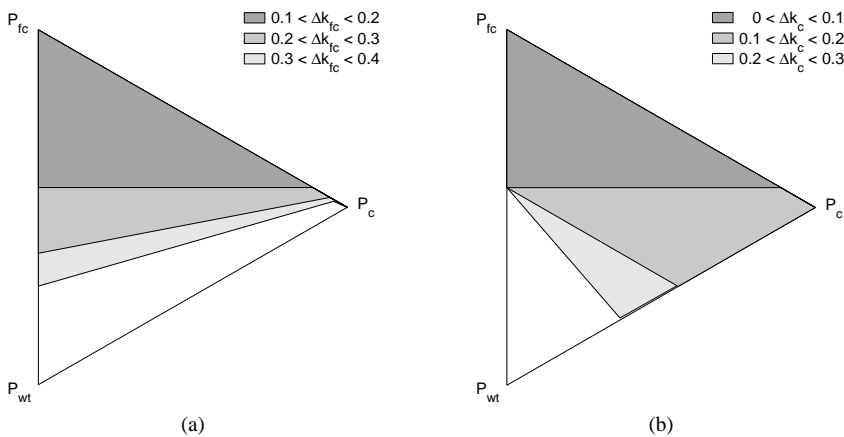

Fig. 6.4. Minimal required utilisation margins for different distributions of the power over fuel cells, wind turbines and conventional generators; (a) required fuel cell margin, $\Delta k_c = 0.1$, $\Delta k_{wt} = 0$; (b) required conventional generator margin, $\Delta k_{fc} = 0.2$, $\Delta k_{wt} = 0$

The same type of diagram is repeated in Fig. 6.4b for a constant value of Δk_{fc} (0.2) and requirements for Δk_c (0.1, 0.2 0.3). Both pictures show that, as expected, the amount of allowable wind power is limited. For increasing utilisation margins, the allowable wind power is also increasing.

The relations in Fig. 6.4a and b are given for conventional generators, fuel cells and wind turbines. They are not limited to those three types however. The fuel cells can be replaced by other DG unit types that have a controllable source, such as for example micro turbines and the wind turbines by other DG units that have a non-controllable source, such as for example solar cells.So far a relation has been laid down between the actual powers of the three generator types. It is also possible to derive requirements for the minimal installed capacity of a certain type of generator. In the next example a relation is obtained for the minimal required installed capacity of fuel cells as a function of the installed capacity of wind turbines. As wind turbines can not contribute to primary frequency control, it is required in this example that fuel cell power has to be installed to provide the primary frequency control contribution of the wind turbines. It is required that the per unit contribution to primary frequency control of wind turbines and fuel cells together is equal to the per unit contribution of the conventional generators. (For example: in a network with 40% DG and 60% conventional, 40% of the additional power that is needed for primary frequency control comes from the DG units and 60% from the conventional generators.)

Fig. 6.5 shows the minimal percentage of installed capacity of fuel cell power that is required as a function of the percentage of actual wind power (both as a percentage of the total installed capacity), for a disturbance that causes a drop in power of 10% of the total installed capacity. The requirements are given for four different values of the minimal utilisation margins which the fuel cells maintain as primary control reserve.
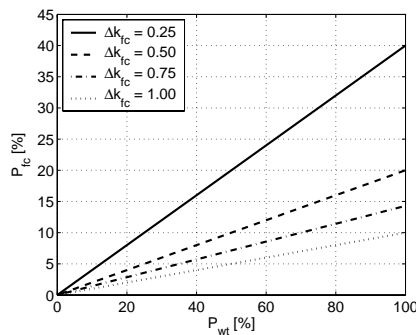
Fig. 6.5. Minimal installed fuel cell capacity (percentage of total generated power) as a function of actual wind power (percentage of total generated power)

In the Netherlands a target of 6 GW of installed wind power has been set. This 6 GW will be about 25% of the total installed capacity. From Fig. 6.5 the minimal required installed fuel cell capacity for 25% wind power can be obtained as 16.7%, 6.3%, 3.8%, and 2.8% for Δk_{fc} is 0.25, 0.5, 0.75, and 1 respectively. When the 6 GW is generated in a low-load situation, it might be much more than 25% of the total power that is generated at that moment. Correspondingly the installed capacity or the maintained utilisation margin of the fuel cells needs to be higher. A possible solution can be to increase the utilisation margin of the fuel cells when the percentage of wind increases.

A similar strategy can be followed to take the changes in wind power as a function of wind speed into account. It is possible to increase the utilisation margin of the fuel cells as a function of the wind speed, as is shown in Fig. 6.6, for three different values of the installed capacity of fuel cells. It is assumed that there is 6 GW of installed wind power.
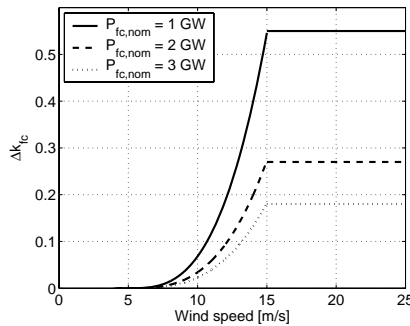
Fig. 6.6. Minimal required fuel cell utilisation margin (primary control reserve) as a function of wind speed for three different values of installed fuel cell power and for 6 GW wind energy

So far it has only been investigated if the primary control reserve is large enough. Another important issue is the implementation of control loops on the DG units. An example of such an implementation, on a fuel cell system, is shown in Fig. 6.7.
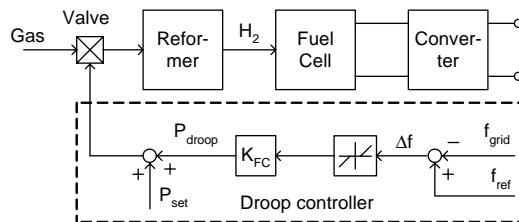
Fig. 6.7. Fuel cell system with droop controller for primary frequency control

The contribution of conventional generators to primary frequency control is determined by their droop constant, as defined in (6.5). The same type of droop control can be implemented on DG unit i:

$$\Delta P_{DG,i} = -K_{DG,i}\Delta f \qquad (6.9)$$

It will now be analysed how the value of $K_{DG,i}$ for each DG unit can be determined. First the total DG power is defined as:

$$P_{DG,tot} = \sum_i P_{DG,i} \qquad (6.10)$$

and the total power of all DG units that can support primary frequency control as:

$$P_{DGpfc,tot} = \sum_j P_{DGpfc,j} \qquad (6.11)$$

In the conventional grid most generators have the same droop. It implies that each of the generators supply the same amount of additional power (as a percentage of the nominal power), when the frequency changes. As has been discussed, not all DG units can contribute to primary frequency control. A good assumption can be however, that all DG units together should be considered as one 'virtual' power plant. This 'virtual' power plant can be obliged to have the same droop as the conventional generators. The droop is then:

$$D_{pf} = \frac{-\Delta f / f_n}{\Delta P_G / P_{DG,tot}} \cdot 100\% \qquad (6.12)$$

The value of the droop constant $K_{DG,i}$ for a DG unit i that can contribute to primary frequency control can then be defined as:

$$K_{DG,i} = \frac{100 \cdot P_{DG,tot}}{D_{pfc} \cdot f_n} \cdot \frac{P_{DG,i}}{P_{DGpfc,tot}} \qquad (6.13)$$

6.4.2 Inertial response

In the conventional power system the inertial response is by definition the behaviour of the grid without control, i.e. it is behaviour that inherently follows from the structure of generators (and motors) that are directly coupled to the grid. This behaviour will be referred to as 'inherent behaviour'. The dynamics of the grid after a disturbance are given by:

$$\frac{d}{dt}\left(\frac{1}{2} J\omega_g^2\right) = P_{dist} \qquad (6.14)$$

with ω_g the grid frequency and P_{dist} the change in power due to a disturbance. The relation between the kinetic energy stored in the rotating mass of a generator and its rated power is given by the inertia constant H [s]. It is normally defined for a single generator, but can also be defined for a total grid:

$$H_{tot} = \frac{\sum_i \left(\frac{1}{2} J_i \omega_g^2 \right)}{\sum_i P_{nom,i}} \qquad (6.15)$$

The term above the line gives the energy stored in rotating masses which are directly coupled to the grid. With an increasing penetration of DG it is to be expected that the inertia J will decrease, implying that the $d\omega_g/dt$ after disturbances will increase. Several types of DG units have some form of energy storage. This stored energy can be used to emulate inertia. The inertia constant becomes then:

$$H_{tot} = \frac{\sum_j \left(\frac{1}{2} J_j \omega_g^2 \right) + \sum_k E_{DG,stored,k}}{\sum_i P_{nom,i}} \qquad (6.16)$$

with $E_{DG,stored,k}$ the stored energy of DG unit k that does not contribute to the inertia by itself, but that can be used to emulate inertia.

The value of H_{tot} of a grid will determine the initial rate of change of the frequency after a disturbance in the power balance. The equations derived in this section are first used to determine how large the inertia constant of a grid with DG units is (or can be). Afterwards they are used to determine which combinations of DG units and conventional generators are needed to obtain a certain minimal value for H_{tot}. The value of H_{tot} depends on:

- types of DG
- installed capacity of each type
- utilisation margin of each type
- the value of emulated inertia of each type

First two examples are given which show the influence of DG units on the inertia constant of the grid. As a first example Fig. 6.8a shows the inertia constant H_{tot} of a network for an increasing DG penetration and for three different mixes of DG types. It is assumed that the DG units replace conventional power plants, thereby reducing the conventional inertia. The inertia constant drops significantly in case that the DG units only consist of fuel cells (or more general: DG units of group III). When also wind turbines are used instead of fuel cells H_{tot} drops less because wind turbines can emulate inertia [Mor 06]. Fig. 6.8 applies to the case where the inertia constant H of the conventional generators and the wind turbines is 5s for both. This clarifies that H_{tot} does not change when only wind turbines are introduced (dotted line). The rate of change of frequency after a disturbance is determined by the inertia constant of the grid. In the second example it is shown how DG units with emulated inertia can change this rate by emulating extra inertia. Fig. 6.8b shows the rate of change of frequency in a grid as a function of the emulated inertia of the wind turbines. The emulated inertia on the

horizontal axis is divided by the average inertia of the conventional generators, J_{conv}. The figure shows that an increase of inertia-less DG will result in a smaller inertia constant and thus a larger initial rate of change of frequency after the occurrence of a disturbance.
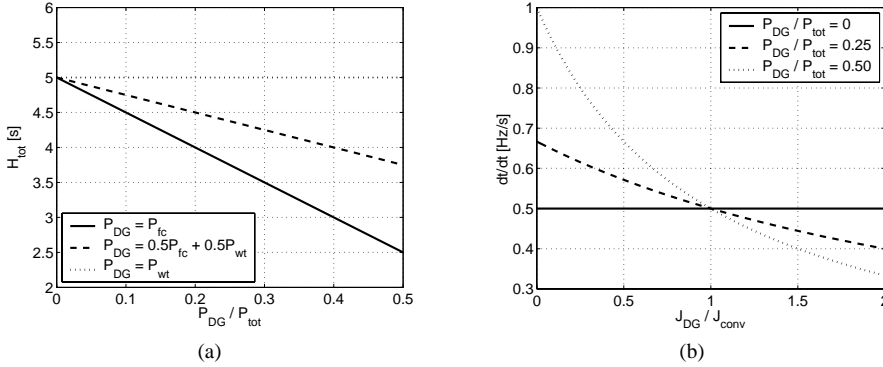
Fig. 6.8. Relation between DG unit power, inertia (constant) and rate of change of frequency; (a) inertia constant of total grid as a function of percentage DG, for different combinations of DG unit types; (b) Rate of change of frequency as a function of emulated inertia J_{emu}, for different DG unit percentages

It is reasonable to assume that there is a lower limit for the inertia constant of the whole grid, as it determines the initial rate of change of frequency after a disturbance:

$$H_{tot} \geq H_{\min} \tag{6.17}$$

with H_{min} for example the average inertia constant of a grid with only conventional generators. Combining this equation with (6.16) gives a lower limit to the minimal amount of energy that should be available for emulating inertia.

An example of possible requirements for a network with conventional generators, fuel cells and wind turbines is given in Fig. 6.9. In this example the conventional generators have an inertia constant of 5 s and the wind turbines have an emulated inertia that corresponds to an inertia constant of 4 s.

Fig. 6.10 shows a DG unit with an additional control loop that emulates inertia. The controller will supply or absorb power according to

$$P_{ine} = J_{emu} \omega_g \frac{d\omega_g}{dt} \tag{6.18}$$

with J_{emu} the emulated inertia. Its value can be chosen freely to some extent, although it is limited by several parameters, such as the rated power of the generator, the time that the power has to be supplied ($E=P \cdot t$) and the speed with which the power has to be increased (dP/dt).
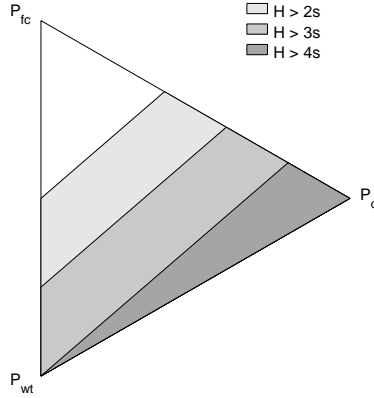
Fig. 6.9. Inertia constant for different combinations of DG unit types (H_c=5s, H_{fc}=0s, H_{wt}=4s)

Normally the speed of the rotating DG unit is controlled. In case of for example micro turbines mostly a constant power is supplied. Renewable generators such as wind turbines have a maximum power point tracking control. In both cases additional power can be subtracted from the kinetic energy of the rotating mass to emulate inertia.

Conventional generators always run at the same speed. Their inertia constant H is independent from the power they supply. This is not the case for most DG units, where the kinetic energy is stored in equipment that rotates at variable speed. Therefore their inertia constant depends on their operating point. In case of a variable speed wind turbine for example, H depends on the actual wind speed. This is discussed in section 6.5.
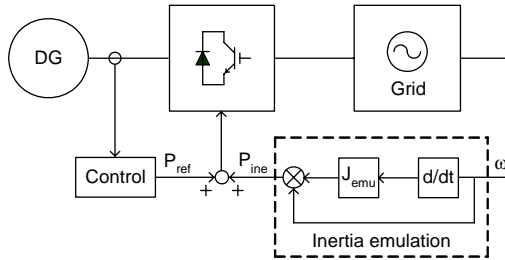
Fig. 6.10. DG unit with control loop that emulates inertia

The last part of this subsection analyses how the value of the emulated inertia J_{emu} of each DG unit can be determined. First the total kinetic energy stored in all DG units together is defined as:

$$E_{DG,stored,tot} = \sum_k E_{DG,stored,k} \tag{6.19}$$

and the relation between the emulated inertia J_{emu} and the kinetic energy of DG unit k as:

$$E_{DG,stored,k} = \frac{1}{2} J_{emu,k} \omega_g^2 \qquad (6.20)$$

It is assumed that the inertia of each DG unit should be proportional to the amount of kinetic energy stored in that DG unit. The equation for the average inertia constant of the total grid, H_{tot}, is given in (6.16). It can be rewritten as:

$$\frac{1}{2} \omega_g^2 \sum_k J_{emu,k} = H_{tot} \cdot \sum_i P_{nom,i} - \sum_j \left(\frac{1}{2} J_j \omega_g^2 \right) \qquad (6.21)$$

Combining (6.19)-(6.21) the value of the emulated inertia for DG unit k is:

$$J_{emu,k} = \frac{2 \cdot H_{tot} \cdot \sum_i P_{nom,i} - \sum_j \left(J_j \omega_g^2 \right)}{\omega_g^2} \cdot \frac{E_{DG,stored,k}}{E_{DG,stored,tot}} \qquad (6.22)$$

6.4.3 Mix Requirements (or: 'Equivalent power plants')

The 2 previous subsections investigated how DG units can contribute to inertial response and primary frequency control. In this subsection this distinction is left behind and it is investigated how a mix of different DG unit types can contribute to frequency control. Requirements for the ratios between the different types will be derived.

In a conventional grid there is a strict distinction between inertial response and primary frequency control. Inertial response is the behaviour that inherently follows from the structure of directly coupled machinery to the grid. It only depends on the dynamic characteristics of the grid and not on the controllers. During primary frequency control the response depends on the control that is implemented. With emulated inertia and DG unit contribution the distinction becomes less clear: Control is implemented to emulate inertia. Inertial response is therefore no longer only inherent behaviour, as it was in the conventional grid. Further, the emulated inertia has not necessarily to be obtained from kinetic energy. If the driving source of the DG unit can increase its energy production fast enough, also this energy can be used to emulate inertia.

It is therefore good to abandon the strict distinction between inertial response and primary frequency control. There is actually only one important point when it comes to frequency control: whether there is enough reserve power available to maintain the power balance. In the conventional grid inertia is only necessary because the mechanical power of the large conventional generators can not be changed fast enough. Therefore the kinetic energy is used to instantaneously restore the power balance. The main goal is to maintain the power balance. In the conventional grid this is done by first using kinetic energy (which is fast) and then using mechanical power (which is slower).

For DG units a distinction will be made between those that can change their output power fast and those that have a slower response and between DG units that have a controllable power source and DG units that have a non-controllable power source, as discussed in section 5.3. Fuel cells, for example, can change their output power. The speed with which this can be done is limited however (as long as no hydrogen storage is used). Variable speed wind turbine, on the contrary, can increase their output power very fast by tapping their kinetic energy. They can supply power during the period that the fuel cell power is increasing. In this way fuel cells and wind turbines can be complementary to each other. The wind turbines use kinetic energy however. After their contribution, their output power is reduced in order to let the wind turbine speed up to its original value. This means that the other generators in the grid have to compensate for this drop in power. An example of a possible combination of responses is shown in Fig. 6.11.
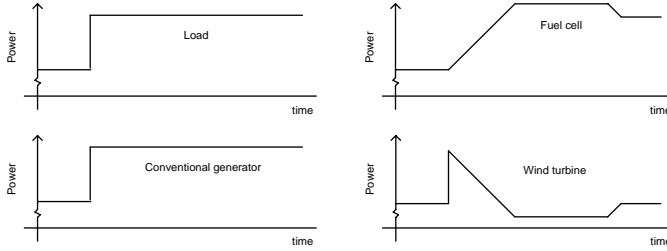
Fig. 6.11. Increase in power; load power (upper left); conventional generator power (lower left); fuel cell power (upper right); wind turbine power (lower left)

During the analyses the DG units are considered as a group: an 'equivalent power plant'. The droop of the equivalent power plant is chosen equal to that of the conventional generators. The change of DG power after a change in power due to a disturbance, P_{dist}, should be:

$$\Delta P_{DG} = PL \cdot P_{dist} \tag{6.23}$$

with PL the penetration level of DG units, which is defined as:

$$PL = \frac{P_{DG,nom}}{P_{DG,nom} + P_{conv,nom}} \tag{6.24}$$

with $P_{DG,nom}$ the sum of the nominal powers of all DG units and $P_{conv,nom}$ the sum of the nominal powers of all conventional generators. Three different DG unit types are considered: fuel cell, micro turbine, and wind turbine. They represent the most important types and it is assumed that other types are comparable to one of these three. They also represent most of the groups that have been defined in section 6.3.

Variable speed wind turbines are driven by an uncontrollable power source (group V). They cannot contribute to primary frequency control. The fuel cells and micro turbines have to provide the steady-state contribution for all DG units together. Therefore their utilisation margin has to be large enough:

$$\Delta k_{fc} P_{fc,nom} + \Delta k_{mt} P_{mt,nom} \geq PL \cdot P_{dist,\max} \tag{6.25}$$

where Δk_{fc} and Δk_{mt} give the utilisation margin of the fuel cell and the micro turbine respectively. (Actually this is the same as their primary control reserve.)

The power balance has to be restored immediately. Some DG units that can provide a steady-state contribution are not fast enough to restore the balance immediately. This has to be done by the fast DG units and the DG units that have kinetic energy available. The maximum power that has to be supplied in this phase is therefore equal to the maximum change in power due to a disturbance. Fuel cells can not contribute to inertial response, as they can change the power of their source only slowly. Therefore during this phase:

$$\Delta k_{mt} P_{mt,nom} + \Delta k_{wt} P_{wt} \geq PL \cdot P_{dist,\max} \tag{6.26}$$

The relations of (6.25) and (6.26) can be represented graphically. An example is given in Fig. 6.12. It is assumed that the utilisation margins of the three types of DG unit are the same. For three different values of the utilisation margin the allowed value of fuel cell, micro turbine and wind turbine power are shown in the figure.
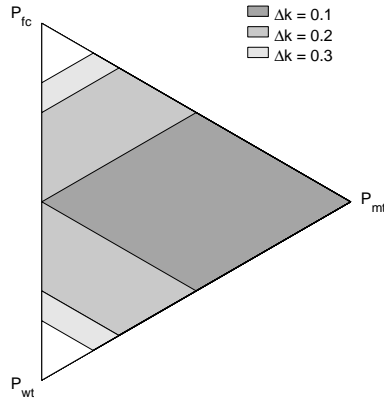
Fig. 6.12. Allowable range of fuel cell, micro turbine and wind turbine power for different utilisation margins and $PL = 0.5$

The requirements are for a case that the maximum drop in load is 10%. The figure shows that micro turbines are always able to control the frequency correctly. When wind turbines or fuel cells form 100% of all DG correct control is not possible. They should always be used in combination with each other or in combination with micro

turbines. The figure shows further that larger percentages of fuel cells and wind turbines are possible, when the utilisation margin increases.

6.5 DG unit contribution to inertia and primary frequency control

In order to be able to analyse the ability of DG units to contribute to inertial response and primary frequency control some basic properties and capabilities of the DG units have to be known. Especially important are the ability to increase the stationary power and the dynamics associated with it and the size of the (emulated) inertia. This section describes the characteristics of three different DG unit types:

- Wind turbine
- Micro turbine
- Fuel cell

Solar cells will not be considered as they have no possibility at all to increase their output power. Other types of DG unit will not be considered as they have no PEC or because they are used on a very limited scale only.

First the most important characteristics of the DG units are discussed. At the end of this section the possibilities of the different DG units are summarised in a number of tables.

6.5.1 Wind turbines

The first type of DG unit that is considered is a variable speed wind turbine. The power supplied by the turbine depends on the wind, which is not controllable. Therefore wind turbines can not participate in primary frequency control. The large blades of the turbine give this type of DG unit a significant inertia. For variable speed turbines this inertia is decoupled from the grid by a PEC to enable variable speed operation. It is possible to give the wind turbines an emulated inertia however.

Variable speed wind turbines have a speed controller, which has the task to keep the optimal tip speed ratio λ over different wind speeds, by adapting the steady state generator speed to its reference value. This reference value is normally obtained from a predefined power-speed curve as shown in Fig. 2.6. For low wind speeds the generator speed is kept at a fixed low speed and for wind speeds above the rated value the rotor/generator speed is limited by progressively pitching the blades in order to limit the aerodynamic power. The reference torque is obtained from the predefined static P-ω characteristic. The error between the actual and the reference torque is sent to a PI controller, which gives a setpoint for the current controller of the turbine. In another loop the pitch angle of the turbine is controlled.

Kinetic energy - Wind turbines can use their kinetic energy to provide inertial response. The energy stored in the rotating mass of their blades is given by:

$$E = \frac{1}{2} J \omega_m^2 \tag{6.27}$$

with J the inertia and ω_m the rotational speed of the turbine. In electrical power engineering often the so-called inertia constant H is used:

$$H = \frac{J \omega_m^2}{2S} \tag{6.28}$$

with S the nominal apparent power of the generator. The inertia constant has the dimension time and gives an indication of the time that the generator can provide nominal power by only using the energy stored in its rotating mass. Typical values for wind turbines are about $2 - 6$ s [Knu 05], which is in the same range as the values for conventional generators ($2 - 9$ s). This implies that introduction of wind turbines in the grid does not necessarily reduce the kinetic energy that is available.

The kinetic energy stored in the rotating mass of a wind turbine depends on the rotational speed of the blades (and thus on the wind speed). The operational output power of the wind turbine is proportional to the cube of the wind speed:

$$P_{wt} \sim v_{wind}^3 \tag{6.29}$$

Variable speed wind turbines operate at a constant tip speed ratio λ. This implies that the rotational speed of the turbine is proportional to the wind speed and thus the rotational speed of the wind turbine is proportional to the cube root of the power:

$$\omega_{wt} \sim \sqrt[3]{P_{wt}} \tag{6.30}$$

The rotational speed of the wind turbine varies between $\omega_{wt,min}$ and $\omega_{wt,nom}$. The power at these two points is defined as $P_{var,min}$ and $P_{var,max}$ respectively. When the power increases further the speed is kept constant. The approximate relation between power and rotational speed is then:

$$\omega_{wt} = \sqrt[3]{\frac{P_{wt}}{P_{var,max}}} \, \omega_{wt,nom} \quad \left(P_{var,min} \le P_{wt} \le P_{var,max} \right)$$
$$\omega_{wt} = \omega_{wt,nom} \quad \left(P_{var,max} < P_{wt} \right) \tag{6.31}$$

Combining (6.28) and (6.31) gives the approximated inertia constant of the turbine:

$$H = \frac{J \omega_{wt,nom}^2}{2 P_{nom}} \left(\frac{P_{wt}}{P_{var,max}} \right)^{2/3} \quad \left(P_{var,min} \le P_{wt} \le P_{var,max} \right)$$
$$H = \frac{J \omega_{wt,nom}^2}{2 P_{nom}} \quad \left(P_{var,max} < P_{wt} \right) \tag{6.32}$$

Primary control reserve - Variable speed wind turbines are controlled in a way that they always capture as much power as possible from the wind, as long as the rated wind speed is not reached. For wind speeds higher than nominal, the pitch controller of the variable speed wind turbine is used to limit the power that is captured by the turbine, to avoid overloading of the mechanical and electrical subsystems.

At first sight wind turbines do not have a primary control reserve and therefore they are not able to contribute to primary frequency control. A possibility to give wind turbines a primary control reserve is to let them operate at a working point below the optimal point. This influences their annual power production however. Another method can be applied when the wind speed is above its nominal value. The power output is then limited by the pitch controller. By decreasing the pitch angle more power can be supplied. This results in overloading of the turbine. When this occurs accidentally this will give no problems. This type of control only works for high wind speeds. The two possibilities are further not considered in this thesis.

6.5.2 Micro turbines

Micro turbines can essentially be considered as small versions of conventional gas-fuelled generators. The important differences however are that they run at much higher speeds and are connected to the grid with a PEC. Similar to conventional plants, micro turbines have inertia. It is decoupled from the grid however, and an additional control loop should be implemented to make the inertia available to the grid. As long as the micro turbine is not running at full power, it can participate in primary frequency control.

The response of a micro turbine to a change in torque setpoint is mainly determined by the gas turbine, which, as a simple approximation, can be modelled as a first order transfer function:

$$G_{gt}(s) = \frac{k_{gt}}{\tau_{gt}s + 1} \tag{6.33}$$

The values for the time constant τ_{gt} that are found in literature vary from tens of milliseconds to tens of seconds.

Kinetic energy - In a situation in which power is needed for a short time, or when it is needed fast, it is possible to use the kinetic energy stored in the rotating mass of the turbine and generator. How much kinetic energy is available can easily be calculated from (6.27) and the corresponding inertia constant from (6.28).

Primary control reserve - As long as the micro turbine is not running at full power it can participate in primary frequency control. How much the output power can be

increased depends on the utilisation margin Δk_{mt} of the micro turbine. The maximum possible increase in power ΔP_{mt}, at a certain moment, can therefore be defined as:

$$\Delta P_{mt} = \Delta k_{mt} P_{mt,nom} \tag{6.34}$$

with $P_{mt,nom}$ the nominal power of the micro turbine.

The speed with which the output power can be increased depends on some typical time constants of the gas turbine. The rate of power increase dP_{mt}/dt is:

$$\frac{dP_{mt}}{dt} = \frac{P_{mt,nom}}{\tau_{mt}} \tag{6.35}$$

with τ_{mt} the time constant of the micro turbine, which is a combination of the delays associated with the different processes and flows in the gas turbine. The expression should be used with care; it gives only an approximation.

6.5.3 Fuel cell

Fuel cells are electrochemical devices. Systems for stationary power applications generally consist of three main parts; a reformer which converts the fuel to hydrogen, the fuel cell itself, where the electrochemical processes take place and the power is generated and the power conditioner, which enables grid connection.

Kinetic energy - The electrical response time of fuel cells is generally fast. It is mainly associated with the speed at which the chemical reaction is capable of restoring the charge that has been drained by the load. Most fuel cells have a reformer however, which produces the hydrogen that is necessary for the electrochemical processes. The processes in the reformer are rather slow, because of the time that is needed to change the chemical reaction parameters after a change in the flow of reactants. This limits the rate with which fuel cells can change their output power. Only when there is some form of hydrogen storage, the fuel cell can increase its power quickly.

Primary control reserve - The capability of fuel cells to contribute to frequency control depends on how much and how fast the output power can be increased. The maximum possible increase in power at a certain moment depends on the primary control reserve, Δk_{fc}, of the fuel cell at that moment. The maximum possible increase in power ΔP_{fc}, at a certain moment, can therefore easily be defined as:

$$\Delta P_{fc} = \Delta k_{fc} P_{fc,nom} \tag{6.36}$$

with $P_{fc,nom}$ the nominal power.

The rate with which the output power can be increased depends on some typical time constants of the fuel cell and the reformer. The rate of power increase dP_{fc}/dt is:

$$\frac{dP_{fc}}{dt} = \frac{P_{fc,nom}}{\tau_{fc}}$$

(6.37)

with τ_{fc} the time constant of the fuel cell, which is a combination of the delays in the reformer and the fuel cell itself. Note that this equation only gives an approximation. Most fuel cells have a large time constant and thus the rate with which the fuel cell can increase its power is limited, also limiting the fuel cell contribution to frequency control.

6.5.4. Summary: Primary control reserve, deployment time and inertia

Three different DG units are described in this paragraph, with specific emphasis on their ability to increase their output power on command. This subsection summarises the capabilities of the three units: first their primary control reserve (power margin) is given, then is it summarised how fast they can change their output power, and finally it is investigated how much kinetic energy is available from rotating DG units.

Primary control reserve - The primary control reserve of a micro turbine and a fuel cell, which depends on the operation point and the nominal power of the DG units are given in table 6.1. Wind turbines do not have a primary control reserve as they are not able to increase the mechanical (wind) power.

Table 6.1: Primary control reserve of DG units

Wind turbine	Micro turbine	Fuel cell
0	$\Delta P_{mt} = \Delta k_{mt} P_{mt,nom}$	$\Delta P_{fc} = \Delta k_{fc} P_{fc,nom}$

Rate of change of power – An important issue is the speed with which the power can be changed. The previous sections showed that the speed of change depends on typical time constants of the micro turbine and fuel cell. Some values that were found in literature are given in table 6.2 and 6.3. Both the ramp up and ramp down time are given (if available). There are significant different in the rate of change of power that can be achieved. It is unclear what causes these differences.

Table 6.2: Ramp up and ramp down speed of micro turbine output power

P_{rated} [kW]	dP/dt up (p.u./sec)	dP/dt down (p.u./sec)	Source
30	0.012	0.015	[Yin 01]
75	0.011	0.015	[Yin 01]
100	0.020		[Per 05]
100	2.0		[Nik 05]

Table 6.3: Ramp up and ramp down speed of fuel cell output power

P_{rated} [kW]	dP/dt up (p.u./sec)	dP/dt down (p.u./sec)	Source
5	0.04	0.09	[El-S 04]
100	0.01		[Zhu 02]

Inertia - Wind turbines do not have a control reserve as they can not increase their mechanical power. Micro turbines have a limited speed with which they can increase their power. Both have kinetic energy available however, which can be used to supply power for a short time. This can be done very fast. The rate of change is only limited by the speed of the controllers. The kinetic energy for several wind turbines and micro turbines that have been found in literature are given in the table below.

Table 6.4: Kinetic energy and inertia constant of wind turbines

P_{rated} [MW]	E [MJ]	H [s]	Source
1.5	7	4.7	[Mil 03]
2.0	6	3	[Per 04]
3.7	18.7	5.1	[Mil 03]

Table 6.5: Kinetic energy and inertia constant of micro turbines

P_{rated} [MW]	E [MJ]	H [s]	Source
20	0.2	10	[Jar 02]
250	2.1	8.2	[Zhu 02]
450	1.8	3.9[1]	[Can 01]

[1] It is not clear from the description in the paper whether this is only for the generator, or for the combination of generator and turbine

6.6 Case study

A case study has been done to show the ability of DG units to contribute to frequency control. First the simulation setup will be described. Next the results of the case study are presented.

6.6.1 Simulation setup

The case studies are performed on a model of a small network that consists of a synchronous generator, fuel cells, wind turbines, and loads. A model of the network is shown in Fig. 6.13. *Load 3* is connected to the network to disturb the power balance. Fig. 6.14 shows a schematic block diagram of the simulation setup.
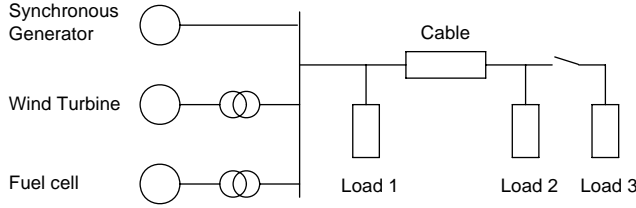
Fig. 6.13. Case study network
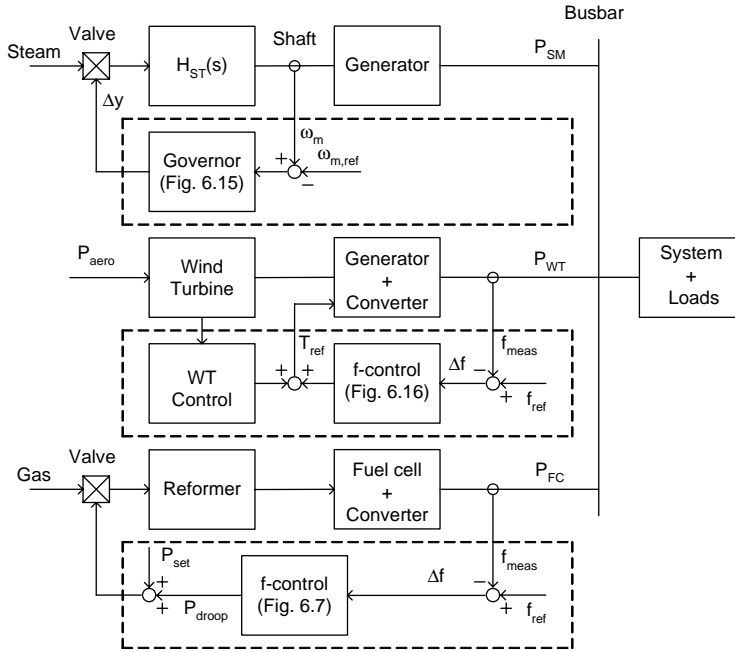
Fig. 6.14. Block diagram of simulation setup

Conventional power plant - The conventional power plant is modelled as a synchronous machine driven by a steam turbine. The synchronous machine is modelled as a three winding representation in *dq* coordinates. The model can be found in [Pie 04]. Damper windings are not taken into account. For the voltage regulator and exciter a so-called type 1 model from [And 77] is used. Primary frequency control is performed by the speed governor shown in Fig. 6.15, which increases or decreases the steam flow to the turbine, depending on the frequency error (ω_m- ω_{ref}). It has a small dead-zone around the nominal frequency.
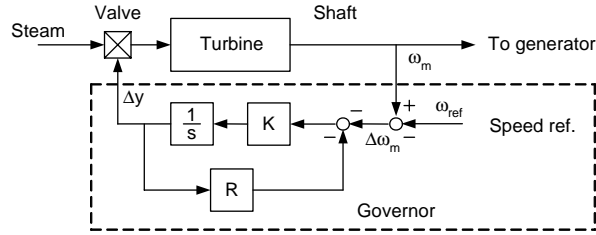
Fig. 6.15. Governor

The reheat steam turbine is modelled as a second order transfer function [Kun 94]:

$$H_{ST}(s) = \frac{1 + sF_{HP}T_{RH}}{(1 + sT_{CH})(1 + sT_{RH})} \tag{6.38}$$

with T_{CH} the time constant of main inlet volumes and steam chest, T_{RH} the time constant of the reheater, and F_{HP} the fraction of total turbine power generated by the high-pressure section. The parameters are obtained from [Kun 94].

Fuel cell – The model of the 100 kW solid-oxide fuel cell (SOFC) that is used is described in appendix C. The fuel cell is connected to the grid with a three-phase voltage source converter. When the fuel cell contributes to primary frequency control, the response of the fuel cell system is mainly determined by the reformer, which can be modelled as a first order transfer function [Zhu 02]:

$$H_R(s) = \frac{1}{1 + sT_R} \tag{6.39}$$

with T_R the time constant of the reformer (5 s). A control loop with a certain droop has been implemented on the system, in order to let it contribute to primary frequency control. The system was already shown in Fig. 6.7.

Wind turbine – The model of the 2.75 MW variable speed wind turbine with doubly-fed induction generator that is used is described in appendix C. Normally the controllers of variable speed wind turbines try to keep the turbine at its optimal speed in order to produce maximum power. The controller gives a torque setpoint that is based on measured speed and power, see Fig. 6.16. An additional controller is implemented that can adapt the torque setpoint to extract power from the rotating mass of the generator, to support primary frequency control. During this support the main dynamics of the turbine are given by the following torque-equation:

$$J \frac{d\omega_{wt}}{dt} = T_a(v_w, \theta, \lambda) - T_e \tag{6.40}$$

with J the inertia and ω_{wt} the rotational speed of the wind turbine, and T_a the aerodynamic torque which depends on the wind speed v_w, the pitch angle θ, and the tip speed ratio λ.

The controller response is chosen in such a way that it complements the power supplied by the fuel cell, such that the sum of their powers is constant. The power increases first to $K_{WT} \cdot \Delta f$ and decreases then with the time constant τ_{fc}, which is the time constant with which the fuel cell output power increases.
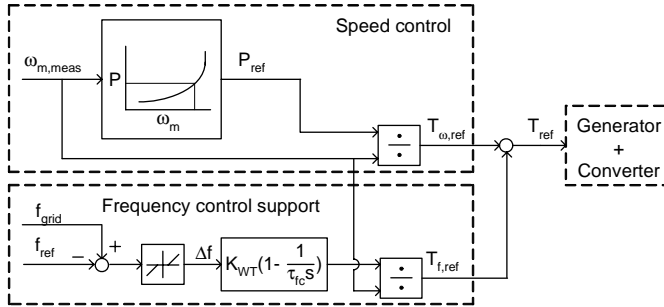
Fig. 6.16. Wind turbine controller; upper branch: maximum power control, lower branch: frequency control support

6.6.2 Parameters

The most important parameters used in the case study are given in table 6.6. Other parameters can be found in the appendices. The total power of the network is small. This is done to be able to see a significant contribution of the DG units, without the necessity to model and simulate a large network. The percentage of wind power in this case study is about 25%. From Fig. 6.5 it can be obtained that the minimal required amount of installed fuel cell capacity should be about 6.5%. The 10% used in this case study should therefore be enough.

The fuel cells and wind turbines are considered together as one equivalent generator. It is required in the case study that the conventional generator and the equivalent generator have the same droop. This strategy is well-known, as it is normally also followed in networks with only conventional generators. It implies that each of the generators supplies the same amount of additional power (as a percentage of their nominal power), when the frequency changes. A droop of 3% has been chosen. The smaller the droop is, the smaller the frequency deviation will be. A droop that is too small can cause instability however.

The value of the droop of the fuel cell has to be much larger than 3% however, as it also has to supply the primary frequency control support of the wind turbines. The droop of the fuel cell is thus given by:

$$D_{FC} = \frac{P_{fc,nom}}{P_{fc,nom} + P_{wt,nom}} \cdot D_{syst} \qquad (6.41)$$

with D_{syst} the droop of the system (3%). Correspondingly the droop of the wind turbine is given by:

$$D_{WT} = \frac{P_{wt,nom}}{P_{wt,nom} + P_{wt,nom}} \cdot D_{syst} \qquad (6.42)$$

With (6.5) the droop constants K_{FC} and K_{WT} can be derived from the droops D_{FC} and D_{WT}. With these equations the values for K that are given in table 6.6 can be calculated. Note that the droop constant of the synchronous machine is given by R, which changes the power setpoint as a function of ω instead of f.

Table 6.6: Parameters for case study

Parameter	Value	Unit	Parameter	Value	Unit
P_{conv}	90	MW	K	$1 \cdot 10^{12}$	W/rad·s^{-1}
$P_{wt,nom}$	27.5	MW	R	$1 \cdot 10^{7}$	W/rad·s^{-1}
$P_{fc,nom}$	10	MW	F_{HP}	0.3	
P_{load1}	10	MW	T_{CH}	0.3	s
P_{load2}	90	MW	T_{RH}	7.0	s
P_{load3}	10	MW	K_{FC}	$2.5 \cdot 10^{7}$	W/Hz
k_{fc}	0.5	-	K_{WT}	$2.5 \cdot 10^{7}$	W/Hz
k_{conv}	0.8	-	τ_{fc}	15	s
k_{w}	0.95	-			

6.6.3 Case study: Frequency control with fuel cells and wind turbines

The case study investigates how fuel cells and wind turbines can work together to contribute to primary frequency control. The fuel cell has a reformer that produces hydrogen from natural gas. The reformer slows down the speed with which the fuel cell power can increase. The wind turbines are used to compensate the slow response of the fuel cells. A load of 10% is suddenly connected to the grid at $t = 5$ s. The load power change is shown in Fig. 6.17a. The frequency response of the network is shown Fig. 6.17b. As a result of the drop in frequency the synchronous generator, the fuel cells, and the wind turbines will increase their output power. Fig. 6.17c shows the power of the synchronous machine. The power of wind turbines and fuel cells together is shown Fig. 6.17d. The output power of the fuel cell and the wind turbine is shown in Fig. 6.17e and Fig. 6.17f respectively.

The power of the fuel cell increases rather slow. The 'gap' is bridged by the wind turbine power however. The speed with which the wind turbine power decreases is

equal to the speed with which the fuel cell power increases. As a result, the combined power stays constant, as can be seen from Fig. 6.17d. The output power of the wind turbine drops below its original value after finishing its frequency control support. This is shown in Fig. 6.17f. The controller determines how large the drop is. The smaller the drop is, the longer the period will be that the power is below its normal value. This drop is compensated by the fuel cell. The deployment time of the wind turbine (the speed with which it increases the power) has been chosen approximately equal to that of the synchronous machine. This gives a better sharing of the power between the conventional generator and the wind turbine.

Oscillations can be seen in the wind turbine power at $t = 5$ s. They are due to the fact that the sudden connection of the load causes a small voltage dip. Although DFIGs are sensitive to voltage dips it can cope with this small dip.
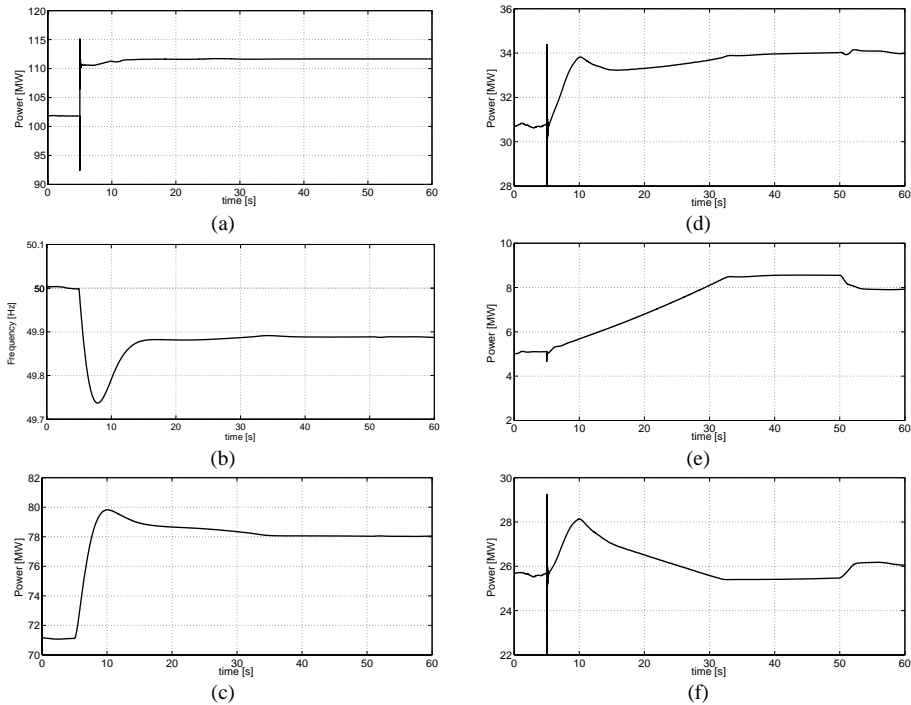
Fig. 6.17. Response of frequency and power to 10% load disturbance at $t = 5$ s: (a) load power; (b) grid frequency; (c) synchronous machine power; (d) combined power of fuel cell and wind turbine; (e) fuel cell power; (f) wind turbine power

6.6.4 Discussion

The case study shows that in principle it is possible to let a combination of DG units contribute to primary frequency control. In the case study only a small network is used.

Some important differences with implementation in a large network are discussed.

In the case studies a percentage of 25% wind power and a load change of 10% have been considered. In a large interconnected system these values will generally be much smaller. Due to the larger inertia in the interconnected power systems the rate of change of frequency will be smaller, which implies that the additional power has to be released slower. Therefore the frequency control will be easier than in small networks. In small (island) networks even more extreme cases might be expected however, especially in low-load situations and high wind speeds. It is possible that a large percentage of the power is generated by wind turbines. At some moment the proposed control no longer works.

Another important issue is the speed with which fuel cells with a reformer can increase their output power. The increase shown in Fig. 6.17 is based on the reformer transfer function that is given in [El-S 04], which is relatively fast. Not all fuel cell system will be able to show this response. With a slower response, the time during which the wind turbines have to supply additional power will also increase. Above a certain fuel cell time constant this will no longer be possible due to the limited amount of kinetic energy that is available.

The primary frequency control re-establishes the power balance at a frequency below 50 Hz, as can be seen from Fig. 6.17b. Secondary frequency control is necessary to bring the frequency back to 50 Hz.

6.7 Summary and conclusion

This chapter investigated which contribution DG units can provide to frequency control. A number of categories are defined for DG units, with respect to their ability to contribute to inertial response and primary frequency control. The contribution will depend on the type of DG unit. It was concluded that with a good mix of different DG unit types, they can participate in frequency control. The inertial response is provided by DG units that have kinetic energy available, such as wind turbines and micro turbines. The primary frequency control is performed by the DG units that are driven by a controllable power source, such as fuel cells and micro turbines. Requirements are derived for which combination of DG units this is possible.

In the Netherlands a target of 6 GW of installed wind power has been set. An example showed that for fuel cells operating at a power margin of 0.5, 1.6 GW of fuel cell power is needed to provide the primary frequency control support for these wind turbines. In case of a margin of 0.75 less than 1 GW is needed.

A case study has been performed on a network with wind turbines and fuel cells. The wind turbines made up 21% of the total installed power and the fuel cells 8%. The simulation results show that with this mix of DG units frequency control can be supported.

Chapter 7

Implementation of grid support control

7.1 Introduction

In the preceding chapters a number of control strategies were developed to let the DG units support the grid. It was analysed how large the contribution of the DG units could be and the control strategies were demonstrated with case study simulations. All control strategies were developed independently from each other. This chapter will analyse how the different strategies can cooperate and can be implemented in the control circuit of a DG unit. In this way a smart DG unit is obtained that supports the grid in different situations.

An important issue is the question how the DG unit 'knows' at what moment which control strategy has to be performed. Preferably this should be done autonomously. Another issue is how the control should react when different disturbances, for example a voltage dip and a frequency deviation, occur at the same time. So far no attention was paid to the question whether the different control strategies can be performed at the same moment.

The goal of this chapter is to investigate how the different control strategies can be implemented. A decision tree will be constructed on the basis of which the different actions can be performed. In the second part of this chapter a number of case study simulations will be done to demonstrate the implementation.

7.2 Controller implementation

This section investigates how the different control strategies derived in chapter 5 and 6 can be implemented. The DG unit should have one overall controller that can handle the different events and can decide which control strategy should be activated. The decision should be made autonomously, based on measured (local) grid parameters and DG unit

parameters. The overall controller output commands are the reference signals for the conventional control (for example current control) of the DG unit and its converter, as is shown by the block diagram in Fig. 7.1.

The only grid quantity that the grid support control measures is the grid voltage. From this measurement the amplitude and frequency of the voltage are derived. Based on the frequency it can decide when the frequency control should be activated. A drop in amplitude will indicate a voltage dip.
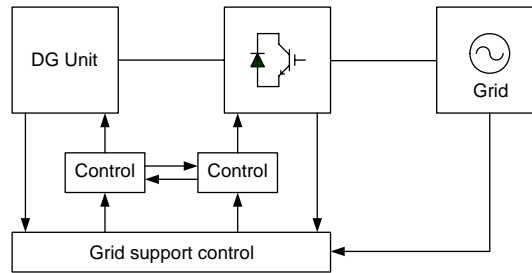
Fig. 7.1. Block diagram of DG unit and converter with overall controller

The grid support controller bases its operation on the state diagram shown in Fig. 7.2. In normal operation the amplitude and frequency of the grid voltage are continuously measured. Further the dc-link voltage of the DG unit is measured. Based on these parameters the decisions are made. The grey circles in Fig. 7.2 represent the (control) states in which the DG unit is operating. The arrows give the conditions for which the system changes from state. Although it is not shown in the figure, there is a hysteresis band around each of the conditions, to avoid oscillations around the condition.

Five different states have been identified:
- Normal operation. None of the grid support strategies is needed in this state.
- Fault ride-through. This state is entered when the controller measures a drop in the amplitude of the grid voltage. Because of the current limitation of the converter the power transferred to the grid is limited. The fault ride-through control proposed in section 5.5 and 5.6 is activated then.
- Grid protection control. This control is necessary for DG units in DNs to avoid disturbance of the over-current protection of the feeders, as described in section 5.3. Depending on the type of protection that is applied and on its settings the DG units can limit their current to the rated current, or to lower values. It is entered when a drop in voltage amplitude is measured.

- Fault ride-through & grid protection control. They will often be needed at the same moment, as they can both be necessary during a voltage dip.
- Frequency control. In this state the DG unit will support the frequency control. It is entered when a change in frequency is measured.
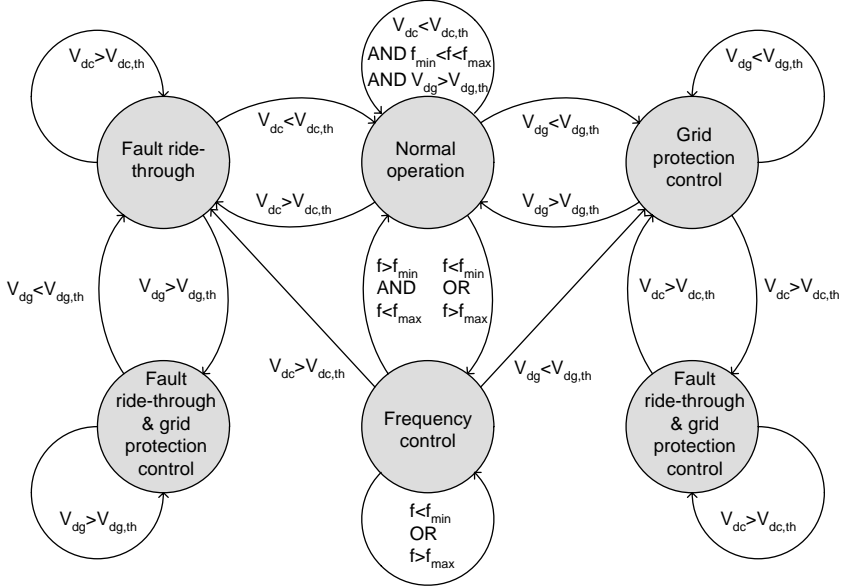
Fig. 7.2. State diagram for overall controller of DG unit (Grey circles represent states and arrows conditions for which is switched between states)

The transition between the different states is based on 3 different conditions:

- $V_{dc} > V_{dc,th}$. During a voltage dip, the power of the DG unit that can be transferred to the grid can be limited. This results in an increase in dc-link voltage and the fault ride-through control should be activated. A wind turbine with doubly-fed induction generator uses the rotor current to detect when the fault ride-through control should be activated.
- $V_{dg} < V_{dg,th}$. The grid voltage is continuously measured to detect when a voltage dip occurs. The dip can be caused by a short-circuit and the grid protection control should be activated to avoid possible distortion of the DN protection.
- $f < f_{min}$ or $f > f_{max}$. When the grid frequency comes outside a pre-defined band the frequency control will be activated.

There is a hierarchy in the order in which the states are entered. The fault ride-through control and grid protection control have a higher priority than the frequency control.

Therefore, when the DG unit is in its frequency control state it will immediately go to the fault ride-through or grid protection control mode when the dc-link voltage or grid voltage exceeds the appropriate limits. This is done to protect the converter.

7.3 Case study

This section presents two case studies that show the performance of the controller implementation described in the previous section.

7.3.1 Setup

The network shown in Fig. 7.3 is used for the case study. It consists of two 10 kV networks that are connected by a 150 kV transmission line. The first part consists of five small synchronous generators, which represent conventional power plants, and two large loads. The second part consists of a 10 kV DN with fuel cells, micro turbines, wind turbines with a doubly-fed induction generator, and loads. The wind turbines are directly connected to the DN, while the fuel cells are connected to a cable. The loads are connected to the substation by a cable. The micro turbines are connected to the same cable as the loads. At locations 1 and 2 faults are applied.
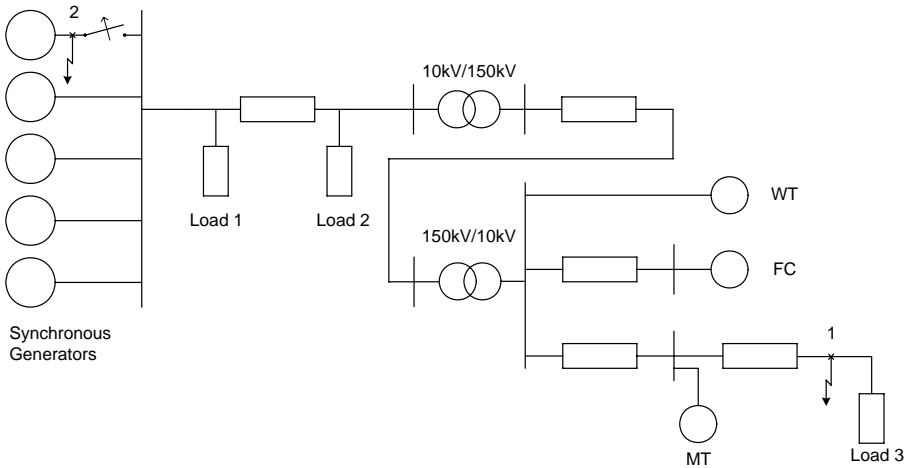

Fig. 7.3. Simulation setup showing two distribution networks connected by a 150kV transmission line; faults are applied at location 1 and 2

7.3.2 Models

The five synchronous generators are modelled according to the description in section 6.6. For the fuel cells, wind turbines, and micro turbines one model is used for each. The output current is multiplied by the appropriate constant to obtain the required total power. A description of the converter and generator models can be found in appendix B and C, respectively. The frequency control implementation of the synchronous generators, fuel cells, and wind turbines is given in section 6.6.

The micro turbine setup is shown in Fig. 7.4. The frequency control is performed in the same way as for the fuel cell. When the frequency change exceeds a limit value the output power is increased according to a droop line.

The wind turbine is protected with the fault ride-through control described in section 5.6. The protection of the fuel cell and micro turbine is similar to that of the wind turbine with permanent magnet generator described in section 5.5.

The models of the transformers and cables that are used can be found in [Pie 04]. All generators, converters and grid components are modelled in the *dq*-reference frame described in appendix E.
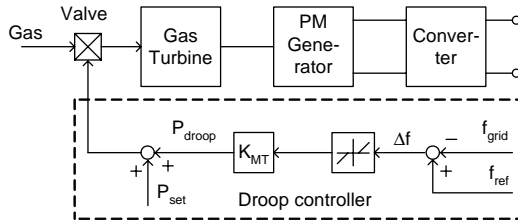
Fig. 7.4. Micro turbine setup with frequency controller

7.3.3 Parameters

The most important parameters used in the case studies are given in table 7.1. Other parameters can be found in table 6.6 and the appendices A, B and C. The total power of the network is small. This is done to be able to see a significant contribution of the DG units, without the necessity to model and simulate a large network. The percentage of DG power is 10%. The droop constants for the DG units are obtained in the same way as in section 6.6. Again a system droop of 3% is chosen. As the DG units now form only 10% of the total power instead of 25% as in section 6.6, also the droop constants are 2.5 times lower than in chapter 6.

Table 7.1: Parameters for case study

Parameter	Value	Unit	Parameter	Value	Unit
P_{conv}	5×50	MW	k_{mt}	0.6	-
$P_{fc,nom}$	5.0	MW	k_{wt}	1.0	-
$P_{mt,nom}$	4.8	MW	τ_{fc}	15	s
$P_{wt,nom}$	16.5	MW	K	$1 \cdot 10^{12}$	W/rad·s^{-1}
P_{load1}	185	MW	R	$1 \cdot 10^7$	W/rad·s^{-1}
P_{load2}	11.5	MW	K_{FC}	$1.1 \cdot 10^7$	W/Hz
P_{load3}	5.5	MW	K_{MT}	$1.1 \cdot 10^7$	W/Hz
k_{conv}	0.7	-	K_{WT}	$1.2 \cdot 10^7$	W/Hz
k_{fc}	0.6	-			

7.3.4 Results case 1

Two events occur during the simulation. The first is that at $t = 5$ s a short-circuit occurs at the end of the distribution feeder with the micro turbines and the load (location 1). The fault is assumed to clear automatically after 0.2 s. The second event occurs at $t = 15$ s, when one of the five synchronous generators is suddenly disconnected (location 2), resulting in a loss of generation of ~20%.

Fig. 7.5a and b show the grid frequency and the voltage at the micro turbine terminals during the two events. The short-circuit results in a small decrease in frequency, whereas the loss of the synchronous generators results in a much larger frequency drop. Due to the short-circuit the voltage at the micro turbine terminals drops almost to zero, as can be seen in Fig. 7.5b. The loss of the synchronous generator does not affect the voltage.

(a)   (b)
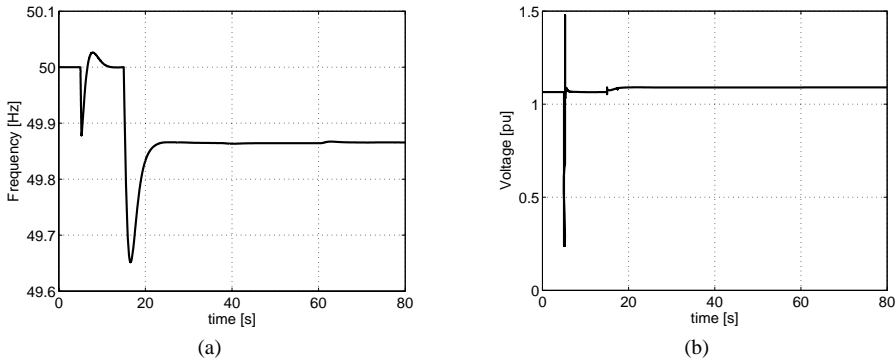
Fig. 7.5. Response to different faults: (a) grid frequency; (b) voltage at micro turbine terminals; (short-circuit in distribution network at $t = 5$ s; disconnection of a large synchronous generator at $t = 15$ s)

The micro turbine detects the short-circuit as a voltage dip at its terminals. Because of the reduced voltage the output power of the converter will be limited. This results in an increase in dc-link voltage and the converter controller goes to its 'fault ride-through & grid protection control' state. The 'grid protection control' operates the micro turbine at its nominal current during the fault, as there is no chance that the DG unit will prevent the proper operation of the DN protection. Fig. 7.6a shows that the micro turbine current is indeed 1 p.u.. The current through the circuit breaker is shown in Fig. 7.6b. There is almost no difference between the current with micro turbine (solid line) and without micro turbine (dashed line).

Due to the current limitation the dc-link current increases, as shown in Fig. 7.7a. The protection technique described in section 6.5 is applied to limit the dc-link voltage. As the protection limits the power of the micro turbine, it will speed up. Because of the short duration of the voltage dip and the high inertia constant of the micro turbine the speed increase is limited, as can be seen in Fig. 7.7b.
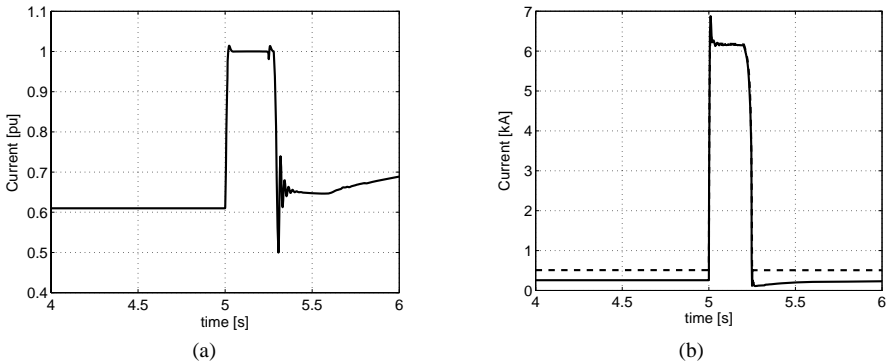
Fig. 7.6. Response to short-circuit at $t = 5$ s: (a) output current of micro turbine; (b) current through circuit-breaker
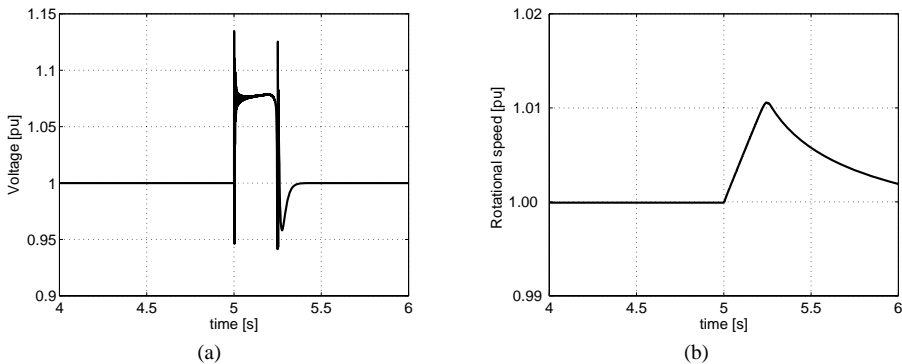
Fig. 7.7. Response of micro turbine to short-circuit at $t = 5$ s: (a) dc-link voltage of micro turbine converter; (b) rotational speed of micro turbine (b)

The second event occurs at $t = 15$ s when one of the five synchronous generators is disconnected. The loss of ~20% of the total generation, results in a significant frequency drop, as shown in Fig. 7.5a. The frequency drop is detected by the DG units, which go to their frequency control state. The output power of the fuel cell, the micro turbine, and the wind turbine are shown in Fig. 7.8a, b, and c respectively. The fuel cell power increases slowly, because of the reformer. It is compensated by the wind turbine, which uses its kinetic energy. The power of all DG units together is shown in Fig. 7.8d. The figure shows that also after the occurrence of the short-circuit at $t = 5$ s the frequency control is activated, because of the frequency drop caused by the short-circuit. The frequency deviation, and therefore the contribution of the DG units, is limited. The synchronous machines bring the frequency back to 50 Hz after the disturbance. This takes about 5 s. After $t = 15$ s a much larger increase in power can be noted.

The results show that the DG units with grid support control can handle different events. They ride through a voltage dip and limit their current to avoid disturbance of protection (micro turbine), followed by a contribution to frequency control.

Fig. 7.8. Response of DG unit output power to different faults: (a) fuel cell; (b) micro turbine; (c) wind turbine; (d) sum of all DG units (short-circuit in distribution network at $t = 5$ s; disconnection of a large synchronous generator at $t = 15$ s)

7.3.5 Results case 2

In the second case the order of the two events is reversed. First, at $t = 5$ s the synchronous generator is disconnected, resulting in a change in frequency, and one second later a short-circuit occurs. The goal of this case is to show that the grid support control goes from its fre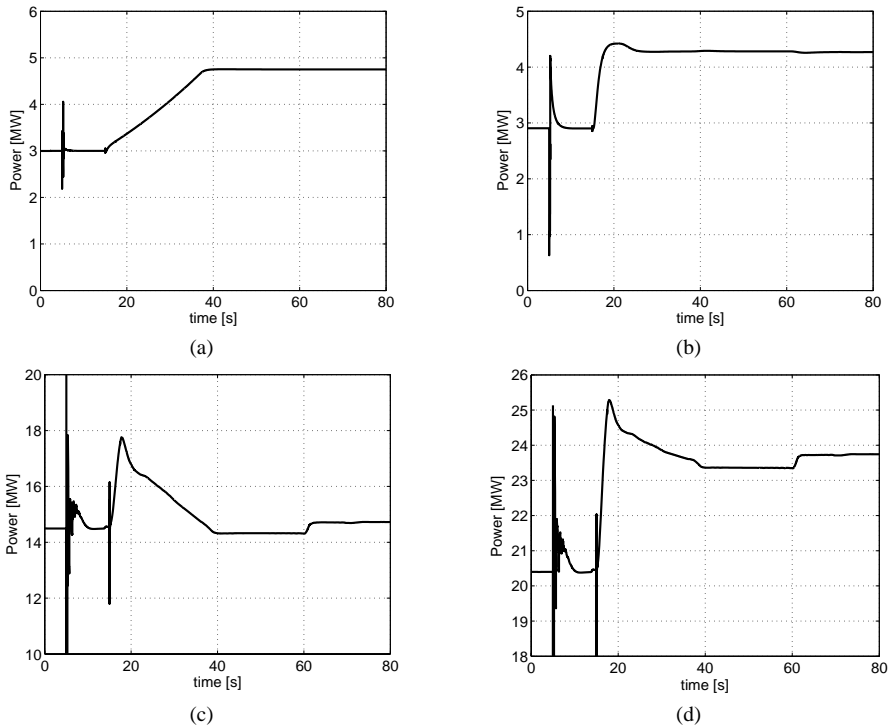quency control state to its fault ride-through state. Fig. 7.9a shows the output power of the micro turbine. After the synchronous machine is disconnected at $t = 5$ s, the power starts increasing. At $t = 6$ s a short-circuit occurs and the micro turbine power is reduced, due to the current limitation in the converter control. An increase in dc-link voltage is the result, as shown in Fig. 7.9b. It is properly limited by the fault ride-through control however.

| (a) | (b) |
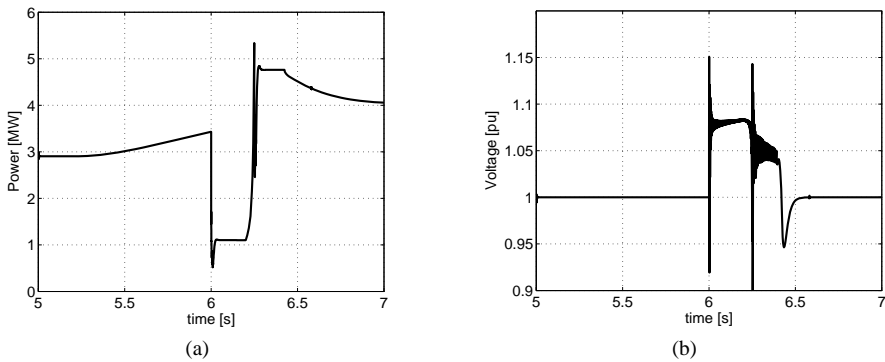
Fig. 7.9. Response to different faults: (a) micro turbine output power; (b) micro turbine dc-link voltage; (disconnection of synchronous generator at $t = 5$ s followed by short-circuit at $t = 6$ s)

7.4 Discussion and conclusion

This chapter investigated whether the different grid support control strategies derived in the previous chapters can be combined in one DG unit. An overall grid support controller has been proposed and a state diagram is derived that can be used to achieve the appropriate control in each situation. This control works almost autonomously. Only the grid voltage at the DG unit terminal needs to be measured.

The grid support controller can be implemented relatively easy. It requires in most cases only adaptation of the control software, and in some cases it can require some additional measurement equipment. This implies that the proposed control can be implemented at low cost.

This chapter focused mainly on the fault ride-through and the frequency control support of DG units. Active damping and voltage control have not been considered in

this chapter but can easily be added to the overall grid support controller. They might require overrating of the converter however, implying some additional investment costs.

Besides these investments related to the overrating of the converter, the main obstacles for implementation of the grid support control are international standards and grid-connection requirements of system operators which in most cases do not allow grid support by the DG units.

Chapter 8

Conclusions and recommendations

8.1 Conclusions

The objective of this thesis is to investigate if and how the power electronic converters (PECs) of DG units can be used to solve some of the problems caused by the introduction of DG. It has been shown that the DG units are able to solve a number of problems or at least mitigate them:

- By implementing an active damping control loop on PECs they can contribute to the damping of harmonics and resonances in the network.
- By controlling their (re-)active power, possibly in combination with overrating of the converter, curtailment of the active power and the use of a variable inductance the DG units can compensate a part of the voltage change they cause. In this way they can increase the maximum allowable DG penetration.
- DG units can ride through grid faults, and minimise the chance on causing malfunctioning of the network protection. They can thus support the grid (voltage) during the fault.
- Although most DG unit types are not able to contribute to frequency control on their own, a combination of different DG unit types can contribute to the conventional frequency control.

In this way a multi-functional DG unit is obtained that can autonomously support the grid in several ways. The general conclusion will be split up in more specific conclusions for each of the issues that were considered.

The first two chapters provided an introduction to the thesis. Chapter 2 explained the basic principles of PECs. It concluded that for frequencies far enough below the bandwidth of the current controller a voltage source converter (VSC), which is the type of converter that is used by most DG units, can be considered as a controlled current source. It was further shown that the behaviour of another type of converter, a current

source converter (CSC), generally is the same as a VSC, as long as the voltage control of the CSC is fast enough. The results of this thesis, which are obtained for a VSC, can therefore also be applied to a CSC.

Detailed simulation of power electronic converters, taking into account the switching of all individual semiconductors, is a time-consuming process. Therefore in this thesis reduced models have been used for simulation of the converters, except in section 3.3.3. Chapter 2 concluded, with reference to appendix F, that for frequency below half the switching frequency reduced models of the converters can be used.

Damping of harmonics – Introduction of DG results in an increase of the capacitance in the grid. Due to this increase there is a risk on harmonics and resonances, as the capacitance forms resonance circuits with the grid inductance. To avoid resonances and a high level of harmonic distortion, there should be enough damping in the grid. In passive grids the damping is obtained from the resistance of the loads and lines. Chapter 3 investigated the influence of DG unit converters on the damping of the harmonics and resonances. It concluded that the contribution is limited. Some types of converter even reduce the damping. They have a current reference waveform that is a copy of the grid voltage. This gives these converters a negative incremental impedance, and thus a negative damping.

Chapter 3 showed that it is possible to implement an additional control loop on the DG unit converter which gives the output impedance of the converter a resistive behaviour for a large frequency range. In this way the damping in the network can be increased and thus harmonics and resonances can be mitigated. Due to the active damping controller the voltage and current of the converter will increase. This limits the maximum damping contribution of the converter. Harmonics at the resonance frequency of the grid can be compensated easily. A 90% reduction requires only a ~10% increase in current and voltage (for a converter with a rated power of 1% of the short-circuit power of the grid). Harmonics at three times the resonance frequency require a ~80% increase in current and a ~180 increase in voltage however, to obtain a reduction of 90%. This implies that harmonics at the resonance frequency, which cause the largest problems, can be most easily damped.

The proposed active damping controller and the analysis how large its contribution to damping can be in a practical network are the main contributions of chapter 3.

Voltage control – In the connection requirements of most grid operators there is a maximum on the allowable voltage change caused by DG units. This limits the maximum amount of DG that can be connected to a network. The DG unit converters can control the voltage to (partly) compensate the voltage change they cause. In this

way a higher penetration can be allowed. Chapter 4 investigated how effective the voltage control of DG unit converters can be. Reactive compensation showed to be of limited effect because of the low inductance in most distribution networks. Converter overrating, generation curtailment and the use of a variable inductance were proposed as solutions to partially overcome these limitations.

An approach has been presented to determine how the maximum allowable DG unit penetration can be determined, and how it can be increased. Due to the active power injection, DG units cause an increase in voltage. The voltage increase offers the possibility to increase the reactive power consumption, which will reduce the voltage again. Using this reactive power to lower the voltage, increases the maximum allowable penetration. Especially in networks with a high X/R ratio a significantly higher penetration of DG can be allowed. An example showed that in a network with an X/R ratio of 0.75 already a 40% higher penetration level can be allowed. For networks with a low X/R ratio generation curtailment and the use of a variable inductance offer good possibilities to increase the DG unit penetration. An example for the rural network showed that a 30% curtailment results in a doubling of the allowable DG power. Overrating was not very effective in this case. An example for the Testnet (which has a two times larger X/R ratio) showed that with an 8% curtailment or a 10% overrating the allowable amount of DG can be doubled already.

The main contribution of chapter 4 is the approach to determine the maximum penetration level of DG units that use their reactive power margin to minimise the voltage change they cause. Another contribution is the proposed variable inductance.

Ride-through and grid support - Most grid operators require the disconnection of DG units when faults occur in the network. One reason for this requirement is that they fear that DG units disturb the classical protection schemes that are applied. It was shown in chapter 5 that power electronic interfaced DG units do not necessarily disturb the protection schemes, as they do not supply large short-circuit currents.

Disconnection of power electronic interfaced DG is thus not necessary, generally. The units can then be used to support the grid (voltage) during the fault. The duration of voltage dips is generally less than 1 s. Overloading of a converter will mostly be allowable for this short period. A combination of DG units and a variable inductance showed to be able to limit the detrimental effect of voltage dips.

Wind turbines with a doubly-fed induction generator are rather sensitive to voltage dips. Some special measures are proposed to protect them. The key of the technique is to limit the high currents in the rotor circuit with a set of resistors, without disconnecting the converter from the rotor or the grid. The wind turbine can resume normal operation when the voltage and current oscillations have decayed enough

(generally within a few hundred milliseconds). In this way the turbine stays synchronised and it can supply reactive power to the grid during a voltage dip.

For the other types of DG units it is not difficult to let them ride through grid faults. Control strategies have been derived to achieve a correct behaviour.

The main contributions of chapter 5 are the proposed protection techniques for variable speed wind turbines (especially those with doubly-fed induction generator).

Frequency control - In order to be able to support frequency control, DG units should have fast controllable power or stored energy and they should be able to increase their output power on command. A number of categories have been defined for DG units, with respect to their ability to contribute to inertial response and primary frequency control. DG units that have kinetic energy available, such as wind turbines and micro turbines, provide the inertial response. Although most individual DG units do not fulfil both requirements, chapter 6 concluded that a combination of different DG unit types can be used to contribute to frequency control. The primary frequency control is performed by the DG units that are driven by a controllable power source, such as fuel cells and micro turbines. Requirements have been derived which can be used to determine the percentage of each of the DG unit types (or groups of types) that is required to obtain a good overall response.

In the Netherlands a target of 6 GW of installed wind power has been set. An example showed that for fuel cells operating at a power margin of 0.5, 1.6 GW of fuel cell power is needed to provide the primary frequency control support for these wind turbines. In case of a margin of 0.75 less than 1 GW is needed. A case study has been performed on a network with wind turbines and fuel cells. The wind turbines made up 21% of the total installed power and the fuel cells 8%. The simulation results show that with this mix of DG units frequency control can be supported.

The main contributions of chapter 6 are the idea to use the kinetic energy stored in the rotating mass of wind and micro turbines to support frequency control, the proposed controller implementations, and the structured analysis of the required percentages of each of the types of DG unit.

Grid support control - Chapter 7 showed that the different grid support control strategies can be combined in one DG unit. An overall grid support controller has been proposed and a state diagram is derived that can be used to achieve the appropriate control in each situation. The control works almost autonomously. Only the grid voltage at the DG unit terminal needs to be measured. It was shown in two case studies that the control handles the different events correctly. The control can be implemented at low cost as it only requires some adaptation of the control software.

The overall grid support controller proposed in chapter 7 forms the main contribution of this chapter.

8.2 Recommendations

From the results of this thesis a number of recommendations for further research can be obtained. First three important general recommendations are given:

- One of the limitations for the grid support by the DG unit is the nominal current of the converter. For most converters it is possible to operate them at a higher current for a short period. The maximum allowable overloading (in magnitude and time) of a converter will depend on the specific converter design. An economical trade-off can be made between the cost of overloading and the economical value of the additional margin, which for example can be used for voltage control or active damping.
- The way of operation of the DG unit converters proposed in this thesis sometimes conflicts with international standards and grid-connection requirements of system operators. To allow grid support the standards and requirements have to be changed.
- This thesis focused on the use of DG unit converters for grid support. Also many loads are connected to the grid with a PEC. Some of the control strategies proposed in this thesis can also be implemented in load converters.

Some more specific recommendations for each chapter are given below.

Damping of harmonics – In chapter 3 only networks with a single converter have been considered. In principle the results can be extended to a network with more converters, by adding up the emulated conductance of each converter. In practice interaction between the converters can occur however. It has to be investigated whether this causes problems. Only single-phase systems have been considered. It should be investigated whether the results can be extended to three-phase systems.

Voltage control – Chapter 4 proposed several methods to increase the voltage control capability of the converter. A methodology should be developed to determine in each practical case the most cost-effective solution.

Each DG unit is assumed to compensate only the voltage change that it causes itself. When a large number of DG units are used, one converter might be able to compensate a larger voltage change than another converter, for example because it has a larger

margin for reactive power. It should be investigated how the contribution to the compensation could be spread in an optimal way amongst a number of DG units.

Different implementations are possible for the variable inductance. In this thesis a device with two anti-parallel thyristors was used. These thyristors result in a significant harmonic distortion. It should be investigated how the variable inductance can be implemented in another way.

Ride-through and grid support –Chapter 5 stated that in case of power electronic interfaced DG units disturbance of protection can be avoided in most cases, because the converters can limit their current during a fault. The issue requires more research however, to determine in which cases and under which conditions disturbance of protection can occur.

It has been shown that it is possible to let a wind turbine with a doubly-fed induction generator ride through a fault. When the dip is cleared the induction generator will absorb a large amount of reactive power from the grid. It has to be studied how this affects the stability of the grid and if it is possible to limit the amount of reactive power that is absorbed.

Frequency control –The simulations in chapter 6 have been done with rather detailed models. More simple models can be derived however, that correctly represent the behaviour of the DG units during their contribution to frequency control. With these simplified models the response of a much larger network with a large number of DG units can be simulated.

When a large number of DG units are used, a good cooperation between the DG units might become problematic. This issue requires more attention. A challenging issue will especially be how the responses of a large number of slow DG unit types (for example fuel cells) and a large number of fast DG unit types (for example wind turbines) can be matched such that they exactly compensate each other.

Another important issue is how secondary frequency control can be implemented when a large number of DG units are connected to the grid.

Grid support control – The case studies in chapter 7 have been done with one fuel cell, one micro turbine and one wind turbine. When a large number of DG units are connected to the network, some form of communication might be necessary. This communication has not to be real-time, but for example setpoints for the frequency control or the appropriate behaviour to avoid disturbance of protection might depend on the number and type of DG units that are connected. When there are large changes in the number of DG units it might be necessary to change the setpoints.

References

[Ack 01]   T. Ackermann, G. Andersson, and L. Söder, "Distributed generation: a definition", *Electric Power Systems Research*, vol. 57, pp. 195-204, 2001.

[Ack 02]   T. Ackermann, V. Knyazkin, "Interaction between distributed generation and the distribution network: operation aspects", in *Proc. 2002 IEEE/PES Asia Pasific Trans. and Distr. Conf. and Exh.*, vol. 2, pp. 1357 – 1362, 6 – 10 Oct. 2002.

[Aka 97]   H. Akagi, "Control Strategy and Site Selection of a Shunt Active Filter for Damping of Harmonic Propagation in Power Distribution Systems", *IEEE Trans. Power Delivery*, vol. 12, no. 1, pp. 354 – 363, Jan. 1997.

[Ana 05]   O. Anaya-Lara, X. Wu, P. Cartwright, J.B. Ekanayake, N. Jenkins, "Performance of Doubly Fed Induction Generator (DFIG) During Network Faults, *Wind Engineering*, vol. 29, no. 1., pp. 49 – 66, 2005.

[Ana 06]   O. Anaya-Lara, F.M. Hughes, N. Jenkins, G. Strbac, "Contribution of DFIG-based wind farms to power system short-term frequency regulation", *IEE Proc.-Gener. Transm. Distrib.* vol. 153, no. 2, pp. 164 – 170, March 2006.

[And 77]   P.M. Anderson, A.A. Fouad, *Power System Control and Stability*, Iowa: Iowa State University Press, 1977.

[Aru 04]   A. Arulampalam, M. Barnes, A. Engler, A. Goodwin, N. Jenkins, "Control of Power Electronic Interfaces in Distributed Generation MicroGrids", *Int. Journal of Electronics*, vol. 91, no. 9, pp. 503 – 523, Sep. 2004.

[Bar 00]   P.P. Barker, R.W. De Mello, "Determining the impact of distributed generation on power systems. I. Radial distribution systems", in *Proc. 2000 IEEE Power Engineering Society General Meeting*, vol. 3, pp. 1645 – 1656, 16-20 July 2000.

[Bar 02]   S. Barsali, M. Ceraolo, P. Pelacchi, D. Poli, "Control techniques of Distributed Generators to improve the continuity of electricity supply", in *Proc. 2002 IEEE Power Engineering Society Winter Meeting*, vol. 2, pp. 789 – 794, 2002.

[Bla 04]   F. Blaabjerg, Z. Chen, S.B. Kjaer, "Power Electronics as Efficient Interface in Dispersed Power Generation Systems", *IEEE Trans. Power Electr.*, vol. 19, no. 5, pp. 1184 – 1194, Sept. 2004.

[Boh 89]   L.J. Bohmann, R.H. Lasseter, "Harmonic interactions in thyristor controlled reactor circuits, *IEEE Trans. Power Delivery*, vol. 4, no. 3, pp. 1919 - 1926, 1989.

[Bol 00]   M.H.J. Bollen, *Understanding Power Quality Problems – Voltage sags and interruptions*, New York: IEEE, 2000.

[Bol 05]   M.H.J. Bollen, A. Sannino, "Voltage Control With Inverter-Based Distributed Generation", *IEEE Trans. Power Delivery*, vol. 20, no. 1, pp 519 - 520, Jan. 2005.

[Bon 01]   A. Bonhomme, D. Cortinas, F. Boulanger, and J.-L. Fraisse, "A new voltage control system to facilitate the connection of dispersed generation to distribution networks", in *Proc. CIRED 2001*, Amsterdam, 18-21 June, 2001.

[Bor 01]   A.-M. Borbely, J.F. Kreider (red), *Distributed Generation: The Power Paradigm for the New Millenium*, Boca Raton, Florida: CRC Press, 2001.

[Cal 05]   R. Caldon, S. Spelta, V. Prandoni, R. Turri, "Co-ordinated voltage regulation in distribution networks with embedded generation", in *Proc. 18th Int. Conf. on Electricity Distribution (Cired)*, 4pp., Turin, 6 – 9 June 2005.

[Can 01]   W.R. Canders, J. Heldt, R.K. Jardan, I. Nagy, H.J. Prümper, "Application of a novel 400 kW Natural Gas Expansion System as a UPS System", in *Proc. 9th European conference on Power Electronics and applications* (EPE), Graz, Austria, 27 – 29 August 2001.

[Con 01]   S. Conti, S. Raita, G. Tina, and U. Vagliasindi, "Study of the impact of PV generation on voltage profile in LV distribution networks", in *Proc. 2001 IEEE Power Tech Conference*, Porto, 10-13 Sept. 2001.

[Dai 03]   C. Dai, Y. Baghzouz, "On the Voltage Profile of Distribution Feeders with Distributed Generators", in *Proc. 2003 IEEE PES General Meeting*, vol. 2, pp. 1136 – 1140, 2003.

[Dit 05]   A. Dittrich, A. Stoev, "Comparison of Fault Ride-Through Strategies for Wind Turbines with DFIM Generators, in *Proc. 11th European Power Electronics Conference (EPE '05)*, Dresden, Germany, 11 – 14 Sept. 2005.

[Don 02]   P. Dondi, D. Bayoumi, C. Haederli, D. Julian, M. Suter, "Network Integration of distributed power generation", *Journal of Power Sources*, No. 106, pp. 1-9, 2002.

[Dug 02]   R.C. Dugan and T.E. McDermott, "Distributed Generation", *IEEE Industry Applications Magazine*, vol. 8, no. 2, pp. 19-25, Mar/Apr 2002.

[Eka 03]   J.B. Ekanayaka, L. Holdsworth, X.G. Wu, N. Jenkins, "Dynamic modelling of doubly-fed induction generator wind turbines", *IEEE Trans. Power Systems*. vol. 18, no. 2, pp. 803 – 809, May 2003.

[Eka 04]   J. Ekanayake, N. Jenkins, "Comparison of the Response of Doubly Fed and Fixed-Speed Induction Generator Wind Turbines to Changes in Network Frequency", *IEEE Trans. Energy Conversion*, vol. 19, no. 4, pp. 800 – 802, Dec. 2004.

[El-S 04] M.Y. El-Shark, A. Rahman, M.S. Alam, A.A. Sakla, P.C. Byrne, T. Thomas, "Analysis of Active and Reactive Power Control of a Stand-Alone PEM Fuel Cell Power Plant", *IEEE Trans. Power Systems*, vol. 19, no. 4, pp. 2022 – 2028, November 2004.

[Ema 04]   A. Emadi, "Modeling of Power Electronic Loads in AC Distribution Systems Using the Generalized State-Space Averaging Method", *IEEE Trans. Industrial Electronics*, vol. 51, no. 5, pp. 992-1000, Oct. 2004.

[Eng 01]   A. Engler, *Regelung von Batteriestromrichtern in modularen und erweiterbaren Inselnetzen*, Universität Gesamthochschule Kassel, PhD- thesis, 2001. (In German)

[Eng 05]   A. Engler, "Applicability of droops in LV grids", *Int. Journal of Distributed Energy Resources*, vol. 1, no. 1, pp. 3 – 16, Jan. 2005.

[Ens 02]   J.H.R. Enslin, W.T.J. Hulshorst, J.F. Groeman, A.M.S. Atmadji, P.J.M. Heskes, *Harmonic interaction between large numbers of photovoltaic inverters and the distribution network*, KEMA Report 40 210 004 TDC 02-29 719A, Arnhem, The Netherlands, Oct. 2002.

[Ens 04]   J.H.R. Enslin, P.J.M. Heskes, "Harmonic Interaction Between a Large Number of Distributed Power Inverters and the Distribution Network", *IEEE Trans. Power Electronics*, vol 19, no. 6, pp, 1586 – 1593, Nov. 2004.

[E.On 03] E.On Netz, *Grid code*, Bayreuth: E.On Netz GmbH, Germany, 1. Aug. 2003.

[Gra 94]   J.J. Grainger and W.D. Stevenson, Jr., *Power System Analysis*, New York: McGraw-Hill, Inc., 1994.

[Had 04]   N. Hadjsaid, "Power industry restructuring: challenges on new technologies – From the State of the Art to future Trends", in *Proc. PCIM 2004*, Nuremberg, 25 – 27 May 2004.

[Han 04]   A.D. Hansen, F. Iov, P. Soerensen, F. Blaabjerg, "Overall control strategy of variable speed doubly-fed induction generator wind turbine", in *Proc. Nordic Wind Power Conference*, Gothenborg, Sweden, 1 – 2 March 2004.

[Har 98]   L. Harnefors, H.-P. Nee, "Model-Based current control of AC Machines using the Internal Model Control Method", *IEEE Trans. Industrial. Applications*, vol. 34, no. 1, pp. 133-141, Jan./Feb. 1998.

[Hat 06]   N. Hatziargyriou, N. Jenkins, G. Strbac, et. al., "Microgrids – Large Scale Integration of Microgeneration to Low Voltage Grids", in *Proc. CIGRE 06*, Paris, paper C6-309, Aug. 2006.

[Hau 02]   M. Hauck, *Bildung eines dreiphasigen Inselnetzes durch unabhängige Wechelrichter im Parallelbetrieb*, Universität Fridericiana Karlsruhe, PhD- thesis, 2002. (In German)

[Hud 03]   R.M. Hudson, F. Stadler, M. Seehuber, "Latest developments in power electronic converters for megawatt class windturbines employing doubly fed generators", in *Proc. Int. Conf. Power Conv. Intelligent Motion*, Nuremberg, Germany, June 2003.

[Ing 03]   S. Ingram, S. Probert, K. Jackson, *The Impact of SmallScale Embedded Generation on the Operating Parameters of Distribution Networks*, DTI Report K/EL/00303/04/01, 2003. (www.dti.gov.uk/renewables/renew_6.1d.htm, Feb. 06)

[Jen 00]   N. Jenkins, *Embedded Generation*, London: Institution of Electrical Engineers, 2000.

[Jen 01]   N. Jenkins, "Impact of Dispersed Generation on Power Systems", *Electra*, no. 199, pp. 6-13, 2001.

[Jar 02]   R.K. Jardan, I. Nagy, T. Nitta, H. Ohsaki, "Environment – Friendly Utilisation of Waste Energies for the Production of Electric Energy in Disperse Power Plans", in *Proc. 2002 IEEE Int. Symp. on Industrial Electronics (ISEI 2002)*, vol. 4, pp. 1119 – 1124, 2002.

[Jer 04]   C. Jeraputra, P.N. Enjeti, "Development of a robust anti-islanding algorithm for utility interconnection of distributed fuel cell powered generation", *IEEE Trans. Power Electronics*, vol. 19, no. 5, pp. 1163 - 1170, 2004.

[Jóo 00]   G. Jóos, B.T. Ooi, D. McGillis, F.D. Galiana, R. Marceau, "The Potential of Distributed Generation to Provide Ancillary Services", in *Proc. 2000 IEEE Power Engineering Society Summer Meeting*, Vol. 3., pp. 1762 – 1767, 2000

[Kar 03]   G. Kariniotakis, et. al., "DA1 – Digital Models for Microsources", MicroGrids project deliverable DA1, 2003.

[Kas 05]   M.A. Kashem, G. Ledwich, "Multiple Distributed Generators for Distribution Feeder Voltage Support", in *IEEE Trans. Energy Conversion* vol. 20, no. 3, pp. 676 -684, Sept. 2005.

[Kat 05]   F. Katiraei, M.R. Iravani, P.W. Lehn, "Micro-Grid Autonomous Operation During and Subsequent to Islanding Process", *IEEE Trans. Power Delivery*, vol. 20, no. 1. pp. 248 – 257, Jan. 2005.

[Kau 04]   K. Kauhaniemi, L. Kumpulainen, "Impact of distributed generation on the protection of distribution networks", in *Proc. 8th IEE Int. Conf. on Developments in Power System Protection 2004*, vol. 1, pp. 315 – 318, 5 – 8 April 2004.

[Kna 04]   V. Knazkins, *Stability of Power Systems with Large Amounts of Distributed Generation*, Ph.D. Thesis, KTH Stockholm, Sweden, 2004.

[Knu 05]   H. Knudsen, J.N. Nielsen, "Introduction to the modelling of wind turbines", in *Wind Power in Power Systems*, T. Ackermann, Ed., Chichester, U.K.: Wiley, 2005, pp. 525 – 585.

[Koj 02]   L. Kojovic, "Impact of DG on Voltage Regulation", in *Proc. 2002 IEEE PES Summer Meeting*, vol. 1, pp. 97 – 102, 2002.

[Kov 59]   K.P. Kovács, I. Rácz, *Transiente Vorgänge in Wechselstrommaschinen – Band II*, Budapest: Verlag der Ungarischen Akademie der Wissenschaften, 1959. (In German)

[Kun 94]   P. Kundur, *Power System Stability and Control*, New York: McGraw-Hill, 1994.

[Kum 04]   L. Kumpulainen, K. Kauhaniem, "Distributed Generation and reclosing coordination", in. *Proc. Nordic Distribution and Asset Management Conference*, 23 – 24 Aug. 2004.

[Kum 05]   L. Kumpulainen, K. Kauhaniemi, P. Verho, O. Vahamaki, "New requirements for system protection caused by Distributed Generation", in *Proc. 18th Int. Conf. on Electricity Distribution (CIRED 2005)*, 4pp., Turin, 6 – 9 June 2005.

[Lal 04]   G. Lalor, J. Ritchie, S. Rourke, D. Flynn, M.J. O'Malley, "Dynamic frequency control with increasing wind generation", in Proc. *2004 IEEE Power Engineering Society General Meeting*, vol. 2, pp. 1715 – 1720, 6 – 10 June 2004.

[Lal 05]   G. Lalor, A. Mullane, M. O'Malley, "Frequency control and wind turbine technologies", *IEEE Trans. Power Systems*, vol. 20, no. 4, pp. 1905 – 1913, Nov. 2005.

[Lee 01]   B.K. Lee, M. Ehsami, "A simplified functional simulation model for three-phase voltage-source inverter using switching function concept", *IEEE Trans. Industrial Electronics*., vol. 48, no. 2. pp. 309 – 321, April 2001.

[Lie 02]   S.N. Liew and G. Strbac, "Maximising penetration of wind generation in existing distribution networks", *IEE Proc.-Gener. Transm. Distrib.*, vol. 149, no. 3, pp. 256-262, May 2002.

[Lis 01]   M. Liserre, F. Blaabjerg, S. Hansen, "Design and Control of an LCL-filter based Three-phase Active Rectifier", in *Proc. 36th IEEE IAS Annual Meeting*, Vol. 1, pp. 299 – 307, 2001.

[Lis 06]   M. Liserre, R. Teodorrescu, F. Blaabjerg, "Stability of Photovoltaic and Wind Turbine Grid-Connected Inverters for a Large Set of Grid Impedance Values", *IEEE Trans. Power Electronics*, vol. 21, no. 1, pp. 263 – 272, Jan. 2006.

[Mac 04]   K.J.P. Macken, K. Vanthournout, J. Van den Keybus, G. Deconinck, R.J.M. Belmans, "Distributed control of renewable generation units with integrated active filter", *IEEE Trans. Power Electronics*, vol. 19, no. 5, pp. 1353 - 1360, Sept. 2004.

[Mäk 04]   K. Mäki, S. Repo, P. Järventausta, "Impact of distributed generation on the protection of distribution networks", in *Proc. 8th IEE Int. Conf. on Developments in Power System Protection 2004*, vol. 1, pp. 327 – 330, 5 – 8 April 2004.

[Mar 02]   M.I. Marei, E.F. El-Saadany, M.M.A. Salama, "Flexible distributed generation, FDG", in *Proc. 2002 IEEE Power Engineering Society Summer Meeting*, vol.1., pp. 49 – 53, 2002.

[Mar 04]   M.I. Marei, E.F. El-Saadany, M.M.A. Salama, "A Novel Control Algorithm for the DG Interface to Mitigate Power Quality Problems, *IEEE Trans. Power Delivery*, vol. 19, no. 2, pp. 1384 – 1392, July 2004.

[Mas 02]   C.L. Masters, "Voltage rise: the big issue when connecting embedded generation to long 11 kV overhead lines, *Power Engineering Journal*, vol. 16, no. 1, pp. 5-12, Feb. 2002.

[McD 03]   T.E. McDermott, R.C. Dugan, "PQ, reliability and DG", *IEEE Industry Applications Magazine*, vol. 9, no. 5, pp. 17 – 23, Sept.-Oct. 2003.

[Mid 76]   R.D. Middlebrook, "Input filter considerations in design and application of switching regulators", in *Proc. IEEE Ind. Appl. Soc. Annual Meeting*, pp. 366-382, 1976.

[Mil 82]   T.J.E. Miller, *Reactive power control in electric systems*, New York: John Wiley & Sons, 1982.

[Mil 03]   N.W. Miller, W.W. Price, J.J. Sanchez-Gasca, *Dynamic Modelling of GE 1.5 and 3.6 Wind Turbine Generators*, Report - GE Power Systems, Schenectady, New York, Oct. 2003.

[Mog 04]   E.F. Mogos, X. Guillaud, "A Voltage Regulation System for Distributed Generation", in *Proc. 2004 IEEE PES Power Systems Conf. and Exhibition*, vol. 2, pp. 787 – 794, 2004.

[Moh 95]   N. Mohan, T.M. Undeland, W.P. Robbins, *Power Electronics – Converters, Applications and Design*, 2nd edition, New York: John Wiley & Sons, 1995.

[Mor 03]   J. Morren, S.W.H. de Haan, J.T.G. Pierik, J. Bozelie, "Comparison of complete and reduced models of a wind turbine with Doubly-Fed Induction Generator", in *Proc. 10th European Conference on Power Electronics and Applications* (*EPE 2003*), Toulouse, Sept. 2003.

[Mor 04]   J. Morren, S.W.H. de Haan, J.A. Ferreira, "Model reduction and control of electronic interfaces of voltage dip proof DG Units", in *Proc. 2004 IEEE Power Engineering Society (PES) General Meeting*, Denver, Co, USA, 6-10 June 2004.

[Mor 05]   J. Morren, S.W.H. de Haan, "Ridethrough of Wind Turbines with Doubly-Fed Induction Generator During a Voltage Dip" *IEEE Trans. Energy Conversion*, vol. 20, no. 2, pp. 435 – 441, June 2005.

[Mor 06]   J. Morren, J. Pierik, S.W.H. de Haan, "Inertial response of variable speed wind turbines", *Electric Power Systems Research*, Vol. 76, pp. 980 – 987, June 2006.

[Mul 05a]   A. Mullane, M. O'Malley, "The Inertial Response of Induction-Machine-Based Wind Turbines" *IEEE Trans. Power Systems*, vol. 20, no. 3, pp. 1496 – 1503, Aug. 2006.

[Mul 05b]   A. Mullane, G. Lightbody, R. Yacamini, "Wind-Turbine Fault Ride-Through Enhancement", *IEEE Trans. Power Systems*, vol. 20, no. 4, pp. 1929 – 1937, Nov. 2005.

[Nav 05]   E. Navarro, *International standard situation concerning components of distributed power systems and recommendations of supplements*, Dispower project deliverable Del_2005_0070, 30 Sept. 2005.

[Nii 04]   J. Niiranen, "Voltage Dip Ride Through of Doubly-fed Generator Equipped with Active Crowbar, in *Proc. Nordic Wind Power Conference 2004*, Gothenburg, Sweden, 1 – 2 March 2004.

[Nii 05]   J. Niiranen, "Experience on voltage dip ride through factory testing of synchronous and doubly fed generator drives", in *Proc. 11th European Power Electronics Conference (EPE '05)*, Dresden, Germany, 11 – 14 Sept. 2005.

[Nik 05]   H. Nikkhajoei, M. Reza Iravani, "A Matrix Converter Based Micro-Turbine Distributed Generation System, *IEEE Trans. Power Delivery*, vol. 20, no. 3, pp. 2182–2192, July 2005.

[Ott 03]   R. Ottersten, *On Control of Back-to-Back Converters and Sensorless Induction Machine Drives*, PhD-thesis, Chalmers University, Götenborg, Sweden, 2003.

[Paa 00]   G.C. Paap, "Symmetrical components in the time domain and their application to power network calculations", *IEEE Trans. Power Systems*, vol. 15, no. 2 pp. 522–528, May 2000

[Pad 00]   J. Padullés. G.W. Ault, J.R. McDonald, "An integrated SOFC plant dynamic model for power systems simulation", *Journal of Power Sources*, vol. 86, no. 2, pp. 495–500, 2000.

[Par 97]   P. Parihar, G.G. Karady, "Characterization of a thyristor controlled reactor", *Electric Power Systems Research*, vol. 41, pp. 141 – 149, 1997.

[Peç 05]   J.A. Peças Lopes, C.L. Moreira, A.G. Madureira, "Defining Control Strategies for Analysing MicroGrids Islanded Operation", in *Proc. 2005 IEEE St. Petersburg PowerTech Conference*, 7 pp., 2005.

[Pen 96]   R. Pena, J.C. Clare, G.M. Asher, "Doubly fed induction generator using back-to-back PWM converters and its application to variable-speed wind-energy generation", *IEE Proc.-Electr. Power Appl.*, vol. 143, no. 3, pp. 231-241, May 1996.

[Pep 05]   G. Pepermans, J. Driesen, D. Haeseldonckx, R. Belmans, W. D'Haeseleer, "Distributed generation: definition, benefits and issues", *Energy Policy*, vol.33, no. 6, pp. 787-798, April 2005.

[Per 04]   A. Perdana, O. Carlson, and J. Persson, "Dynamic Response of Grid-Connected Wind Turbine with Doubly Fed Induction Generator during Disturbances" in *Proc. Nordic Workshop on Power and Ind. El. (NORPIE 2004)*, Trondheim, Norway, 2004.

[Per 05]   O. Perego, S. Belloni, *Dispower project, The CESI cogeneration plant based on Turbec T100 microturbine CHP system*, Dispower Project Highlight No. 16, www.dispower.org, 30 March 2005.

[Pet 03]   A. Petersson, *Analysis, Modelling and Control of Doubly-Fed Induction Generators for Wind Turbines*, Licentiate thesis, Technical report no. 464L, Chalmers University, Göteborg, Sweden, 2003.

[Pet 04]   A. Petersson, S. Lundberg. T. Thiringer, "A DFIG Wind-Turbine Ride-Through System Influence on the Energy Production", in *Proc. Nordic Wind Power Conference 2004*, Gothenburg, Sweden, 1 – 2 March 2004.

[Pie 04]   J.T.G. Pierik, J. Morren, E.J. Wiggelinkhuizen, S.W.H. de Haan, T.G van Engelen, J. Bozelie, *Electrical and control aspects of offshore wind turbines II (Erao-2), Vol. 1: Dynamic models of wind farms*, Technical report ECN-C--04-050, ECN, 2004, June 2004.

[Pro 05]   F. Provoost, J. Myrzik, W.L. Kling, "Optimized Voltage Control in Autonomously Controlled Networks", in *Proc. Int. Conf. on Future Power Systems (FPS 2005),* Hoofddorp, The Netherlands, 16 – 17 Nov. 2005, 5pp.

[Püt 03]   H.B. Püttgen, P.R. MacGregor, F.C. Lambert, "Distributed generation: Semantic hype or the dawn of a new era?", *IEEE Power and Energy Magazine*, vol. 1, no. 1, pp. 22 – 29, Jan-Feb 2003.

[Rez 03]   M. Reza, P.H. Schavemaker, W.L. Kling, L. van der Sluis., "A research program on intelligent power systems: Self controlling and self adapting power systems equipped to deal with the structural changes in the generation and the way of consumption", In P*roceedings of CIRED 2003 Conference*, Barcelona, Spain, 12-15 May 2003.

[Rez 05]   M. Reza, J. Morren, P.H. Schavemaker, W.L. Kling, L. van der Sluis, "Power Electronic Interfaced DG Units: Impact of Control Strategy on Power System Transient Stability", in *Proc. 3rd IEE Int. Conf. on Reliability of Transmission and Distribution systems, (RTDN '05)*, London, UK, 15-17 February 2005.

[Ryc 06a]   W.R. Ryckaert, K. De Gussemé, D.M. Van de Sype, L. Vandevelde, J.A. Melkebeek, "Damping potential of single-phase bidirectional rectifiers with resistive harmonic behaviour, *IEE Proc.-Electr. Power Appl.*, vol. 153, no. 1, pp. 68 – 74, Jan. 2006.

[Ryc 06b]   W. Ryckaert, *Vermindering van de spanningsvervorming in distributienetten met resistieve shunt-harmonische impedanties*, PhD- thesis, Universiteit Gent, 2006 (in Dutch).

[Saa 98]   Z. Saad-Saoud, M.L. Lisboa, J.B. Ekanayake, N. Jenkins, G. Strbac, "Application of STATCOMs to wind farms", *IEE Proc. Generation, Transmission and Distribution*, vol. 145, no. 5, pp. 511 – 516, Sept. 1998.

[Sac 02]   G. Saccomando, J. Svensson, and A. Sannino, "Improving voltage disturbance rejection for variables-speed wind turbines", *IEEE Trans. Energy Conversion*, vol. 17, no. 3, pp. 422-428, Sep. 2002.

[Sac 03]   Fabio Saccamanno, *Electric Power Systems – Analysis and control*, New York: Wiley-Interscience, 2003.

[Sco 02]   N.C. Scott, D.J. Atkinson, and J.E. Morrell, "Use of load control to regulate voltage on distribution networks with embedded generation", *IEEE Trans. Power Systems*, vol. 17, no. 2, pp. 510-515, May 2002.

[Slo 02]   J.G. Slootweg, W.L. Kling, "Modelling of large wind farms in power system simulations," in Proc. *IEEE Power Engineering Soc. Summer Meeting*, vol. 1, pp. 503 – 508, 2002.

[Slo 03a]   J.G. Slootweg, S.W.H. de Haan, H. Polinder, and W.L. Kling, "General model for representing variable speed wind turbines in power system dynamics simulations", *IEEE Trans. Power Systems*, vol. 18, no. 1, pp. 144-151, Feb. 2003.

[Slo 03b]   J.G. Slootweg, *Wind Power – Modelling and Impacts on Power System Dynamics*, PhD- thesis, Delft University of Technology, 2003.

[Soe 05]   J. Soens, *Impact of wind energy in a future power grid*, PhD- thesis, KU Leuven, 2005.

[Str 02]   G. Strbac, N. Jenkins, M. Hird, P. Djapic, G. Nicholson, *Integration of operation of embedded generation and distribution networks*, Report University of Manchester, 2002

[Sud 00]   S.D. Sudhoff, S.F. Glover, P.T. Lamm, D.H. Schmucker, D.E. Delisle, "Admittance Space Stability of Power Electronic Systems", *IEEE Trans. Aerospace and Electronic Systems*, vol. 36, no. 3, pp. 965-973, 2000.

[Sun 04a]   T. Sun, Z. Chen, F. Blaabjerg, "Flicker mitigation of grid connected wind turbines using STATCOM", in *Proc. 2nd Int. Conf. on Power Electr., Machines and Drives, (PEMD 2004)*, Vol. 1, pp. 175 – 180, 31 March-2 April 2004.

[Sun 04b]   T. Sun, *Power Quality of grid-connected wind turbines with DFIG and their interaction with the grid*, Ph.D. Thesis, Aalborg Univeristy, Denmark, 2004.

[Tak 03]   T. Takeshita, N. Matsui, "Current Waveform Control of PWM Converter System for Harmonic Suppression on Distribution System", *IEEE Trans. Industrial Electronics*, vol. 50, no. 6, pp. 1134 – 1139, Dec. 2003.

[Tan 04]   Y.T. Tan, *Impact on the power system with a large penetration of photovoltaic generation*, PhD- thesis, UMIST, Manchester, 2004.

[Ton 05]   Matteo Tonso, Johan Morren, Sjoerd W.H. de Haan, J.A. Ferreira, "Variable Inductor for Voltage Control in Distribution Networks", in *Proc. 11th European conference on Power Electronics and applications* (EPE 2005), Dresden, Germany, 11 – 14 September 2005

[Tra 03]   T. Tran-Quoc, C. Andrieu, N. Hadjsaid, "Technical impacts of small distributed generation units on LV networks", in *Proc. 2003 IEEE Power Engineering Society General Meeting*, vol. 4, 6 pp., 13-17 July 2003.

[UCT 04]   UCTE, *Operation Handbook – Appendix 1: Load-Frequency Control and Performance*, July 2004.

[Ver 04]   P. Vermeyen, J. Driesen, R. Belmans, "Protection of grids with distributed generation", in *Proc. 2nd IEEE Young Researcher Symposium*, 18-19 March 2004, Delft, The Netherlands.

[Vu 05]   T. Vu Van, J. Driesen, R. Belmans, "Power Quality and voltage stability of distribution system with distributed energy resources," *International journal of distributed energy resources*, vol.1, no.3, pp. 227 – 240, Sept. 2005.

[Vu 06]   T. Vu Van, *Impact of Distributed Generation on power system operation and control*, Ph.D. Thesis, KU Leuven, 2006.

[Wal 01]   Simon R. Wall, "Performance of Inverter Interfaced Distributed Generation", in *Proc. 2001 IEEE/PES Transmission and Distribution Conference and Exposition*, vol. 2, pp. 945-950.

[Wil 95]   C.M. Wildrick, F.C. Lee, B.H.Cho, B.Choi, "A method of defining the load impedance specification for a stable distributed power system", *IEEE Trans. Power Electronics*, vol. 10, no. 3, pp. 280-285, May 1995.

[Woy 03]   A. Woyte, *Design issues of photovoltaic systems and their grid integration*, PhD- thesis, KU. Leuven, 2003.

[Ye 04]   Z. Ye, A. Kolwalkar, Y. Zhang; P. Du; R. Walling, "Evaluation of anti-islanding schemes based on nondetection zone concept", *IEEE Trans. Power Electronics*, vol. 19, no. 5, pp. 1171 – 1176, 2004.

[Yin 01]   R.J. Yinger, Behaviour of Capstone and Honeywell Microturbine Generators during Load Changes, *CERTS Report LBNL-49095*, July 2001.

[Yin 04]   J. Yin, L. Chang, C. Diduch, "Recent developments in islanding detection for distributed power generation", in Proc. *2004 Large Eng. Systems Conf. on Power Eng., LESCOPE-04*, pp. 124 – 128, 28 – 30 July 2004.

[Zhu 02]   Y. Zhu, K. Tomsovic, "Development of models for analyzing the load-following performance of microturbines and fuel cells", *Electric Power Systems Research*, vol. 62, no. 1, pp. 1 -11, 2002.

Appendix A

Network model description

For the case studies that are done in this thesis simplified models of an electricity network are used. The networks will be described shortly in this appendix.

A.1 Urban network

The Nuon 'Testnet' is a 10kV cable distribution network in a residential area in Lelystad, The Netherlands, and it can be characterised as a strong MV network. It consists of a MV distribution substation with a number of radial feeders. A simplified layout of the network is shown in Fig. A.1. Only the feeders that are used in this thesis are shown.
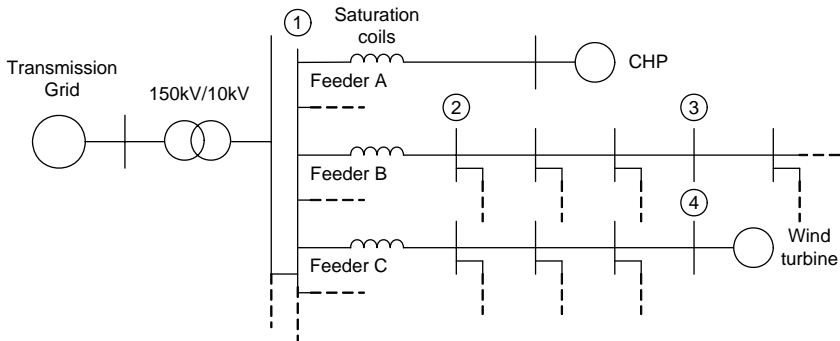
Fig. A.1. Schematic layout of 10 kV 'Testnet' cable network

The 10 kV substation is connected with the 150 kV HV transmission network by a 47 MVA transformer. The feeders are connected to the substation by a series reactor to limit the short-circuit current. The total load of the Testnet is about 8 MW and 4 MVAr.

Three small wind turbines with a total installed capacity of about 1.5 MW are connected to feeder C. They are modelled as one equivalent turbine. Feeder A has a CHP plant of about 2.5 MW. The network is rather lightly loaded and can be considered as a 'strong' network.

When the network is used, it is modelled as a Thévenin equivalent circuit, with the impedance given by the short-circuit impedance of the node under consideration. The parameters of the four nodes that are used are given in table A.1.

Table A.1. Parameters of the Testnet

Node	S_{sc} [MW]	X_{sc}/R_{sc}
1	320	45
2	105	1.25
3	60	0.75
4	50	0.75

A.2 Rural network

The Maarhuizen network is an extensive rural 10 kV cable network in the north of the Netherlands. It can be characterised as a weak MV network. It is fed from a 110 kV transmission network by 3 parallel 30 MVA transformers. One feeder is considered in the studies. Three wind turbines with a total rated power of 1.6 MW are connected to this network. The feeder has a high impedance. In some cases this results in large voltage deviations. The layout of the network is shown in Fig. A.2. The short-circuit impedance at the three nodes that have been used is given in table A.2. When the network is used, it is modelled as a Thévenin equivalent circuit, with the impedance given by the short-circuit impedance of the node under consideration.
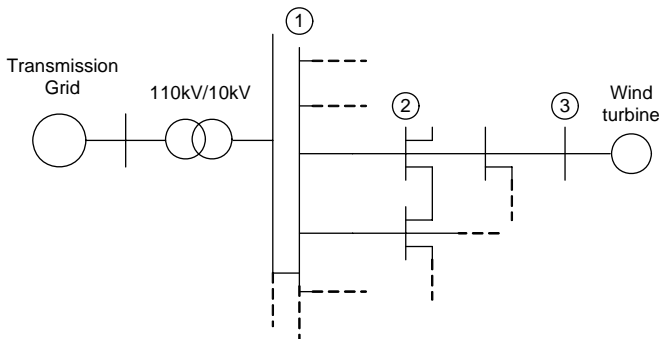
Fig. A.2. Layout of a part of the Maarhuizen 10 kV rural cable network

Table A.2. Parameters of the rural network

Node	S_{sc} [MW]	X_{sc}/R_{sc}
1	153	41
2	103	2.20
3	21	0.35

A.3 Low-voltage network

The low-voltage network in Vroonermeer-Zuid, a suburb of Alkmaar, is a typical 400 V network with a large fraction of DG (solar cells). The maximum power feedback from the PV generators in the area is planned to be 36 MW [Ens 04]. The complete network is still under development and not all PV systems are installed yet. The maximum loading of the area is around 60 MVA. The individual homes with roof mounted PV arrays are connected to a number of network sections that are supplied from separate 10 kV/400 V transformers. The network is of particular interest because severe problems with harmonic distortion and resonances have been noted in it [Ens 04]. The problems are due to the low resonance frequencies in the grid, which are due to the high amount of capacitance. The capacitance is mainly formed by the output capacitance of the power electronic converters (loads and PV inverters) in the grid.

In this thesis a lumped model of one of the 400 V networks is used. The model is shown in shown in Fig. A.3. The section has a peak solar generation of 235 kW and an average load of 26 kW. The grid impedance consists of a resistance R_g and an inductance L_g which are mainly determined by the transformer and cable impedance. The capacitance C_l is formed by the parallel connection of the filter capacitance of the solar inverters and load. The resistance R_l represents the loads in the network. The parameters are given in table A.3.
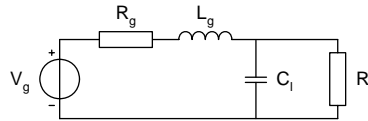

Fig. A.3. Lumped representation of one 400V feeder of the Low-voltage network

Table A.3 Parameters of the Vroonermeer-Zuid network

Parameter	Value	Unit	Parameter	Value	Unit
L_g	140	μH	C_l	300	μH
R_g	0.1	Ω	R_l	2	Ω

148

Appendix B

Converter model description

This appendix describes the power electronic converter models that have been used.

B.1 Single-phase full-bridge converter

The case studies in chapter 3 are performed with a model of a 5 kW single-phase full-bridge converter switching at 20 kHz. The converter has an LCL-filter, with a resonance frequency of ~9 kHz. The filter design is based on the procedure described in [Lis 01]. Fig. B.1 shows the complete converter model. The converter has been modelled in the SimPowerSystems blockset of Matlab. For the full-bridge IGBT-converter the universal switch block is used. Fig. B.2 shows the structure of the current controller.
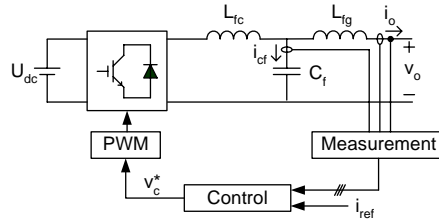
Fig. B.1. Model of single-phase converter with LCL filter
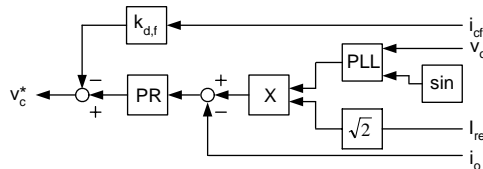
Fig. B.2. Structure of current controller of single-phase converter with LCL filter

The reference sine wave for the current control is obtained from an internally generated waveform that is synchronised to the grid voltage with a PLL. This sine wave is

multiplied with the rms value of the reference current I_{ref}. The current is controlled with a PR controller. It uses second-order generalised integrators to achieve zero steady-state error [Hau 02]. The transfer function of the PR-controller shown in Fig. B.2 is:

$$G_{PR}(s) = K_p + \frac{K_r s}{s^2 + \omega_0^2}$$
(B.1)

The gain of the transfer function becomes infinite at ω_0 and thus it can bring the steady-state error at this frequency back to zero. The size of the proportional gain K_p from the PR controller determines the bandwidth and phase margin of the system, in the same way as for classical PI-controllers [Lis 06]. In the high-frequency range (above the bandwidth of the PR-controller) the stability is related to the damping of the LCL-filter. A feed-forward control loop is used to avoid oscillations in the filter. The parameters that have been used for the filter and the controller are given in table B.I.

Table B.1 Parameters of single-phase inverter

Parameter	Value	Unit	Parameter	Value	Unit
P_{nom}	5	kW	L_{fc}	0.2	mH
V_{nom}	230	V	L_{fg}	0.8	mH
f_s	20	kHz	K_p	10	-
V_{dc}	600	V	K_r	10000	-
C_f	2	μF	$k_{d,f}$	10	-

For the comparison in section 3.3.3 the model described above is used. For the other simulations the PWM-block and the switches are replaced by a controlled voltage source that is directly controlled by the output of the current controller.

B.2 Three-phase full-bridge converter

The DG units in chapter 4, 5, 6, and 7 are connected to the grid by a three-phase full-bridge IGBT-converter. The converter model is shown in Fig. B.3. The dc-link of the converter is modelled as a voltage source when the converter is used without DG unit. The converter uses a first-order filter, with inductance L_f and resistance R_f. The output current and voltage of the converter are measured and transformed to the dq-reference frame. The currents are controlled by PI-controllers to get the reference voltage for the full-bridge. The reference voltages are transformed back to the abc-reference frame. A triangular-carrier-based PWM circuit converts the reference signals to the on/off signals for the switches. The structure of the control is shown in Fig. B.4. The reference currents are obtained from the active and reactive power controllers.
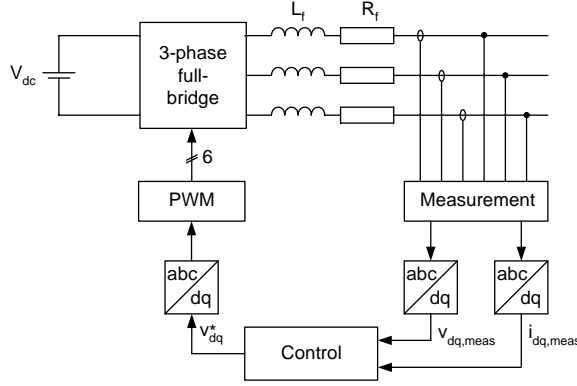
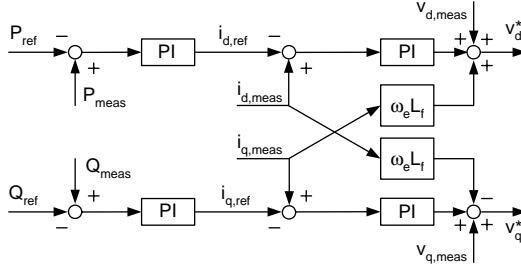Fig. B.3. Model of three-phase full-bridge converter with RL filter

Fig. B.4. Scheme of the power and current controller of a three-phase inverter

The remaining part of this section discusses how the controller constants for the current controller can be obtained. The voltage difference across the filter is:

$$\Delta v_d = R_f i_d + L_f \cdot \frac{di_d}{dt} + \omega_e L_f i_q$$

$$\Delta v_q = R_f i_q + L_f \cdot \frac{di_q}{dt} - \omega_e L_f i_d$$

(B.2)

The last terms in the equations cause a cross-coupling of the *d*- and *q*-axes. They are treated as disturbances on the output, as shown in Fig. B.4. The PI controller tracks the i_d and i_q errors to give Δv_d and Δv_q respectively. To ensure good tracking of thee currents, the cross-related flux terms are added to v_d and v_q to obtain the reference voltages.

The transfer function of the filter, from voltage to current, is:

$$G(s) = \frac{1}{L_f s + R_f}$$

(B.3)

Using the Internal Model Control principle [Har 98] to design the controllers yields:

$$K(s) = K_p + \frac{K_i}{s} = \frac{\alpha_c}{s} G^{-1}(s) \tag{B.4}$$

where α_c is the bandwidth of the current control loop, K_p is the proportional gain and K_i is the integral gain of the controller. The gains become [Pet 03]:

$$K_p = \alpha_c L_f; \quad K_i = \alpha_c R_f \tag{B.5}$$

Generally some fine-tuning is done to optimise the response.

The converter has an outer control loop that controls the active and reactive power of the converter. The measured active and reactive power are calculated from:

$$
\begin{aligned}
P_{meas} &= v_{d,meas} i_{d,meas} + v_{q,meas} i_{q,meas} \\
Q_{meas} &= v_{q,meas} i_{d,meas} - v_{d,meas} i_{q,meas}
\end{aligned} \tag{B.6}
$$

In chapter 5 simulations are presented that are done with a 2 MW converter. The parameters of this converter are given in table B.2.

Table B.2 Parameters of three-phase inverter

Parameter	Value	Unit	Parameter	Value	Unit
P_{nom}	2	MW	$K_{p,d}$	0.2	-
V_{nom}	960	V	$K_{i,d}$	12.5	-
f_s	5	kHz	$K_{p,q}$	0.1	-
V_{dc}	1500	V	$K_{i,q}$	6.25	-
L_f	0.2	mH	$K_{p,P}, K_{p,Q}$	0.1	
R_f	12.5	mΩ	$K_{i,P}, K_{i,Q}$	0.001	

In most cases a 'reduced model' of the converter is used, which does not take into account the modulation and the switching of the IGBTs. Appendix F shows that this model can be used as long as the frequency of the phenomena that are investigated is much lower than the switching frequency of the converter. This condition is met in steady-state situations, but not always during transient phenomena such as short-circuits and voltage dips. It is shown in [Mor 04] that there are some differences between the 'full' and 'reduced' model in these situations, but they are limited.

The reduced model is modelled in the *dq0*-reference frame and simulated in Simulink. The block diagram of the model is shown in Fig. B.5. The filter block contains the transfer functions that can be obtained from (B.2). The control block contains the controller structure shown in Fig. B.4. The reference value for the power, P_{ref}, is obtained from the DG unit control or from the dc-link control.
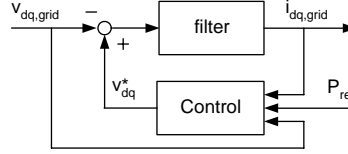
Fig. B.5. Block diagram of three-phase full-bridge converter in *dq0*-reference frame

B.3 Three-phase back-to-back converter

Introduction - Several types of DG unit use a back-to-back converter, consisting of two full-bridge IGBT-converters with a dc-link in between. They are modelled according to the block diagram shown in Fig. B.6. The DG unit and its converter are modelled as one sub-system. The models are described in appendix C. The 3-phase full bridge converter model is described in the previous section. It has the task to control the dc-link voltage. It receives its power setpoint from the dc-link control. The dc-link model is shown in Fig. B.7. The dc-link control is described in this subsection. The controller design is based on [Ott 03]. The parameters of the back-to-back converter are given in appendix C, together with the DG unit parameters.
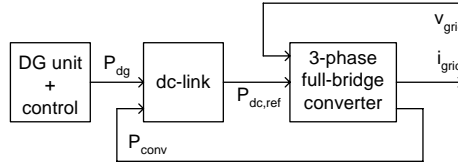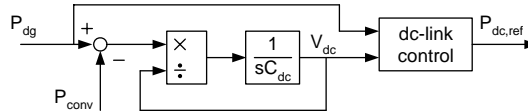

Fig. B.6. Block diagram of a model of a DG unit with back-to-back converter in *dq0*-reference frame

Fig. B.7. Model of dc-link of back-to-back converter

dc-link control - The dc-link capacitor behaves as an energy storage device. Neglecting losses, the time derivative of the stored energy equals the difference between the DG unit power P_{dg} and the converter power P_{conv}:

$$\frac{1}{2} C_{dc} \frac{dv_{dc}^2}{dt} = P_{dg} - P_{conv} \qquad (B.7)$$

This equation is nonlinear with respect to v_{dc}. Therefore a new state-variable is introduced: $W = v_{dc}^2$. Substituting this in (B.7) gives:

$$\frac{1}{2}C\frac{dW}{dt} = P_{dg} - P_{conv} \tag{B.8}$$

which is linear with respect to W. The physical interpretation of this state-variable substitution is that the energy is chosen to represent the dc-link characteristics [Ott 03]. The dc-link voltage is assumed to be controlled by the converter. P_{conv} is written as $v_{dc} \cdot i_{dc}$. The transfer function from i_{dc} to W is then:

$$G(s) = -\frac{2}{sC_{dc}} \tag{B.9}$$

As this transfer function has a pole in the origin it will be difficult to control it. An inner feedback loop for active damping is used [Ott 03]:

$$i_{dc} = i_{dc}^{'} + G_a W \tag{B.10}$$

with G_a the active conductance, performing the active damping, and i_{dc}' the reference current provided by the outer control loop, see Fig. B.8. Substituting (B.10) into (B.8) gives:

$$\frac{1}{2}C_{dc}\frac{dW}{dt} = P_{dg} - v_{dc}i_{dc}^{'} - v_{dc}G_a W \tag{B.11}$$

The transfer function from i_{dc}' to W becomes:

$$G^{'}(s) = -\frac{2}{sC_{dc} + 2G_a} \tag{B.12}$$

Using the internal model control principle [Har 98], the following parameters for the PI-controller can be obtained [Ott 03]:

$$k_p = -\frac{\alpha_d C_{dc}}{2}, \quad k_i = -\frac{\alpha_d^2 C_{dc}}{2} \tag{B.13}$$

When the pole of $G'(s)$ is placed at $-\alpha_d$ the following active conductance is obtained:

$$G_a = \frac{\alpha_d C_{dc}}{2} \tag{B.14}$$

The controller is completed by a feed-forward term from P_{dg} to $P_{dc,ref}$', which improves the dynamic response of the dc-link controller.
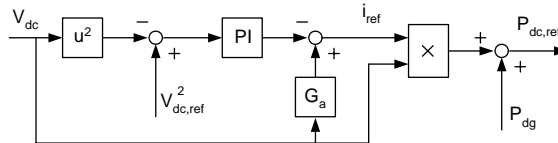

Fig. B.8. Model of dc-link control of back-to-back converter

Appendix C

DG unit model description

This appendix describes the DG unit models that are used and gives the used parameters.

C.1 Fuel cell

In this section the model of the fuel cell system is described. The block diagram of the model is shown in Fig. C.1. It consists of a reformer, a fuel cell stack, a dc/dc converter, a dc-link, a three-phase VSC and a controller. The dc/dc converter is modelled with a fixed transfer ratio between input and output voltage. The dc-link control and the inverter are described in appendix B. The combined model of the fuel cell, reformer and its control is shown in Fig. C.2. It is obtained from [Zhu 02].
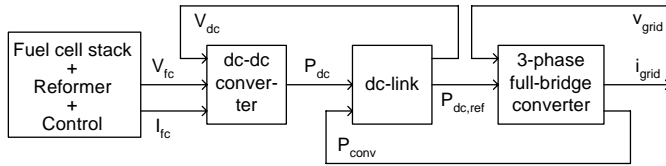

Fig. C.1. Fuel cell system block diagram

Reformer - The response of the chemical processes in the reformer is usually slow, because of the time that is needed to change the chemical reaction parameters after a change in the flow of reactants. The dynamic response function is modelled as a first-order transfer function with a time constant T_f.

Fuel cell stack - A model of a SOFC fuel cell is used. The modelling is based on [Kar 03], [Pad 00] and [Zhu 02]. The overall fuel cell reaction is

$$H_2 + \frac{1}{2}O_2 \rightarrow H_2O \tag{C.1}$$

The stoichiometric ratio of hydrogen to oxygen is 2 to 1. The fuel cell is controlled in such a way that there is always an oxygen excess, to let hydrogen react with oxygen more completely. In [Zhu 02] a ratio of 1.145 is proposed.
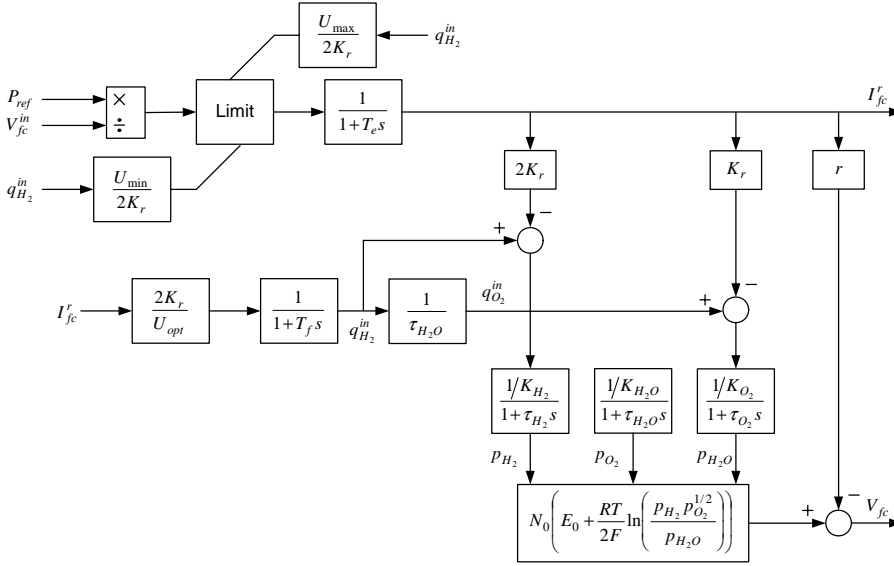

Fig. C.2. SOFC schematic diagram [Zhu 02]

The anode is assumed to be supplied with H_2 only and the cathode with O_2 only. The potential difference between the anode and cathode can be calculated with the Nernst equation, minus the voltage drop due to ohmic polarisation

$$V_{fc} = N_0 \left(E_0 + \left(\frac{RT}{2F} \right) \ln \left(\frac{p_{H_2} \sqrt{p_{O_2}}}{p_{H_2O}} \right) \right) - rI_{fc} \tag{C.2}$$

where $p_{H_2}, p_{H_2O}, p_{O_2}$ are the partial pressures of H_2, H_2O and O_2 respectively.

An important parameter for a fuel cell is the fuel utilisation U_f. It is defined as the ratio between the fuel flow that reacts and the input fuel flow. Typically an 80% – 90% utilisation is used [Zhu 02]. For a certain input hydrogen flow, the demand current of the fuel cell can then be restricted in the range

$$\frac{0.8 q_{H_2}^{in}}{2 K_r} \leq I_{fc} \leq \frac{0.9 q_{H_2}^{in}}{2 K_r} \tag{C.3}$$

The optimal utilisation factor (U_{opt}) is assumed to be 85% and thus [Kar 03]:

$$q_{H_2}^{in} = \frac{2 K_r}{0.85} I_{fc} \tag{C.4}$$

The molar flow of hydrogen that reacts is [Pad 00]:

$$q_{H_2}^{r} = \frac{N_0 I_{fc}}{2F} = 2 K_r I_{fc} \tag{C.5}$$

with K_r [kmol/(s·A)] defined for modelling purposes.

Model implementation and parameters - Fig. C.1 and Fig. C.2 show the block diagram of the complete system and of the dynamic model of the SOFC. Parameters of the 100 kW fuel cell that is used are given in table C.1. Parameters of the converter that is used are given in table C.2

Table C.1 Fuel cell parameters

Parameter	Value	Unit	Parameter	Value	Unit
P_{rate}	100	kW	K_{H2}	$8.43 \cdot 10^{-4}$	kmol/(s·atm)
P_{ref}	100	kW	K_{H2O}	$2.81 \cdot 10^{-4}$	kmol/(s·atm)
T	273	K	K_{O2}	$2.52 \cdot 10^{-3}$	kmol/(s·atm)
F	$96.487 \cdot 10^{3}$	C/kmol	τ_{H2}	26.1	s
R	8314	J/(kmol·K)	τ_{H2O}	78.3	s
E_0	1.18	V	τ_{O2}	2.91	s
N_0	384	-	r	0.126	V
K_r (=N_0/4F)	$0.996 \cdot 10^{-6}$	kmol/(s·A)	T_e	0.8	s
U_{max}	0.9	-	T_f	5	s
U_{min}	0.8	-	r_{H_O}	1.145	-
U_{opt}	0.85	-			

Table C.2 Parameters of back-to-back converter of micro turbine

Parameter	Value	Unit	Parameter	Value	Unit	Parameter	Value	Unit
P_{nom}	100	kW	L_{conv}	0.1	mH	$K_{p,dc}$	$7.5 \cdot 10^{-5}$	-
$V_{conv,nom}$	400	V	R_{conv}	12.5	mΩ	$K_{i,dc}$	$7.5 \cdot 10^{-3}$	-
V_{dc}	750	V	$K_{p,conv}$	0.02	-	G_a	$7.5 \cdot 10^{-5}$	-
C_{dc}	1	mF	$K_{i,conv}$	4	-			

C.2 Micro turbine

This section describes the micro turbine model. The system, shown in Fig. C.3, consists of a gas turbine, a permanent magnet generator and a back-to-back converter. The converter was already described in appendix B. The gas turbine and the permanent magnet generator are described in this section. The parameters of the permanent magnet generator and the gas turbine are given in table C.3. The parameters of the 300 kW converter are given in table C.4.

Gas turbine - The gas turbine consists of a compressor, a combustor and a turbine. A detailed description of the modelling of the individual parts of the system can be found in [Nik 05]. In the thesis an approximation is used, that models the gas turbine as a first order transfer function:

$$G_{gt}(s) = \frac{1}{\tau_{gt}s + 1}$$ (C.6)

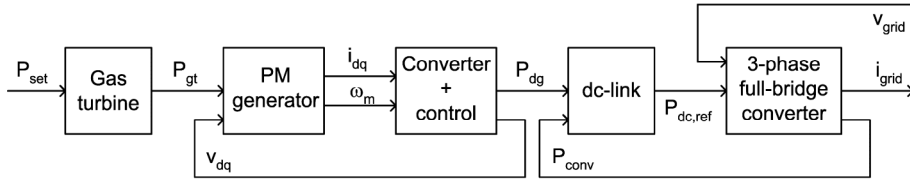In literature the values of τ_{gt} vary from tens of milliseconds to tens of seconds.

Fig. C.3. Micro turbine system block diagram

Permanent magnet generator – Using the generator convention, the stator voltage equations of a synchronous machine are given by:

$$v_{ds} = -R_s i_{ds} - \omega_s \psi_{qs} - \frac{d\psi_{ds}}{dt} \quad \text{with} \quad \begin{array}{l} \psi_{ds} = L_s i_{ds} + \Psi_f \\ \psi_{qs} = L_s i_{qs} \end{array}$$

$$v_{qs} = -R_s i_{qs} + \omega_s \psi_{ds} - \frac{d\psi_{qs}}{dt}$$ (C.7)

The electrical torque T_e of the permanent magnet generator is given by [Sch 01]:

$$T_e = 2 p i_{qs} \Psi_f$$ (C.8)

with p the number of pole pairs. The stator electrical angular velocity is given by $\omega_s = p\omega_m$, with ω_m the mechanical angular velocity [rad/s], which can be obtained from:

$$\frac{d\omega_m}{dt} = \frac{1}{J}(T_m - T_e)$$ (C.9)

with J the inertia constant of the rotor [kg·m^2] and T_m the mechanical torque [Nm]. The generator model is based on these three equations.

Control - In order to apply independent control for the two coordinates the influence of the q-axis on the d-axis-components and vice versa must be eliminated. This can be done by decoupling the two components, in the way shown in Fig. C.4. With the decoupling applied, the linear transfer function of i_{ds} to v_{ds} is:

$$\frac{i_{ds}(s)}{v_{ds}(s)} = \frac{1}{L_s s + R_s} \tag{C.10}$$

The proportional and integral constants for the PI-controller can be obtained as [Pet 03]:

$$k_p = \alpha_c L_s, \quad k_i = \alpha_c R_s \tag{C.11}$$

with α_c is the bandwidth of the current control loop. The angular velocity ω_m can be controlled by T_e which is proportional to i_{qs}. The constants for the speed controller are [Sch 01]:

$$k_p = \frac{2 p^2 \psi_f}{J}, \quad k_i = \frac{2 p^2 \psi_f R_s}{J L_s} \tag{C.12}$$

Table C.3 Micro turbine parameters

Parameter	Value	Unit	Parameter	Value	Unit	Parameter	Value	Unit
τ_{gt}	1	-	L_s	40	μH	$K_{p,d}$	0.145	-
P_{rate}	300	kW	ψ_f	0.06	Vs	$K_{i,d}$	$2.9 \cdot 10^{-3}$	-
V_s	400	V	J	0.31	kgm^2	$K_{p,q}$	0.145	-
ω_m	3000	rad/s	τ_{gt}	0.3	s	$K_{i,q}$	$2.9 \cdot 10^{-3}$	-
R_s	0.0022	Ω						

Table C.4 Parameters of back-to-back converter of micro turbine

Parameter	Value	Unit	Parameter	Value	Unit	Parameter	Value	Unit
P_{nom}	300	kW	L_{conv}	0.1	mH	$K_{p,dc}$	$7.5 \cdot 10^{-4}$	-
$V_{conv,nom}$	400	V	R_{conv}	12.5	mΩ	$K_{i,dc}$	$7.5 \cdot 10^{-2}$	-
V_{dc}	750	V	$K_{p,conv}$	0.02	-	G_a	$7.5 \cdot 10^{-4}$	-
C_{dc}	1	mF	$K_{i,conv}$	4	-			

Fig. C.4. Converter + control block diagram

C.3 Wind turbine with doubly-fed induction generator

This section presents the model of the wind turbine with Doubly-Fed Induction Generator (DFIG) that is used. This type of wind turbine has a converter connected to the rotor windings instead of the stator windings. A block diagram of the model is shown in Fig. C.5. This section gives first a short description of the aerodynamical and mechanical (turbine) model, followed by a description of the electrical generator and its control. The dc-link model and the model of the full-bridge converter are given in appendix B. The model of the three-winding transformer can be found in [Pie 04].

Fig. C.5. Block diagram of wind turbine with doubly-fed induction generator

Wind turbine model and control - The description of the turbine model will be brief. A more detailed description can be found in [Pie 04]. A wind model is used to calculate a realisation of the stochastically changing wind speed. From this the averaged wind speed over the turbine rotor is determined to obtain the instantaneous aerodynamic torque, including the variations caused by the passing of the blades through the

inhomogeneous wind field over the rotor area. The effect of wind speed variations on the aerodynamic torque is determined by a $C_p(\lambda)$ curve.

The wind turbine model consists of sub-models for the aerodynamic behaviour of the rotor, the rotating mechanical system (drive-train), the tower, power limitation by pitch control and the electrical generator and control. The mechanical model for turbine rotor, low and high-speed shaft, gearbox and generator rotor is a two-mass spring and damper model. The tower model consists of a mass-spring-damper model for the translation of the tower top in two directions: front-aft and sideways.

Since electrical and mechanical dynamics in a wind turbine are of different time scales (i.e. the electrical dynamics are much faster than the mechanical dynamics), the whole system can be controlled in a cascade structure. The fast electrical dynamics can be controlled in an inner loop and a speed controller can be added in a much slower outer loop. The speed controller of the wind turbine was described in chapter 2 already. The control of the electrical generator will be described below.

Generator model – The induction generator is represented by a 5th order model in the *dq* reference frame. Using the generator convention, the following set of equations results:

$$
\begin{aligned}
v_{ds} &= -R_s i_{ds} - \omega_s \psi_{qs} + \frac{d\psi_{ds}}{dt} \\
v_{qs} &= -R_s i_{qs} + \omega_s \psi_{ds} + \frac{d\psi_{qs}}{dt} \\
v_{dr} &= -R_r i_{dr} - \omega_r \psi_{qr} + \frac{d\psi_{dr}}{dt} \\
v_{qr} &= -R_r i_{qr} + \omega_r \psi_{dr} + \frac{d\psi_{qr}}{dt}
\end{aligned}
\quad \text{with} \quad
\begin{aligned}
\psi_{ds} &= -(L_s + L_{ms})i_{ds} - Mi_{dr} \\
\psi_{qs} &= -(L_s + L_{ms})i_{qs} - Mi_{qr} \\
\psi_{dr} &= -(L_r + L_{mr})i_{dr} - Mi_{ds} \\
\psi_{qr} &= -(L_r + L_{mr})i_{qr} - Mi_{qs}
\end{aligned}
\tag{C.13}
$$

with $M = \sqrt{L_{ms}L_{mr}}$ the mutual inductance.

The electrical angular velocity of the rotor, ω_r, is:

$$
\omega_r = \omega_s - p\omega_m \tag{C.14}
$$

with p the number of pole pairs [-] and ω_m the mechanical angular velocity [rad/s]. The electrical torque of the generator is given by:

$$
T_e = p(\psi_{dr}i_{qs} - \psi_{qr}i_{ds}) \tag{C.15}
$$

The rotational speed of the generator is given as:

$$
\frac{d\omega_m}{dt} = \frac{1}{J}(T_m - T_e) \tag{C.16}
$$

The active and reactive power delivered by the stator are given by:

$$
P_s = v_{ds}i_{ds} + v_{qs}i_{qs} \tag{C.17}
$$

$$Q_s = v_{qs}i_{ds} - v_{ds}i_{qs} \tag{C.18}$$

The model of the induction generator that has been used is based on (C.13) - (C.18).

Generator control – The structure of the control of the induction generator is shown in Fig. C.6. Since the stator flux is almost fixed to the stator voltage, it is practically constant. This implies that the derivative of the stator flux and of the stator magnetizing current are close to zero, and can be neglected [Pen 96], [Pet 03]. The voltage equations of the rotor which have previously been given in (C.13) can then be written as:

$$v_{dr} = -R_r i_{dr} - L_r \frac{di_{dr}}{dt} - \omega_r \psi_{qr}$$
$$v_{qr} = -R_r i_{qr} - L_r \frac{di_{qr}}{dt} + \omega_r \psi_{dr} \tag{C.19}$$

This equation is comparable to equation (B.2) for the three-phase full-bridge converter in appendix B.2. The PI-controller parameters for the generator control can be obtained in the same way as described in appendix B.2.

A synchronously rotating *dq* reference frame with the direct *d*-axis oriented along the stator flux vector position is used to control the generator. Due to the chosen reference frame, ψ_{qs} and v_{ds} are zero. Therefore the reactive power and the active power delivered by the stator can be written as:

$$P_s = v_{qs}i_{qs} = v_{qs}\left(\frac{L_m}{L_r + L_m}\right)i_{qr} \tag{C.20}$$

$$Q_s = v_{qs}i_{ds} = \omega_s\left(-\left(L_s + L_m\right)i_{ds} - L_m i_{dr}\right)i_{ds} \tag{C.21}$$

As the stator current is equal to the supply current, it can be assumed that it is constant. The reactive power is then proportional to the direct component of the rotor current i_{dr}. The active power, and thus the speed, can be controlled by i_{qr}.

It is assumed that the current controller is much faster than the speed controller. The electrical torque is then $T_e = T_{e,ref}$. The reference torque is set to:

$$T_{e,ref} = T'_{e,ref} - B_a\omega_m \tag{C.22}$$

where B_a is an "active damping torque" [Pet 03]. The transfer function from rotational speed to electrical torque becomes now:

$$G_s(s) = \frac{1}{Js + B_a} \tag{C.23}$$

Using again the IMC method, the following gains of the controller are obtained [Pet 03]:

$$k_{ps} = \alpha_s J, \quad k_{is} = \alpha_s B_a \tag{C.24}$$

where α_s is the desired closed-loop bandwidth of the speed controller. When B_a is chosen to be $B_a=J\alpha_s$, changes in the mechanical torque are damped with the same time constant as the bandwidth of the speed control loop [Pet 03].
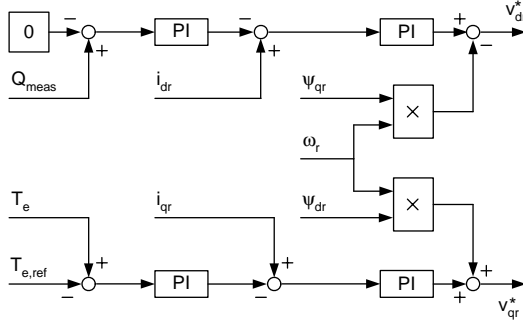

Fig. C.6. Converter + control block diagram

Converter – A DFIG has a back-to-back converter connected between its rotor terminals and the grid. The generator side converter is used to control the rotor currents of the machine, according to (B.2) - (B.5) and (C.19), while the grid side converter controls the DC-link voltage. The converter model is described in appendix B.3.

Parameters – The parameters that have been used for the wind turbine with doubly-fed induction generator are given in table C.5. The parameters for the converter model are given in table C.6.

Table C.5 Doubly-fed induction generator machine parameters

Parameter	Value	Unit	Parameter	Value	Unit	Parameter	Value	Unit
P_{nom}	2.75	MW	L_{mr}	18.2	mH	$K_{p,q}$	0.2	-
$V_{s,nom}$	960	V	L_s	0.118	mH	$K_{i,q}$	0.32	-
$V_{r,nom}$	670	V	L_r	0.31	mH	$K_{p,s}$	25	-
ω_m	1000	rad/s	R_s	1.2	mΩ	$K_{i,s}$	155	-
p	3	-	R_r	5.2	mΩ	$K_{p,Q}$	0.00032	-
J	240	kgm^2	$K_{p,d}$	0.02	-	$K_{i,Q}$	0.0032	-
L_{ms}	4.55	mH	$K_{i,d}$	3.2	-			

Table C.6 Parameters of back-to-back converter of doubly-fed induction generator

Parameter	Value	Unit	Parameter	Value	Unit	Parameter	Value	Unit
P_{nom}	750	kW	L_{conv}	0.1	mH	$K_{p,dc}$	$2.5 \cdot 10^{-4}$	-
$V_{conv,nom}$	670	V	R_{conv}	12.5	mΩ	$K_{i,dc}$	$2.5 \cdot 10^{-2}$	-
V_{dc}	1100	V	$K_{p,conv}$	0.01	-	G_a	$2.5 \cdot 10^{-4}$	-
C_{dc}	1	mF	$K_{i,conv}$	0.1	-			

C.4 Wind turbine with synchronous generator and full-size converter

The fourth type of DG unit that is used is a variable speed wind turbine with a synchronous generator and a full-size converter. The variable speed wind turbine is equal to that of the model described in section C.3, for a wind turbine with a DFIG. A permanent magnet generator is used and the generator and converter model are equal to that of the micro turbine described in section C2. The parameters for the permanent magnet generator are given in table C.7. The parameters of the 1.5 MW converter are given in table C.8.

Table C.7 Permanent magnet synchronous machine parameters

Parameter	Value	Unit	Parameter	Value	Unit	Parameter	Value	Unit
P_{rate}	1.5	MW	J	240	kgm^2	$K_{p,d}$	$6.8 \cdot 10^{-4}$	-
V_s	960	V	Ψ_f	9.8	Vs	$K_{i,d}$	$3.4 \cdot 10^{-3}$	-
ω_m	1.7	rad/s	L_s	1.3	mH	$K_{p,q}$	$1.4 \cdot 10^{-3}$	-
p	60	-	R_s	0.014	Ω	$K_{i,q}$	$2.9 \cdot 10^{-4}$	-

Table C.8 Parameters of back-to-back converter of permanent magnet generator

Parameter	Value	Unit	Parameter	Value	Unit	Parameter	Value	Unit
P_{nom}	1.5	MW	L_{conv}	0.1	mH	$K_{p,dc}$	$2.5 \cdot 10^{-4}$	-
$V_{conv,nom}$	960	V	R_{conv}	12.5	mΩ	$K_{i,dc}$	$2.5 \cdot 10^{-2}$	-
V_{dc}	1750	V	$K_{p,conv}$	0.01	-			
C_{dc}	3	mF	$K_{i,conv}$	0.1	-			

Appendix D

Short-circuit response of induction machine

This appendix determines the response of an induction machine to a symmetrical short-circuit at its stator terminals. Based on this analysis, section 5.6 analyses the response of a wind turbine with doubly-fed induction generator to a voltage dip. The analysis in this appendix is based on the analyses in [Kov 59].

For the analysis a space-vector description is used. In a synchronously rotating reference frame the equations describing an induction machine are [Kov 59]:

$$\vec{v}_s = R_s \vec{i}_s + \frac{d\vec{\psi}_s}{dt} + j\omega_s \vec{\psi}_s \qquad (D.1)$$

$$\vec{v}_r = R_r \vec{i}_r + \frac{d\vec{\psi}_r}{dt} + j(\omega_s - \omega_r)\vec{\psi}_r \qquad (D.2)$$

$$\vec{\psi}_s = L_s \vec{i}_s + L_m \vec{i}_r \qquad (D.3)$$

$$\vec{\psi}_r = L_m \vec{i}_s + L_r \vec{i}_r \qquad (D.4)$$

In these equations all parameters are reduced to the stator side. The equations can also be written in a fixed reference frame (fixed to the stator of the machine). In that case ω_s is zero. Based on these equations the equivalent circuit of the induction machine shown in Fig. D.1 can be obtained. It can be used for transient analysis of an induction machine.
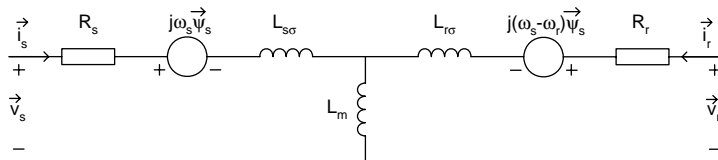

Fig. D.1. Equivalent circuit of induction machine for transient analysis

Based on (D.3) and (D.4) the currents can be written as a function of the fluxes:

$$\dot{i}_s = \frac{1}{L_s - \frac{L_m^2}{L_r}} \vec{\psi}_s - \frac{L_m}{L_r} \frac{1}{L_s - \frac{L_m^2}{L_r}} \vec{\psi}_r \tag{D.5}$$

$$\dot{i}_r = -\frac{L_m}{L_s} \frac{1}{L_r - \frac{L_m^2}{L_s}} \vec{\psi}_s + \frac{1}{L_r - \frac{L_m^2}{L_s}} \vec{\psi}_r \tag{D.6}$$

In these equations the term $L_s - \frac{L_m^2}{L_s}$ is similar to the transient inductance of a synchronous machine [Kov 59]. It will be denoted as $L_s^{'}$. Knowing that $L_s = L_{s\sigma} + L_m$ and $L_r = L_{r\sigma} + L_m$, the transient stator inductance can be written as:

$$L_s^{'} = L_{s\sigma} + \frac{L_{r\sigma}L_m}{L_{r\sigma} + L_m} \tag{D.7}$$

Similarly the transient rotor inductance can be introduced as:

$$L_r^{'} = L_{r\sigma} + \frac{L_{s\sigma}L_m}{L_{s\sigma} + L_m} \tag{D.8}$$

The equations can further be simplified by introducing the stator and rotor coupling factors:

$$k_s = \frac{L_m}{L_s} \tag{D.9}$$

$$k_r = \frac{L_m}{L_r} \tag{D.10}$$

And the leakage factor:

$$\sigma = 1 - \frac{L_m^2}{L_s L_r} \tag{D.11}$$

With the inductances and coupling factors the current equations (D.5) and (D.6) become:

$$\dot{i}_s = \frac{\vec{\psi}_s}{L_s^{'}} - k_r \frac{\vec{\psi}_r}{L_s^{'}} \tag{D.12}$$

$$\dot{i}_r = -k_s \frac{\vec{\psi}_s}{L_r^{'}} + \frac{\vec{\psi}_r}{L_r^{'}} \tag{D.13}$$

The equations that have been obtained so far will be used to derive an approximate equation for the maximum short-circuit current supplied by an induction machine. The rotational speed of the rotor differs only a few percent from the grid frequency and is assumed to stay constant during a transient event. This introduces only a limited error [Kov 59].

The voltage equations of an induction machine are given by (D.1) and (D.2). Solving these differential equations will give a particular solution, which give the current in a steady-state situation. The general solution can be obtained by adding the solution of the homogeneous differential equation to the steady-state currents. The solution of the homogeneous equation gives the 'free currents', which separately satisfy the homogenous differential equation. The solution of the homogeneous equation can be obtained by setting the stator and rotor voltage to zero.

During the occurrence of a short-circuit the currents go from the original stationary state to a new stationary state. The continuity of the transition is assured by the 'free currents'. The 'free currents' that occur during this compensation process can be investigated separately from the stationary currents, as if both stator and rotor are short-circuited [Kov 59]. The 'free currents' of an induction machine that rotates approximately synchronous, are similar to those in a synchronous machine. During the transition from one stationary state to another the following currents are present in the induction machine:

1. Stationary currents with frequency f_s (stator) and $f_r=s \cdot f_s$ (rotor)
2. Stator dc-current. It can be considered as a space-vector with a fixed position. As the rotor rotates with $\omega_m=(1-s)\omega_s$ (assuming one pole-pair) with respect to this fixed space-vector, the rotor adds an alternating current with $f=(1-s)\omega_s$ to this dc-current.
3. Rotor dc-current. This current rotates with the rotor and creates the alternating current in the stator.

The dc-components are no real dc-currents. In reality the space-vector rotates slowly and it is damped exponentially. The space-vector rotates faster for a larger stator and rotor resistance. The time-constant for the damping of the dc-components in stator and rotor are given by [Kov 59]:

$$T_s^{'} = \frac{L_s^{'}}{R_s}$$
(D.14)

$$T_r^{'} = \frac{L_r^{'}}{R_r}$$
(D.15)

The currents and fluxes in the machine during a short-circuit are determined in two steps. In the first step the stator and rotor resistance are neglected. The current- and

flux-components that are obtained are considered as the start-values. In the next step the components are multiplied by a damping factor, which is based on the resistance and leakage inductance of the machine. The results that are obtained in this way have an error of 10 - 20% [Kov 59].

The short-circuit current of an idle running machine will be determined. Neglecting the mechanical losses the machine rotates at the synchronous rotational speed ω_s. The stator resistance can be neglected in steady-state. Before the occurrence of the short-circuit the rotor current is zero: $I_r=0$. The stator current is:

$$I_s e^{j\omega_s t} = \frac{V_s e^{j\omega_s t}}{jX_s} = \frac{V_s e^{j\omega_s t}}{j\omega_s L_s}$$
(D.16)

the stator flux is:

$$\Psi_s e^{j\omega_s t} = I_s e^{j\omega_s t} L_s = \frac{V_s e^{j\omega_s t}}{j\omega_s}$$
(D.17)

and the rotor flux is (in a fixed reference frame):

$$\Psi_r e^{j\omega_s t} = I_s e^{j\omega_s t} L_m = \frac{L_m}{L_s}\frac{V_s e^{j\omega_s t}}{j\omega_s} = k_s \frac{V_s e^{j\omega_s t}}{j\omega_s}$$
(D.18)

At time $t = 0$ a three-phase short-circuit is assumed to occur at the stator of the machine. Both the rotor and the stator are short-circuited then. This implies that the flux in both windings does not change. The stator flux is given by:

$$\psi_s = \Psi_{s,0} = \frac{\sqrt{2}V_s}{j\omega_s}$$
(D.19)

The rotor flux has to stay fixed to the rotor winding. As the rotor rotates synchronously with the angular velocity ω_s, also the rotor flux ψ_r rotates with that angular velocity, as shown in Fig. D.2. In a fixed reference frame the rotor flux is thus given by:

$$\psi_r = \Psi_{r,0} = k_s \frac{\sqrt{2}V_s}{j\omega_s} e^{j\omega_s t}$$
(D.20)

At the moment that the short-circuit occurs, the rotor and stator flux ψ_r and ψ_s have the same angle and approximately the same amplitude. The stator flux is fixed to the stator, but the rotor flux will change with the rotor and after half a period it will be 180° out of phase and have an opposite direction. The currents in the machine will reach their maximum value then. They can become very high and are only limited by the leakage inductances.
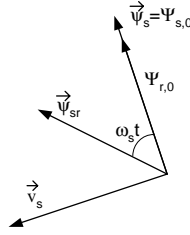
Fig. D.2. Induction machine flux vectors during a three-phase short-circuit (with resistance neglected)

The stator short-circuit current can be obtained by substituting (D.19) and (D.20) in (D.12):

$$\vec{i}_s = \frac{\vec{\psi}_s}{L_s^{'}} - k_r \frac{\vec{\psi}_r}{L_s^{'}} = \frac{\vec{\psi}_s - k_r \vec{\psi}_r}{L_s^{'}} = \frac{\sqrt{2}V_s}{j\omega_s L_s^{'}} \left[1 - k_r k_s e^{j\omega_s t} \right] \tag{D.21}$$

Writing $k_r k_s$ as $1 - \sigma$ (see (D.9) - (D.11)) the equation becomes:

$$\vec{i}_s = \frac{\sqrt{2}V_s}{j\omega_s L_s^{'}} \left[1 - (1-\sigma)e^{j\omega_s t} \right] \tag{D.22}$$

This equation is obtained under the assumption that the stator and rotor resistance can be neglected, implying that the current is undamped. In reality the current will always decline.

The first term inside the rectangular brackets of (D.22) represents the dc-component in the stator current. This current will be damped with the transient time constant $T_s^{'}$. The second term represents the ac-component in the stator current, to which a dc-component in the rotor current belongs. This term will thus be damped with the transient time constant $T_r^{'}$. Taking into account these two damping factors, (D.22) becomes [Kov 59]:

$$\vec{i}_s = \frac{\sqrt{2}V_s}{jX_s^{'}} \left[e^{-\frac{t}{T_s^{'}}} - (1-\sigma)e^{j\omega_s t} e^{-\frac{t}{T_r^{'}}} \right] \tag{D.23}$$

When the voltage v_s has an angle $\alpha + \frac{\pi}{2}$ with respect to stator phase a, at the moment that the short-circuit occurs, then $v_s = j\sqrt{2}V_s e^{j\alpha}$. The short-circuit current in this phase is then the projection of the vector is on the a-phase, i.e. its real part:

$$i_{sa} = \frac{\sqrt{2}V_s}{X_s^{'}} \left[e^{-\frac{t}{T_s^{'}}} \cos\alpha - (1-\sigma)e^{j\omega_s t} e^{-\frac{t}{T_r^{'}}} \cos(\omega_s t + \alpha) \right] \tag{D.24}$$

The current is shown in Fig. D.3.

Although the current-vector does not reach the maximum value exactly at $t=T/2$, the current after half a period gives a good approximation of the maximum current [Kov 59]. The maximum current can thus be obtained by substituting $t=T/2$ in (D.23):

$$i_{s,\max} = \frac{\sqrt{2}V_s}{X_s'}\left[e^{-\frac{T}{2T_s'}} + (1-\sigma)e^{-\frac{T}{2T_r'}} \right] \qquad (D.25)$$
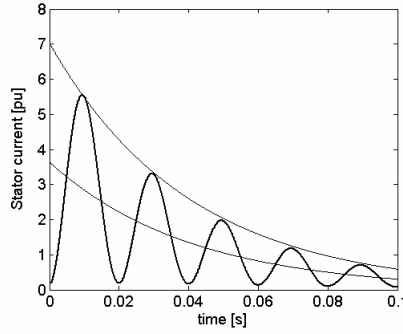

Fig. D.3. Short-circuit current in one phase of an induction machine

Appendix E

Park transformation

For most simulations in chapter 5, 6 and 7 the Park transformation is used to transform the models to the *dq0* reference frame. As this stationary reference frame is chosen to rotate with the grid frequency, all voltages and currents in the *dq0* reference frame are constant in steady state situations. Therefore, modelling in the *dq0* reference frame is expected to increase the simulation speed significantly, as a variable step-size simulation program can apply a large time step during quasi steady-state phenomena. This is especially useful for the simulations in chapter 6. This appendix describes the basic properties of the Park transformation and it shows how models in an *abc* reference frame can be transformed to the *dq0* reference frame.

The Park transformation is instantaneous and can be applied to arbitrary three-phase time-dependent signals. For $\theta_d = \omega_d t + \varphi$, with ω_d the angular velocity of the signals that should be transformed and φ the initial angle, the Park transformation is given by:

$$\begin{bmatrix} x_d \\ x_q \\ x_0 \end{bmatrix} = \left[\mathbf{T}_{dq0}(\theta_d) \right] \cdot \begin{bmatrix} x_a \\ x_b \\ x_c \end{bmatrix} \tag{E.1}$$

with the Park transformation matrix $\mathbf{T}_{dq0}$ defined as:

$$\left[\mathbf{T}_{dq0}(\theta_d) \right] = \sqrt{\frac{2}{3}} \begin{bmatrix} \cos\theta_d & \cos\left(\theta_d - \dfrac{2\pi}{3}\right) & \cos\left(\theta_d + \dfrac{2\pi}{3}\right) \\ -\sin\theta_d & -\sin\left(\theta_d - \dfrac{2\pi}{3}\right) & -\sin\left(\theta_d + \dfrac{2\pi}{3}\right) \\ \dfrac{1}{\sqrt{2}} & \dfrac{1}{\sqrt{2}} & \dfrac{1}{\sqrt{2}} \end{bmatrix} \tag{E.2}$$

The positive *q*-axis is defined as leading the positive *d*-axis by $\pi/2$, as shown in Fig. E.1. Voltages and currents of electrical systems are often given as a set of differential equations. These differential equations can easily be transformed to the *dq0* reference system. The derivative of a vector in the *abc* reference system is given by:

$$\frac{d}{dt}\left[\mathbf{x}_{abc}\right] = \frac{d}{dt}\left(\left[\mathbf{T}_{dq0}(\theta_d)\right]^{-1}\cdot\left[\mathbf{x}_{dq0}\right]\right) \tag{E.3}$$

With the chain-rule for derivatives and knowing that for $x=x(t)$:

$$\frac{d}{dt}\sin x = \cos x\frac{dx}{dt} \text{ and } \frac{d}{dt}\cos = -\sin x\frac{dx}{dt} \tag{E.4}$$

and that $\omega_d=d\theta_d/dt$, the following result is obtained:

$$\left[\mathbf{T}_{dq0}(\theta_d)\right]\cdot\frac{d}{dt}\left[\mathbf{x}_{abc}\right] = \frac{d}{dt}\left[\mathbf{x}_{dq0}\right] + \omega_d\cdot y\cdot\left[\mathbf{x}_{dq0}\right] \tag{E.5}$$

with y given by:

$$y = \frac{1}{\omega_d}\cdot\left(\frac{d}{dt}\left[\mathbf{T}_{dq0}(\theta_d)\right]\right)\cdot\left[\mathbf{T}_{dq0}(\theta_d)\right]^{-1} = \begin{bmatrix} 0 & -1 & 0 \\ 1 & 0 & 0 \\ 0 & 0 & 0 \end{bmatrix} \tag{E.6}$$

It can be seen from (E.6) that differential equations will cause a cross-relation between the d and the q axis.
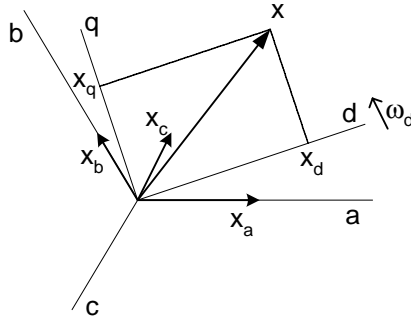

Fig. E.1. Relationship between *abc* and *dq* quantities

Some additional properties of the Park transformation can be derived. As the transformation is orthogonal, it holds that:

$$\left[\mathbf{T}_{dq0}(\theta_d)\right]\cdot\left[\mathbf{T}_{dq0}(\theta_d)\right]^{-1} = \left[\mathbf{T}_{dq0}(\theta_d)\right]\cdot\left[\mathbf{T}_{dq0}(\theta_d)\right]^{T} = [\mathbf{I}] \tag{E.7}$$

The transformations of (E.2) is unitary. Note that by replacing the factor $\sqrt{2/3}$ by a factor $2/3$ the transformation will be amplitude-invariant, implying that the length of the current and voltage vectors in both *abc* and *dq0* reference frame are the same. This amplitude-invariant transformation is generally used for modelling of electrical machines [Paa 00].

The Park transformation does not only transform the fundamental frequency signals. Also non-fundamental harmonics are correctly transformed as x_a, x_b and x_c are time

signals, including all harmonics. In steady state a non-fundamental frequency component with frequency ω_h will appear as a sinusoidal signal with frequency $(\omega_h\text{-}\omega_d)$ in the *dq0* domain. The highest frequency that can be represented accurately in the *dq0* frame depends on the time step that is used.

With (E.7) it can be shown that the Park transformation conserves power:

$$
\begin{aligned}
p(t) &= \left[\mathbf{v}_{abc}\right]^{T}\cdot\left[\mathbf{i}_{abc}\right] \\
&= \left[\left[\mathbf{T}_{dq0}(\theta_d)\right]^{-1}\left[\mathbf{v}_{dq0}\right]\right]^{T}\cdot\left[\mathbf{T}_{dq0}(\theta_d)\right]^{-1}\left[\mathbf{i}_{dq0}\right] \\
&= \left[\mathbf{v}_{dq0}\right]^{T}\left[\left[\mathbf{T}_{dq0}(\theta_d)\right]^{-1}\right]^{T}\cdot\left[\mathbf{T}_{dq0}(\theta_d)\right]^{-1}\left[\mathbf{i}_{dq0}\right] \\
&= \left[\mathbf{v}_{dq0}\right]^{T}\left[\mathbf{T}_{dq0}(\theta_d)\right]\cdot\left[\mathbf{T}_{dq0}(\theta_d)\right]^{-1}\left[\mathbf{i}_{dq0}\right] \\
&= \left[\mathbf{v}_{dq0}\right]^{T}\cdot\left[\mathbf{i}_{dq0}\right]
\end{aligned}
\tag{E.8}
$$

The instantaneous active and reactive power can be obtained directly from the voltages and currents in the *dq0* reference system:

$$
\begin{aligned}
p &= v_d i_d + v_q i_q \\
q &= v_q i_d - v_d i_q
\end{aligned}
\tag{E.9}
$$

The simulations in chapter 6 and 7 and in section 5.5 and 5.6 are done with models in the *dq0* reference frame. The *0*-axis has not been modelled, as only symmetrical situations are considered. Besides models for the electrical machines and converters also models for grid components such as cables and transformers have been used. A description of these models in the *dq0* reference frame can be found in [Pie 04].

174

Appendix F

On the use of reduced converter models

For the simulations that have been done in this thesis reduced models of power electronic converters have been used. This means that no modulation is applied and that the switches are replaced by controlled voltage sources (one voltage source per phase), which are directly controlled by the reference waveforms. This appendix will investigate under which conditions the reduced models can be used. The analyses and derivations in this appendix are based on [Zio 85], [Moh 95], [Lee 01], [Hol 03].

F.1 Switching functions

The basic principle of a half-bridge converter was described in chapter 2. For convenience the phase arm shown in Fig. 2.7 is repeated here in Fig. F.1a. The two switches are controlled by a pulse width modulation circuit, which compares the reference waveform to a triangular carrier waveform. When the reference waveform is above the carrier waveform the output is switched to the upper rail, and when it is below the carrier waveform it is switched to the lower rail. The output voltage $v_{an}(t)$ can be written as:

$$v_{an}(t) = SF(t) \cdot V_{dc} \tag{F.1}$$

with $SF(t)$ the switching function which can be expressed as [Zio 85]:

$$SF = \sum_{n=1}^{\infty} A_n \cos n\omega_0 t \tag{F.2}$$

An example of a switching function is shown in Fig. F.1b. The switching function is time-dependent and is a function of the carrier waveform:

$$x(t) = \omega_c t + \theta_c \tag{F.3}$$

and the reference waveform:

$$y(t) = \omega_0 t + \theta_0 \tag{F.4}$$

with ω_c and ω_0 the angular frequency of the carrier waveform and the reference waveform respectively and θ_c and θ_0 the angle of the two waveforms respectively.

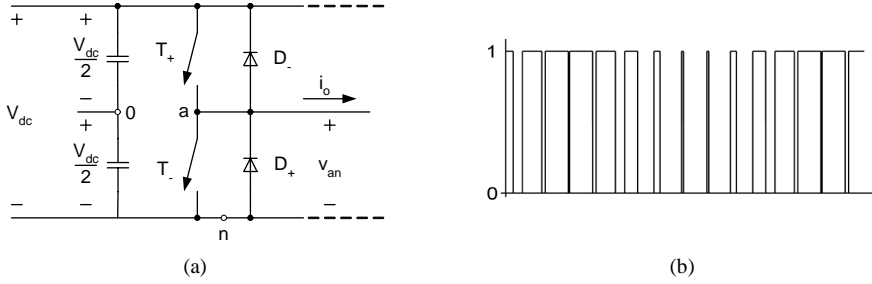(a)   (b)

Fig. F.1. Phase-arm of converter

F.2 Fourier analysis theory

From Fourier analysis theory it is known that any time-varying function $f(t)$ can be expressed as a summation of its harmonic components:

$$f(t) = \frac{a_0}{2} + \sum_{m=1}^{\infty} \left[a_m \cos m\omega t + b_m \sin m\omega t \right] \tag{F.5}$$

with

$$a_m = \frac{1}{\pi} \int_{-\pi}^{\pi} f(t) \cos m\omega t \, d\omega t \qquad\qquad m = 0, 1, \ldots, \infty \tag{F.6}$$

$$b_m = \frac{1}{\pi} \int_{-\pi}^{\pi} f(t) \sin m\omega t \, d\omega t \qquad\qquad m = 1, 2, \ldots, \infty \tag{F.7}$$

For a function based on two time-varying parameters, (F.5) can be written as [Hol 03]:

$$f(x, y) = \frac{A_{00}}{2} + \sum_{n=1}^{\infty} \left[A_{0n} \cos ny + B_{0n} \sin nyt \right] + \sum_{m=1}^{\infty} \left[A_{m0} \cos mx + B_{m0} \sin mx \right]$$

$$\sum_{m=1}^{\infty} \sum_{\substack{n=-\infty \\ (n \neq 0)}}^{\infty} \left[A_{mn} \cos(mx + ny) + B_{mn} \sin(mx + ny) \right] \tag{F.8}$$

with

$$A_{mn} = \frac{1}{2\pi^2} \int_{-\pi}^{\pi} \int_{-\pi}^{\pi} f(x, y) \cos(mx + ny) \, dx \, dy \tag{F.9}$$

$$B_{mn} = \frac{1}{2\pi^2} \int\limits_{-\pi}^{\pi} \int\limits_{-\pi}^{\pi} f(x, y)\sin(mx + ny)\, dx\, dy \qquad \text{(F.10)}$$

The two equations can be written in complex form as:

$$\underline{C}_{mn} = A_{mn} + jB_{mn} = \frac{1}{2\pi^2} \int\limits_{-\pi}^{\pi} \int\limits_{-\pi}^{\pi} f(x, y)e^{j(mx+ny)}\, dx\, dy \qquad \text{(F.11)}$$

F.3 Harmonic spectrum of triangular carrier modulation

In this section the harmonic spectrum of the switching function will be determined. The modulation circuit uses a triangular carrier waveform, which is compared with a reference waveform that is defined as:

$$v_{an}^* = M\cos(\omega_0 t + \theta_0) \qquad \text{(F.12)}$$

with M the modulation index ($0 < M < 1$). In [Hol 03] it is shown that for a triangular carrier waveform the instants that the switching function changes between 0 and 1 can be expressed as (assuming that θ_c and θ_0 are zero):

$$x = 2\pi p - \frac{\pi}{2}(1 + M\cos\omega_0 t) \qquad\qquad p = 0,\ 1,\ 2,\ \ldots,\ \infty \qquad \text{(F.13)}$$

when SF changes from 0 to 1 and

$$x = 2\pi p + \frac{\pi}{2}(1 + M\cos\omega_0 t) \qquad\qquad p = 0,\ 1,\ 2,\ \ldots,\ \infty \qquad \text{(F.14)}$$

when SF changes from 1 to 0. With these equations the harmonic components of the switching function can be determined. First (F.8) will be written in another form however. Replacing $f(x,y)$ by $SF(x,y)$, x by $\omega_c t + \theta_c$ and y by $\omega_0 t + \theta_0$, (F.8) can be written as:

$$
\begin{aligned}
SF(t) = {} & \frac{A_{00}}{2} && \text{dc offset} \\[1em]
& + \sum_{n=1}^{\infty}\left[A_{0n}\cos n[\omega_0 t + \theta_0] + B_{0n}\sin n[\omega_0 t + \theta_0]\right] && \begin{array}{l}\text{Fundamental}\\ \text{component \&}\\ \text{baseband harmonics}\end{array} \\[1em]
& + \sum_{m=1}^{\infty}\left[A_{m0}\cos m[\omega_c t + \theta_c] + B_{m0}\sin m[\omega_c t + \theta_c]\right] && \text{Carrier harmonics} \\[1em]
& + \sum_{m=1}^{\infty}\sum_{\substack{n=-\infty\\(n\neq 0)}}^{\infty}\left[\begin{array}{l}A_{mn}\cos(m[\omega_c t + \theta_c] + n[\omega_0 t + \theta_0])\\ + B_{mn}\sin(m[\omega_c t + \theta_c] + n[\omega_0 t + \theta_0])\end{array}\right] && \text{Sideband harmonics}
\end{aligned}
\qquad \text{(F.15)}
$$

with m the carrier index variable and n the baseband index variable. This form clearly shows the different components of the harmonic components of $SF(t)$ as a function of the carrier and the reference waveform frequency.

With the equations (F.13) and (F.14), (F.11) can be written as:

$$A_{mn} + jB_{mn} = \frac{1}{2\pi^2} \int\limits_{-\pi}^{\pi} \int\limits_{-\frac{\pi}{2}(1+M\cos y)}^{\frac{\pi}{2}(1+M\cos y)} e^{j(mx+ny)} \, dx \, dy \qquad (F.16)$$

This equation can be used to determine expressions for all four terms in (F.15). The dc offset is given for $m=0$ and $n=0$:

$$A_{00} + jB_{00} = \frac{1}{2\pi^2} \int\limits_{-\pi}^{\pi} \int\limits_{-\frac{\pi}{2}(1+M\cos y)}^{\frac{\pi}{2}(1+M\cos y)} dx \, dy = \frac{1}{2\pi^2} \int\limits_{-\pi}^{\pi} \pi(1+M\cos y) \, dy = 1 \qquad (F.17)$$

The offset in $SF(t)$ is thus ½. The baseband harmonics ($m=0$, $n>0$) can be expressed as:

$$A_{0n} + jB_{0n} = \frac{1}{2\pi^2} \int\limits_{-\pi}^{\pi} \int\limits_{-\frac{\pi}{2}(1+M\cos y)}^{\frac{\pi}{2}(1+M\cos y)} e^{jny} \, dx \, dy = \frac{1}{2\pi^2} \int\limits_{-\pi}^{\pi} \left[\pi(1+M\cos y)e^{jny} \right] dy$$

$$= \frac{1}{2\pi} \int\limits_{-\pi}^{\pi} \left[e^{jny} + \frac{M}{2} \left(e^{j[n+1]y} + e^{j[n-1]y} \right) \right] dy \qquad (F.18)$$

As $\int\limits_{-\pi}^{\pi} e^{jny} \, dy = 0$ for any nonzero value of n, (F.18) can be reduced to:

$$A_{01} + jB_{01} = \frac{1}{2\pi} \int\limits_{-\pi}^{\pi} \frac{M}{2} \, dy = M \qquad (F.19)$$

for $n=1$. For all other $n>1$, $A_{0n}+jB_{0n}=0$ [Hol 03]. This fundamental frequency component term is equal to the amplitude of the reference waveform defined in (F.12).

The carrier and side-band harmonics are defined as [Hol 03]:

$$A_{m0} + jB_{m0} = \frac{2}{m\pi} J_0\left(m\frac{\pi}{2} M \right) \sin m\frac{\pi}{2} \qquad (F.20)$$

$$A_{mn} + jB_{mn} = \frac{2V_{dc}}{m\pi} J_n\left(m\frac{\pi}{2} M \right) \sin\left([m+n]\frac{\pi}{2} \right) \qquad (F.21)$$

F.4 Harmonic voltages in a half-bridge converter

The output voltage $v_{an}(t)$ of the half-bridge converter shown in Fig. F.1a can be obtained by substituting (F.17), (F.19), (F.20), and (F.21) in the equation for the switching function, (F.15), and substituting the switching function in (F.1):

$$
v_{an}(t) = \frac{V_{dc}}{2} + \frac{V_{dc}}{2} M \cos(\omega_0 t + \theta_0)
$$
$$
+ \frac{2V_{dc}}{\pi} \sum_{m=1}^{\infty} \frac{1}{m} J_0\left(m\frac{\pi}{2}M\right) \sin m\frac{\pi}{2} \cos(m[\omega_c t + \theta_c])
$$
$$
+ \frac{2V_{dc}}{\pi} \sum_{m=1}^{\infty} \sum_{\substack{n=-\infty \\ (n\neq 0)}}^{\infty} \frac{1}{m} J_n\left(m\frac{\pi}{2}M\right) \sin\left([m+n]\frac{\pi}{2}\right) \times \cos(m[\omega_c t + \theta_c] + n[\omega_0 t + \theta_0])
$$

(F.22)

where J_0 and J_n are Bessel functions with argument 0 and n.

The harmonic components of the voltage can be split up in the four groups that have been defined:

- a dc offset of ½V_{dc}. This term disappears when the voltage v_{a0} is used instead of v_{an}. Also in full-bridge converters (such as the one used in this thesis) the dc term disappears).
- a fundamental frequency component that equals the reference waveform defined in (F.12) times V_{dc}.
- a group of harmonics with the carrier frequency and multiples of it.
- a group of harmonics defined by the sum and difference between the modulating carrier waveform harmonics and the reference waveform and its associated baseband harmonics. They exist as groups around the carrier harmonic frequencies.

F.5 Discussion and conclusion

The fundamental frequency component of the voltage generated by the converter is thus equal to the reference voltage. The voltage generated by the converter will also contain higher harmonics, which are centred around the carrier frequency. When the carrier frequency is much higher than the fundamental frequency ($f_c \gg f_0$) the harmonics created by the pulse-width modulation and the switching of the converter will not interfere with the fundamental frequency behaviour of the converter and other phenomena with a relatively low frequency. This implies that a reduced model can be used, as long as the frequency of the phenomena under investigation is sufficiently lower than the carrier frequency.

As the carrier frequency is generally much higher than the fundamental frequency of the reference waveform, the fundamental frequency can generally easily be separated from the harmonic frequencies by a low-pass filter. This filter will also limit the harmonic currents that are injected in the network.

List of symbols

Abbreviations

CSC	Current source converter
DFIG	Doubly-fed induction generator
DG	Distributed Generation
DN	Distribution network
FC	Fuel cell
HV	High-voltage
LV	Low-voltage
MT	Micro turbine
MV	Medium-voltage
PEC	Power electronic converter
SF	Switching function
VI	Variable inductor
VSC	Voltage source converter
WT	Wind turbine

Notation

For the variables in the equations different notations have been used:

x(t)	time-dependent signal
x(s)	frequency-dependent signal (Laplace domain)
X	RMS value
$\underline{X}$	Complex value
$\vec{x}$	vector

Symbols

B	damping torque [N·m]
C	capacitance [F]
D	droop [-]
E	energy [J]
f	frequency [Hz]
F	Faraday's constant [C/mol]
F	fraction of total turbine power [-]
G	conductance [S]
G	transfer function [-]
H	inertia constant [s]
i, I	current [A]
J	inertia [kg·m^2]
k	controller constant [-]
k	utilisation factor [-]
K	controller constant [-]
K	droop constant [W/Hz]
K	valve molar constant [kmol/(s·A)]
L	inductance [H]
m, M	modulation ratio [-]
n, N	number [-]
p	number of pole pairs [-]
p	partial pressure [N/m^2]
P	active power [W]
PL	penetration level [-]
q	molar flow [kmol/s]
Q	reactive power [VA]
r	ratio [-]
R	resistance [Ω]
R	governor constant [-]
R	universal gas constant [J/(mol K)]
s	Laplace operator [-]
S	apparent power [VA]
T	temperature [K]
T	time constant [s]
T	torque [N·m]
U	utilisation factor [-]
v	speed [m/s]
v	voltage [V]
V	voltage [V]
V	volume [m^3]
X	reactance [Ω]
Z	impedance [Ω]

α	bandwidth [Hz]
φ	angle [rad]
ω	angular velocity [rad/s]
τ	time constant [s]
θ	pitch angle [degrees]
λ	tip speed ratio [-]
Ψ	flux [Wb]

Subscripts

0	fundamental
a	active
a	amplitude
a	aerodynamic
a	phase a
c	conventional
c	current control
conv	converter
cb	circuit breaker
d	d-axis, damping
dg, *DG*	Distributed Generation
dip	voltage dip
dist	disturbance
dyn	dynamic
CPL	constant power load
CPS	constant power source
dc	dc
df	damping in filter
e	electrical
emu	emulated
f	filter
f	fundamental
fc	fuel cell
fc	converter side of filter
FC	fuel cell
fg	grid side of filter
fl	fault location
g	grid
G	generator
gen	generator
gt	gas turbine
h	harmonic
HP	high-pressure

i	input, integral
ine	inertial response
inv	inverter
l	load
load	load
m	mechanical
max	maximum
min	minimum
mt, *MT*	micro turbine
n	node
nom	nominal
o	output
p	proportional
pfc	primary frequency control
PR	proportional-resonant
q	q-axis
r	real (real-imaginary)
r	resonant
r	ripple
r	resistance
R	reformer
rect	rectifier
ref	reference
rt	response time
s	source
s	switching
syst	system
sc	short-circuit
th	threshold
tot	total
var	variable
wt, *WT*	wind turbine
x	imaginary

Superscripts

*	complex-conjugate
'	reduced on stator side
r	resistance
in	in
out	out

Dankwoord

Dit proefschrift is het resultaat van vier jaar onderzoek binnen de vakgroep Electrical Power Processing van de Technische Universiteit Delft. Vele mensen zijn direct of indirect betrokken geweest bij mijn promotie-onderzoek en de realisatie van dit proefschrift. Zonder volledig te kunnen zijn wil ik een aantal van hen in het bijzonder bedanken.

De eerste die ik wil bedanken is mijn toegevoegd promotor ir. S.W.H. de Haan. Als mijn dagelijks begeleider heeft hij een belangrijke bijdrage geleverd aan de totstandkoming van dit proefschrift. Hij hield steeds de grote lijnen van het onderzoek in het oog en heeft een grote bijdrage geleverd aan het steeds weer scherp formuleren van de vraagstellingen. Ook de leesbaarheid van het proefschrift is er dankzij hem sterk op vooruitgegaan. Sjoerd, bedankt dat ik met mijn vragen altijd bij je terecht kon.

Als promotor heeft ook prof. dr. J.A. Ferreira een belangrijke bijdrage geleverd aan de totstandkoming van dit proefschrift. Braham, bedankt voor je frisse blik op het onderzoek, het waardevolle commentaar dat je gaf tijdens onze voortgangs-besprekingen, en je aandacht voor de praktische relevantie van mijn onderzoek.

Mijn onderzoek maakte deel uit van het IOP-EMVT project "Intelligentie in Netten". De samenwerking met de 9 andere promovendi had zeker haar meerwaarde. Bij deze wil ik, Andrej, Anton, Cai, Frans, George, Jody, Reza, Roald en Sjef dan ook bedanken voor de plezierige samenwerking. Hetzelfde geldt voor alle begeleiders die bij het project betrokken waren.

SenterNovem wil ik bedanken voor het mogelijk maken van dit project. De leden van de IOP-begeleidingscommissie worden bedankt voor het commentaar en de adviezen tijdens de halfjaarlijkse bijeenkomsten.

Tijdens mijn promotie heb ik veel baat gehad bij het werk dat ik samen met Jan Pierik van ECN gedaan heb in de Erao-projecten. Jan, bedankt voor de plezierige en leerzame samenwerking.

Gedurende de jaren die ik aan de TU werkte heb ik met veel plezier de kamer gedeeld met Bart Roodenburg. Bart, bedankt voor alles: de koffie die 's ochtends klaarstond, de vele gesprekken over van alles en nog wat, de mogelijkheid om 'domme vragen' te kunnen stellen en je op de praktijk gebaseerde visie op veel van mijn wilde theoretische plannen.

Zonder ze allemaal bij naam te noemen wil ik ook alle andere collega's, medewerkers, promovendi en studenten bij de EPP vakgroep bedanken. Hetzelfde geldt voor mijn collega's van de EPS vakgroep. Mijn onderzoek bevond zich op het grensvlak tussen electriciteitsvoorziening en vermogenselektronica. Vaak kwam ik dan ook bij hen over de vloer.

During my research I had the opportunity to cooperate with a number of (Ph.D.-) students. Especially I would like to thank Matteo Tonso, who did a master-project on the use of a variable inductance for voltage control. Some of his results have been used in this thesis. Further I would like to thank Jean-Baptiste Defreville, Ivo van Vliet and Mariel Triggianese. Also the cooperation with them has been very pleasant and helpful.

Mijn huisgenoten hebben jarenlang een 'burger' in hun midden geduld. Hoewel onze ritmes soms wat uit fase liepen heeft dit zelden tot problemen geleidt en heb ik met plezier op Don Quichotte gewoond. Bedankt voor het samenwonen en jullie betrokkenheid.

Hoewel misschien wat minder direct bij het onderzoek betrokken, wil ik ook mijn familie, vrienden en kennissen bedanken voor de belangstelling en interesse die ze de afgelopen jaren getoond hebben in (de voortgang van) mijn onderzoek. Hoewel ik misschien niet altijd duidelijk heb kunnen maken wat ik precies deed hebben jullie toch regelmatig blijk gegeven van jullie betrokkenheid, hartelijk dank daarvoor. In het bijzonder wil ik Hans Teerds bedanken die de omslag van dit proefschrift ontworpen heeft. Hans, bedankt.

Mijn leven is in Gods hand. Hij heeft mij de talenten gegeven om dit onderzoek te doen en Hij heeft mij de afgelopen jaren gezondheid en alles wat ik nodig had gegeven. Hem komt bovenal de dank voor dit proefschrift toe.

Delft, september 2006
Johan Morren

List of publications

Journal papers

- Johan Morren, Bart Roodenburg, Sjoerd W.H. de Haan, "Electrochemical reactions and electrode corrosion in Pulsed Electric Field (PEF) treatment chambers", *Innovative Food Science and Emerging Technologies*, Vol. 4 No. 3, September 2003, pp. 285 – 295.
- Johan Morren, Sjoerd W.H. de Haan, "Ridethrough of Wind Turbines with Doubly-Fed Induction Generator During a Voltage Dip" *IEEE Trans. Energy Conversion*, Vol. 20, No. 2, pp. 435 – 441, June 2005.
- Bart Roodenburg, Johan Morren, H.E. (Iekje) Berg and Sjoerd W.H. de Haan, "Metal release in a stainless steel Pulsed Electric Field (PEF) system: Part I. Effect of different pulse shapes; theory and experimental method", *Innovative Food Science and Emerging Technologies*, Vol. 6 No. 3, September 2005, pp. 327 – 336.
- Bart Roodenburg, Johan Morren, H.E. (Iekje) Berg and Sjoerd W.H. de Haan, "Metal release in a stainless steel pulsed electric field (PEF) system: Part II. The treatment of orange juice; related to legislation and treatment chamber lifetime", *Innovative Food Science and Emerging Technologies*, Vol. 6 No. 3, September 2005, pp. 337 – 345.
- Johan Morren, Jan T. G. Pierik, Sjoerd W. H. de Haan, Jan Bozelie, "Grid interaction of offshore wind farms. Part 1. Models for dynamic simulation", *Wind Energy*, Vol. 8, No. 3, pp. 265 – 278, 2005, DOI: 10.1002/we.158
- Johan Morren, Jan T. G. Pierik, Sjoerd W. H. de Haan, Jan Bozelie, "Grid interaction of offshore wind farms. Part 2. Case study simulations", *Wind Energy*, Vol. 8, No. 3, pp. 279 – 293, 2005, DOI: 10.1002/we.159
- Johan Morren, Sjoerd W.H. de Haan, Wil L. Kling, J.A. Ferreira, "Wind Turbines Emulating Inertia and Supporting Primary Frequency Control", *IEEE Trans. Power Systems*, Vol. 21, No. 1, pp. 433 – 434, February 2006.
- Johan Morren, Jan Pierik, Sjoerd W.H. de Haan, "Inertial response of variable speed wind turbines", *Electric Power Systems Research*, Vol. 76, pp. 980 – 987, June 2006.
- J. Morren, S.W.H. de Haan, J.A. Ferreira, "Contribution of DG Units to Primary Frequency Control", *European Transactions on Electric Power*, article in press, 2006.
- Johan Morren, Sjoerd W.H. de Haan, "Short-Circuit Current of Wind Turbines with Doubly-Fed Induction Generator", *IEEE Trans. Energy Conversion*, accepted for publication, 2006.

Conference papers

- K. Burges, E.J. van Zuylen, J. Morren, "DC Transmission for Offshore Wind Farms: Concepts and Components", in *Proc. 2nd International Workshop on Transmission Networks for Offshore Wind Farms*, Stockholm, Sweden, 29 – 30 March 2001.
- J. Morren, S.W.H. de Haan, J.A. Ferreira, "Design and scaled experiments for high-power DC-DC conversion for HVDC systems", in *Proc. 32nd IEEE annual Power Electronics Specialists Conference (PESC)*, Vol. 3, pp. 791-796, 17 – 21 June 2001.

- J. Morren, M. Pavlovsky, S.W.H. de Haan, J.A. Ferreira, "DC-DC conversion for offshore windfarms", in *Proc. 9th European conference on Power Electronics and applications* (EPE), Graz, Austria, 27 – 29 August 2001.
- B. Roodenburg, G. de Jong, I.E. Pol, J. Morren, N. Dutreux, P.C. Wouters, R.H.S.H. Beurskens, S.W.H. de Haan, "Preservation of Liquid Food by Pulsed High-Voltage Arc Discharges", in Proc. Society For Applied Microbiology (SFAM) annual meeting, pp. 145-147, Wageningen, The Netherlands, 9 – 11 January 2002.
- J. Morren, S.W.H. de Haan, J.A. Ferreira, "High-voltage DC-DC converter for offshore windfarms", in *Proc. IEEE Young Researchers Symposium in Electrical Power Engineering*, Leuven, Belgium, 7 – 8 February 2002.
- B. Roodenburg, J. Morren, S.W.H. de Haan, H.A. Prins, Y.L.M. Creyghton, "Modeling a 80 kV Pulse Source for Pulsed Electric Fields (PEF)", In *Proc. 10th Power Electronics and Motion Control conference (EPE-PEMC)*, Cavtat & Dubrovnik, Croatia, 9 – 11 September 2002.
- S.W.H. de Haan, B. Roodenburg, J. Morren, H. Prins, "Technology for Preservation of Food with Pulsed Electric Fields (PEF), in *Proc 6th IEEE Africon Conference*, Vol. 2, pp. 791-796, 2 – 4 October 2002.
- B. Roodenburg, J. Morren, S.W.H. de Haan, P.C. Wouters, G. de Jong, I.E. Pol, Y.L.M. Chreyghton, "High-Voltage Arc Pulser for Preservation of Liquid Food", in *Proc. European Pulsed Power Symposium*, pp. 26/1 26/6, Saint Louis, France, 22 – 24 October 2002.
- J. Morren, S.W.H. de Haan, P. Bauer, J.T.G. Pierik, J. Bozelie, "Comparison of complete and reduced models of a wind turbine with Doubly-Fed Induction Generator" in *Proc. 10th European conference on Power Electronics and applications* (EPE 2003), Toulouse, France, 2 – 4 September 2003.
- B. Roodenburg, J. Morren, S.W.H. de Haan, H.E. Berg, "Corrosion Experiments in a Pulsed Electric Field (PEF) Treatment Chamber with Stainless Steel Electrodes", in Proc. Workshop on Nonthermal Food Preservation, Vol. 1, pp. 1 – 4, Wageningen, The Netherlands, 7 – 10 September 2003.
- J. Morren, S.W.H. de Haan, J.T.G. Pierik, J. Bozelie, Fast Dynamic Models of Offshore Wind Farms for Power System Studies", in *Proc. 4th International Workshop on Large-scale Integration of Wind Power and Transmission Networks for Offshore Wind Farms*, Billund, Denmark, 20 – 21 October 2003.
- Jan Pierik, Johan Morren, Sjoerd de Haan, Tim van Engelen, Edwin Wiggelinkhuizen, Jan Bozelie, "Dynamic models of wind farms for grid-integration studies", in *Proc. Nordic Wind Power Conference 2004*, Gothenburg, Sweden, 1 – 2 March 2004.
- M. Reza, J. Morren, P.H. Schavemaker, J.G. Slootweg, W.L. Kling, L. van der Sluis, "Impacts of converter connected distributed generation on power system transient stability", in *Proc. 2nd IEEE Young Researchers Symposium in Electrical Power Engineering*, Delft, The Netherlands, 18 – 19 March 2004.
- Johan Morren, Sjoerd W.H. de Haan, J.A. Ferreira, "Distributed Generators providing ancillary services", *Distribution Europe 2004,* Amsterdam, The Netherlands, 27-28 April 2004.
- Johan Morren, Jan T.G. Pierik, Sjoerd W.H. de Haan, "Fast dynamic modelling of direct-drive wind turbines", in *Proc PCIM Europe 2004*, Nürnberg, Germany 25 – 27 May 2004.
- J. Morren, S.W.H. de Haan, J.A. Ferreira, "Model reduction and control of electronic interfaces of voltage dip proof DG units", in *Proc. 2004 IEEE Power Engineering Society (PES) General Meeting*, Denver, 6- 10 June 2004.
- J. Morren, S.W.H. de Haan, J.A. Ferreira, "Distributed Generation Units contributing to voltage control in distribution networks", in *Proc. 39th International Universities Power Engineering Conference (UPEC 2004)*, Bristol, UK, 6- 8 September 2004.
- J. Morren, J.T.G. Pierik, S.W.H. de Haan, "Voltage dip ride-through of direct-drive wind turbines", in *Proc. 39th International Universities Power Engineering Conference (UPEC 2004)*, Bristol, UK, 6- 8 September 2004.
- Johan Morren, Jan. T.G. Pierik, Sjoerd W.H. de Haan, Voltage dip ride-through control of wind turbines with doubly-fed induction generators, in *Proc. IEA Topical Expert Meeting on System Integration of Wind Turbines (IEA TEM 44)*, Dublin, Ireland, 7-8 November 2005.
- M. Reza, J. Morren, P.H. Schavemaker, W.L. Kling, L. van der Sluis, "Power Electronic Interfaced DG Units: Impact of Control Strategy on Power System Transient Stability", in *Proc. 3rd IEE Int. Conf. on Reliability of Transmission and Distribution systems, (RTDN '05)*, London, UK, 15-17 February 2005.
- G. Papaefthymiou, J. Morren, P.H. Schavemaker, W.L. Kling, L. van der Sluis, "The Role of Power Electronic Converters in Distributed Power Systems: Stochastic Steady State Analysis", in *Proc. Cigré Symposium on Power Systems with Dispersed Generation*, Athens, Greece, April 13 – 16, 2005.

- Henk Polinder, Johan Morren, "Developments in Wind Turbine Generator Systems", in *Proc. 8th Int. Conf. on Modelling and Simulation of Electric Machines, Converters and Systems (ELECTRIMACS '05)*, Hammamet, Tunesia, April 17 – 20, 2005.
- Johan Morren, Sjoerd W.H. de Haan, J.A. Ferreira, "Contribution of DG units to voltage control: active and reactive power limitations", in *Proc. 2005 IEEE St. Petersburg PowerTecch*, St. Petersburg, Russia, 27- 30 June 2005.
- Johan Morren, Sjoerd W.H. de Haan, J.A. Ferreira, "(De-)Stabilising Effect of Power Electronic Interfaced DG Units in Distribution Networks", in *Proc. 11th European conference on Power Electronics and applications* (EPE 2005), Dresden, Germany, 11 – 14 September 2005.
- Matteo Tonso, Johan Morren, Sjoerd W.H. de Haan, J.A. Ferreira, "Variable Inductor for Voltage Control in Distribution Networks", in *Proc. 11th European conference on Power Electronics and applications* (EPE 2005), Dresden, Germany, 11 – 14 September 2005.
- Johan Morren, Sjoerd W.H. de Haan, J.A. Ferreira, "Contribution of DG Units to Primary Frequency Control", in *Proc. Int. Conf. on Future Power Systems (FPS 2005)*, Hoofddorp, The Netherlands, 16 – 18 November 2005.
- Jan Pierik, Johan Morren, Tim van Engelen, Sjoerd de Haan, Jan Bozelie, "Development and validation of wind farm models for power system studies", in *Proc. European Wind Energy Conference & Exhibition (EWEC 2006)*, Athens, Greece, 27 February – 2 March, 2006.
- Johan Morren, Sjoerd W.H. de Haan, J.A. Ferreira, "Primary Power/Frequency Control with Wind Turbines and Fuel Cells", in *Proc. 2006 IEEE Power Engineering Society (PES) General Meeting*, Montreal, Canada, 18 – 22 June 2006.

Other publications

- J.T.G. Pierik, J. Morren, E.J. Wiggelinkhuizen, S.W.H. de Haan, T.G van Engelen, J. Bozelie, *Electrical and control aspects of offshore wind turbines II (Erao-2), Vol. 1: Dynamic models of wind farms*, Technical report ECN-C--04-050, ECN, 2004, June 2004.
- J.T.G. Pierik, J. Morren, E.J. Wiggelinkhuizen, S.W.H. de Haan, T.G van Engelen, J. Bozelie, *Electrical and control aspects of offshore wind turbines II (Erao-2), Vol. 2: Offshore wind farm case studies*, Technical report ECN-C--04-050, ECN, 2004, June 2004.

Curriculum Vitae

Johan Morren was born on 23 October 1976 in Wekerom. From 1989 to 1995 he visited the athenaeum at the Jacobus Fruytier scholengemeenschap in Apeldoorn. In 1995 he started his study at the Delft University of Technology, where he received the M.Sc. degree in Electrical Engineering in 2000. In 2001 he started as a research assistant in the Electrical Power Processing group of the Delft University of Technology. He worked on different projects regarding the preservation of food with pulsed electric field (PEF) treatment and the grid-connection of renewable energy sources. From 2002 to 2006 he worked, in the same group, on a Ph.D. project on the power electronic aspects of grid integration of Distributed Generation units. Since 1 October 2006 Johan Morren is with Essent Netwerk.
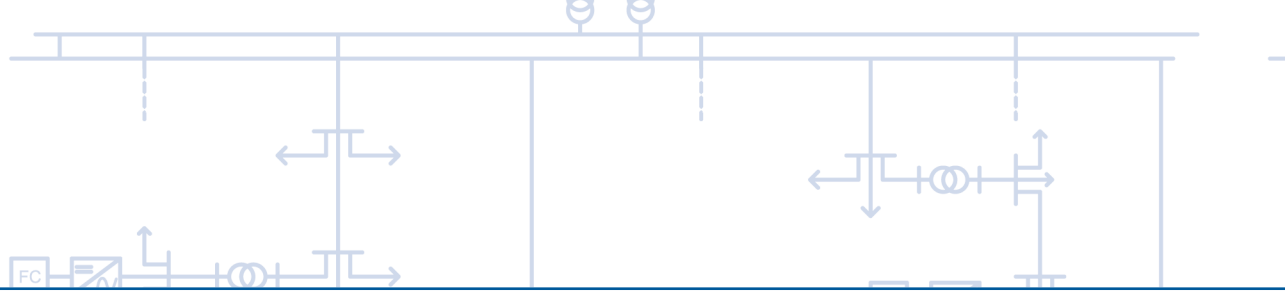
The introduction of Distributed Generation (DG) causes several problems, which are mainly related to the differences between DG units and conventional generators. A large part of the DG units are connected to the grid via power electronic converters. The main task of these converters is to convert the power that is available from the prime source to the characteristic voltage and frequency of the grid. The flexibility of the converters offers the possibility to configure them in such a way that, in addition to their main task, they can support the grid. Four issues have been considered in this thesis: damping of harmonics, voltage control, the behaviour of DG units during grid faults, and frequency control. The different control strategies that are required to achieve the grid support can all be implemented simultaneously in the control of a DG unit. In this way a multi-functional DG unit is obtained that can autonomously support the grid in several ways.